NOTE TO USERS

An Investigation Of Cellular Responses To Tetrafluoroethylcysteine-induced Mitochondrial Dysfunction

Han Kiat Ho

A dissertation submitted in partial fulfillment of the requirements for the degree of

Doctor of Philosophy

University of Washington

2005

Program Authorized to Offer Degree:
School of Pharmacy, Department of Medicinal Chemistry

INFORMATION TO USERS

The quality of this reproduction is dependent upon the quality of the copy submitted. Broken or indistinct print, colored or poor quality illustrations and photographs, print bleed-through, substandard margins, and improper alignment can adversely affect reproduction.

In the unlikely event that the author did not send a complete manuscript and there are missing pages, these will be noted. Also, if unauthorized copyright material had to be removed, a note will indicate the deletion.

ProQuest Information and Learning Company
300 North Zeeb Road
P.O. Box 1346
Ann Arbor, MI 48106-1346

University of Washington
Graduate School

This is to certify that I have examined this copy of a doctoral dissertation by

Han Kiat Ho

and have found that it is complete and satisfactory in all respects,

and that any and all revisions required by the final

examining committee have been made.

Chair of Supervisory Committee:

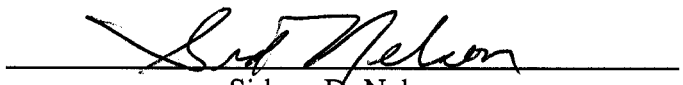

Sidney D. Nelson

Reading Committee:

Sidney D. Nelson

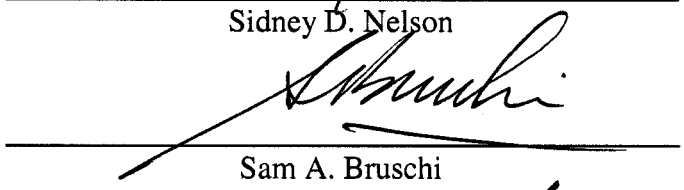

Sam A. Bruschi

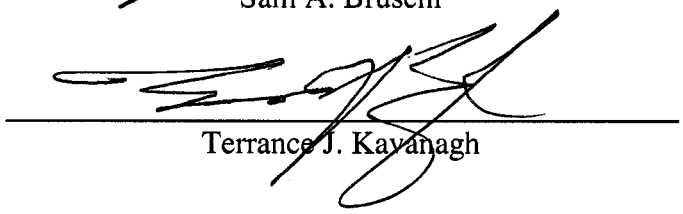

Terrance J. Kavanagh

Date: 24 October 2005

In presenting this dissertation in partial fulfillment of the requirements for the doctoral degree at the University of Washington, I agree that the Library shall make its copies freely available for inspection. I further agree that extensive copying of the dissertation is allowable only for scholarly purposes, consistent with "fair use" as prescribed in the U.S. Copyright Law. Requests for copying or reproduction of this dissertation may be referred to Proquest Information and Learning, 300 North Zeeb Road, Ann Arbor, MI 48106-1346, to whom the author has granted "the right to reproduce and sell (a) copies of the manuscript in microform and/or (b) printed copies of the manuscript made from microform."

Signature Ho Han Kut

Date 24 October 2005

University of Washington

Abstract

An Investigation Of Cellular Responses To Tetrafluoroethylcysteine-induced Mitochondrial Dysfunction

Han Kiat Ho

Chair of the Supervisory Committee:
Professor Sidney D. Nelson
Department of Medicinal Chemistry

Several disease states and chemical-induced toxicities are mediated through an early mitochondrial dysfunction. A better understanding of the molecular and biochemical events that transpire during such mitochondrial damage will help improve accuracy in preclinical screening of drug toxicities, and also in identifying potential drug targets for disease modulation. The studies described herein employ *S*-(1,1,2,2,-tetrafluoroethyl)-L-cysteine (TFEC), a major metabolite of tetrafluoroethylene (TFE), which covalently adducts a select subset of mitochondrial proteins, and causes mitochondrial stress. Results of these studies revealed that early mitochondrial changes, including the inhibition of the TCA cycle and ATP production, trigger a series of biochemical events that transcend organellar boundaries. The immediate impact of TFEC on the mitochondria is discussed in Chapter 2. The subsequent cascade of events are relayed through various signal transduction pathways that affect nuclear transcriptional responses and the induction of a number of cytosolic heat shock proteins (HSPs) as described in Chapter 3. An unexpected oxidative stress response, related to the activation of the Nrf2 transcriptional pathway was discovered and is described in Chapter 4. A further link between oxidative stress and a prior ER stress response is discussed. Finally, Chapter 5 speculates about a possible role for a

critical TFEC adduct and explores new routes of toxicity based on other observations. Overall, the results support an important role for mitochondrial dysfunction in the initiation, progression and outcome of some chemical-induced toxicities. Multiple signaling pathways can emerge from a focal subcellular lesion, leading to a plethora of targeted cellular responses in various organelles. Future investigations are suggested to better characterize these responses for identifying potential toxicity biomarkers, and/or potential drug targets.

TABLE OF CONTENTS

LIST OF ABBREVIATIONS

AD	Alzheimer's disease
ADP	Adenosine diphosphate
AIF	Apoptosis inducing factor
AMAP	N-acetyl-*m*-aminophenol
AMC	7-amino-4-methylcoumarin
ANT	Adenine nucleotide translocase
AOAA	Aminooxyacetic acid
APAP	N-acetyl-*p*-aminophenol; acetaminophen
ARE	Antioxidant response element
AST	Aspartate aminotransferase
ATF	Activating transcription factor
ATP	Adenosine triphosphate
BSS	Buffered saline solution
BUN	Blood urea nitrogen
CHAPS	3-[(3-cholamidopropyl)-dimethylammonio]-1-propanesulfonate
CoA	Coenzyme A
DCVC	Dichlorovinylcysteine
DEAE	Diethylaminoethyl
DEM	Diethylmaleate
DFTAF	Difluorothionoacetyl-fluoride
DFTAL	Difluorothionoacetyl-lysyl
DNA	Deoxyribonucleic acid
DP	Dipeptidase
DR	Death receptor

DTT	Dithiothreitol
EDTA	Ethylenediamine tetraacetic acid
ER	Endoplasmic reticulum
ETC	Electron transport chain
$FADH_2$	Flavin adenine dinucleotide
FBS	Fetal bovine serum
GAPDH	Glyceraldehyde 3-phosphate dehydrogenase
GCL	Glutamylcysteine ligase
GGT	Gamma-glutamyl transferase
GSH	Glutathione
GSSG	Oxidized glutathione
γGTP	Gamma-glutamyl transpeptidase
H_2DCFDA	Dihydro-dichlorofluorescein diacetate
HO-1	Heme oxygenase-1
HSP	Heat shock protein
IAP	Inhibitor of apoptosis protein
INT	Iodonitrotetrazolium chloride
IVT	In vitro transcription
JNK	c-Jun N-terminal kinase
αKGDH	Alpha-ketoglutarate dehydrogenase
KMV	Alpha-ketomethylvaleric acid
LDH	Lactate dehydrogenase
MAPK	Mitogen-activated protein kinase
MEF	Mouse embryonic fibroblast
MPP^+	1-methyl-4-phenylpyridinium
MPT	Mitochondrial permeability transition
MPTP	Mitochondrial permeability transition pore

mRNA	Messenger ribonucleic acid
mtDNA	Mitochondrial DNA
MTPT	1-methyl-4-phenyl-1,2,3,6-tetrahydropyridine
MTT	3-(4,5-dimethylthiazol-2-yl)-2,5-diphenyl-tetrazolium bromide
NAD^+	Nicotinamide adenine dinucleotide (oxidized)
NADH	Nicotinamide adenine dinucleotide (reduced)
NAPQI	N-acetyl-*p*-quinoneimine
NQO1	NADPH-dependent quinone oxidoreductase-1
Nrf2	NF-E2 related factor 2
NSAIDs	Non-steroidal anti-inflammatory drugs
PBS	Phosphate buffered saline
PERK	PKR-like ER kinase
PI3K	Phosphoinositol-3-kinase
PIPES	Piperazine-N,N'-bis(2-ethanesulfonic acid)
Pi	Pyrophosphate
PMSF	Phenylmethyl-sulfonylfluoride
PMT	Photomultiplier tube
RNS	Reactive nitrogen species
ROS	Reactive oxygen species
Rpm	Revolutions per minute
RTG	Retrograde system
RT-PCR	Reverse transcription-polymerase chain reaction
SDS-PAGE	Sodium dodecylsulfate-polyacrylamide gel electrophoresis

SEM	Standard error about the mean	TFEC	Tetrafluoroethylcysteine
		TNFα	Tumor necrosis factor-α
SiRNA	Small interfering RNA	TNFR	Tumor necrosis factor receptor
SnPP	Tin protoporphyrin IX		
SOD	Superoxide dismutase		
TAMH	Transforming growth factor-α mouse hepatocytes	UPR	Unfolded protein response
TCA	Tricarboxylic acid	UV	Ultraviolet
TCEP	Tris(2-carboxyethyl)phosphine	VDAC	Voltage-dependent anion selective channel
TFE	Tetrafluoroethylene	WT	Wild-type

LIST OF FIGURES

LIST OF TABLES

ACKNOWLEDGMENTS

I would like to thank the faculty, staff and students of the Department of Medicinal Chemistry for their support, guidance and friendship throughout the entire period of my PhD education.

Specifically, I would like to thank:

My advisor, Dr. Sid Nelson, for his guidance and teachings that stretches far beyond the realm of science.

My co-advisor, Dr. Sam Bruschi, for imparting the skills, knowledge and passion in pursuing toxicology research.

My supervisory committee, Dr. Terry Kavanagh, Dr. Bill Atkins and Dr. Richard S. Morrison for their assistance and support on my scientific development.

The Nelson Lab, both past and present, for the camaraderie and support through all the joys and pains of research. Particularly to Dr. Michael Adams, Dr. Zhonghua Hu, Dr. Yankai Jia and Kevin Coe who have taught and helped me through a number of experiments.

And to the many friendship forged over the past five years that have made my stay in Seattle so pleasant, eventful and unforgettable.

DEDICATION

To my parents

For their love, support and encouragement

To my wife, Ivane

Who has made this journey extraordinary, sweet, and meaningful.

To my child, eagerly awaiting to see this world

For giving me a better tomorrow.

Chapter 1

An Investigation Of Cellular Responses To Tetrafluoroethylcysteine-Induced Mitochondrial Dysfunction

1.1 Introduction: The critical roles of mitochondria in eukaryotes

The mitochondrion is a eukaryotic organelle critical for cellular viability in most eukaryotic cells. It is a double-membraned organelle consisting of a phospholipid-rich outer membrane and an inner membrane. The inner membrane is folded into cristae (Figure 1.1), enclosing the mitochondrial matrix within. Each mitochondrion carries genetic material (mtDNA) that is distinctively different from the nuclear DNA of its host cell. More intriguingly, it contains its own machinery for protein synthesis and is responsible for the expression of 13 unique mitochondrial proteins in humans. These discoveries, among others, have led many to propose that mitochondria trace their evolutionary origin to prokaryotes that became incorporated with pseudoeukaryotes, with subsequent selection for a symbiotic relationship between the two organisms (Scheffler 1999).

Today, the mitochondrion is known for its role in harnessing the energy necessary to sustain most cellular activities. This energy, stored in the form of adenosine triphosphate (ATP), is derived from a cascade of biochemical events centered in the mitochondria through the transfer of high-energy phosphates. The electrochemical potential across the inner mitochondrial membrane, the relay of electrons through a stretch of protein complexes, as well as a redox potential generated by reduced nicotinamide adenine dinucleotide (NADH) and reduced flavin adenine dinucleotide ($FADH_2$) formation through the tricarboxylic acid (TCA) cycle, and fatty acid β-oxidation within the mitochondrial matrix, cooperatively provide the precursors and chemical environment for ATP synthesis.

However, within the last decade, other physiological roles for mitochondria have also gained much attention. Mitochondria has been shown to be an important organelle for maintaining intracellular calcium homeostasis. This regulation is critical in many signal transduction pathways where calcium is the second messenger (Duchen 2000, 2004). This, together with the discovery of a mitochondrial signaling pathway for the ubiquitous programmed cell death mechanism, apoptosis, expanded the current understanding of the major function of mitochondria as an energy source. Members of the BCL-2 family including BAX, BAK and BID, provide important and early triggers for mitochondrial membrane perturbations, resulting in the opening of a mitochondrial permeability transition pore (MPTP) and the subsequent release of cytochrome *c* for caspases activation. These biochemical changes systematically drive the execution of apoptotic as well as necrotic processes. The manifestation of this cell death pathway involves both physiological and pathological stimuli, a common but relatively new observation in many fields of cell biology.

Clearly, mitochondria influence both "life and death" events in most organisms: oxidative phosphorylation providing the sustenance for cellular activities, and apoptotic signaling regulating growth and termination. Undoubtedly, such highly polarized activities have to be kept in a fine balance to ensure optimal survival for the entire organism. Thus, dysfunction of this organelle can have detrimental outcomes. Mitochondrial disturbances have been implicated in a number of disease states including Parkinson's disease, Alzheimer's disease (AD), cardiomyopathies, diabetes, as well as a number of organ specific drug-induced toxicities.

1.1.1 Mitochondria: Maintenance of cellular bioenergetics

The first recognized of the mitochondria is as the powerhouse of the cell, harnessing energy in the form of ATP to drive metabolic activities. The entirety of bioenergetics is highly complex and involves a number of intertwining biochemical processes. The mitochondrial matrix contains the all-important tricarboxylic acid cycle (TCA or Krebs cycle). This process was first proposed by Krebs in 1937, and is now one of the

most well-studied metabolic pathways in the cell (Scheffler 1999). It comprises eight sequential catalytic steps. For ease of discussion, the cycle is conveniently described as commencing, with the entry of acetyl-Coenzyme A (CoA), generated by the reaction of the multi-enzyme complex, pyruvate dehydrogenase (Figure 1.2). Acetyl-CoA is the key substrate, wherein the acetyl group condenses with oxaloacetate to form citrate. Subsequent metabolic steps in the cycle involve dedicated enzymes including aconitase, isocitrate dehydrogenase, α-ketoglutarate dehydrogenase (αKGDH), succinyl-CoA synthase, succinate dehydrogenase, fumarase and malate dehydrogenase. Details of the catalytic reactions are further illustrated as shown in Figure 1.2. These enzymes operate by relaying a 4-6 carbon substrate through each enzyme complex, eventually converting one molecule of citrate to oxaloacetate through each completed cycle. The important products generated from the cycle include reduced pyridine nucleotides, namely NADH, $FADH_2$ as well as guanosine triphosphate (GTP). NADH and $FADH_2$ are both reducing equivalents needed to drive the electron transport chain on the mitochondrial inner membrane (to be discussed later). Of equal importance is the fact that cycle intermediates generated in the process are also essential precursors for a number of biochemical processes. For example, succinyl-CoA is necessary for the biosynthesis of heme, and α-ketoglutarate is drained off and transaminated to form glutamate, a non-essential amino acid (Scheffler 1999). Intuitively, the plurality of the enzymatic steps involved in the cycle suggests that the overall efficiency of the process can be regulated at several different stages. From a toxicological point of view, it also implies that there are multiple ways in which this physiological process can be disrupted. One obvious consequence of TCA cycle interference is a depletion of the reducing equivalents (e.g. NADH), necessary for the electron transport chain (ETC).

The ETC on the inner mitochondrial membrane culminates in reducing equivalents for ATP synthesis, through oxidative phosphorylation of adenosine diphosphate (ADP). It consists of four macromolecular protein complexes: NADH-coenzyme Q reductase (Complex I), succinate-coenzyme Q reductase (Complex II), coenzyme Q-cytochrome

c reductase (Complex III or bc_1-complex) and cytochrome *c* oxidase (Complex IV) (Figure 1.3). Electrons from NADH and $FADH_2$ are released and traverse along this chain on the protein complexes, successively reducing and oxidizing each complex as electrons move to their final acceptor, molecular oxygen. This electron relay converts chemical energy to pump protons kinetically across the inner mitochondrial membrane in order to build up a concentration gradient. Ultimately, protons will flow back into the mitochondrial matrix through ATP synthase (also known as Complex V) to catalyze the formation of ATP from ADP and pyrophosphate (Pi). This electron transport system is more commonly referred to as Mitchell's chemiosmotic theory.

Another significant source of reducing equivalents in the mitochondria for ATP synthesis is lipid catabolism. After hydrolysis of cholesterol esters and phospholipids in the cytosol, fatty acids translocate into the mitochondria and covalently bind to coenzyme A, forming acyl-CoAs. Here, the hydrocarbon chain in fatty acids undergoes two-carbon reduction through a β-oxidation process involving 4 enzymatic steps: elimination of hydrogen from the α and β carbons, hydration, oxidation and cleavage (Figure 1.4). This results in the formation of acetyl CoA (which subsequently enters the TCA cycle), as well as NADH and $FADH_2$. The fatty acid, which is now two carbons shorter, will undergo successive β-oxidations to yield more acetyl-CoA and reducing equivalents. Because of the multi-cyclic oxidation for each substrate, each molecule of fatty acid yields a significantly higher energy (3233 KJ/mol) than sugars (2937 KJ/mol) and is therefore, an important source of energy for cellular processes (Garrett and Grisham 1995).

The generation of ATP is vital for most cellular processes. For example, proper folding of new proteins requires the activity of molecular chaperones, like HSP70, which possess an ATPase domain. A lack of sufficient ATP may result in a pathological accumulation of unfolded translated proteins. In the ER, this phenomenon is referred to as the unfolded protein response (UPR). For this reason, perturbation of the mitochondrial TCA cycle and/or ETC can lead to a detrimental outcome in the

host cell or tissue. The wide plethora of mechanisms by which these disturbances occur, as well as their consequences, will be more comprehensively discussed in a later section.

1.1.2 Mitochondria: A storehouse for messengers of death

In the past decade, there has been a surge of biochemical research focusing on the critical roles of mitochondria in cell physiology, apart from ATP synthesis. Much of this work originated from studies describing the participation of mitochondria in cell death processes, encompassing both apoptosis and necrosis (Desagher and Martinou 2000; Green and Reed 1998; Halestrap *et al.* 2000; Orrenius 2004; Robertson and Orrenius 2002; Van Loo *et al.* 2002). The word "apoptosis", first coined in 1972, is an energy-dependent form of cell death that is manifested as a series of ordered biochemical changes that progress in a well-defined chronological fashion (Kerr *et al.* 1972). Taking a very simplistic overview of these pathways, apoptosis is a highly regulated cell death mechanism with the purpose of removing aged, unwanted or dysfunctional cells, without causing excessive disturbance to neighboring cells or tissues. This process transcends different stages of an organism's life cycle. For example, in primate embryonic tissue, apoptosis is essential for the proper formation of interdigital spaces. In healthy individuals, it supports the maintenance of immune responses, whereby unselected B and T-cells are continually removed to help maintain homeostasis (Gewies 2003). More applicable to this dissertation, apoptosis is a major mechanism for removal of damaged cells from tissue. Morphologically, apoptosis is manifested by cell shrinkage, chromatin condensation, internucleosomal DNA fragmentation, and the formation of buds on the plasma membrane, which eventually break off into tiny apoptotic bodies. For this purpose, apoptosis is also referred to as a programmed cell death (Kaufmann and Hengartner 2001). This is unlike necrosis, a rapid cell death process with uncontrolled cellular swelling and subsequent lysis, which often results in the release of cellular contents including proteases that leads to more extensive damage and inflammatory reaction (Figure 1.5).

It is well known that cell death can arise through the disruption of mitochondrial oxidative phosphorylation (Duchen 2004; Leist *et al.* 1997; Lieberthal *et al.* 1998). Interference of ATP synthesis in mitochondria can lead to global cellular energy depletion and inhibition of ATP-dependent biochemical processes. Additionally, decreased production of ATP to 10-25% of physiological concentrations can switch the mechanism of cell death from apoptosis to necrosis (Lieberthal *et al.* 1998). ATP depletion is also a key "trigger" that activates cell death pathways (Leist *et al.* 1997). Mitochondria can influence cell death in other ways by participating in the signaling events involved in apoptosis and necrosis. Release of mitochondrial proteins caused by specific signals can result in the execution of either/or both of these forms of cell death (Green and Reed 1998).

1.1.3 Mitochondria and apoptosis

A myriad of insults can trigger the activation of apoptosis in cells: DNA damage, UV irradiation, growth factor withdrawal and chemotherapeutic drugs are some examples. There are two major pathways for apoptosis that are currently established: a receptor-mediated pathway and a mitochondrial pathway (Hengartner 2000; Kaufmann and Hengartner 2001; Zimmermann *et al.* 2001) (Figure 1.6). The receptor-mediated pathway involves the binding of specific ligands to cell surface receptors generally termed "death receptors" (DR). This family of receptors includes Fas and tumor necrosis factor-α receptor (TNFR), which are expressed in various tissue types. Their respective ligands, FasL and TNFα, are inducible proteins that are part of a battery of responses to immune-mediated reactions and inflammation. The association of such ligands to their surface receptors stimulates the recruitment of receptor death domains (DD), thus forming an activated death-inducing signaling complex (DISC) (Zimmermann *et al.* 2001) that subsequently hydrolyzes and activates an apoptosis-specific cysteine protease, caspase-8 (Figure 1.6).

Caspase-8 belongs to a family of intracellular cysteine proteases that target specific peptides by cleaving off the C-terminal end of aspartate residues. Caspases can be

classified into two major classes: the initiator caspases, including caspase-2, -8 and –9, that hydrolyze other downstream procaspases into active forms. The downstream caspases, also known as "executioners" (caspase-3, -6 and-7), are ultimately responsible for the biochemical and morphological manifestations of apoptosis by cleaving more than 100 different protein substrates, many of which have known functions in propagating cell death (Fischer *et al.* 2003). In receptor-mediated apoptosis, caspase-8 turns on the apoptotic machinery by cleaving pro-caspase-3. The activation of caspase-3 is, in fact, one of the traditional hallmark indicators of apoptosis.

The second major pathway for apoptotic cell death is the mitochondrial-dependent pathway. This pathway has been well-studied in recent years, but the complexity of its regulatory mechanisms seems to increase as new information surfaces. To date, many aspects of the pathway are not well understood. It is common to trace the origin of the mitochondrial pathway from the participation of the BCL2 family of proteins. The BCL2 family of proteins can be classified as pro-apoptotic (e.g. BAX, BAK, BID, BAD) or anti-apoptotic (e.g. BCL2, BCL-xL). Both classes possess at least one BCL2 homology domain (BH1-BH4) (Desagher and Martinou 2000; Gross *et al.* 1999). In an unstimulated state, these proteins are predominantly localized to the cytosol or on the outer surface of the mitochondrial membrane. Upon receipt of a death signal, pro-apoptotic members like BAX undergo rapid translocation from the cytosol to the mitochondria, presumably through conformational changes that result in an insertion of the otherwise buried hydrophobic C-terminus α9 helix of the protein into the outer mitochondrial membrane (Degli Esposti and Dive 2003; Hsu *et al.* 1997; Putcha *et al.* 1999; Wolter *et al.* 1997; Zhang *et al.* 1998). This binding has been demonstrated in a number of studies to be a critical trigger for the subsequent release of important intramitochondrial proteins (e.g. cytochrome *c*) to the cytosol, as well as the opening of the permeability transition pore (Degli Esposti and Dive 2003; Finucane *et al.* 1999; Pastorino *et al.* 1999; Robertson and Orrenius 2000).

The release of cytochrome *c* from the intermembranal spaces results in the formation of an activated multimeric complex in the cytosol, which also includes Apaf1, ATP/dATP and procaspase-9. This activated complex (a.k.a apoptosome) cleaves the pro-domain of caspase-9, which in turn activates downstream caspase-3 to elicit their proteolytic activities (Jiang and Wang 2004; Robertson and Orrenius 2000; Zou *et al.* 1999). Within the past few years, other intramitochondrial proteins released through this process have been discovered. The flavoprotein, apoptosis inducing factor (AIF), and endonuclease G, translocate to the nucleus and are responsible for some of the nuclear changes, including chromatin condensation and DNA fragmentation (van Gurp *et al.* 2003; Van Loo *et al.* 2002). Smac/DIABLO and Omi/HtrA2 are released into the cytosol where they sequester inhibitors of apoptosis proteins (IAPs). IAPs antagonize the proteolytic action of caspases under basal conditions. Thus, when mitochondrial Smac/DIABLO and Omi/HtrA2 are released, they block the inhibitory action of IAPs on caspases (Hengartner 2000; van Gurp *et al.* 2003; Van Loo *et al.* 2002). Thus, this serves as an intrinsic mechanism to amplify/propagate the apoptotic machinery.

A pivotal part of the execution of the mitochondrial pathway of cell death is the opening of the mitochondrial permeability transition pore (MPTP). It is a multimeric protein complex that forms a channel wide enough to enable the release of molecules < 1500 Da from the mitochondrial matrix to the cytosolic spaces (Desagher and Martinou 2000; Kim *et al.* 2003). This channel spans across the inner and outer mitochondrial membrane and is comprised of a voltage dependent anionic channel (VDAC) on the outer membrane, the adenine nucleotide translocase (ANT) on the inner membrane, and cyclophilin D in the matrix. There are also specific binding pockets for interaction with BCL2 and hexokinase (Figure 1.7). After an external trigger, such as BAX translocation, increased cytosolic redistribution of intracellular calcium and other physiological changes, the channel opens, facilitating an influx of ions and a depolarization of the inner membrane (loss of $\Delta\Psi_m$). This increases the osmotic potential of the mitochondrial matrix, resulting in matrix swelling and the

release of intramitochondrial proteins (Desagher and Martinou 2000). This phenomenon is more commonly referred to as the mitochondrial permeability transition (MPT). A prolonged MPT can block ATP synthesis and is therefore implicated as an important event in necrotic cell death.

While BAX translocation, cytochrome c release and MPT are well-characterized and are crucial for activating the mitochondrial pathway of cell death, their inter-relationships are not clear. There are many hypotheses about how BAX translocation results in the release of cytochrome *c*. Some groups have reported that BAX undergoes oligomerization at the outer mitochondrial membrane to form channels in the lipid membrane that promote the release of cytochrome *c* (Antonsson *et al.* 2000; Antonsson *et al.* 2001; Mikhailov *et al.* 2003; Scorrano and Korsmeyer 2003). Others have invoked an initial binding of BAX to the MPTP resulting in its opening and the consequences of mitochondrial swelling and permeabilization, such as the release of cytochrome c and other small molecules through non-specific pores on the outer mitochondrial membrane (Desagher and Martinou 2000; Marzo *et al.* 1998). Another proposed mechanism involves the truncated form of a BCL2 protein, BID (tBID), that decreases the stability of the lipid membrane, thereby promoting the formation of lipid pores (Desagher and Martinou 2000; Scorrano and Korsmeyer 2003). More recent evidence suggests that cytochrome *c* interacts with membrane phospholipids and can be released through oxidation of cardiolipin by reactive oxygen/nitrogen species (ROS/RNS) or binding with tBID (Kagan *et al.* 2004; Orrenius 2004).

Another dimension of complexity emerges from the cross-regulatory actions of the pro- and anti-apoptotic members of BCL2. It is known that anti-apoptotic BCL-xL and BCL2 can mitigate the effects of BAX on mitochondria through both direct and indirect mechanisms. Overexpression of BCL2 and BCL-xL have been shown to prevent BAX translocation (Murphy *et al.* 2000; Robertson *et al.* 1997) possibly by heterodimerization of BAX with BCL2/BCLxL (Antonawich *et al.* 1998; Mikhailov *et al.* 2001; Oltvai *et al.* 1993), or by modulation of protein phosphorylation of BCL2

and subsequent signaling events (Ganju and Eastman 2002). Finally, regulation of apoptosis by BCL2 can occur downstream of cytochrome *c* release. For example, BCL-xL has been shown to form a ternary inhibitory complex with Apaf-1 and caspase-9 that prevents the activation of effector caspases (Pan *et al.* 1998).

While mitochondrial and the death receptor mediated pathways are in some ways distinct, significant cross-talk occurs between the two pathways in the execution of apoptosis. The activation of caspase-8 through the death receptor pathway has been shown to stimulate mitochondrial changes through the proteolytic cleavage of BID. Truncated BID (tBID) subsequently translocates to the outer mitochondrial membrane to mediate cytochrome *c* release in a manner similar to BAX. This process can also be inhibited by BCL2 (Jiang and Wang 2004; Luo *et al.* 1998; Zimmermann *et al.* 2001). Additionally, it has been shown that t-BID can bind BAX to trigger the latter's oligomerization (Eskes *et al.* 2000). Hence, mitochondrial pathways may serve in parallel to perpetuate and amplify apoptotic signals originating from the receptor-mediated pathway (Jiang and Wang 2004).

Although this section has focused more on apoptosis, it should be noted that necrosis can also result from similar mitochondrial perturbations and often have common initiating events (Kim *et al.* 2003; Raffray and Cohen 1997). For example, cytochrome *c* release from the mitochondria does not necessarily lead to apoptosis. HepG2 cells treated with the pro-oxidant menadione underwent cytochrome *c* release and necrosis (Samali *et al.* 1999). Moreover, early BAX translocation in acetaminophen-treated mice, did not lead to the activation of downstream caspases (El-Hassan *et al.* 2003). Features of both apoptosis and necrosis have also been observed in other experimental models where apoptosis is initiated but not executed, and necrosis ensues (Pierce *et al.* 2002; Raffray and Cohen 1997). Lemasters and coworkers has done extensive work in characterizing MPT as a critical bifurcation point between necrosis and apoptosis. A widespread or prolonged MPT will dramatically decrease membrane potential such that ATP synthesis is suppressed. Under such circumstances, necrosis will prevail. On

the other hand, a transient MPT will maintain ATP synthesis to drive apoptosis to completion (Kim *et al.* 2003). Thus, mitochondrial dysfunction is strongly implicated in cell death caused by both apoptotic and necrotic mechanisms.

1.1.4 Mitochondrial dysfunction in diseases and chemical toxicities

As it has been clearly illustrated in the earlier sections that mitochondria play crucial roles in both "life" (ATP synthesis) and "death" (apoptosis and necrosis) events, one can presume that disruption of these activities would have serious and detrimental consequences to the well-being of the host cell/tissue. A representative list of several of these mitochondrial dysfunctions is shown in Table 1.1 and are discussed below.

The TCA cycle is the primary reaction pathway for the generation of NADH/$FADH_2$ in the mitochondria, and is easily disrupted because inhibition at any point in the cycle can halt the overall process. For example, small doses of arsenite ($NaAsO_2$) are sufficient to trap sulfydryl groups of the lipoyl moieties in pyruvate and αKGDH complexes (Chacin *et al.* 1979). Fluoroacetate (a.k.a. Compound 1080), a compound derived from certain South African plants was used as a rodenticide during World War II and has been shown to be a specific inhibitor of aconitase. It is metabolized to fluorocitrate and is irreversibly bound to aconitase as a pseudo-substrate. When accumulated in humans through accidental exposure, it can cause cardiac arrhythmias and fibrillation (Boelsterli 2003). In later chapters, we will also demonstrate how TFEC is a selective inhibitor of aconitase and αKGDH, and how this inhibition is important in the initiation of mitochondrial dysfunction.

Also in the mitochondrial matrix, metabolism of fatty acids can be disrupted by a number of NSAIDs (non-steroidal anti-inflammatory drugs) and pentenoate (Krahenbuhl 2001). For example, valproic acid is desaturated by P450, conjugated with CoA and forms an intermediate that can directly inhibit enzymes in the β-oxidation pathway. Damage may ensue with further depletion of CoA (Boelsterli 2003; Fromenty and Pessayre 1995; Krahenbuhl 2001). The *R* enantiomers of

ibuprofen and flurbiprofen are also known to form thioester linkages with CoA, inhibiting β-oxidation and causing microvesicular steatosis (Browne *et al.* 1999).

The mitochondrial membranes are another important site for eliciting targeted mitochondrial dysfunction. Two components are key: the ETC and the MPTP. The cardiolipin-rich mitochondrial inner membrane attracts a number of hydrophobic xenobiotics where binding and inhibition of the various complexes of the ETC (Complex I-V) can occur. The pesticide rotenone is a classical inhibitor of Complex I. It blocks the flow of electrons down the ETC and thereby increases the release of ROS leading to apoptosis (Darrouzet *et al.* 1998; Li *et al.* 2003). The toxin cyanide binds to ferric heme iron in Complex IV and blocks its redox cycling capacity. This directly inhibits ATP synthesis in Complex V. Another drug, doxorubicin, used as a chemotherapeutic agent, has high affinity for cardiolipin (Goormaghtigh *et al.* 1983). It accumulates at the inner mitochondrial membrane and undergoes rapid redox cycling at Complex I (between the semiquinone radical and quinone) that reduces molecular to superoxide anion (Boelsterli 2003).

These actions not only serve to reduce ATP production and arrest other ATP-dependent metabolic activities, but more importantly, they provide an alternative route where excessive buildup of electrons along the ETC is dissipated as ROS through a direct interaction with localized molecular oxygen. Although most nucleated cells are equipped with the necessary antioxidants (glutathione, thioredoxin, vitamins A, C and E) and other detoxification enzymes (catalase, superoxide dismutases and glutathione peroxidases), these protective mechanisms can be overwhelmed with heightened ROS production (Halliwell and Gutteridge 1999). The detrimental consequences of ROS arise because of the inherent reactivity of ROS towards various endogenous molecules that can culminate in cellular dysfunction through lipid peroxidation, oxidation of protein thiols with subsequent disruption of protein folding and function, and DNA damage as shown in Figure 1.8 (Cotran *et al.* 1999). Mitochondrial DNA (mtDNA) is susceptible to ROS-mediated damage, not only because of its proximity to the site of

ROS production, but also because of the lack of protein histones that can protect DNA from ROS damage. Hence, deletions in mtDNA and its depletion can aggravate the reduction in ATP synthesis because several subunits of the mitochondrial complexes are mitochondrially-encoded (e.g. cytochrome *c* oxidase subunits). Finally, ROS is an important trigger that facilitates opening of the MPTP and exacerbates downstream processes of membrane depolarization, mitochondrial swelling and apoptosis/necrosis as described earlier.

Apart from these major routes of mitochondrial dysfunction, other significant pathways include inhibition of phosphorylation (e.g., by oligomycin), which directly inhibits ATP synthase, and uncoupling in the ETC (e.g., by pentachlorophenol) which shuttles protons back into the mitochondrial matrix, bypassing ATP synthase. Ionophores like valinomycin and nigericin permeabilize the mitochondrial inner membrane such that it becomes leaky to various ions necessary for maintenance of mitochondrial energetics. Some transport inhibitors block the export of ATP or import of precursors for ATP generation (e.g., N-ethylmaleimide, atractyloside and bongkrekic acid). Some of these agents, like bongkrekic acid, can inhibit the MPTP thus blocking apoptosis. It also has been reported that pathogenesis of salicylate-induced Reye's syndrome involves modulation of the MPTP (Trost and Lemasters 1997).

In addition to chemically-induced mitochondrial dysfunction, similar dysfunction occurs in several disease states. Neurological disorders like Parkinsonism and Alzheimer's are intricately linked to early mitochondrial changes, resulting in a protracted degeneration of normal cellular function. Parkinsonism is a result of progressive loss of dopaminergic neurons in the substantia nigra of the brain. A mitochondrial involvement in its pathophysiology was first observed when 1-methyl-4-phenyl-1,2,3,6-tetrahydropyridine (MTPT) was found to cause Parkinson-like behavior in drug users (Gerlach *et al.* 1991; Scheffler 1999). MTPT was later found to be metabolized by monoamine oxidases (MAO) to 1-methyl-4-phenylpyridinium

(MPP^+), which readily inhibits Complex I in these neurons (Chiba *et al.* 1985; Gerlach *et al.* 1991; Krueger *et al.* 1990; Nicklas *et al.* 1985). Similarly, the pesticide, rotenone, blocks Complex I, and has been used on occasion as a chemical model for Parkinsonism (Darrouzet *et al.* 1998; Jenner 2001; Tada-Oikawa *et al.* 2003). Rotenone has been shown to increase the release of ROS and effect MPT and caspase-driven apoptosis following Complex I inhibition (Isenberg and Klaunig 2000; Li *et al.* 2003; Pei *et al.* 2003; Tada-Oikawa *et al.* 2003). Some evidence suggests that ATP depletion might not be as critical as the release of ROS in the pathogenesis of Parkinsonism (Jenner 2001; Sherer *et al.* 2002). BAX upregulation and BCL2 inhibition was observed in MPP^+-administered mice, with subsequent activation of the mitochondrial apoptosis pathway (Vila *et al.* 2001).

Mitochondrial dysfunction also has been implicated in the etiology of Alzheimer's disease which is pathologically linked to a premature death of cholinergic neurons in the brain. Though the exact mechanism for AD onset is highly complex, one well-characterized triggering factor is the formation of amyloid plaques through accumulation of the amyloid β peptide (AβP) (Scheffler 1999). AβP has been proposed to inhibit the activity of mitochondrial ETC complexes and Krebs cycle enzymes, and induce the MPT (Abramov *et al.* 2004). These plaques can also increase formation of ROS, which increases the rate of mtDNA mutation (Abramov *et al.* 2004; Aliev *et al.* 2003; Aliev *et al.* 2002). Others have reported elevated mtDNA mutation and an associated deficiency in mitochondrially-encoded cytochrome *c* oxidase activity in AD patients (Aliev *et al.* 2002; Castellani *et al.* 2002; Cottrell *et al.* 2002). The significance of each of these mitochondrial disturbances to the clinical outcome of AD is yet to be determined.

Contrary to inhibition of mitochondrial function, excessive stimulation of specific mitochondrial activities can have adverse effects on the integrity of the mitochondria and the whole cell, as well. Altered cell signaling within the mitochondria has been shown to prolong the lifespan of cells, propagating neoplastic behavior. For example,

the anti-apoptotic protein BCL2 was first discovered to be overexpressed in follicular B-cell lymphoma (Andersen *et al.* 2005; Gross *et al.* 1999; Oltvai *et al.* 1993). Its cytoprotective activity represses programmed cell death, hence becoming pro-oncogenic. In the past decade, anti-sense oligonucleotides of BCL2 and BCL-xL, as well as small molecule antagonists, have been investigated as potential chemotherapeutic agents to treat many types of cancer (including chronic lymphocytic leukemia, multiple myeloma and non-small-cell lung carcinoma (Andersen *et al.* 2005). Studies are in progress to induce the expression of BAX, a BCL2 member whose expression is silenced in some cancer types, through DNA manipulation (Roth and Reed 2002).

1.2 Tetrafluoroethylcysteine (TFEC)

Tetrafluoroethylene (TFE, Figure 1.9) is an industrial gas used as a precursor for synthesizing the polymer, TEFLON™. Due to the popularity of this product as an "anti-stick" coating agent, TFE is ranked among the most widely used industrial chemicals. While the polymerized form of the gas is extremely inert and hence, perceived to be relatively safe, TFE itself is mildly hazardous. A study conducted by the National Toxicology Program revealed that long-term exposure (2 years) resulted in significant increased incidences of renal tubule and hepatocellular neoplasms in both mice and rats (NTP 1997). Another potential concern about the safety issues of handling and exposure to TFE came from studies which demonstrated TFE-induced kidney tubular damage, and its likely link to the metabolism of TFE to its GSH conjugates (Odum and Green 1984). A number of follow-up studies identified the toxic species as a reactive intermediate derived from tetrafluoroethylcysteine (TFEC, Figure 1.9), the penultimate metabolite of a TFE-GSH conjugate (Commandeur *et al.* 1989). TFEC metabolism and the current understanding of the mechanism of its toxicity will be highlighted in this section.

1.2.1 Metabolism of TFEC

The major metabolite of TFE is tetrafluoroethylcysteine (TFEC), generated through multi-step sequential metabolism of the GSH conjugate of TFE. Presumably, this involves an initial glutathione S-transferase (GST) mediated reaction. GSTs are Phase II xenobiotics metabolizing enzymes found in almost all cells in cytosol, microsomes and mitochondria. P450-mediated oxidation, though a common metabolic route for other related haloalkenes (e.g., perchloroethylene), has not been shown to play a major role in TFE metabolism. The first complete metabolism study *in vitro* that demonstrated the processing of TFE to a single addition product, S-(1,1,2,2-tetrafluoroethyl)glutathione was performed in 1984 (Odum and Green 1984). Using an *in vivo* rat model, they also identified cysteinylglycine and cysteine conjugates in rat bile, indicating that subsequent processing of the glutathione conjugate occurred rapidly. This enzymatic processing likely is catalyzed by the enzymes γ-glutamyltransferase (GGT) and aminopeptidase M (a.k.a cysteinylglycine dipeptidase or DP), respectively (Figure 1.10). The relevance of this metabolic pathway to toxicity was confirmed through studies showing that the cysteine conjugates are responsible for most, if not all, of the toxicity seen with TFE (Anders and Dekant 1998).

1.2.2 Toxicity of TFEC

Glutathione conjugation has been known for years to be an important route for detoxification of xenobiotics. Electrophilic intermediates formed by bioactivation are often detoxified by high levels of intracellular GSH (about 2 mM). Additionally, GSH itself participates in the maintenance of cellular redox potential by reducing ROS with concomitant oxidation to the disulfide GSSG. Surprisingly, GSH or cysteine conjugates generated from a number of haloalkenes, are found to be highly toxic. Dichlorovinylcysteine (DCVC), the major cysteine conjugate of trichloroethylene, was shown to be responsible for aplastic anemia caused by trichloroethylene (Anders and Dekant 1998; Dekant 2001). A number of other cysteine conjugates, including pentachlorobutadienylcysteine and chlorotrifluoroethylcysteine were found to cause

severe nephrotoxicity after administration to mice and rats (Anders 2004). TFEC is another classical example of this unusual bioactivation reaction.

A link between TFEC and the nephrotoxic effects of TFE in rats was suggested by large increases in plasma urea and urine output after administration of either compound (Odum and Green 1984). TFEC-mediated nephrotoxicity and mild hepatotoxicity were observed by others as well (Lock and Ishmael 1998). The first cross-species comparison of TFEC toxicity between mice and rats was carried out, and nephrotoxicity occurred in both species, whereas hepatotoxicity in mice was limited to elevated cell proliferation (Keller *et al.* 2000). Several other studies corroborated these results by demonstrating subcellular and biochemical perturbations in cells after TFEC treatment. Increase in free cytosolic calcium after exposure of rat renal proximal tubules to TFEC was observed in addition to lipid peroxidation that was determined to be inconsequential to the outcome of TFEC toxicity (Groves *et al.* 1990, 1991). In contrast, calcium-dependent calpain activation was found to play a significant role in TFEC-mediated renal cell death (Waters *et al.* 1997).

The formation of the ultimate toxic metabolite of TFEC, as well as the other haloalkene cysteine conjugates is catalyzed by β-lyases (EC 4.4.1.13). These enzymes catalyze the cleavage of the C-S bond in cysteine S-conjugates to an unstable thiolate intermediate plus aminoacrylate, which quickly decomposes into pyruvate and ammonia (Cooper *et al.* 2002b; Park *et al.* 1999). TFEC releases a thiolate intermediate that undergoes favorable rearrangement into difluorothionoacetylfluoride (DFTAF). This species readily binds to lysine residues of renal proteins through a condensation reaction resulting in the formation of the thioacetamide adduct, difluorothionoacetylysine (DFTAL) (Hayden *et al.* 1991b) (Figure 1.11).

The importance of DFTAL adducts to the toxicity of TFEC has been demonstrated consistently over the years. The use of the β-lyase selective inhibitor, aminooxyacetic acid (AOAA) reversed the toxicity and/or associated functional loss in mitochondria

(Hayden and Stevens 1990). AOAA also blocked covalent binding of the reactive metabolite to renal proteins and blocked cell death after TFEC (Groves *et al.* 1993). However, only partial recovery with similar treatment in rats and human renal tubular cells was observed (Lock and Ishmael 1998; McGoldrick *et al.* 2003). Taken together, the findings support protein-adduct formation as a critical determinant in cell death after TFEC treatment, although the extent of its involvement may vary from system to system.

1.2.3 TFEC adducts specific mitochondrial proteins

Protein modification can impact cellular survival in a number of ways: The most direct effect is the defunctionalization of the adducted protein. Subsequently, this change may trigger signaling pathways, resulting in activation of the apoptotic cascade. The modified protein also might be recognized by cellular defense mechanisms to mount an inflammatory and/or immune response in attempts to remove damaged proteins or cells from the tissue/organ. For these reasons, protein modification (as well as oxidative stress) is often a primary consideration by molecular toxicologists when studying the mechanism of toxicity of a new compound.

The foundation for the role of covalent binding in toxicity can be traced back to the work of James and Elizabeth Miller who demonstrated that covalent modification of DNA and proteins by metabolites of carcinogenic dyes resulted in carcinogenesis (Miller and Miller 1981). Subsequently, metabolites of acetaminophen and bromobenzene were found to covalently bind to hepatic proteins, and binding was highest in necrotic areas of the liver (Brodie 1971, Jollow 1973). This binding phenomenon was later incorporated into a "Critical Target Hypothesis" where modification of selective proteins might have more significant detrimental impact to the cells than others. A comparison that supports this hypothesis comes from investigations of acetaminophen (APAP) and its regioisomer, 3-hydroxyacetanilide (AMAP). Both compounds are bioactivated by cytochrome P450 into quinoneimines and quinones, but only APAP is hepatotoxic. Two-dimensional gel electrophoresis of

liver proteins from mice treated with either APAP or AMAP showed that AMAP reactive metabolite adduct mainly cytosolic proteins, whereas APAP modified proteins in the mitochondria as well as the cytosol (Qiu *et al.* 1998, 2001). Consequently, significantly higher calcium dysregulation and protein thiol arylation and oxidation occur after APAP treatment as compared with what occurs after AMAP treatment (Tirmenstein and Nelson 1989, 1990). Hence, these mitochondrial targets could be pivotal to the manifestation of toxicity, likely triggering mitochondrial dysfunction as an early event as described in the previous sections.

Protein adducts to TFEC metabolite(s) were demonstrated to form in a β-lyase dependent reaction in kidney mitochondria of rats administered with ^{35}S-radiolabelled TFEC (Hayden and Stevens 1990). Subsequently, an antibody generated against halothane protein adducts (Satoh *et al.* 1985) which has high structural resemblance to DFTAL adducts was found to cross-react with DFTAL-bound renal proteins and binding could be localized to the mitochondrial fraction (Hayden *et al.* 1991a). The same antibody was used to narrow the localization of the adducts to the inner and outer membrane compartment of the mitochondria and six major adducts were isolated. Through the use of automated Edman sequencing of the major bands in these fractions resolved by SDS-PAGE, three adducts were identified as HSP60, mitochondrial HSP70 (a.k.a. mortalin, mtHSP70) and aspartate aminotransferase (AST) (Bruschi *et al.* 1993). Further efforts led to the identification of E2 and E3 subunits of αKGDH, and aconitase (Table 1.2) (Bruschi *et al.* 1998; James *et al.* 2002).

In order to establish that adduction of these proteins is critical to TFEC-mediated toxicity, the functional consequences of the adduction must be determined. An *in vivo* model was used to show that αKGDH activity was inhibited in kidneys of rats after a nephrotoxic dose of TFEC, and this inhibition correlated with various indices of renal failure such as blood urea nitrogen (BUN) and urinary glucose output (Bruschi *et al.* 1998). Presumably, this effect is due to the role of αKGDH as the rate-limiting step in

the TCA cycle (Huang *et al.* 2003a). Inhibition of αKGDH would deplete mitochondria of NADH necessary for oxidative phosphorylation. Separately, the inhibition of αKGDH in PC12 cells after TFEC treatment was reported (Park *et al.* 1999). Additionally, the inhibition of aconitase by TFEC treatment was observed. The extent of inhibition of aconitase was greater than that of αKGDH, not only in rat kidneys, but also in a transgenic mouse hepatocyte cell line, TAMH, as shown in Figure 1.13 (James *et al.* 2002; Wu *et al.* 1994).

The significance of DFTAL adducted HSP60 and mtHSP70 in TFEC-mediated toxicity has also been studied extensively. Both of these proteins are important stress proteins that respond to mitochondrial damage. They have the ability to associate with the hydrophobic, exposed region of newly synthesized or misfolded polypeptides to mediate the proper refolding process to generate functionally active proteins. HSP60 was shown to interact with DFTAL modified αKGDH after TFEC treatment using reciprocal immunoprecipitation techniques (Bruschi *et al.* 1998). Subsequently, mtHSP70 was found to co-purify with protein disulfide isomerase and a high molecular weight cysteine-S conjugate β-lyase, most likely to be AST (the minor DFTAL protein adduct) in TFEC-treated rat kidneys (Cooper *et al.* 2001). Taken together, these findings support the working hypothesis that specific mitochondrial stress proteins are recruited in an attempt to "rescue" DFTAL modified proteins (Table 1.2).

Up to this point, it has been found that DFTAL adducts are all located in the mitochondria. This observation is unexpected given the fact that β-lyase activity is ubiquitously expressed in different compartments (cytosol and mitochondria) of most cell types. Nine mammalian cysteine S-conjugate β-lyases are currently known, including cytosolic kynureninase, glutamine transaminase and mitochondrial branched-chain aminotransferase among others (Cooper *et al.* 2002a). Mitochondrial AST has been determined to be another enzyme with cysteine S-conjugate β-lyase activity, and 15-20% of the β-lyase activity toward TFEC was found to be catalyzed

by AST (Cooper *et al.* 2002b). Furthermore, processing of TFEC by AST lead to thioacylation and inactivation of the enzyme (Cooper *et al.* 2002b; Park *et al.* 1999). Overall, the cumulative evidence has led to a proposed scheme of events wherein TFEC is taken into mitochondria and bioactivated specifically by AST. The reaction inactivates AST and also releases electrophilic DFTAF which binds to other proximal key TCA enzymes. It is possible that there is a direct substrate channeling effect from AST to αKGDH and/or aconitase since mitochondrial AST is localized on the inner mitochondrial membrane as part of the malate-aspartate shuttle that connects to the TCA cycle. Subsequently, HSP60 and mtHSP70 are recruited in a futile attempt to salvage damaged mitochondrial proteins (Figure 1.12) (James *et al.* 2002). The possibility remains to be tested that DFTAF migration occurs from the initial aconitase, αKGDH and AST adducts to HSP60 and mtHSP70.

1.2.4 TFEC as a model for mitochondrial dysfunction

From the prior section, it appears that TFEC selectively adducts mitochondrial proteins. This adduction is important to the subsequent toxicity since aminooxyacetic acid restores cell viability after treatment with toxicologically relevant concentrations of TFEC (Groves *et al.* 1993). Because initial reactions of TFEC occur selectively in the mitochondria and can be precisely defined, TFEC is a potentially important model compound to investigate the mechanistic details of mitochondrial dysfunction caused by chemicals. Therefore, we conducted a number of experiments with TFEC to address mechanisms of cytotoxicity caused by this mitochondrial toxin.

Primarily, these studies were conducted *in vitro* with a well-characterized TAMH cell line. This cell line was derived from a long-term culture of the hepatocytes of transgenic mice overexpressing transforming growth factor-α (Wu *et al.* 1994). It is highly appropriate for toxicological studies for a number of reasons. Firstly, it maintains a number of P450 phenotypes including 2E1 and 3A4 (Bruschi *et al.*, unpublished data) which drives the bioactivation reaction of a number of toxicants. For example, it reproduces the *in vivo* toxicity of acetaminophen (Pierce *et al.* 2002),

unlike other commercially available hepatocyte cell lines. Secondly, TAMH cells can be cultured under serum-free conditions, which helps evade complications of non-specific protein binding in toxicokinetics studies. More importantly, the cell line can undergo successive passaging with minimal change to its cell type specific differentiation. This creates a consistent model to aid comparative studies with drug effects performed at different times.

A time-dependent increase in fluoride concentration confirmed the bioactivation of TFEC in TAMH cells (Chapter 2, Figure 2.1). A necrotic pattern of cell death was observed by light microscopy after treatment of TAMH cells with concentrations of TFEC that cause necrosis in kidney cells in rats treated with TFEC (Figure 1.13). It was also demonstrated that the same pattern of protein adduction occurs in TAMH cells as in rat kidneys, based on studies with anti-TFA polyclonal antibodies. Immunoreactive bands that match the molecular weights of aconitase, the E2 and E3 subunits of αKGDH, AST, HSP60 and mtHSP70 were all detected in TFEC treated lysates of TAMH cells (James *et al.* 2002). Moreover, these DFTAL adducts were almost completely absent in cells that were pretreated with AOAA (Figure 1.14, Bruschi *et al.*, unpublished data). Similar AOAA treatment also blocked cytotoxicity (complete recovery observed after 125 μM TFEC treatment for 24 h) as determined by MTT viability (Chapter 2, Figure 2.2). Overall, there is convincing evidence to support that the β-lyase mediated protein binding and toxicity is a major pathway in TAMH cells, treated with TFEC in parallel with what occurs *in vivo* in rats and mice.

In the subsequent chapters, we examine in greater depth, the biochemical consequences of TFEC adduction within the mitochondria, as well as the propagation of the injury to other organelles and cellular response to the injury. Chapter 2 focuses on the early mitochondrial perturbations, with particular emphasis on the pathway and possible signaling events leading to apoptosis and necrosis after TFEC treatment. The use of DNA microarrays as a tool to examine global gene expression helped us generate and test hypotheses regarding the involvement of an extramitochondrial heat

shock response (Chapter 3) and an Nrf2-mediated antioxidant response (Chapter 4). Finally, Chapter 5 proposes the existence of a TFEC adduct critical for initiating cell death and explores other possible mechanisms for toxicity as a result of most recent findings.

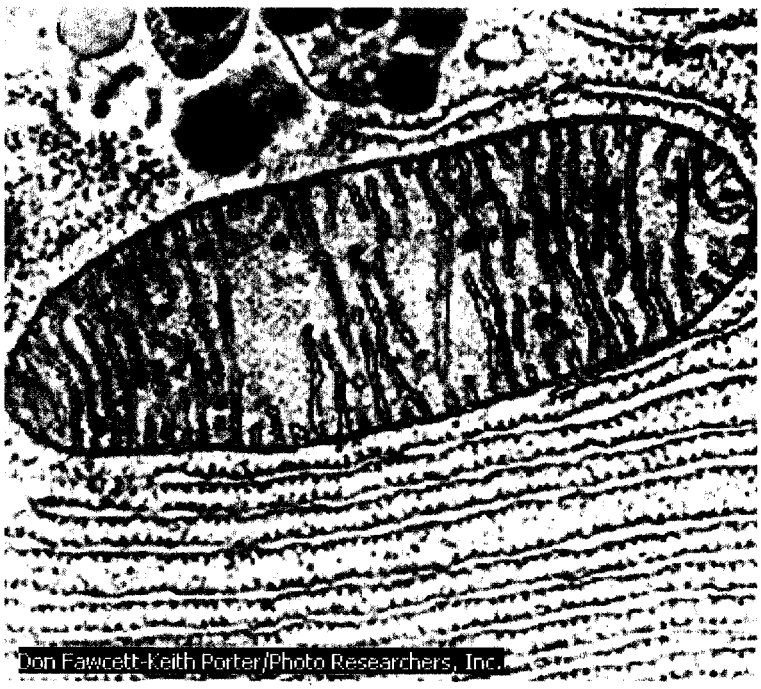

Figure 1.1 **Mitochondrial structure.** Two mitochondrial membranes create four distinct regions called the mitochondrial outer membrane, intermembranal spaces, mitochondrial inner membrane and the mitochondrial matrix. Figure taken from Fawcett, A Textbook of Histology, 12th Edition, 1994.

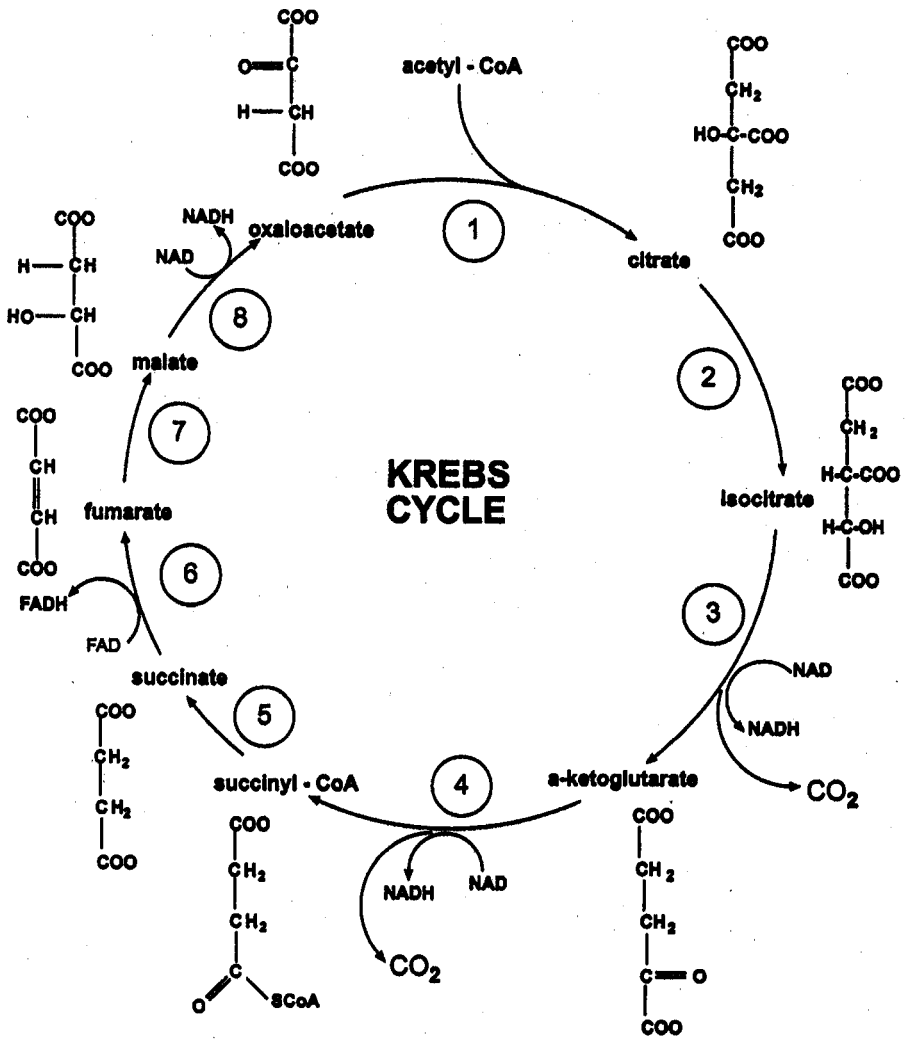

Figure 1.2 **Krebs cycle.** Acetyl CoA, derived from β-oxidation of fatty acids or glycolysis through pyruvate dehydrogenase, enters the cycle at (1) citrate synthase. Sequential metabolism of citrate to oxaloacetate involves multiple enzymes connected in series: (2) aconitase, (3) isocitrate dehydrogenase, (4) α-ketoglutarate dehydrogenase, (5) succinyl-CoA synthetase, (6) succinate dehydrogenase, (7) fumarase, and (8) malate dehydrogenase. Figure taken from Sheffler, Mitochondria, 1999.

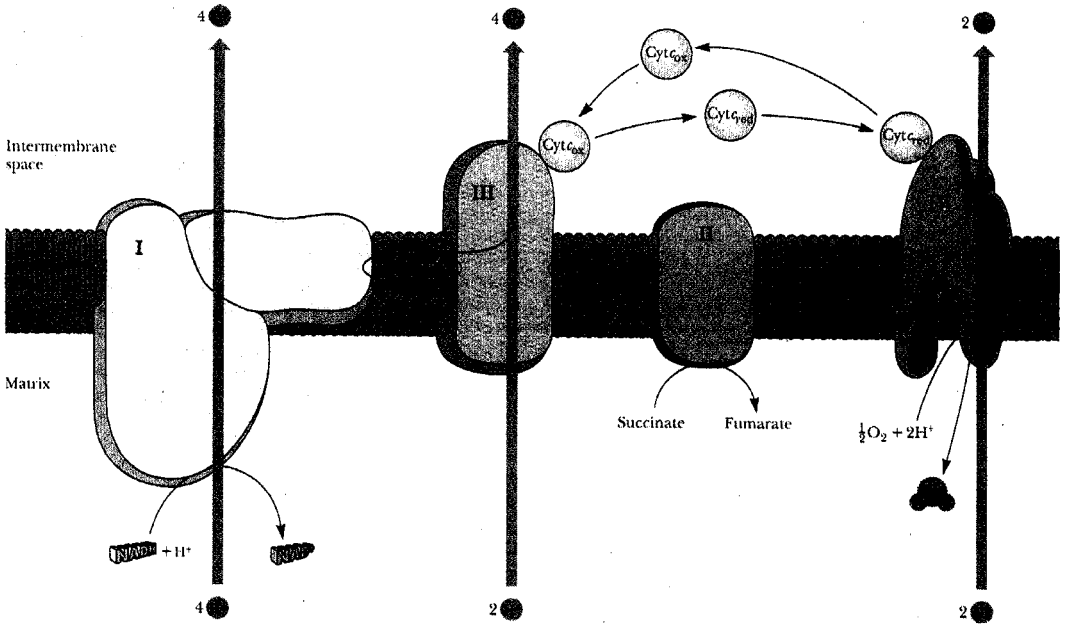

Figure 1.3 **The electron transport chain (ETC).** The ETC reoxidizes reduced NADH and $FADH_2$ while releasing free energy in the form of electrons and protons. It is organized into 4 major protein complexes: Complex I (NADH-Coenzyme Q reductase) transfers two electrons from NADH to Coenzyme Q (ubiquinol) via a flavin mononucleotide (FMN) intermediate. Complex II (succinate-Coenzyme Q reductase or succinate dehydrogenase) reduces FAD to $FADH_2$ and transfers the electrons directly to ubiquinol (reduced Coenzyme Q). Complex III (Coenzyme Q-cytochrome *c* reductase) passes electrons from ubiquinol to cytochrome *c*. Complex IV (cytochrome *c* oxidase) accepts electrons from cytochrome *c* and mediates a 4-electron reduction of molecular oxygen to water. These processes are accompanied with the generation of protons from Complex I, II and IV, which are pumped across the mitochondrial inner membrane to establish an electrochemical gradient that drives ATP synthase (Complex V). Figure taken from Garrett and Grisham, Biochemistry, 1995.

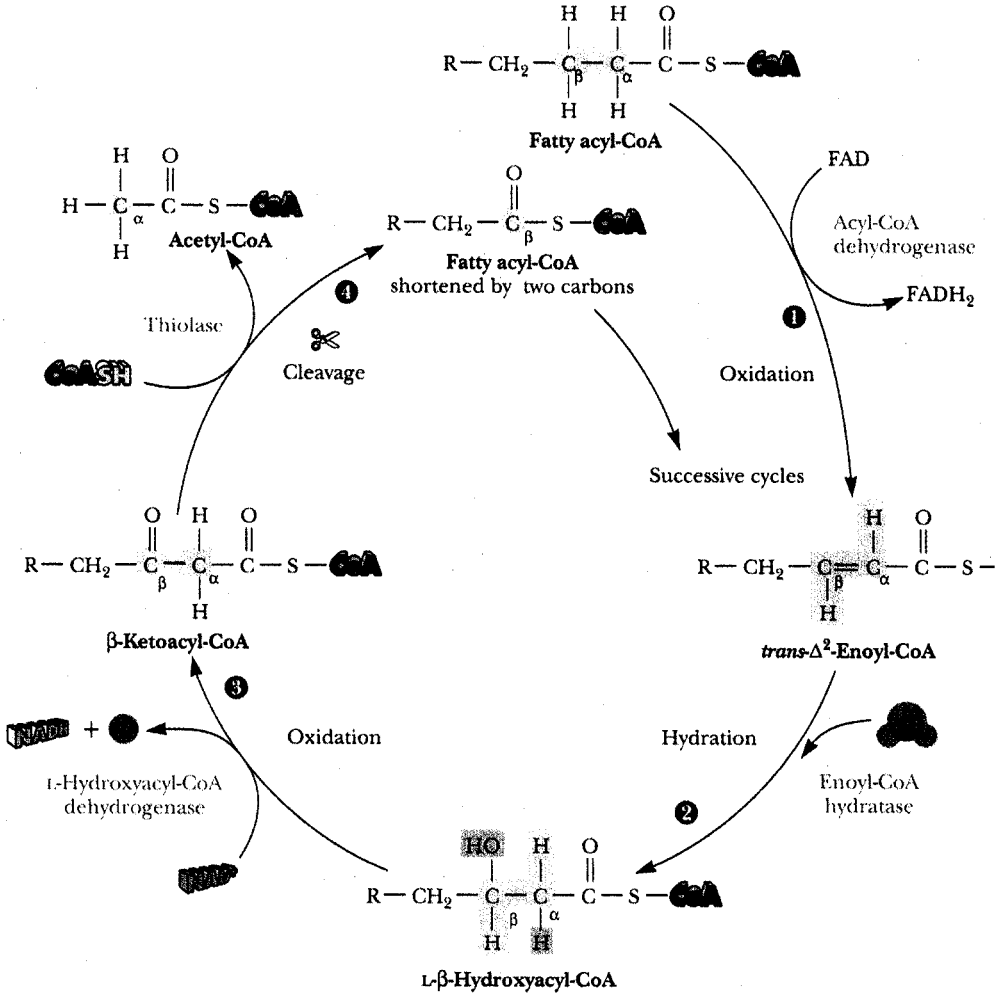

Figure 1.4. **Fatty acid catabolism.** The β-oxidation of saturated fatty acids involves a cycle of four enzymatic reactions with each cycle producing single molecules of $FADH_2$, NADH, acetyl-CoA and a resultant fatty acid shortened by 2-carbon length. Figure taken from Garrett and Grisham, Biochemistry, 1995.

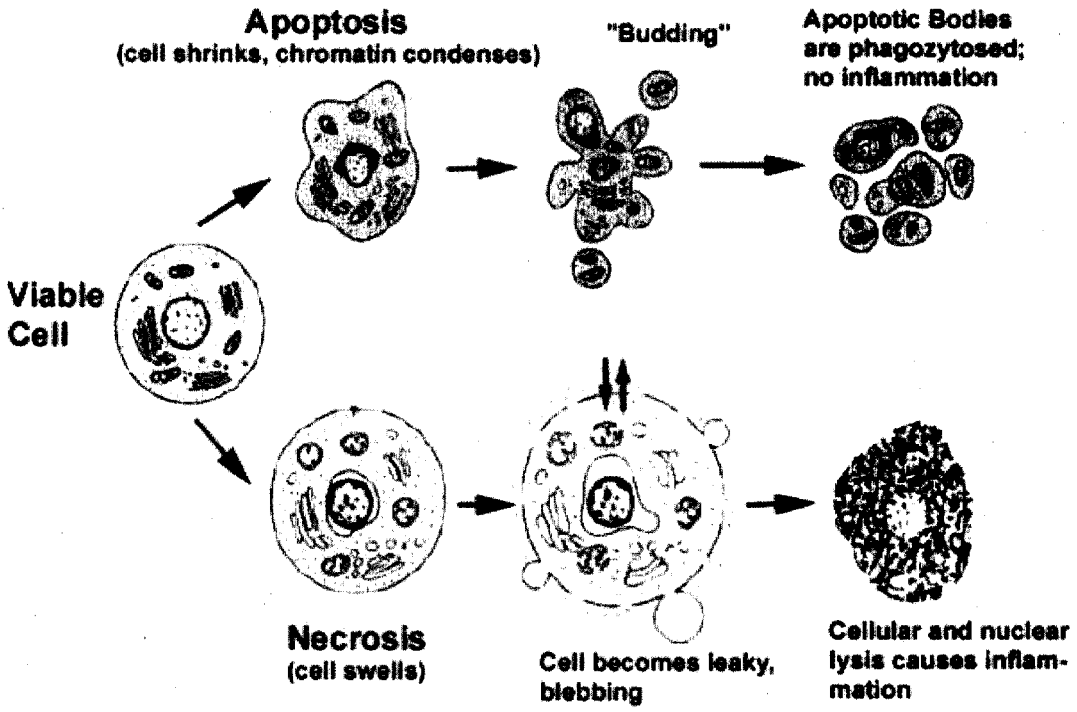

Figure 1.5 **Hallmarks of the apoptotic and necrotic cell death processes.** Apoptosis includes cellular shrinking, chromatin condensation and margination at the nuclear periphery with the eventual formation of membrane-bound apoptotic bodies that contain organelles, cytosol and nuclear fragments and are phagocytosed without triggering inflammatory processes. The necrotic cell swells, becomes leaky and finally is disrupted and releases its contents into the surrounding tissue resulting in inflammation. Figure taken from Gewies, 2003.

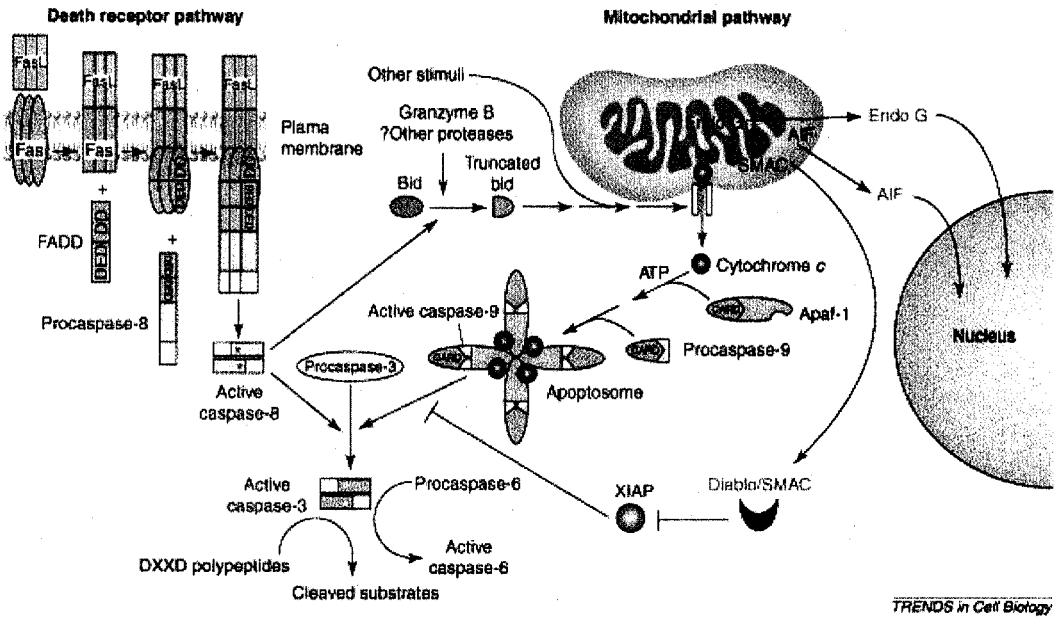

Figure 1.6. **Pathways in apoptosis.** Two major pathways exist in apoptosis: Death receptor pathway (extrinsic pathway) as well as the mitochondrial pathway (intrinsic pathway). Major events in the death receptor pathway involve ligand binding to the cell surface receptor, which results in sequential binding of death domains and procaspase-8. Caspase-8 in turn activates caspase-3 mediated proteolysis, and BID, which relays a secondary apoptotic signal to the mitochondria. The mitochondrial pathway involves the release of cytochrome *c* and the formation of the apoptosome complex in the cytosol which activates procaspase-9. This complex subsequently converges with the death receptor pathway at the activation of caspase-3. Other regulatory factors like AIF and Diablo/SMAC are also released from the mitochondria to amplify the apoptotic responses. Figure taken from Kaufmann, 2001.

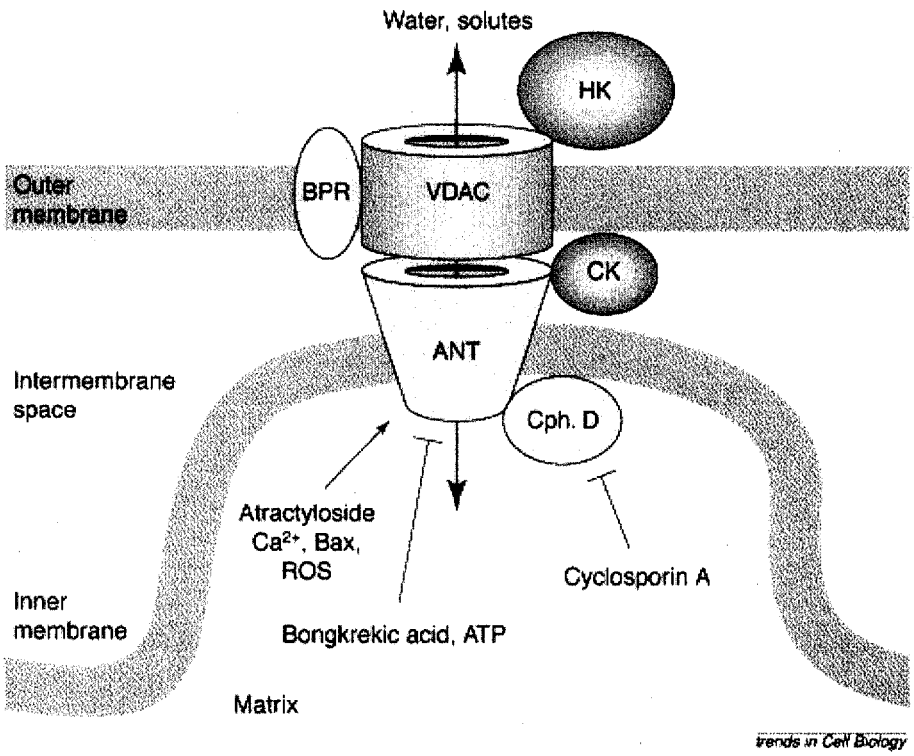

Figure 1.7. **Mitochondrial permeability transition pore (MPTP).** This channel spans across the outer and inner mitochondrial membrane, forming a hydrophilic pore in the center. It is formed with the association of the voltage-dependent anion channel (VDAC) in the outer membrane, adenine nucleotide translocase (ANT) in the inner membrane and cyclophilin D in the matrix. Other associated proteins include hexokinase (HK), creatine kinase (CK) and benzodiazepine receptor (BPR). Opening of the pore allows free movement of solutes <1500 Da to traverse across into the cytosolic spaces, a phenomenon more commonly termed the mitochondrial permeability transition (MPT). A prolonged opening of the pore can result in mitochondrial swelling and a rupturing of outer membrane, resulting in the collapse of $\Delta\Psi_m$ and a loss of cytochrome *c* and other mitochondrial proteins. Opening of the pore can be modulated by an influx of calcium, ROS and binding of pro-apoptotic BAX to the outer membrane. Bongkrekic acid and cyclosporin A can block MPT by binding and inhibiting the pore at ANT and cyclophilin D respectively. Figure taken from Desagher and Martinou, 2000.

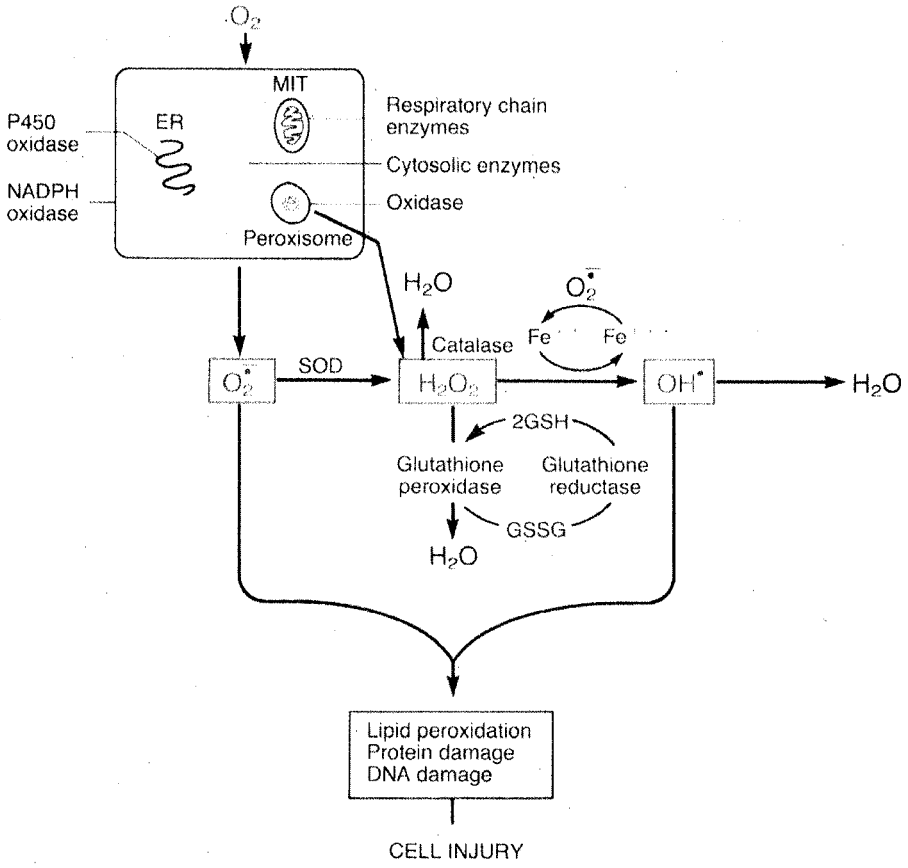

Figure 1.8. **Consequences of ROS in the cell.** Reactive oxygen species can be generated as a by-product in many cellular metabolic processes including ETC, peroxisomal activities, cytosolic enzymatic activities as well as microsomal P450 and NADPH-dependent oxidases. One electron reduction of molecular oxygen yields superoxide, which can be further reduced to hydrogen peroxide and hydroxyl radical, before terminal reduction to water. When these ROS are not adequately removed or quenched by glutathione peroxidases and other endogenous antioxidants, ROS can result in lipid peroxidation and protein and DNA damage. Figure taken from Robbins Pathologic Basis of Disease, 1989.

Table 1.1 **Principle mechanisms for mitochondrial dysfunction in diseases and drug toxicities.** Table adapted and modified from Krahenbuhl, 2001.

Principle Mechanism	Examples
Inhibition of the electron transport chain	Rotenone, Parkinson's disease, Alzheimer's disease
Uncoupling of oxidative phosphorylation	Pentachlorophenol, amiodarone, tacrine
Mitochondrial permeability transition	Salicylates, valproic acid
Inhibition of fatty acid metabolism	Valproic acid
Inhibition of TCA cycle	Arsenite, fluorocitrate
Modulation of mitochondrial DNA	Nucleoside analogs, alcohol
Inhibition of apoptosis	Follicular B-cell lymphoma

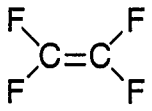

Tetrafluoroethylene

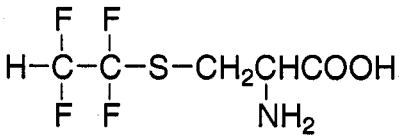

S-(1,1,2,2-tetrafluoroethyl)-L-cysteine (TFEC)

Figure 1.9. **Study compounds**. Tetrafluoroethylene (TFE) and S-(1,1,2,2-tetrafluoroethyl)-L-cysteine (TFEC).

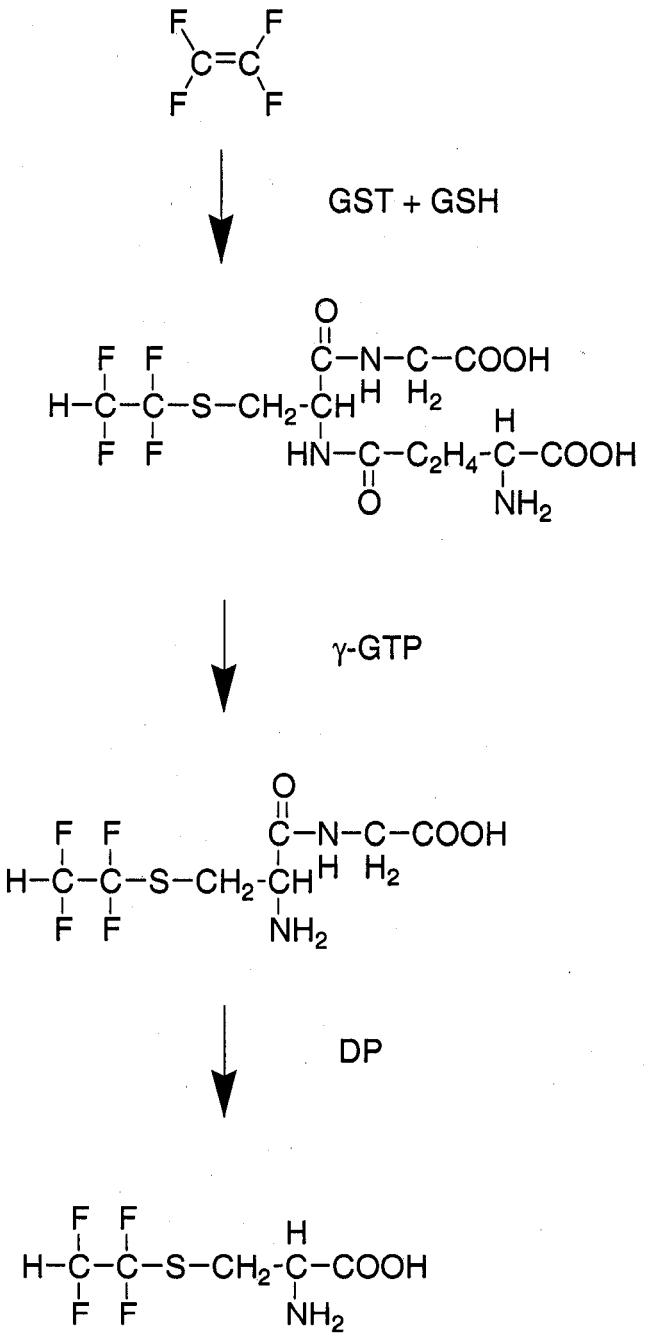

Figure 1.10. **Metabolism of TFE to TFEC.** Glutathione (GSH) is added to TFEC by glutathione S-transferase (GST) forming the TFE-glutathione adduct (TFE-GS). The TFE-GS adduct is further metabolized by γ-glutamyltranspeptidase (γ-GTP) forming a TFE-cysteinylglycine conjugate, which is processed by cysteinylglycine dipeptidase (DP) to TFEC.

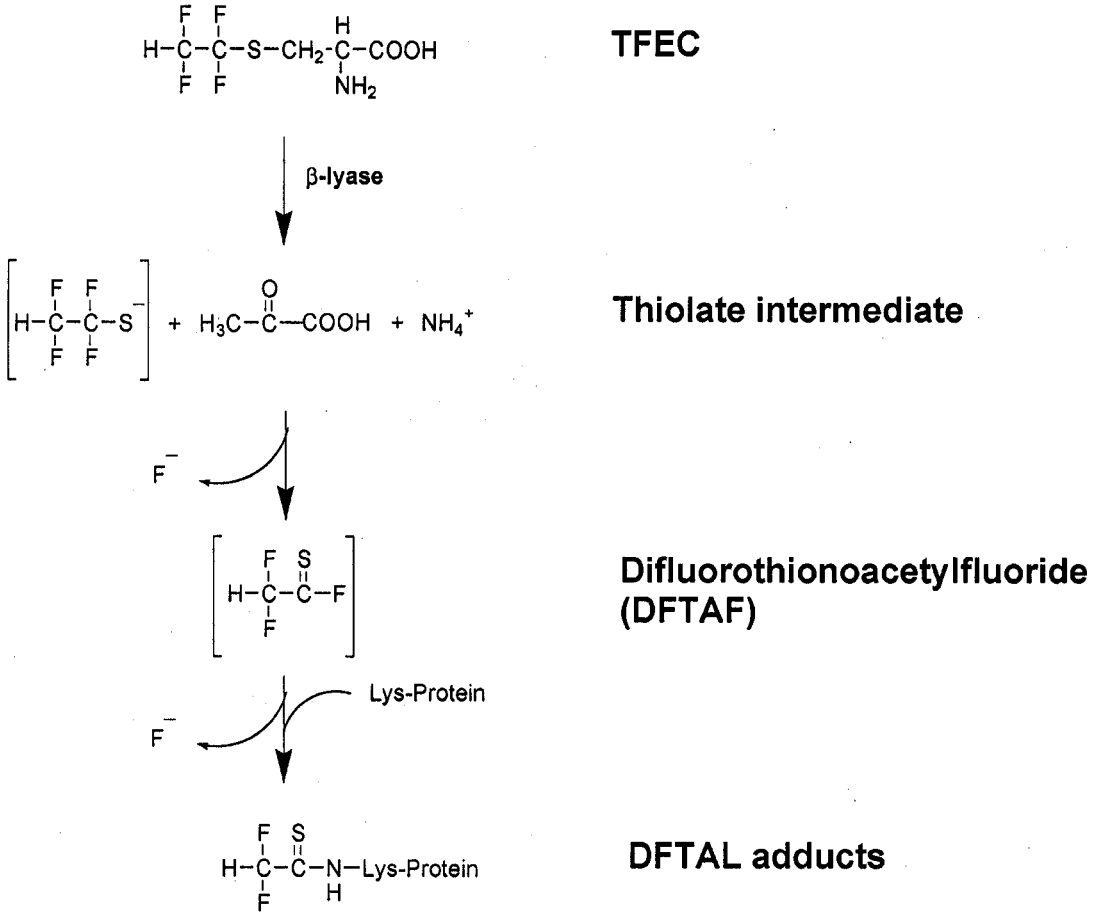

Figure 1.11. **Bioactivation of TFEC.** TFEC is metabolized by β-lyase into tetrafluoroethanethiolate, pyruvate and ammonia. The loss of a fluoride promotes the rearrangement of the molecule into the highly electrophilic difluorothionoacetylfluoride (DFTAF). This species readily adducts exposed lysine residues, generating difluorothionoacetyllysyl adducts (DFTAL).

Table 1.2 **Identification of DFTAL adducts after TFEC treatment**

Protein modified	Function	Localization	Reference
mtHSP70 (mortalin)	Stress protein	Mitochondrial matrix	(Bruschi *et al.* 1993)
HSP60	Stress protein	Mitochondrial matrix	(Bruschi *et al.* 1993)
Dihydrolipoamide dehydrogenase (E3o) subunit (α-KGDH)	TCA cycle	Mitochondrial matrix	(Bruschi *et al.* 1998)
Dihydrolipoamide dehydrogenase (E3) subunit (BCKDK)	TCA cycle	Mitochondrial matrix	(Bruschi *et al.* 1994)
Lipoamide succinyltransferase (E2o) subunit (α-KGDH)	TCA cycle	Mitochondrial matrix	(Bruschi *et al.* 1998)
Aspartate aminotransferase (AST)	Intermediary metabolism	Mitochondrial membrane	(Bruschi *et al.* 1993)
Aconitase	TCA cycle	Mitochondrial matrix	(James *et al.* 2002)
L-arginine:glycine amidinotransferase	Intermediary metabolism	Mitochondrial matrix	Bruschi *et al.*, unpublished observation

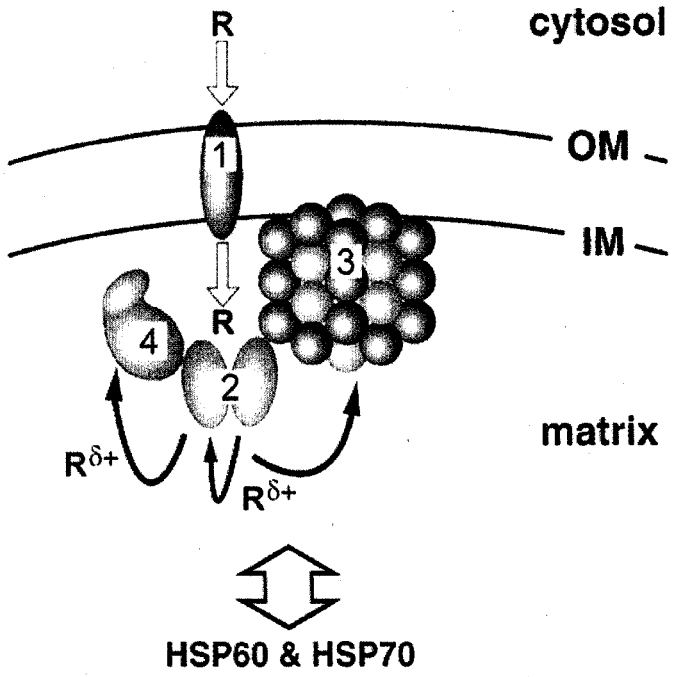

Figure 1.12. **Proposed mechanism of DFTAL adduct formation in the mitochondria.** Transport of the protoxicant TFEC (R) into the mitochondrion by an unidentified transporter (1) results in the formation of reactive intermediate ($R^{\delta+}$) and is proposed to be undertaken primarily by native, homodimeric mitochondrial AST (2). Mitochondrial AST-generated $R^{\delta+}$ is removed to other proximal targets, e.g., the α KGDH complex (3) and bilobular monomeric aconitase (4), by inherent substrate channeling between these components. Secondarily, DFTAL-induced conformational alterations in target proteins signal the recruitment of mitochondrial stress proteins HSP60 and HSP70 for downstream repair processes. The relative positions of the mitochondrial outer membrane (OM), inner membrane (IM), and matrix are indicated. Figure and text adapted and modified from James et. al., 2002.

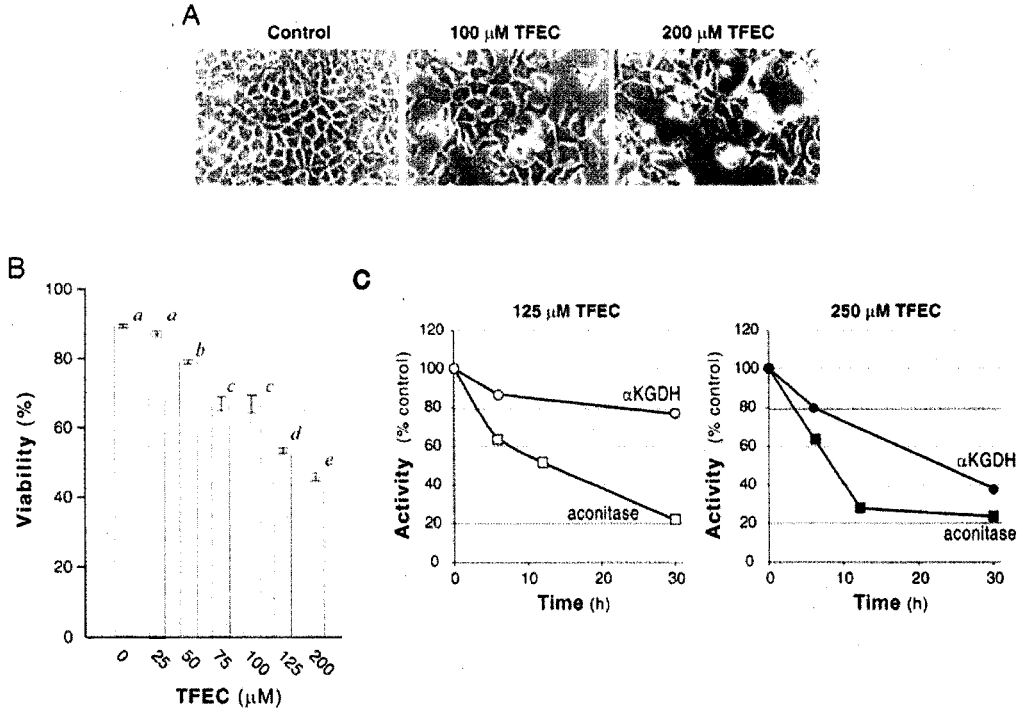

Figure 1.13. **Early TFEC-induced alterations to mitochondrial function.** (A) Cellular morphology by light microscopy of TFEC-induced cytotoxicity in TAMH cultures exposed to saline vehicle (control) or 100 or 200 μM TFEC for 12 h. Non-adherent and dead cells were observed as smaller, light-colored, spheres out of the plane of focus for all TFEC treatments whereas adjacent healthier cells remained in the culture monolayer (300X magnification). (B) Quantitative evaluation of cell viabilities in TAMH cultures exposed to TFEC (0-200 μM) for 12 h using Live/Dead assay (Molecular Probes). Treatments with differing designations were statistically distinct (*a-e*, $0.05 > p < 0.001$). (C) Relative time course and extent of aconitase inhibition *in vitro* with respect to another confirmed TFEC target, the αKGDH complex. Aconitase activities in TAMH cultures ranged from control values of 7.98 μmol of *cis*-aconitate consumed min^{-1} (mg of protein)$^{-1}$ (±0.0003 μmol min^{-1} mg^{-1}, SD; n = 3 independent experiments) to 2.06 μmol of *cis*-aconitate min^{-1} mg^{-1} in cultures treated with 250 μM TFEC for 30 h (n = 2). αKGDH activities ranged from a maximum of 0.397 μmol of NADH produced min^{-1} (mg of protein)$^{-1}$ to a minimum of 0.153 μmol of NADH produced min^{-1} mg^{-1} (values are the average of two independent determinations). Figure and text adapted and modified from James *et al.*, 2002.

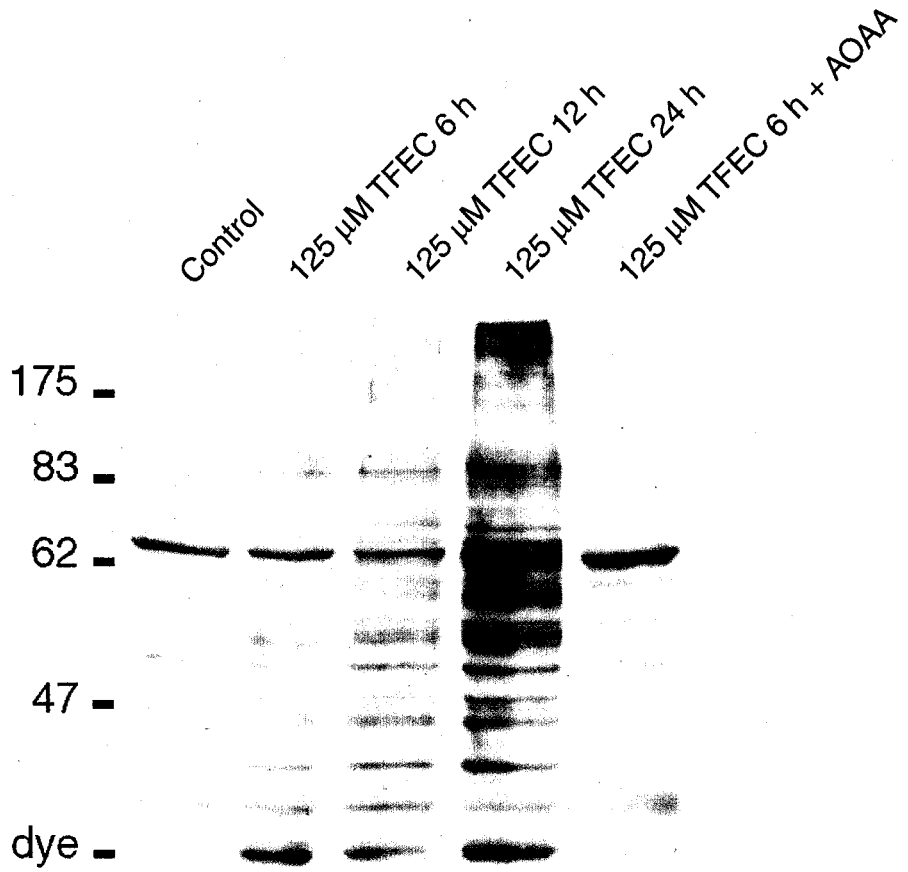

Figure 1.14. **Inhibition of DFTAL adduct formation by AOAA.** Total lysates of TFEC-treated (125 µM) TAMH cells were probed with anti-TFA polyclonal antibody. A progressive increase in adduct formation is observed over 6-24 h. Aminooxyacetic acid (AOAA) at 500 µM effectively prevented adduct formation. Figure taken from Bruschi *et al.*, unpublished data.

Chapter 2

Mitochondrial Changes: From Early Apoptotic Signals To Secondary Necrosis

2.1 Introduction

Previously, our lab characterized biochemical changes following TFEC exposure *in vitro* using a TGFα-overexpressing mouse hepatocyte cell line (TAMH) and observed dose- and time-dependent inhibition for both aconitase and αKGDH protein target activities which closely resembled comparable mitochondrial deficits in these enzymes *in vivo* (James *et al.* 2002; Wu *et al.* 1994). Protein binding could be decreased by co-administration of the β-lyase inhibitor, AOAA (as discussed in Chapter 1). This demonstrated that the TAMH cell line contains sufficient TFEC bioactivation capability to reproduce important aspects of the nephrotoxicity of TFEC at toxicologically relevant doses (James *et al.* 2002; Pierce *et al.* 2000; Pierce *et al.* 2002). The studies reported in this chapter confirm the bioactivation of TFEC in TAMH cells with the release of fluoride (Figure 2.1), as well as demonstrating a complete restoration of viability of the cells by the coadministration of AOAA (Figure 2.2). Additional experiments were carried out to investigate specific mitochondrial changes that occurred in TAMH cells after the initial binding of a TFEC reactive metabolite to mitochondrial proteins. Since the initiating lesions of TFEC originate within the mitochondria, it is our hypothesis that early mitochondrial changes play an important role in the progression of cellular injury.

BCL2 pro- and anti-apoptotic proteins are positioned near the apex of the hierarchy of events in mitochondrial-mediated cell death mechanism(s). Although they are predominantly cytosolic, members of this family, e.g. BAX, are rapidly translocated to the mitochondrial outer membrane to activate other downstream processes in promoting apoptosis. This involves the mitochondrial pathway for apoptosis, as opposed to the receptor-mediated pathway represented e.g. by TNFα. BAX

subcellular translocation was assessed in TFEC-mediated cytotoxicity using stable transfectants of the parental TAMH cell line either overexpressing the BAX dimerization partner, BCL-xL (TAMH-BCL-xL) or, overexpressing an empty vector control (Takehara *et al.* 2001; Tzung *et al.* 1997). Since BCL-xL represents the predominant anti-apoptotic BCL-2 family member observed in mouse hepatocytes, these stable lines are most suited to examine BAX translocation following TFEC treatment (Tzung *et al.* 1997). Events following BAX translocation usually include the release of cytochrome *c* from the mitochondria, and the activation of caspases. However, variations to this pathway have been reported, and the impact on subsequent cell viability may also differ. Thus, the role of these downstream mitochondrial events was investigated in the same system, as was the relationship between activation of BAX and upstream mitogen-activated protein kinases (MAPK) stress signaling pathways, and possible receptor-mediated apoptotic pathways. Parts of this chapter were previously published in *Biochemical Pharmacology* (Ho *et al.* 2005a).

2.2 Materials and Methods

2.2.1 Cell culture

Serum-free cell culture of the TAMH line between passages 21-35 was undertaken as previously described (Pierce *et al.* 2002; Wu *et al.* 1994). Details regarding the stable TAMH-BCL-xL cell line have been previously reported (Tzung *et al.* 2001). All chemicals were obtained from Sigma (St. Louis, MO) unless otherwise stated. Briefly, cells were grown in serum free Dulbecco's modified Eagle's medium/Ham's F12 (Invitrogen, Carlsbad, CA) supplemented with 5 μg/mL insulin, 5 μg/mL transferrin, 5 ng/mL selenium (Collaborative Biomedical Products, Boston, MA), 100 nM dexamethasone, 10 mM nicotinamide and 0.1% v/v gentamicin (Invitrogen). Maintenance of the stable transfectant TAMH-BCL-xL line and the null vector control, TAMH-Vc, were with additional supplementation of 400 μg/mL G418 sulfate (Invitrogen). Cultures were maintained in a humidified incubator with 5% carbon dioxide/95% air at 37°C and passaged at 70-90% confluence.

2.2.2 Dosing and harvesting of cells

Cultures were treated at confluence by replacement of growth medium with fresh medium containing 250 μM of freely soluble TFEC. TFEC was synthesized according to procedures previously described (Adams 2003; Hayden and Stevens 1990). To provide sufficient material for immunoblot assays, TAMH-Vc or TAMH-BCL-xL cultures were grown in larger 150 cm^2 tissue culture flasks (cf. 25 or 75 cm^2). During harvesting, medium was aspirated and cells washed twice with ice-cold PBS. Two hundred μL of lysis buffer containing 20 mM Tris, 0.25 mM sucrose, 1 μM dithiothreitol (DTT), and protease inhibitor cocktail (Roche, Switzerland) were added to each dish. Cells were scraped off using a rubber policeman and kept at 0°C prior to generation of whole-cell lysates by sonication with an ultrasonic probe tip (Series 4710, Cole-Palmer, Vernon Hills, IL). For immunoblots examining BAX translocation and cytochrome *c* release, isolation of TAMH-Vc or TAMH-BCL-xL subcellular fractions was carried out prior to sonication as detailed below.

2.2.3 Fluoride release assay

Cells were grown on T150 dishes to confluence and treated with TFEC (250 μM) for 0, 2, 4 or 6 h, after which cell culture medium was harvested. A 1 mL sample was transferred to a microcentrifuge tube and dried using a Jouan RC 1022 SpeedVac (Thermo Electron Corp., Waltham, MA). The dried medium was re-dissolved in 100 μl of cell culture medium to generate a 10-fold concentrate for fluoride analysis. Fluoride concentration was determined by voltametric analysis using fluoride electrodes, according to method previously described (Castillo *et al.* 2001) in collaboration with Dr. Evan Kharasch, University of Washington.

2.2.4 Subcellular fraction isolation

Mitochondria-enriched fractions were isolated with slight modifications to the protocol described previously (Single *et al.* 1998). Briefly, the harvested cells were pelleted using a bench top microcentrifuge. Supernatant was removed and the pellet

was lysed in 100 μL (per million cells) of digitonin lysis buffer (75 mM NaCl, 1 mM NaH_2PO_4, 8 mM Na_2HPO_4, 250 mM sucrose, 200 μg/mL digitonin, and protease inhibitor cocktail) with gentle but thorough resuspension for 10 min. The lysate was centrifuged at 13,000 g for 5 min at 4°C. The resultant supernatant was collected as the cytosolic fraction. The pellet was then resuspended with a fresh volume of digitonin lysis buffer, sonicated for 5 s, and centrifuged at 13,000 g for 5 min at 4°C. The supernatant contained the mitochondria-enriched fraction. The purity of sub-cellular fractions was confirmed by immunoblotting with antisera to mitochondrially-located VDAC or cytosolic glyceraldehyde 3-phosphate dehydrogenase (GAPDH) as described below.

2.2.5 Immunoblotting

All fractions collected were assayed for protein concentration using a BCA protein assay kit (Pierce, Rockford, IL). Sample proteins (30-50 μg) were resolved by denaturing electrophoresis using 15% SDS-PAGE (Mini-PROTEAN II, Bio-Rad Laboratories, Hercules, CA) and transferred to nitrocellulose membranes for 1 h at 15 V using Trans-Blot SD Semi-Dry Transfer Cell (Bio-Rad). Immunodetection was by chemiluminescence (SuperSignal ULTRA, Pierce) using specific antibodies diluted in PBS with 0.05% (v/v) Tween 20 and 5% (w/v) powdered milk. Anti-ATF3, anti-VDAC and anti-BCL-xL were from Santa Cruz Biotechnology; anti-Hsp70i (1:1,000) from Stressgen (Victoria, BC); anti-BAX and anti-cytochrome *c* from BD Bioscience (San Jose, CA); anti-p38 from Cell Signaling Technology (Beverly, MA) and anti-GAPDH (1:2,500) was made in-house (Dietze *et al.* 1997). Secondary anti-mouse and anti-rabbit horseradish peroxidase conjugated secondary antibodies (Pierce) were used at 1:20,000 dilution. All antibodies were used at 1:2,000 dilution unless otherwise stated.

2.2.6 Densitometric analysis

Nitrocellulose membranes and X-ray films were analyzed after immunoblotting using Bio-Rad ChemiDoc and the Quantity One Version 4.3.0 program (Bio-Rad). The bands were cropped and their optical densities were quantified.

2.2.7 Immunocytochemistry

Cells were grown on 2 and 4-well chambered slides (Labtek II, Nalgene, Rochester, NY). Cultures were dosed as described above. After treatment, medium was aspirated and cells were stained with 500 nM MitoTracker™ Red (Invitrogen) for 20 min, washed twice with Hank's buffered saline solution (BSS) and fixed with 3.7% (v/v) paraformaldehyde (EMS, Hatfield, PA) in Hank's BSS for 20 min at room temperature. Ice-cold acetone was added and the mixture was allowed to stand for 5 min to permeabilize the plasma membrane. Non-specific binding was blocked by soaking the chambers overnight in PBS with 10% fetal bovine serum (FBS) at 4°C. Immunostaining was with anti-BAX (Invitrogen) and AlexaFluor 488-conjugated anti-mouse IgG (Invitrogen) for 2 h incubation each (dilutions between 1:50 and 1:200). Saponin (0.2%; w/v) was added with the immunostaining reagents to enhance antibody accessibility. Slides were mounted with Fluoromount G (Southern Biotechnologies, Birmingham, AL) and examined using a Nikon Diaphot 200 fluorescence microscope (Nikon, Melville, NY) with 40X magnification. The images were captured with a Princeton Instruments MicroMax CCD (Molecular Devices, Sunnyvale, CA).

2.2.8 Viability assay using MTT

Cells were seeded and grown to confluence on 96-well plates (approximately 10,000 cells in each well). After TFEC treatment, 50 µL MTT dye (2.5 mg/mL in PBS) was added per well with another 200 µL HEPES-buffered growth medium and incubated at 37°C in the dark for 3-4 h. The dye solution was then aspirated and 25 µL of Sorenson's buffer (0.1 M glycine, 0.1 M NaCl equilibrated to pH 10.5 with 0.1 M

NaOH) and 200 μL of dimethylsulfoxide (DMSO) were added immediately to each well. The plates were read at 560 nm using a microtiter plate reader (Molecular Devices) as previously described (Plumb *et al.* 1989).

2.2.9 Cytotoxicity assay using LDH release

Lactate dehydrogenase (LDH) release was determined quantitatively using microtiter plate modifications of standard iodonitrotetrazolium chloride (INT)- coupled colorimetric methods (Decker and Lohmann-Matthes 1988). Briefly, cells grown on 96-well plates were subjected to respective TFEC doses made up in 100 μL of growth medium. At the end of treatment, 20 μL of freshly prepared lactate solution (36 mg/mL in Tris.Cl 10 mM, pH 8.5), 20 μL of INT solution (2 mg/mL in PBS) and 20 μL of NAD^+ solution (3 mg/mL with 13.5 U/mL of diaphorase in PBS containing 0.03% BSA and 1.2% sucrose) were added to each well. The mixture was incubated for 10-30 min at ambient temperature with periodic shaking of the plate. Reactions were quenched with a solution of aminooxoacetic acid (AOAA, 16.6 mg/mL in PBS). The plates were read at 490 nm on a microtiter plate reader. The data were converted into an arbitrary unit of absorbance/time (*per* min) before they were expressed as a ratio of non-treated control.

2.2.10 Caspase activation assays

Caspase activation was determined by incubating 30-60 μg of homogenized cell lysates at 37°C in 100 μL of caspase assay buffer (50 mM PIPES, pH 7.4, 100 mM NaCl, 1 mM EDTA, 10% w/v sucrose, 0.1% w/v CHAPS, and 10 mM DTT) with 20 μM fluorogenic caspase substrates: Ac-DEVD-AMC, Ac-VDVAD-AMC, Ac-VEID-AMC, Ac-IETD-AMC, LEHD-AMC (Axxora, San Diego, CA). Fluorescence was monitored on a Packard Fluorocount (PerkinElmer, Boston, MA) microplate fluorometer with an excitation wavelength of 360 nm and an emission of 460 nm. Data are presented as *p*mol of AMC hydrolyzed/μg lysate protein/microtiter plate incubation time. The levels of activation were compared against a positive control

treated with 200 nM actinomycin-D and 5 ng/mL TNFα for 8 h (TNFα was added 1 h after addition of actinomycin-D).

2.2.11 Calpain activation assays

Calpain activation was determined using the same methodology as described for caspases with slight modification. Briefly, 30-60 μg of homogenized cell lysates were incubated at 37°C in 100 μL of caspase assay buffer (see above) with 20 μM fluorogenic calpain substrate, Suc-LLVY-AMC (Axxora). Fluorescence from the hydrolyzed products was determined on the plate reader as described previously. Data are presented as *p*mol of AMC hydrolyzed/μg lysate protein/microtiter plate incubation time. The specificity of activation was determined by inhibiting the hydrolysis using calpain inhibitors, 100 μM of the peptides ALLM or ALLN (Roche), made from a 10 mM stock in DMSO.

2.2.12 Phosphoprotein analysis

TAMH cells were treated with TFEC (200 μM) for 1, 2 or 4 h, and processed for phosphoprotein analysis according to the procedure provided by the manufacturer of the assay kit (Biosource, Camarillo, CA). Briefly, treated cells were rinsed with ice-cold PBS and harvested by scraping. They were lysed with the proprietary NP40 cell lysis buffer (Biosource) supplemented with 1 mM PMSF and protease inhibitor cocktail (Roche) for 30 min on ice. The lysates were then spun down at 13,000 g for 10 min at 4 °C. The clear supernatant was removed for phosphorylation analysis on the Bioplex system (Luminex Corp., Austin ,TX) using AKT, JNK1/2, p38 3-plex antibody beads (Biosource).

2.2.13 Death receptor pathway analysis

TAMH cells were grown on 6-well plates to confluence, and were treated with TFEC (250 μM) for 4 and 8 h. Cell culture medium was harvested after respective treatments and processed for death receptor analysis according to the procedure provided by the manufacturer of the assay kit (Biosource). The samples were assayed for the release of

TNFR-I, TNFR-II and DR5 (Death receptor 3-plex, Biosource) on the Bioplex system as described for phosphoprotein analysis above.

2.3 Results

2.3.1 Release of fluoride during β-lyase mediated metabolism of TFEC

To assess β-lyase mediated metabolism of TFEC in TAMH cells, release of fluoride was measured. TAMH cells were treated with 250 μM TFEC, and fluoride concentration in the cell culture medium was determined from 0-6 h. A linear increase in fluoride concentration over the duration of TFEC incubation was observed (Figure 2.1). A detectable level of fluoride concentration at 0 h was likely due to degradation of the TFEC stock solution during prolonged storage (i.e. more than a week at 4 °C).

2.3.2 Cytoprotective effect of AOAA on TFEC toxicity

Subsequently, a specific β-lyase inhibitor, aminooxyacetic acid (AOAA), was coadministered with cytotoxic doses of TFEC (125 to 250 μM). At 24 h after treatment with TFEC (125 μM), coincubation with 500 μM of AOAA were completely protected from loss of viability as assessed using the MTT assay. Cell viability was restored to 80% of controls in the presence of TFEC (250 μM) and AOAA (500 μM) compared to 20% in the absence of AOAA (Figure 2.2).

2.3.3 Effect of TFEC on BAX cytosolic and mitochondrial localization

Immunoblot analyses of TAMH cultures treated with TFEC (250 μM, 0-8 h) revealed a shift in a 21 kDa immunoreactive BAX species from the cytosol to mitochondria at 4 h and 8 h post-treatment (Fig. 2.3A). Although some BAX localization to mitochondria in the control samples was observed, there was nonetheless, a prominent increase in BAX-specific band intensity and mitochondrial translocation with TFEC treatment. In particular, TFEC-specific increases were much more pronounced in the null vector line (TAMH-Vc) in comparison to the TAMH line stably overexpressing BCL-xL (TAMH-BCL-xL; Fig. 2.3A cf. Fig. 2.3B). In addition, densitometric analyses confirmed that TAMH-BCL-xL cultures overexpressed BCL-xL at

approximately 8-fold higher levels in comparison to the null vector line (Fig. 2.3C and 2.3D). Consistent with previous reports, an approximately 60 kDa BAX-immunoreactive species that matches previously reported BAX oligomerization products was observed (Mikhailov *et al.* 2003; Mikhailov *et al.* 2001) (data not presented). The exact composition of any BAX oligomers have yet to be determined.

2.3.4 Immunocytochemical determination of BAX translocation in TAMH-Vc and TAMH-BCL-xL cultures

Independent confirmation of immunoblot assays for BAX intracellular movement *in vitro* following TFEC treatments was by immunocytochemistry (Fig. 2.4). Mitotracker™ Red was used as a mitochondrial specific marker, and BAX was localized by immunostaining with polyclonal anti-BAX primary antibodies and AlexaFluor 488-conjugated secondary antibodies (refer to Experimental Procedures). Punctate red staining of mitochondria was evident from 2 h to 6 h of TFEC treatment of TAMH-Vc cultures, which transformed to an orange coloration (merging of AlexaFluor 488 and Mitotracker™ Red staining). Merged staining was at its most intense in cultures treated for 2 h (Fig. 2.4; left panels). FITC-immunostained cytosolic BAX was simultaneously reduced in intensity. Vanishing green and increased colocalization of Mitotracker™ Red and BAX staining (orange merged image) clearly demonstrated that BAX translocated to mitochondria during the course of TFEC treatment in TAMH-Vc cultures, thereby, validating the immunoblot data of Fig. 2.4. Additionally, a small fraction of BAX in the mitochondria of 0 h samples was detected (Fig. 2.4), suggesting that a minor proportion of the total BAX population is constitutively located on the mitochondrial membrane, consistent with the immunoblot data of Fig. 2.3. In addition, later stage TFEC-treated cultures appeared altered with respect to morphology, and were comparatively low in confluence, indicating a loss of cellular adhesion during the progression of TFEC-induced cellular injury (Fig. 2.4; 4 h and 6 h panels of TAMH-Vc).

In comparison, TAMH-BCL-xL cultures displayed little overt morphological change from 2 h to 6 h of TFEC treatment (Fig. 2.4; lower right panels). Qualitatively, AlexaFluor 488 labeling (i.e. green fluorescence) and cytosolic BAX localization remained intense throughout the course of TFEC exposure in TAMH-BCL-xL overexpressing cultures consistent with a failure to activate cytosolic BAX and its subsequent translocation to mitochondria.

2.3.5 Cytochrome *c* release following BAX translocation

Cytochrome *c* release was also examined by Western blot assay. Cytochrome *c*, which was localized exclusively within mitochondria, was released into the cytosol 8 h after TFEC treatment of TAMH-Vc cells (Fig. 2.5A). These data support a well-established model in apoptosis of early BAX translocation to the mitochondria followed by subsequent cytochrome *c* release into the cytosol. On the other hand, TAMH-BCL-xL cells did not show significant change in the mitochondrial localization of cytochrome *c* for up to 8 h after TFEC treatment (Fig. 2.5B).

2.3.6 Inhibition of cell death with BCL-xL overexpression

Stable transfectant TAMH-Vc and TAMH-BCL-xL cell lines were compared to the parental TAMH line for TFEC-induced toxicity using cell viability and cytotoxicity assays. An MTT assay was used to assess 24 h survival of cells following continuous TFEC exposure (0-600 μM). BCL-xL overexpression maintained cell viability with remarkable cytoprotection evident, even in the presence of high TFEC concentrations (400-600 μM; Fig. 2.6). Cellular viability was still about 55% after 8 h exposure to 600 μM TFEC. On the other hand, TAMH-Vc and parental TAMH lines showed progressive cell killing from TFEC concentrations ranging from 200 μM to 600 μM. Nearly complete cytotoxicity was observed at 600 μM TFEC in the TAMH-Vc and TAMH parental cells where cell viability was less than 20% (Fig. 2.6). Since the MTT viability assay relies on active mitochondrial respiration, these results may be confounded by TFEC-mediated mitochondrial dysfunction. Thus, an alternative measure of toxicity was employed.

Complementary results were obtained for cytotoxicity measured as a function of intracellular LDH released into the culture medium due to plasma membrane rupture (Fig. 2.7). This assay was performed at 8 h TFEC treatment in order to avoid confounding effects of protease digestion of released LDH, which contributes to a short half-life in the culture medium (approximately 9 h in the medium[1]). Consistent with the MTT data, both parental TAMH and TAMH-Vc cultures showed proportional increases in LDH release, which doubled between 200-400 μM TFEC concentrations. In contrast, LDH release remained at basal levels in BCL-xL overexpressing cells exposed to TFEC concentrations up to 400 μM. However, at TFEC concentrations of 600 μM, LDH release was similar in all 3 cell lines. A likely explanation for this discrepancy with results of the MTT assay is that inhibition of mitochondrial function by TFEC accentuates the differences between BCL-xL overexpressed and the control cell lines in the MTT assay. Nonetheless, BCL-xL effectively blocked cell death induced by high concentrations of TFEC using two independent methods of assessment.

2.3.7 BCL-xL mediated prevention of TFEC-induced proteotoxicity

The impact of BCL-xL overexpression on other determinants of cellular survival was also examined. Induction of cytosolic HSP70i represents a robust marker for cellular stress and protein damage (Kregel 2002). In addition, ATF3 (activating transcription factor-3) has also been established as a transcriptional repressor that is highly induced in cells treated with numerous chemicals and stressors (Hai *et al.* 1999; Pierce *et al.* 2002; Zhang *et al.* 2002). The levels of expression of HSP70i and ATF3 were examined by immunoblot in both TAMH-BCL-xL and TAMH-Vc lines in a pulse/chase type of experiment (Fig. 2.8). Cultures were exposed to vehicle or TFEC (400 μM) for 4 h, and then were allowed to recover in the presence of fresh growth medium for an additional 8 h (i.e. total time of 12 h) prior to preparation of cell lysates and subsequent analysis. ATF3 was observed to be strongly induced after TFEC

[1] Information taken from Promega Technical Bulletin No. 306, Version 5/03

treatment (Fig. 2.8, right lanes). Interestingly, the expression level of ATF3 was similar for both TFEC-treated TAMH-BCL-xL and TAMH-Vc cell lines. HSP70i levels were also strongly upregulated after TFEC exposure but only in TAMH-Vc cultures (Fig. 2.8). In comparison, neither ATF3 nor HSP70i could be detected in TAMH-BCL-xL and TAMH-Vc cultures in the absence of added TFEC (Fig. 2.8, left lanes). Hence, BCL-xL overexpression suppressed TFEC-mediated increases in HSP70i but not ATF3.

2.3.8 Caspase activity assays

Based on the observations of early mitochondrial changes, BAX translocation and cytochrome *c* release, the contribution of various caspase activities in the mechanism of TFEC-mediated TAMH cell killing was investigated. Caspases are known as downstream effectors of "classical" apoptosis in response to the release of cytochrome *c* and apoptosome formation in the cytosol. Five key caspases, including the "initiators" (caspase-2, -8 and –9) and the "executioners" (caspase-3/7, -6) were investigated using hydrolysis of directed tetrapeptide/pentapeptide fluorogenic substrates (Fig. 2.9). For all of the caspase activities studied, only modest activation (at most <10% of positive control levels) were observed with TFEC-treatment at any of the time points examined (Fig. 2.9). Caspase 3/7 activities in the BCL-xL overexpressing cell line were even below detection limits. Furthermore, activities generally appeared diminished in TAMH-BCL-xL versus TAMH-Vc or TAMH lines (Fig. 2.9). However, the levels of activity were minor in comparison to levels of caspase activities after TNFα/actinomycin-D treatment as a positive control for apoptosis (Fig. 2.9).

2.3.9 Calpain activity assays

The lack of significant caspase activation across the three cell lines prompted us to examine alternative intracellular proteolytic activities. Calpains are another class of cysteine proteases that show increased activities during necrotic as well as apoptotic cell death (Wang 2000). Increases in calpain activity were monitored by the hydrolysis

of the specific fluorogenic calpain substrate (Suc-LLVY-AMC) after treatment of all three cell lines with 250 μM TFEC for 0-8 h. As shown in Figure 2.10, a progressive increase in calpain activity was observed in TAMH-Vc cells, and the activity peaked after 6 h treatment (absolute activity 86.5 ± 8.1 *p*mol hydrolyzed product per hour). This reflects an approximate 2-fold increase in basal calpain activity ($p<0.05$). On the other hand, the activation seen in BCL-xL cells in comparison was insignificant from 0-6 h ($p>0.05$) with a modest increase observed after 8 h (i.e. 69.5 ± 9.3) ($p<0.05$). There was a statistical difference between activities in the two cells lines at early time points after TFEC treatment as determined by an unpaired t-test (i.e. 2 and 4 h; $p<0.05$), indicating either a delayed response or attenuation of calpain activation in TAMH-BCL-xL cells. Specificity of this assay was determined by reversal of calpain mediated hydrolysis using the calpain inhibitors acetyl-L-leucyl-L-leucyl-L-methioninal and acetyl-L-leucyl-L-leucyl-L-norleucinal (ALLM and ALLN). A 100 μM inhibitor concentration inhibited calpain activity to less than 20 % of the non-inhibitor treated samples. Overall, these results suggest that calpains rather than caspases are the proteases activated in TAMH cells after TFEC treatment.

2.3.10 Phosphorylation of stress-activated protein kinases

Phosphorylation of a group of stress-activated protein kinases after treatment with TFEC was investigated in an attempt to relate the proteotoxic mitochondrial effects to earlier signal transduction events. Using a newly established platform (i.e. Bioplex system), phosphorylation of AKT, JNK1/2 and p38 were quantified and expressed as a ratio of their respective total protein levels. As shown in Figure 2.11, a dramatic increase in phosphorylation of p38 (more than 5-fold) was observed 4 h after TFEC treatment. The same conditions produced a slight increase in JNK1/2 phosphorylation (approx. 1.5-fold) and basal pertubations for AKT. Since the Bioplex system is not widely reported in the literature, we validated our findings of the phosphorylation of p38 with a traditional immunoblot assay. As shown in Figure 2.12, the same treatments demonstrated similar phosphorylation trends as observed using the Bioplex assay system. Polyclonal antibodies against p38 phosphorylated at Thr180 and Tyr182

were used, and revealed increased phosphorylation (approx. 4-fold) compared to controls, 4 h after TFEC treatment (Figure 2.11).

2.3.11 Death receptor assays

Separately, to rule out the role of a receptor-mediated pathway in the early apoptotic signaling, release of death receptors were measured by the Bioplex System. The secretion of death receptors, including TNF-R1, TNF-R2 and DR5 by injured cells to the extracellular medium is an indication of receptor-mediated apoptosis. No significant increases in the release of these three receptors after either 4 or 8 h treatment with 250 μM TFEC (Figure 2.13) was detected. Cells treated with TNFα/actinomycin D was used as a positive control for the release of death receptors (data not shown).

2.4 Discussion

In recent years, several studies in molecular toxicology have focused on BCL-2 proteins as central to early events in drug-induced cytotoxicity. Among them, pro-apoptotic BAX is probably one of the best studied members. BAX is known to be constitutively expressed in the cytosol and found to relocate to the mitochondrial membrane upon induction of cellular injury by many factors (Hsu *et al.* 1997; Wolter *et al.* 1997; Zhang *et al.* 1998). BAX evokes an early response, which initiates downstream mitochondrial changes predisposing to apoptosis. The precise mechanism(s) of BAX activation and function are not yet known, and there are different schools of thought as to how its subcellular migration confers a pro-apoptotic character. Some studies have reported that BAX enables the release of several effectors of apoptosis like AIF, cytochrome *c*, and SMAC/DIABLO, by creating a channel in the mitochondrial membrane (Eskes *et al.* 2000). Others have provided evidence for homodimerization and oligomerization (Antonsson *et al.* 2001; Mikhailov *et al.* 2001) with anti-apoptotic members, like BCL-xL, to inhibit the latter's cytoprotective actions (Antonawich *et al.* 1998; Oltvai *et al.* 1993; Shangary and Johnson 2002). In general agreement with these studies, our immunoblot and

immunocytochemical studies suggest that BAX translocation is an early event in TFEC-induced cytotoxicity occurring within 2 h of treatment of TAMH cells with TFEC (Fig 2.3).

Although native BAX resides in the cytosol, a small amount was constitutively present in the outer mitochondrial membrane, in agreement with other studies (Figs. 2.3 and 2.4) (Putcha *et al.* 1999). The physiological significance of this constitutive mitochondrial BAX could imply that an equilibrium exists between the pro-apoptotic and anti-apoptotic BCL-2 proteins such that when BAX is in excess, some can be distributed to the mitochondrial membrane (Chao and Korsmeyer 1998; Oltvai *et al.* 1993). This is supported by our data with the BCL-xL overexpressed TAMH cell line, which had a significantly lower content of BAX in the mitochondria, even though the overall expression level of BAX was not altered (Figs. 2.3 and 2.4).

Numerous reports confirm a role for anti-apoptotic BCL-2 members in inhibiting BAX activation, notably at the level of its translocation to the mitochondria (Finucane *et al.* 1999; Ganju and Eastman 2002; Murphy *et al.* 2000). In particular, it has been reported that BCL-xL, but not BCL-2, is the major anti-apoptotic protein in hepatocytes (Takehara *et al.* 2001; Tzung *et al.* 1997). As a result, the effects of BCL-xL overexpression on TFEC cytotoxicity was determined in the TAMH cell line and were found to inhibit BAX translocation and maintained near complete cell viability to all but unrealistically high concentration of TFEC (i.e. > 400 μM). Furthermore, this study also indicated that BCL-xL overexpression prevented the release of cytochrome *c*, supporting the proposition that BAX translocation is, at least in part, required for cytochrome *c* release during TFEC-induced cytotoxicity.

Interestingly, some of our findings deviate from expectations, based on current understanding of the BAX-mediated cell death pathway. Results here demonstrate that TFEC-induced BAX expression and translocation promote the subsequent release of cytochrome *c* (see Chapter 1 for in-depth discussion). However, this resulted in only

limited caspase activation. On the other hand, activation of an alternative cysteine protease, calpain, was detected, and calpain activation was inhibited by BCL-xL overexpression. Calpain activation is driven by intracellular calcium mobilization and its proteolytic activities can proceed even in an ATP-independent fashion. Our current findings are consistent with a recent report of a role for calpain in TFEC-mediated kidney cell injury (Schnellmann and Williams 1998). These results, in addition to prior morphological evidence, strongly support necrosis as the dominant pathway for TFEC-mediated cytotoxicity (Bruschi *et al.* 1998). Therefore, we hypothesize that the covalent modification of intramitochondrial targets by TFEC initiates intracellular stress signaling pathways (e.g. p38 MAPK), which facilitates the early mitochondrial manifestation of apoptosis. However, inhibition of critical TCA cycle enzymes through DFTAL adduct formation (especially that of aconitase and αKGDH) rapidly depletes cellular ATP levels, shifting the mechanism of cell death from apoptosis to secondary necrosis. Further evidence to support this hypothesis will be presented in Chapter 4 where ATP depletion and mobilization of intracellular calcium supports the activation of calpains.

An important aspect yet to be addressed is the origin of the early apoptotic signaling. Some signal transduction pathways that trigger BAX translocation and other early mitochondrial apoptotic responses have been established, even though mechanistic details are still poorly understood. For example, ionizing radiation-induced DNA damage activates the tumor suppressor gene, p53, which increases the expression of BCL2 proteins, such as BAX, and also leads to permeabilization of the mitochondrial membrane (Brady and Gil-Gomez 1998; Chipuk *et al.* 2004). Some members of the MAPK family have also been shown to participate in the activation of apoptosis: For example, c-Jun NH2-terminal kinase (JNK), activated by several environmental stresses, activates BAX, and causes cytochrome *c* release and cell death (Lee *et al.* 2005a; Lei *et al.* 2002). Another member, p38, also activates BAX translocation during both nitric oxide and cyanide- induced apoptosis (Ghatan *et al.* 2000; Shou *et al.* 2003).

Aside from the stress-activated protein kinase pathway, receptor-mediated pathways of apoptosis may lead to cytochrome *c* release. This occurs through an increased expression of the soluble, extracellular death receptors and subsequent binding by specific ligands, leading to the activation of caspase-8 (as further described in Chapter 1). Caspase-8 in turn cleaves BID to generate an activated truncated BID (tBID) that translocates to the mitochondrial outer membrane (Zimmermann *et al.* 2001). The effects of BID translocation parallel that of BAX leading to subsequent mitochondrial effects (Jiang and Wang 2004; Luo *et al.* 1998; Orrenius 2004). However, the lack of caspase-8 activation (Figure 2.9) and the absence of death receptor release into the extracellular medium (Figure 2.13), exclude such a possibility in TFEC-mediated mitochondrial dysfunction.

Hence, the role of possible upstream signal transduction pathways was investigated using a representative set of stress-activated protein kinases, including AKT, JNK and p38 MAPK. Results from both the Bioplex system and immunoblot assays confirmed a selective activation of the p38 MAPK pathway (Fig 2.11 and 2.12). However, the mechanism of p38 participation in the mitochondrial pathway of apoptosis is not clear. Presumably, p38 catalyzes phosphorylation of critical amino acids on BAX, resulting in global conformational changes such that BAX undergoes translocation to the mitochondrial outer membrane (Shou *et al.* 2003).

HSP70i induction was used in these studies as an indicator of TFEC-induced protein damage in TAMH cells (Fig. 2.8). Increased BCL-xL levels resulted in a lack of observable HSP70i induction following TFEC treatment. This finding is consistent with the prominent role that the HSP70 family plays in the recognition of protein native state. In particular, the highly inducible HSP70i isoform is known to confer cytoprotective effects in response to many stressors by limiting excessive protein aggregation and misfolding (Beere and Green 2001; Kabakov *et al.* 2002). An alternative term "proteotoxicity", first coined by Hightower in 1991, adequately

describes such loss of protein homeostasis (Hightower 1991). The literature also defines additional roles for HSP70i including inhibition of specific apoptotic steps such as JNK activation and apoptosome complex formation (Beere and Green 2001; Salminen *et al.* 1997). Elevated HSP70i levels in our studies are viewed as indicative of TFEC-mediated proteotoxicity in both TAMH and TAMH-Vc cultures. Therefore, the most likely interpretation for the lack of HSP70i upregulation in BCL-xL overexpressing cells is a reduction in proteotoxic damage caused by TFEC (Fig. 2.8). Nonetheless, further work is required to provide a direct mechanistic link between BCL-xL overexpression and HSP70i regulation. Of relevance, similar observations have also been reported with BCL-xL-mediated protection from heat shock (Robertson *et al.* 1997). This subject will be more comprehensively discussed in Chapter 3.

Analogous to these findings with HSP70i, increased levels of expression of stress–responsive ATF3 following TFEC treatment of TAMH cells were observed (both with and without BCL-xL overexpression). ATF3 belongs to a family of transcription factors that contain the basic region-leucine zipper (bZip) DNA binding domain (Hai *et al.* 1999). Induction of the *atf3* gene appears as an early response to several forms of cellular stress, including liver dysfunction (Allen-Jennings *et al.* 2002). Increased transcriptional upregulation of the *atf3* gene in TAMH cells after TFEC treatment was confirmed by both microarray analyses and quantitative RT-PCR (Hu *et al.*, manuscript in preparation). Since BCL-xL overexpression does not directly alter the expression of TFEC-induced ATF3 upregulation, the observed cytoprotective effects of BCL-xL must either be downstream from ATF3, or through a mechanism that is independent of the ATF3-mediated stress response. More recently, studies have revealed that ATF3 serves an integral role in the endoplasmic reticulum (ER) stress response (Jiang *et al.* 2004; Zhang *et al.* 2001). Subsequent investigations have also confirmed the transcriptional (*gadd153, gadd34, gadd45*) and translational upregulation (Gadd153) of some established ATF3-regulated ER dependent stress response genes (Chapter 4). Taken together, these findings suggest an early ER stress

response associated with TFEC-induced mitochondrial events, that are not inhibited by BCL-xL overexpression. Further investigations of the interrelationship(s) among these two proteins will be necessary to address these questions.

The effects of BCL-xL on TFEC-treated TAMH cells extend beyond modulation of early events of cell death as exemplified by BAX translocation, HSP70i induction and cytochrome *c* release. Our results also revealed that BCL-xL overexpression has an important and reproducible function in determining the overall level of cell survival to chemical insult. TAMH-BCL-xL cells were less susceptible to TFEC-induced cell death as compared to both the parental TAMH and the TAMH-Vc cell lines. The possibility remains that this cytoprotective effect of BCL-xL on chemically-mediated necrotic damage may translate into an effective chemo-preventative therapeutic strategy.

In summary, a cytoprotective action of BCL-xL on BAX-mediated toxicity has been demonstrated in TFEC-induced cell death. BAX activation appears as an early event in TFEC-induced cell death and our findings may open new avenues for the design of BCL-xL mimetics in the treatment of adverse effects from other compounds, previously considered necrotic in mechanism, but similarly acting through a BAX pathway.

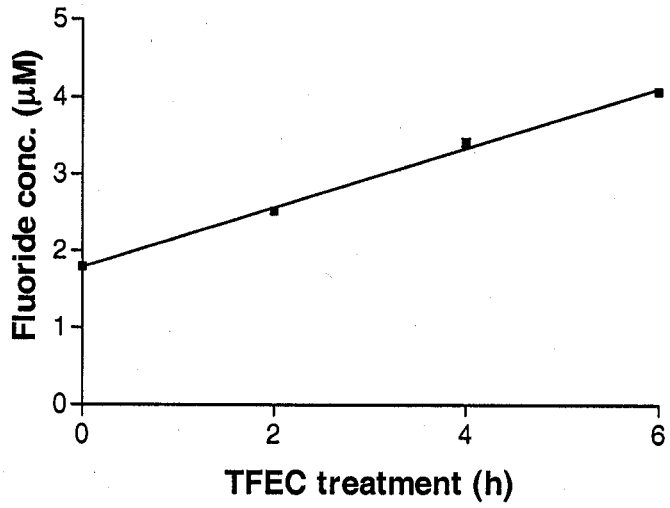

Figure 2.1 **Metabolism of TFEC by β-lyase**. TFEC undergoes rapid defluorination after the formation of the thiolate intermediate from a β-lyase cleavage. Subsequent protein adduction by DFTAL will release another fluoride ion.. Hence, a quantification of fluoride is an indirect indication of β-lyase mediated metabolism of TFEC. Results confirm a time-dependent linear increase in fluoride concentration after incubation of TAMH cells with TFEC (250 μM) for 0-6 h. A detectable level of fluoride concentration at 0 h was likely due to degradation of the TFEC stock solution during prolonged storage (i.e. more than a week at 4 °C).

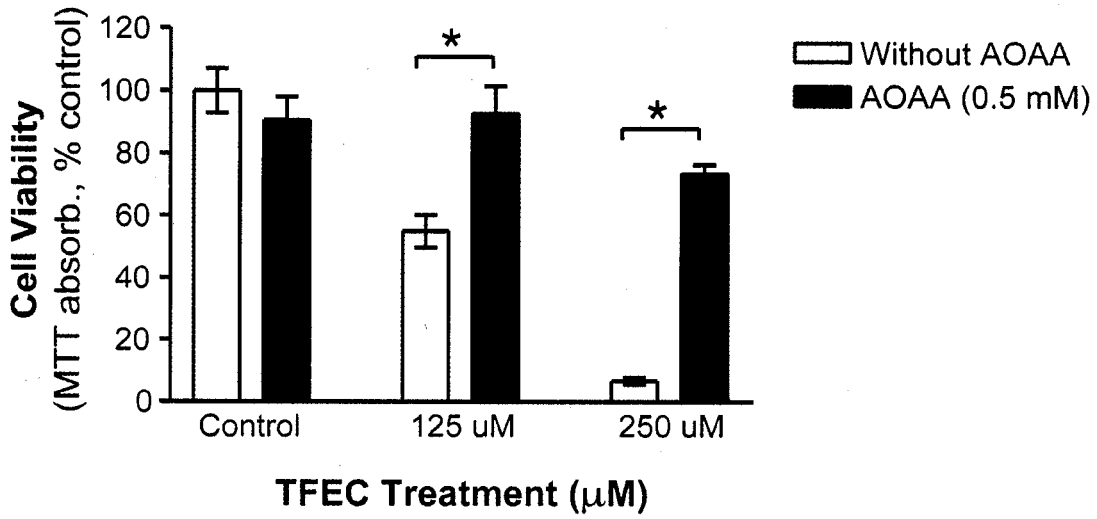

Figure 2.2. **Cytoprotective effect of AOAA on TFEC toxicity.** TAMH cells were treated with 125-250 μM of TFEC for 24 h, with or without AOAA (0.5 mM) administration. AOAA completely blocked TFEC toxicity at 125 μM, as determined by MTT viability assay. More than 6-fold increase in viability was observed at 250 μM TFEC treatment. (* denote statistically significant differences between AOAA treated and non-treated samples).

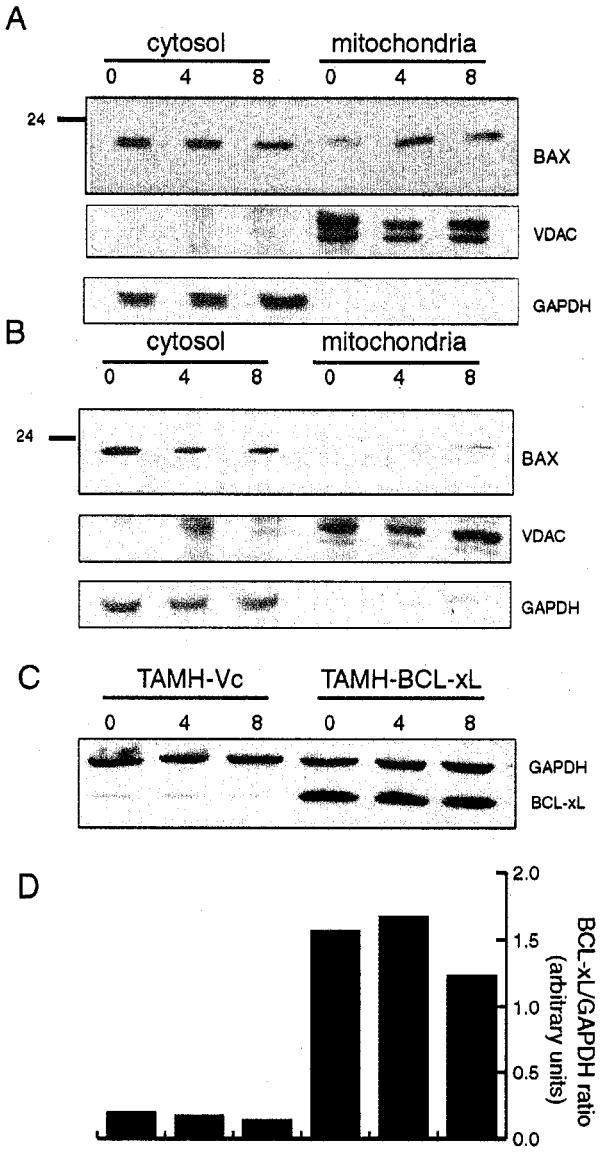

Figure 2.3 **Immunoblot assay for BAX following TFEC treatment of TAMH-Vc and TAMH-BCL-xL cells.** (A) TAMH-Vc cells were treated with 250 μM TFEC for 0, 4 and 8 h. Subcellular fractions of cytosol and mitochondria were separated and immunoblotted with monoclonal anti-BAX. Polyclonal anti-GAPDH and anti-VDAC were employed as loading controls for cytosol and mitochondria, respectively. (B) TAMH-BCL-xL cells were treated and immunoblotted in the same manner as for TAMH-Vc cells above. (C) Total cell lysates from TAMH-Vc and TAMH-BCL-xL cells treated with 250 μM of TFEC for 0, 4 and 8 h immunoblotted with polyclonal anti BCL-xL to confirm the extent of its overexpression in TAMH-BCL-xL cells as compared to TAMH-Vc cells. (D) Densitometric analysis of BCL-xL expression in TAMH-Vc and TAMH-BCL-xL cells, displayed as a ratio of GAPDH to BCL-xL for each treatment time point.

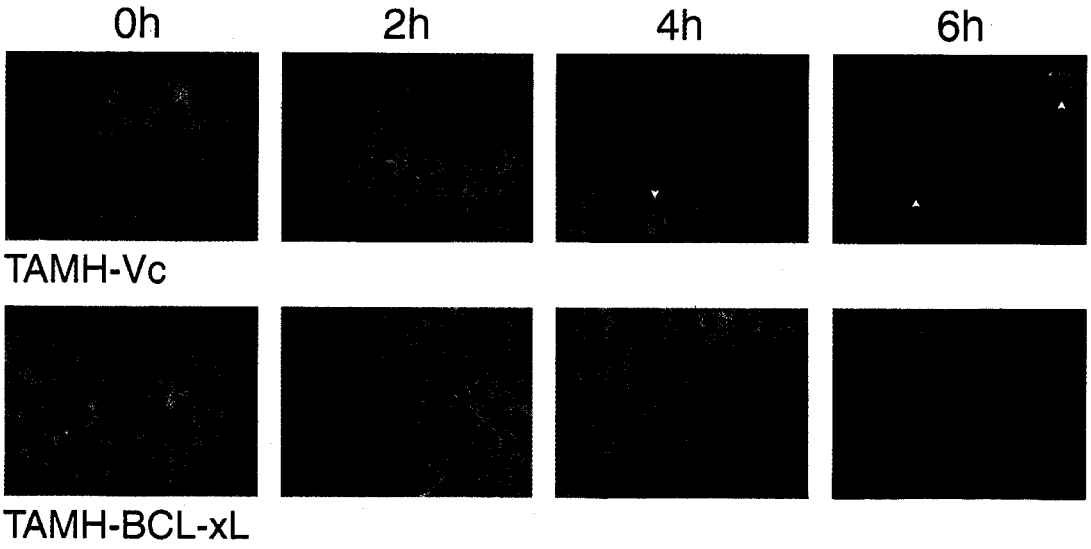

Figure 2.4 **Immunocytochemical detection of BAX localization**. TAMH-Vc (left panel) and TAMH-BCL-xL cells were treated with 250 μM TFEC for 2, 4 and 6 h. Mitochondria were stained with MitoTracker™ Red and BAX with AlexaFluor 488-conjugated anti-mouse antibodies. The cells were fixed on a slide and viewed with a fluorescent microscope. Movement of BAX from the cytosol to mitochondria was observed with a progressive decrease in green and corresponding increases in orange/yellow – indicative of dye-merging between FITC and MitoTracker Red. (Arrows indicate cells having advanced necrotic morphology).

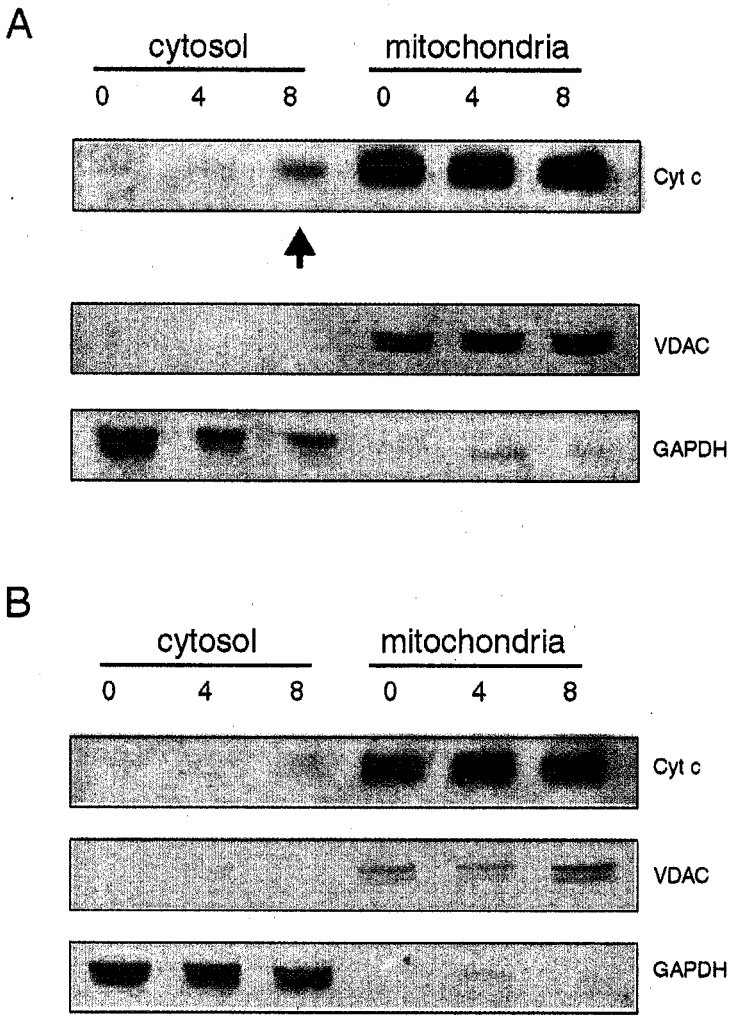

Figure 2.5 **Immunoblot assay for cytochrome *c* release following TFEC treatment of TAMH-Vc and TAMH-BCL-xL cells**. (A) TAMH-Vc cells were treated with 250 μM TFEC for 0, 4 and 8 h. Subcellular fractions of cytosol and mitochondria were separated and immunoblotted with monoclonal anti-cytochrome *c*. Polyclonal anti-GAPDH and anti-VDAC were employed as loading controls for cytosol and mitochondria, respectively. (B) TAMH-BCL-xL cells were treated and immunoblotted in the same manner as for TAMH-Vc cells above. (Arrow indicates a significant release of cytochrome c into the cytosol of TFEC treated TAMH-Vc cells).

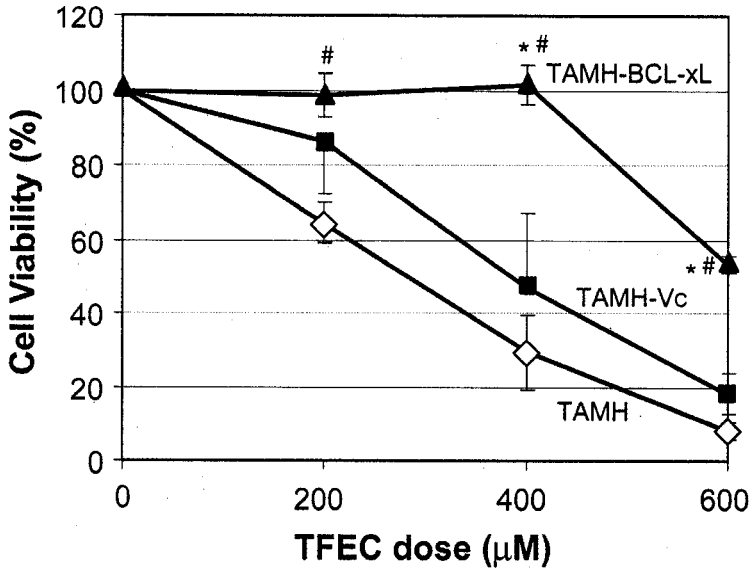

Figure 2.6 **Viability of TFEC-treated TAMH, TAMH-Vc and TAMH-BCL-xL cells**. Cells were treated with 200, 400 or 600 μM TFEC for 12 h in total. Viability was measured by MTT assay. Results are expressed as a percentage of viable cells in the untreated controls with +/- SD. (* indicates statistical difference between the TAMH-BCL-xL and TAMH-Vc and # indicates difference between TAMH-BCL-xL with TAMH by unpaired t-test, $p<0.05$).

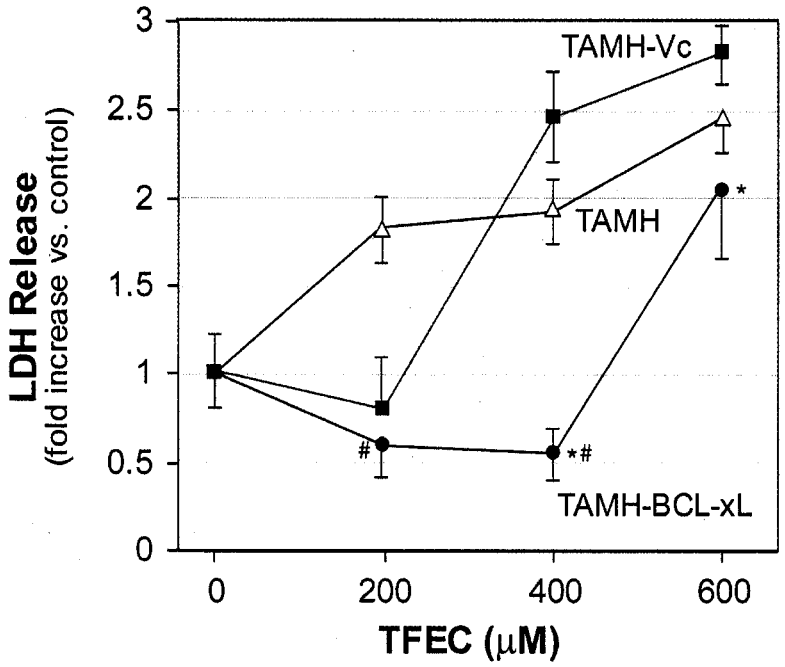

Figure 2.7 **Cytotoxicity of TFEC-treated TAMH, TAMH-Vc and TAMH-BCL-xL cells.** Cells were treated with 200, 400 or 600 μM of TFEC for 8 h in total. Cytotoxicity was measured by the cumulative release of LDH into the culture media. Results are expressed as the number of fold increase in LDH activity (n=8) vs. untreated cells (number of fold activity = 1). (* indicates statistical difference between the TAMH-BCL-xL and TAMH-Vc and # indicates difference between TAMH-BCL-xL with TAMH by unpaired t-test, $p<0.05$).

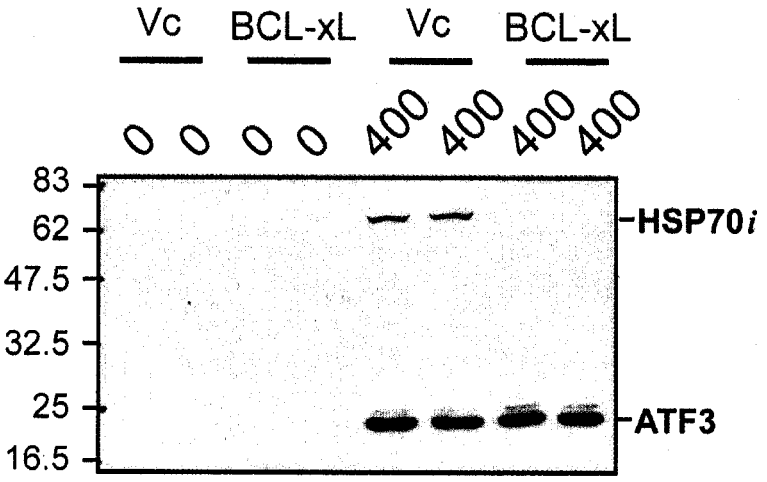

Figure 2.8 **Effects of TFEC treatment on HSP70i and ATF3 expression.** TAMH-Vc and TAMH-BCL-xL cells were treated with TFEC (400 μM) for 4 h followed by incubation in standard growth medium not containing TFEC for a further 8 h (12 h in total). Immunoblot assays were performed using 20 μg total cell lysate protein loaded onto each lane and blotted with polyclonal anti-ATF3 and monoclonal anti-HSP70i.

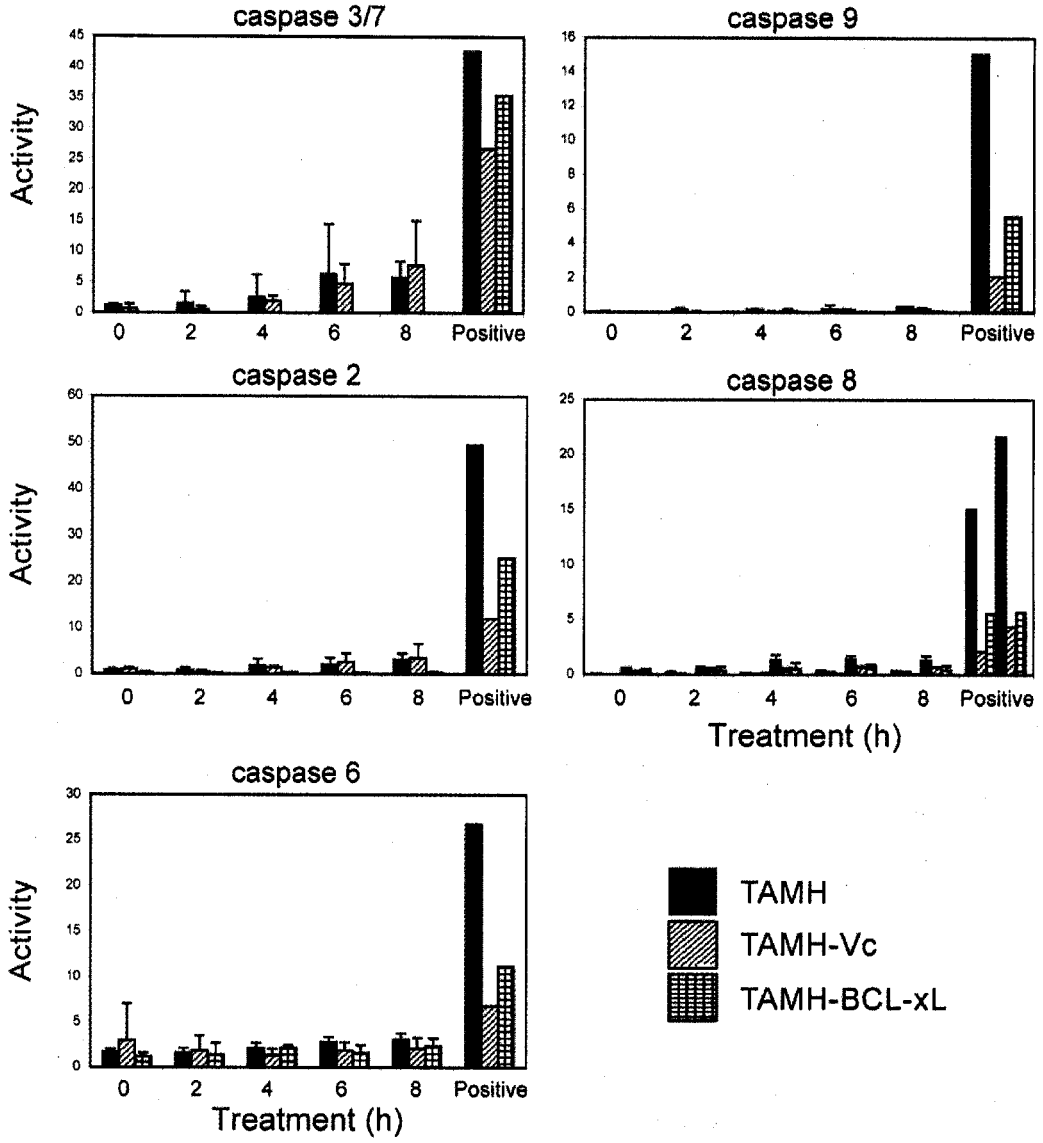

Figure 2.9 **Caspase activity assays for TFEC treated TAMH, TAMH-Vc and TAMH-BCL-xL cells.** Cells were treated with 250 mM of TFEC for 2, 4, 6 and 8 h. Caspase activities were quantified by the amount of specific fluorogenic caspase-substrates hydrolyzed (pmol of AMC substrates) per μg total lysate protein per minute of incubation for the assay with +/- SD (n=3). These values were compared against an actinomycin-D/TNF-α treated positive control for 8 h. The substrates used were (A) Ac-DEVD-AMC for caspase-3/7; (B) Ac-VDVAD-AMC for caspase-2; (C) Ac-VEID-AMC for caspase-6; (D) Ac-IETD-AMC for caspase-8; (E) Ac-LEHD-AMC for caspase-9.

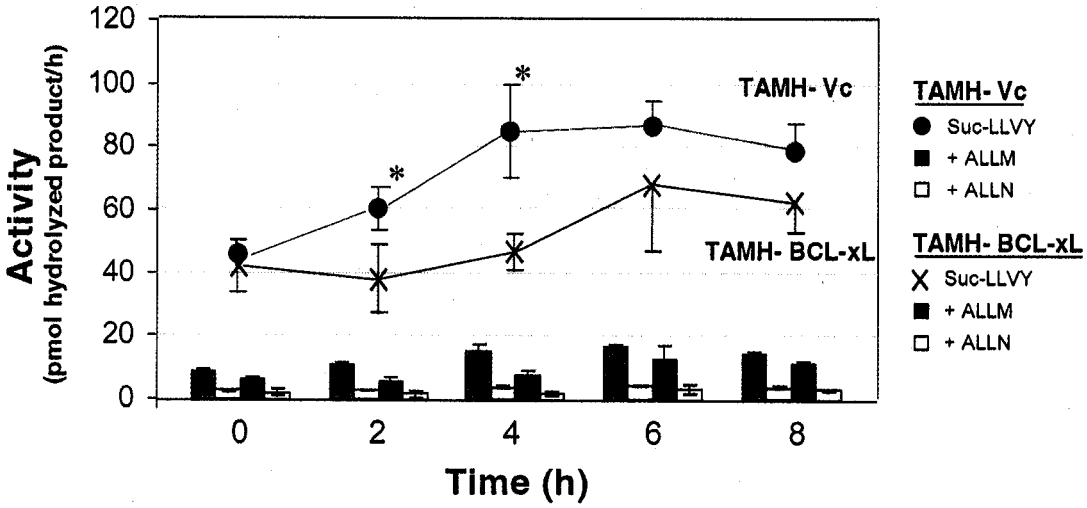

Figure 2.10 **Calpain activity assays for TFEC treated TAMH-Vc and TAMH-BCL-xL cells.** Cells were treated with 250 mM of TFEC for 2, 4, 6 and 8 h. Calpain activity was quantified by the amount of specific fluorogenic calpain substrate hydrolyzed (pmol of Suc-LLVY-AMC) per μg total lysate protein per minute of incubation for the assay with +/- SD (n=3). Specific calpain inhibitors, ALLM and ALLM were coadmininstered in parallel experiments to demonstrate the selectivity of the activation. (* indicates statistical difference between the two cell lines by unpaired t-test, $p<0.05$)

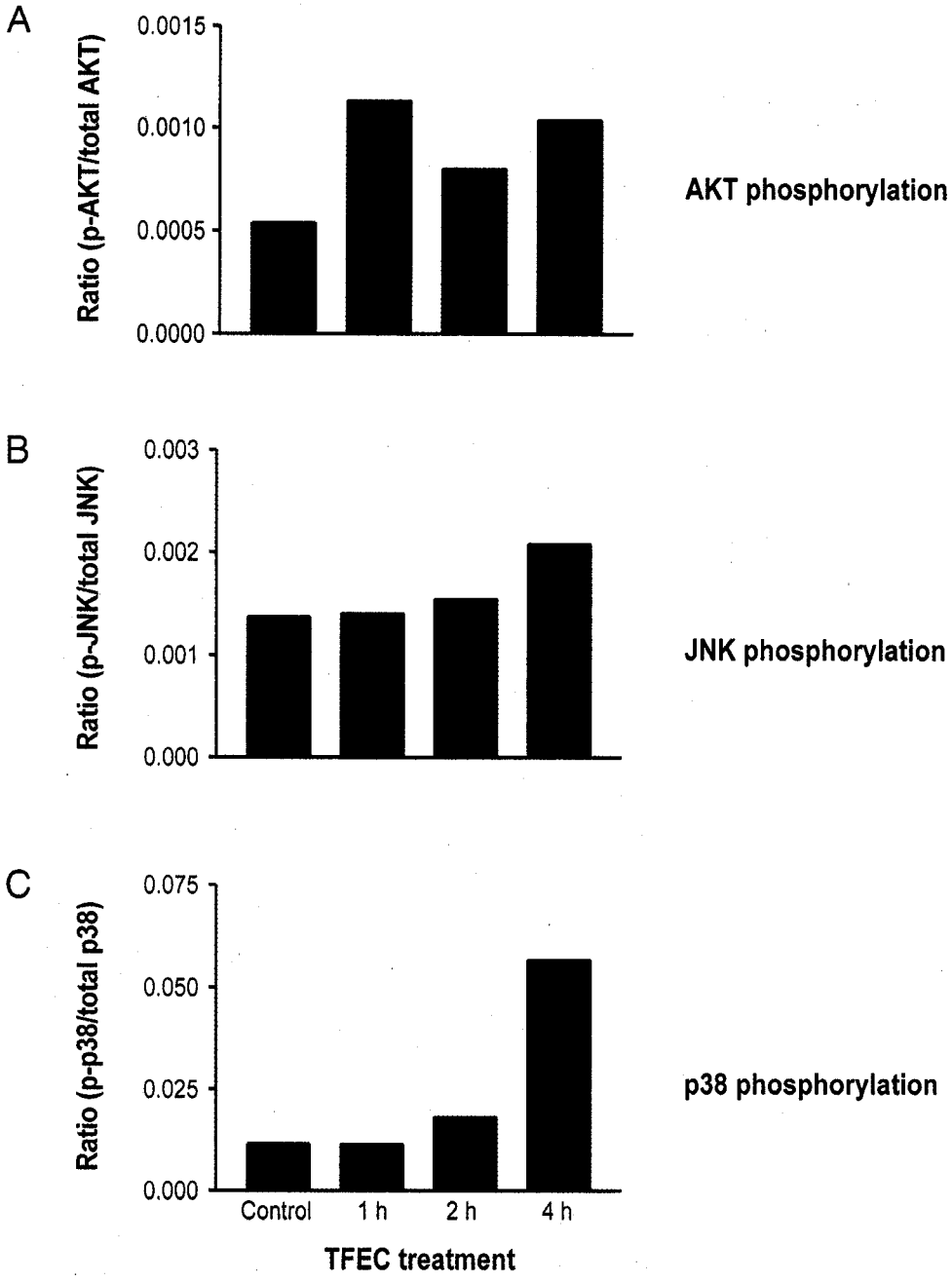

Figure 2.11 **Phosphorylation of stress-activated protein kinases by Bioplex™ system.** TAMH cells were treated with TFEC (200 μM) for 1, 2 or 4 h. The cell lysates were then subjected to a mouse 3-plex phosphorylation analysis. The results of protein kinase phosphorylation is expressed as an average of the ratio of phosphorylated protein to their respective total protein levels (n = 2). The 3 stress-activated protein kinases examined include (A) AKT, (B) JNK, (C) p38.

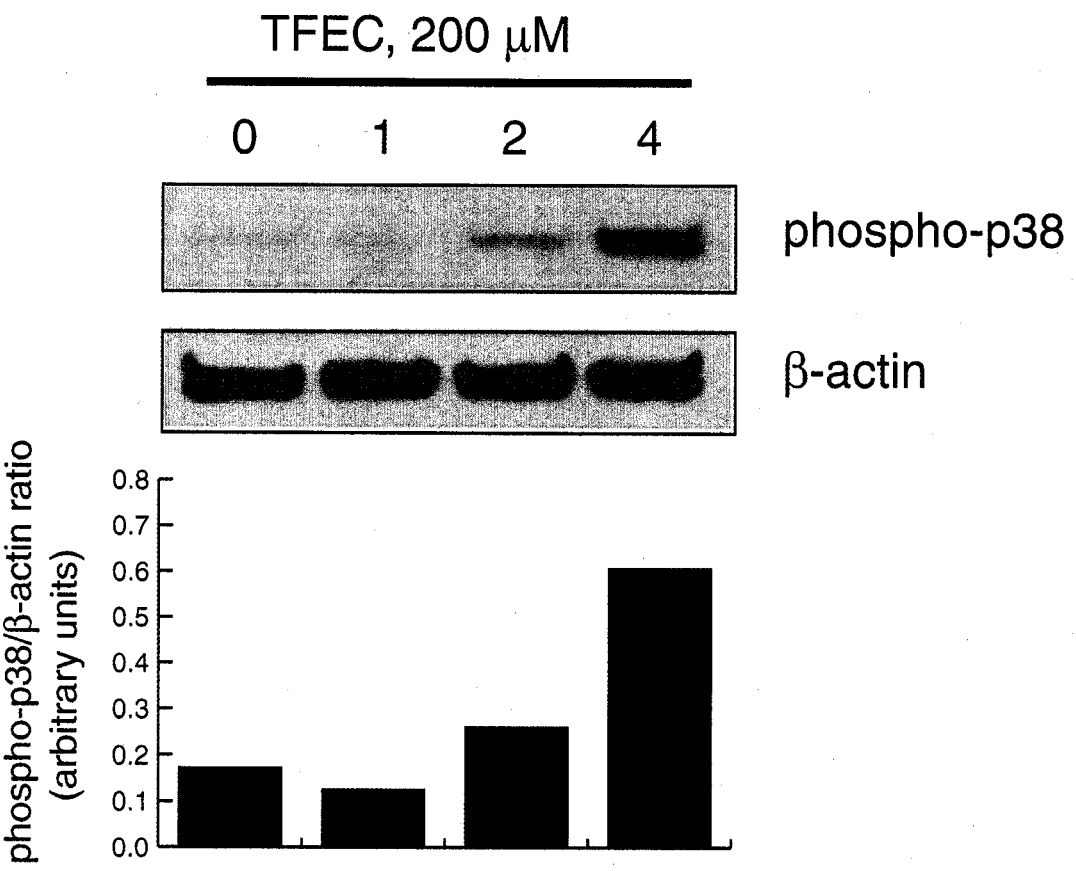

Figure 2.12 **Immunoblot analysis of p38 phosphorylation following TFEC treatment.** TAMH cells were treated with TFEC (200 μM) for 1, 2 or 4 h. The cell lysates were separated by SDS-PAGE and probed with anti-phospho-p38 polyclonal antibody. Monoclonal anti-β-actin was employed as a loading control.

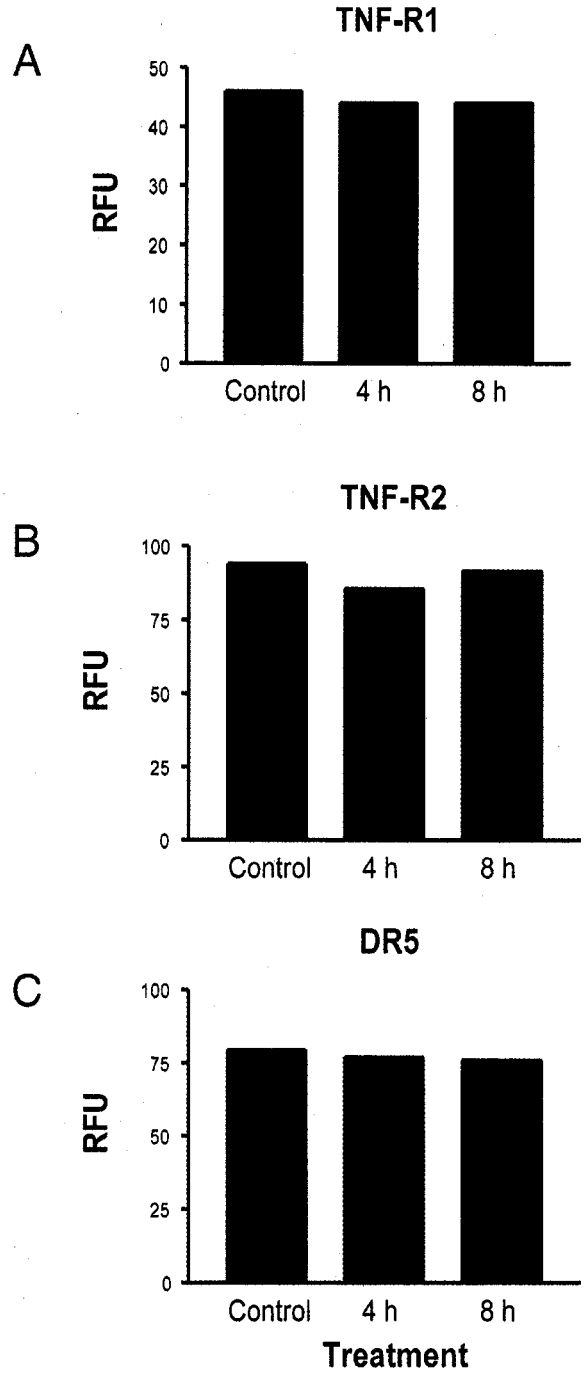

Figure 2.13 **Quantifying release of death receptors by Bioplex™ system.** TAMH cells were treated with TFEC (250 μM) for 4 and 8 h. The cell culture medium after treatment were harvested and subjected to a 3-plex death receptor analysis on the Bioplex™ system. The release of death receptors: (A) TNF-R1, (B) TNF-R2 and (C) DR5 is expressed as relative fluorescence unit (RFU).

Chapter 3

Extramitochondrial Responses: Selective Induction Of Cytosolic Heat Shock Proteins

3.1 Introduction

Although biochemical pathways affected by mitochondrial dysfunction have been well studied in several systems, there remain many effects that are not completely understood. For example, it is not clear how mitochondrial lesions evoke a communication with the nucleus to induce transcription of nuclear-encoded response genes. This phenomenon, often referred to as mitochondria-to-nucleus retrograde signaling, is analogous to the RTG system in yeast (Butow 2002; Butow and Avadhani 2004). Earlier work has identified cytochrome *b*, an integral part of Complex III of the electron transport chain, as a likely mammalian equivalent of RTG3 in yeast through homology matching by RT-PCR (Adams 2003). In a more recent report, further evidence for a mitochondria-to-nucleus signaling was demonstrated with altered nuclear gene expression (such as depletion of cathepsin and BCL2 mRNAs) and phenotypic changes following mitochondrial dysfunction and mtDNA damage (Biswas *et al.* 2005). Further data were presented to support a role for calcium dysregulation in initiating this stress signaling. Clearly, events culminating in cell death resulting from "mitochondrial diseases" involve organelles other than the mitochondria, either directly or tangentially, and the extramitochondrial responses may either protect the cells or propagate the injury. Thus, we were interested in investigating the generalized cellular responses to mitochondrial damage in an attempt to identify signature events and also, to pinpoint potential subcellular targets that might be exploited for therapy against such pathologies.

To work towards this objective, TFEC was used as a toxicant that is known to elicit intramitochondrial stress as an initiating event in cytotoxicity. As described in Chapter

2, a mouse hepatocyte cell line (TAMH) was used as a model for TFEC-induced cytotoxicity (James *et al.* 2002; Pierce *et al.* 2002; Wu *et al.* 1994). The goals of the studies reported in this chapter were to identify early transcriptional and translational changes that might be crucial in the manifestation and progression of cytotoxicity.

3.2 Materials and Methods

3.2.1 Cell culture

Serum-free cell culture of the TAMH line was cultured as described in Chapter 2.

3.2.2 RNA isolation

Cells were grown to confluence in 150 cm^2 tissue culture dishes in quadruplicate for each sample, and treated with 200 μM TFEC for 2, 4 and 6 h. At the end of respective treatments, cells were harvested by scraping with a rubber policeman. The resultant cell pellets were spun down and washed once with Dulbecco's PBS (Invitrogen). Immediately, 1 mL of Trizol reagent (Invitrogen) per 10^7 cells was added for cell lysis. After vortexing, the lysate was passed through 22G needles 10 times to ensure complete lysis. Quickly, 0.2 mL of chloroform was added to every 1 mL of cell lysate and vortexed vigorously for 15 s (1 mL aliquots of lysates were measured out into microcentrifuge tubes). The tubes were left to stand for 2-3 min before spinning at 10,000 rpm for 15 min at 4°C. Gently, 0.5 mL of aqueous phase was transferred to a fresh tube, and an equivolume of 70% ethanol was added. This resulting mix was loaded onto an RNeasy column (Qiagen, Valencia, CA) and purified total RNA was extracted according to the manufacturer's protocol.

3.2.3 Microarray analysis procedures

Gene expression analyses were performed using the Amersham, Codelink 10K mouse array (Amersham Biosciences, Piscataway, NJ) according to manufacturer's protocols. Briefly, total RNA from each sample was quantified before first and second strand cDNA synthesis. The resulting double-stranded cDNA was purified with a QIAquick spin column (Qiagen). After drying the cDNA in a SpeedVac concentrator, cRNA was

synthesized by *in vitro* transcription (IVT) and purified using the RNeasy kit (Qiagen). The quality of the cRNA was evaluated using an Agilent 2100 Bioanalyzer (Agilent, Palo Alto, CA) and samples with A260:A280 ratio of 1.8-2.1 were used for subsequent microarray analysis. Each 10 μg of cRNA sample was hybridized onto Codelink microarray slides and incubated for 18 h at 37 °C. At the end of incubation, the arrays were washed with 0.75X TNT buffer (0.1 M Tris-HCl pH 7.6, 0.15 M NaCl, 0.05 % Tween-20) at 46°C for 1 h and incubated with streptavidin-Alexa 647 (Molecular Probes, Eugene, OR) working solution at 25°C for 30 min to label the fluorogenic probe. The arrays were scanned with an Axon GenePix 4000B fluorescent scanner and the GenePix Pro imaging software (Axon Instruments, Foster City, CA). Fluorescent intensity of each spot in the image was determined using ImaGene™ 5 (Biodiscovery, Marina del Rey, CA) for spot finding and analysis.

3.2.4 Quantitative RT-PCR

Quantitative RT-PCR was carried out using an ABI Prism 7700 Sequence detection system (Applied Biosystems, Foster City, CA) with SYBR Green dye as the fluorogenic probe. The thermal cycling condition comprised an initial denaturation step at 95 °C for 10 min, followed by 40 cycles at 95 °C for 20 s and 62 °C for 60 s. The gene-specific sequences of the primer pairs and probes used in the assays were as follows: *HSP25* (NM_013560): forward primer, TGTCCCTGGACGTCAACCACTT; reverse primer, ACCTGGAGGGAGCGTGTATTTC. *HO-1* (NM_010442): forward primer, GCACAGGGTGACAGAAGAGGCTA; reverse primer, ATCTGTGAGGGACTCTGGTCTTTGT. *HSP40* (NM_006145): forward primer, GGGACCAGACCTCGAACAACAT; reverse primer, ACCACAGAGAGCCTCCCGAA. *HSP105* (NM_006644): forward primer, GAGGCAAGGATGAGAAATACAACCAC; reverse primer, CAATTCCTTGACCTTCGCTCTGAT. *HSP60* (X53584): forward primer, AAGCTGAACGAGCGACTTGCTAA; reverse primer, GCTGCTCTTGTAGCATTGAGAGCA. *mtHSP70* (NM_010481): forward primer,

CAGCGCTCATTGAAACTCTTC; reverse primer, GTGCCAGAACTTCCAGAACCTTC. *HSP70i* (M12573): forward primer, TCCTATGCCTTCAACATGAAGAGC; reverse primer, GAGATGACCTCCTGGCACTTGTC. *GAPDH* (NM_008084): forward primer, TCCTGCACCACCAACTGCTT; reverse primer, GAGGGGCCATCCACAGTCTT.

3.2.5 Statistical analysis and data normalization

Statistical analysis and data normalization were carried out with Bioconductor software (Harvard University, Boston, MA). The foreground spot intensities from all the bioarrays used for the experiment were normalized as a group using quantile normalization as described previously (Bolstad *et al.* 2003). Heat maps of selected HSP expression profiles were generated using GeneSifter software (VizXlabs, Seattle, WA).

3.2.6 Subcellular fraction isolation

Mitochondrial-enriched fractions were isolated as described in Chapter 2.

3.2.7 Immunoblotting

All fractions collected were assayed for protein concentration using the BCA protein assay kit (Pierce Chemical Co., Rockford, IL). Each 30-50 μg of sample proteins were resolved by denaturing electrophoresis using 8-15% SDS-PAGE (Mini-PROTEAN II, Bio-Rad Laboratories, Hercules, CA) and transferred to nitrocellulose membranes for 1 h at 15 V using Trans-Blot SD Semi-Dry Transfer Cell (Bio-Rad). Immunodetection was by chemiluminescence (SuperSignal ULTRA, Pierce, Rockford, IL) using specific antibodies diluted in PBS with 0.05% (v/v) Tween 20 and 5% (w/v) powdered milk. Anti-HSP25, anti-HO-1, anti-HSP40, anti-HSP60, anti-HSP70i and anti-grp75 were from Stressgen (Victoria, BC); anti-HSP105 was from Santa Cruz and anti-GAPDH (1:2500) was made in-house (Dietze *et al.* 1997). Secondary anti-mouse and anti-rabbit horseradish peroxidase conjugated secondary antibodies (Pierce) were used

at 1:20,000 dilution. All antibodies were used at 1:2,000 dilution unless otherwise stated.

3.2.8 DEAE-sepharose column purification of HSP25

Cells were grown to confluence in fifteen T150 dishes and treated with TFEC (6 h, 250 μM). Whole cells were washed in ice-cold PBS and harvested by scraping. The cells were pelleted in microcentrifuge tubes and lysed in 4.5 mL of lysis buffer with sonication (as described in Chapter 2). The resulting cell lysates were centrifuged at 14,000 rpm for 15 min and supernatant was applied to a 2 x 10 cm column composed of diethylaminoethyl (DEAE)-sepharose fast-flow resin (Sigma) was used in a 2 x 10 cm column, pre-equilibrated with buffer containing 20 mM Tris, 0.1 mM EDTA, 2 mM DTT and 0.1% CHAPS. After adding the sample, equilibration buffer was passed through with a continuous gradient from 0 to 1 M NaCl (total volume of 400 mL), maintained at a flow rate of 1 mL/min. Eighty fractions were collected (approx. 5 mL each). Every third fraction was screened for HSP25 by Western blot and the fraction with the highest concentration of the HSP25 was subjected to subsequent analysis.

3.2.9 HSP25 silencing by siRNA

Cells were grown on 6-well plates to 60-70% confluence before transfection with siRNA (small interfering RNAs). Custom-made siRNA designed for silencing *HSP25* (Accession number: NM_013560) expression was obtained from Santa Cruz. Various volumes (4-8 μL) of 10 μM siRNA were added to 80 μL of transfection medium (OptiMEM, Invitrogen) and incubated at room temperature for 5 min. Separately, transfection reagent (4-8 μL; Dharmafect4, Dharmacon, Chicago, IL) was incubated with transfection medium (80 μL) for the same duration. The two tubes were mixed gently and incubated at room temperature for 20 min. Immediately following this incubation period, TAMH cells were washed with transfection medium. Six hundred and forty μL of transfection medium were added to the siRNA/transfection reagent mix and the entire volume was added onto the cells. After incubation at 37 °C for 6 h, 800 μL of normal growth medium (DMEM/F12) was added to each well. Incubation

was continued for 24 h and thereafter, medium was replaced with fresh growth medium and cells were incubated for another 24 h. Cells were harvested by trypsinization and subjected to immunoblot analysis for evaluation of transfection efficiency. Cells with an optimum siRNA/transfection reagent ratio for gene silencing were treated with TFEC. TFEC was administered 30 h after the initial transfection. A scrambled siRNA sequence was used as a negative control (Ambion, Austin, TX)

3.2.10 Viability assays by MTT

Cells were seeded and grown to confluence on 96-well plates. After TFEC treatment, the MTT assay was performed as previously described in Chapter 2. For heat shock experiments, 96-well plates were suspended in a shaking water bath maintained at 43 °C for 1 h. TFEC was administered 12 h after the initial heat shock. Hemin pretreatment involved incubation of TAMH cells with hemin (20 μM) for 1 h. Hemin was removed and TFEC treatment was administered at 4 h after the initial hemin pretreatment.

3.3 Results

3.3.1 Microarray analysis of TFEC treated TAMH cells

To assess genomic responses to TFEC-induced intramitochondrial damage, microarray analysis was performed on TFEC-treated TAMH cells over a period of 2-6 h. A total of 67, 179 and 303 genes were differentially regulated (> 2 fold or < 0.5 fold) at 2, 4 and 6 h, respectively (Table 3.1). Briefly, a large number of genes relating to homeostatic stress responses, apoptosis, metabolism, transporters and transcriptional regulation were upregulated, while genes associated with cell cycling and immune response were down-regulated after TFEC treatment (Table 3.2).

Among the early stress responses detected, the most significant were upregulation of a number of genes belonging to the heat shock protein superfamily. More than two-fold increases were observed for *HSP70i* (denoted as HSP68 and HSP68A on the array), *HSP40* (*HSP40B*1 and *HSP40B9*), *HSP25*, *HSP86* and *HSP105* 4 h after treatment

with TFEC (Figure 3.1A). The most highly upregulated gene was *HSP70i*, whose expression increased by 19.6 and 35.7-fold at 4 and 6 h, respectively. Heme oxygenase-1 (HO-1) also demonstrated a dramatic induction of 17.2-, 29.4- and 31.0-fold vs. control cells at 2, 4 and 6 h, respectively (Table 3.3). More importantly, this HSP regulation profile is unique to TFEC, as other known hepatotoxicants treated at concentrations that caused approximately the same extent of lethality in TAMH cells (including acetaminophen, rotenone, diquat and flutamide), do not yield a similar pattern (Figure 3.1). As shown in the heat-map of nine representative *hsp* gene expression profiles, TFEC (4 and 6 h) treated cells clustered closely together (Figure 3.1).

3.3.2 Quantitative RT-PCR analysis of heat shock proteins

To validate the upregulation of these *hsp* transcripts, quantitative real-time PCR was performed on selected HSPs. As clearly demonstrated in Figure 3.2, we have confirmed the transcriptional upregulation of *HO-1* (or *HSP32*), *HSP70i*, *HSP25*, *HSP40* and *HSP105*. In contrast, mitochondrial *HSP60* and *mtHSP70* both showed a lack of induction at any time point examined.

3.3.3 Immunoblot analyses of heat shock protein expression

Confirmatory Western blots were performed to determine if increased protein expression paralleled transcriptional upregulation. Accordingly, TAMH cells were treated with 250 μM TFEC and total cell lysates were probed with specific antibodies/antisera to heat shock proteins of interest using standard procedures as described in Materials and Methods. We observed a significant upregulation of HSP70i from 2- 8 h (Fig. 3.3A). Microsomal HO-1 also showed a time-dependent induction. However, levels of HSP40 and HSP105 did not show any significant increase despite obvious transcriptional changes. Other ER-bound and mitochondrial HSPs did not manifest TFEC-dependent induction.

A novel immunoreactive band against HSP25 was observed that was inducible after continued incubation with TFEC. This protein had a MW of approximately 50 kDa, suggestive of a dimer of HSP25. Interestingly, it was non-dissociable, even under an extreme denaturing and reducing environment using high concentrations of DTT (up to 500 mM) and β-mercaptoethanol (up to 2 M) as shown in Figure 3.3B. When cell lysates were partially purified with DEAE-sepharose column, the 50 kDa band became more sensitive to DTT (100 and 200 mM) and Tris(2-carboxyethyl)phosphine (TCEP; 1 and 10 mM) reducing conditions. At 10 mM TCEP, the band completely dissociated into its corresponding monomer at 25 kDa (Figure 3.3C). The subcellular localization of HSP25 was determined by probing cytosolic and mitochondrial fractions of TAMH cells treated for 0, 4 and 8 h with TFEC. As shown in Figure 3.3D, the 25 kDa immunoreactive band decreased in the cytosol with a corresponding increase in the mitochondria after 4 and 8 h. The higher molecular weight bands were only apparent after treatment with TFEC, and were localized in both compartments. However, the apparent dimer decreased in the cytosol with a concomitant increase in mitochondria over time (Figure 3.3D). Minute quantities of GAPDH was detected in the mitochondrial fraction at 8 h treatment with TFEC. This could be due to contamination of mitochondria fraction with cytoslic material during fraction subcellular fraction isolation.

3.3.4 HSP25 silencing by siRNA

To provide evidence for the formation of an HSP25 dimer, the gene was silenced by siRNA. Effective gene silencing was achieved with 4 μL of siRNA (10 mM) plus 6 μL of transfection reagent for each well in a 6-well dish. The efficiency of the silencing was approximately 85% 48 h after initial transfection (Figure 3.4A). Cells treated under these conditions were subsequently treated with TFEC. At 8 h post-treatment (250 μM), HSP25 protein expression was reduced to about 25% of control. Likewise, the expression of the apparent dimer was reduced to 20% of control, with little change in expression level of HSP25 in either untransfected or scrambled siRNA transfected cells (Figure 3.4B).

To determine the functional impact of a reduced HSP25 expression by gene silencing, MTT viability assay was performed on TFEC (250 and 500 μM for 8 h) treated TAMH cells with prior vehicle transfection or HSP25 siRNA transfection. However, no significant change in viability was observed between them (Figure 3.4C).

3.3.5 Heat shock pretreatment of TAMH cells

The functional significance of the apparently coordinated upregulation of heat shock proteins was evaluated using a "gain-of-function" approach. A mild heat shock pretreatment can be used to non-selectively induce HSP without causing lethality in host cells, a phenomenon also known as heat shock preconditioning (De Maio 1999; Kregel 2002; Ritossa 1996). Since HSP response is cell-type dependent, the heat shock response in TAMH cultured cells was examined using an initial 43 °C/30 min incubation, and HSP expression at various timepoints after the initiation of the temperature shock was then assessed by Western analysis. As shown in Figure 3.5, HSP70i, HSP40, HSP25 and HSP105 were all upregulated between 4-16 h after heat shock pretreatment. The mitochondrial levels of HSPs including mtHSP70 (a.k.a. grp75) and HSP60 were mildly upregulated relative to cytosolic HSP responses. In separate experiments, the expression of these HSPs was optimized by changing the duration of heat shock (15 min to 3 h) as well as varying the temperature (37 to 45 °C) (data not shown). These results helped us establish the optimum conditions for heat shock in TAMH cells at 42-43 °C for 30-60 min, and the maximum induction of HSPs occurred between 4-16 h after the initial heat shock.

3.3.6 Cytoprotective effects of heat shock pretreatment on TFEC-induced toxicity

TAMH cells were incubated with TFEC (250 μM) for 0-12 h after an initial heat shock treatment. Cellular viability was assessed using MTT assay. Results demonstrated a significant increase in viability of TAMH cells at 8 and 12 h after TFEC treatment. Cells treated with higher doses of TFEC (500 μM) showed improved

survival after heat shock, although a complete reversal to control cell viability was not apparent (Figure 3.6).

3.3.7 Cytoprotective effect of heme oxygenase-1 induction

Since HO-1 is the most strongly upregulated gene observed based on microarray analysis, its potential role in cytoprotection was investigated in a separate "gain-of-function" experiment. Hemin was administered to induce the expression of HO-1. A concentration of 20 μM for 1 h was sufficient to induce HO-1 expression over a period of 48 h with peak levels occurring between 8-24 h (Figure 3.7A). Based on this information, TAMH cells were pretreated with hemin 4 h prior to various TFEC doses and incubated for 4, 8 and 24 h. No significant protection occurred after 4 and 8 h. After 24 h, more than 3-fold improvement in viability was observed. However, this protection did not occur after incubation with supratoxicological concentrations of TFEC (400 and 600 μM) (Figure 3.7B).

To evaluate if the apparent cytoprotective effect of hemin at 24 h post-TFEC administration is due to the enzymatic role of HO-1, we inhibited the catalytic activity of HO-1 with tin protoporphyrin-IX (SnPP). Treatment with SnPP (20 μM) caused a modest, but significant increase in toxicity after 6 h and 24 h treatment with TFEC (Figure 3.8).

3.3.8 Delayed induction of ferritin by hemin pretreatment

One important consequence of heme oxygenase endogenous activity is the metabolism of heme and the release of free iron, which then induces ferritin expression. The extent of ferritin induction has been shown to correlate with the cytoprotective effect, potentially resulting from its antioxidant potential (Gonzales *et al.* 2002; Otterbein and Choi 2000). Hence, ferritin induction was measured by immunoblot assay after administration of hemin (20 μM), just as in the preconditioning experiment with TFEC shown in Figure 3.7. A time-dependent increase in ferritin expression over the

entire incubation period of 0-48 h was observed (Figure 3.9). The most pronounced increase was at 24 h.

3.4 Discussion

In this study, TFEC was used to induce mitochondrially-directed subcellular damage in an attempt to investigate the early genomic responses to mitochondrial dysfunction. Microarray analysis of TAMH cells treated with TFEC showed time-dependent increases in gene expression over the first 6 h. Apart from genes known to inhibit cell cycling, signal transduction, transcriptional regulation and metabolism, TFEC demonstrated a robust induction of heat shock proteins that was different from what was observed after incubation of TAMH cells with other cytotoxicants. This result is consistent with the hypothesis that heat shock response is an important cellular defense mechanism in the face of intramitochondrial dysfunction (Sammut and Harrison 2003).

Heat shock proteins are now recognized as a superfamily of stress proteins, first observed in 1962 during transient heat shock experiments with *Drosophila melanogaster* (De Maio 1999; Kregel 2002; Ritossa 1996). Subsequent work has shown that HSP induction is responsive to a broad range of endogenous and exogenous cell stressors. Most HSPs have well-defined subcellular localization. For example, HSP60 is predominantly mitochondrial, HSP70i is cytosolic and GRP78 is ER-bound. A generalized, but not exclusive role, for heat shock proteins is to bind exposed hydrophobic regions of unfolded, misfolded or modified proteins in order to help attain/restore biological function. HSP70 is the most well-characterized chaperone for its binding of nascent, transported and misfolded proteins together with the co-chaperones HSP40 and GrpE. Refolding processes requiring these HSPs are energy-dependent and require ATP hydrolysis to avoid kinetically trapped intermediates (De Maio 1999).

TFEC treatment of TAMH cells resulted in dramatic inductions of *HSP70i*, *HO-1*, *HSP40*, *HSP25*, and *HSP105* within the first 4 h of treatment as confirmed by both microarray and RT-PCR. Corresponding increases in protein expression were also observed for HSP70i and HO-1 over the first 8 h. Although we did not observe commensurate evidence of protein upregulation for *HSPs* other than HSP70i and HO-1 by Western blot analyses, this could suggest a delayed translational effect in comparison to HSP70i and HO-1, and/or the existence of multi-modal signaling pathways in the regulation of specific HSP isoforms. Somewhat surprising was the observation that cytosolic HSPs (with the exception of microsomal HO-1) were the most highly upregulated, even though TFEC damage originates within the mitochondrial matrix. While other ER and mitochondrial HSPs are known to be inducible after other kinds of stress (Maniratanachote *et al.* 2005; Schafler *et al.* 2002), TFEC did not demonstrate similar responses. The expression profile was also different from the pattern commonly observed after a mild temperature shock, where HSP60 and HSP105 are significantly upregulated (Figure 3.5).

The underlying significance of this unexpected cytosolic HSP response is not clear. However, it can be assumed that there is an early signaling event from the mitochondria that is directed towards the cytosol (as well as other subcellular compartments) where transcription factors become activated, leading to the induction of cytosolic stress proteins. Evidence for such events will be reported in Chapter 4 which shows that the cytosolic "cap-and-collar" transcription factor, Nrf2, is rapidly activated (within 1 h) after TFEC treatment to mediate an antioxidant response. Induction of ATF3 also supports the conclusion that other ER-driven transcriptional changes are a consequence of intramitochondrial damage (Chapter 2 and 4). Hence, early mitochondrial injury rapidly generates secondary responses that affect the rest of the cell.

Accordingly, experiments were carried out to determine if the specific induction of cytosolic HSPs confers protection from TFEC damage. Mild heat shock pretreatment

caused upregulation of several HSPs in TAMH cells and was found to improve cell viability after TFEC treatment. However, a complete reversal of TFEC toxicity by pre-emptive HSP induction was not observed, most likely because the HSPs induced did not reside in the mitochondria. As it is known that the majority of the mitochondrial proteins are synthesized in the cytoplasm and transported into the mitochondria in an unfolded state, where mitochondria-accessible chaperones (including HSP60 and HSP10) will then mediate the folding process from within (Schafler *et al.* 2002), it is unlikely that elevations in cytosolic HSPs can greatly affect mitochondrial protein lesions. Nonetheless, the increased viability observed indicates that the elevations in cytosolic HSPs might play some role in the progression of cellular injury. It is also possible that heat shock induce other non-HSP stress responses that confer cytoprotection. An interesting future investigation would be to subject TAMH cells to low levels of TFEC to mimic heat shock preconditioning, before exposing them to toxic concentrations for determination of possible cytoprotection.

There are a few possible mechanisms to explain this cytoprotection. For example, there is evidence that nonspecific hydrophobic interactions of HSP70i (the major HSP induced during heat shock) with other proteins may have effects beyond restoration of protein damage. The promiscuity of HSPs to bind various proteins, likely participates in modulating other cell signaling events including apoptosis (Garrido *et al.* 2001). Studies on HSP70i have provided evidence for its inhibition of JNK, which would lead to a disruption of some early signaling events in apoptosis (Mosser *et al.* 1997). Other studies have demonstrated binding of HSP70i to Apaf1, thus inhibiting the formation of the apoptosome and subsequent activation of caspases (Beere *et al.* 2000). Similarly, HSP70 association with AIF blocks apoptosis, as well as interference with the balance between BAX/BCL-2 in favor of cellular survival, further prevent the activation of BAX and decreasing its translocation to the outer mitochondrial membrane (Gotoh *et al.* 2004; Ravagnan *et al.* 2002; Zhou *et al.* 2003).

Additionally, induction of HO-1 by hemin pretreatment provided a delayed cytoprotection at 24 h post-treatment. HO-1 is known to be intricately linked to cytoprotection from oxidative stress (Chen *et al.* 2000; Otterbein and Choi 2000; Shimizu *et al.* 2000). It catalyzes the rate-limiting step of heme degradation to biliverdin, carbon monoxide and ferrous iron as by-products. Each of these by-products may contribute to the antioxidant potential of HO-1. Firstly, biliverdin/bilirubin can undergo redox cycling that, when coupled to ROS, biliverdin reductase and $NADPH/NADP^+$, functions as a free radical scavenger. As such, bilirubin has been shown to be a potent antioxidant in the brain, with activity equivalent to α-tocopherol (Stocker *et al.* 1987). Secondly, physiological concentrations of carbon monoxide provide anti-inflammatory activity (Otterbein *et al.* 2000). Thirdly, free ferrous iron released from heme is rapidly sequestered by an intracellular iron storage protein, ferritin (Otterbein and Choi 2000). This binding prevents the generation of the highly toxic hydroxyl radical through the free-iron mediated Fenton reaction (Halliwell and Gutteridge 1999). Therefore, release of free iron from HO-1 catalysis of heme degradation, counter-intuitively, creates antioxidant potential through ferritin induction.

The mechanism of the HO-1 mediated cytoprotective effect on TFEC was further investigated with a selective inhibitor, tin protoporphyrin-IX (SnPP). Increased cytotoxicity was observed after SnPP coadministration, and suggests that the cytoprotective action of HO-1, albeit delayed, is closely related to its endogenous enzymatic function in heme degradation. Furthermore, induction of ferritin by the release of free iron might be contributing to the delayed cytoprotection. This can be rationalized from our results showing significantly increased ferritin levels only 24 h after hemin treatment. Delayed induction of ferritin occurred 6 h after hemin treatment in rat brain as well (Gonzales *et al.* 2002). It is possible that early release of ferrous iron potentiates the toxicity of TFEC transiently, before a threshold concentration of intracellular ferritin is reached to sequester the iron. Thus, HO-1 induction by TFEC treatment is playing a greater role in modulating downstream stress and apoptotic

processes. The modest effects of HO-1 induction on cytoprotection suggests that oxidative stress does not play a major role in the cytotoxicity caused by TFEC (for further discussion, see Chapter 4). This is consistent with previous studies which showed that blocking lipid peroxidation did not affect cell survival toward TFEC (Groves *et al.* 1991).

Another interesting result from the investigation was the observation of a 50 kDa protein that was recognized by an antibody to HSP25, and was only present after TFEC treatment. This band was responsive to specific HSP25 silencing by siRNA, indicating that it is most likely a HSP25 dimer by its apparent molecular weight. It was reported that under highly oxidative conditions, native HSP25 formed a dimer through a disulfide bridge linking the monomers (Zavialov *et al.* 1998). By employing a redox immunoblotting technique, it was suggested that this HSP25 dimer played a role in maintaining cellular thiol status. HSP25 is known to interact with GSH/GSSG to preserve oxidative balance (Arrigo 2001; Zavialov *et al.* 1998). More recently, substitution of Cys141 by alanine in murine HSP25 was found to inhibit dimer formation, and also decreased the cytoprotective activity of the protein after treatment of transfected L929 cells with hydrogen peroxide (Diaz-Latoud *et al.* 2005). This mechanism is even more attractive, taking into account the high inducibility and cellular abundance of HSP25 after specific stress events (Ehrnsperger 1997). Hence, our observation of the formation of an apparent HSP25 dimer could be a cellular response to oxidative stress. This raises the possibility that TFEC pretreatment may induce cross-tolerance to purely oxidative insults (e.g. H_2O_2) if TFEC-mediated induction of HSP25 dimer is a real and functional corollary. Evidence of redox disturbances in TAMH cells after TFEC treatment are depletion of NAD(P)H and increase in intracellular hydrogen peroxide 4-6 h post-treatment (see Chapter 4). However, the situation is more complex because, contrary to earlier reports, the apparent dimer formed in TAMH cells after TFEC treatment is resistant to standard protein denaturing and reducing environments (high DTT and β-mercaptoethanol concentrations etc.) (Diaz-Latoud *et al.* 2005). It was however dissociable when a

partially purified sample was applied to the extreme reducing conditions of 10 mM TCEP. This finding suggests that the apparent dimer was likely held together by strong disulfide bonds that were either well-protected by neighboring peptides, and/or have undergone further oxidation that rendered the dimer resistant to reduction with DTT or β-mercaptoethanol. Mass spectrometric characterization of this dimer will be necessary to further confirm these postulations.

Furthermore, there appear to be two separate pools of HSP25 within the cells: cytosolic and mitochondrial. Cytosol-to-mitochondria subcellular relocalization of HSP25 after treatment with TFEC suggests that there is some pathophysiological role of HSP25 in the mitochondria. In recent years, a few groups have described HSP25 relocalization and cytoprotective roles within the mitochondria in various cell lines (Downs *et al.* 1999; He and Lemasters 2003; Samali *et al.* 2001). For example, its was demonstrated that mitochondrial HSP25 can block mitochondrial cytochrome *c* release and inhibit apoptosis (Samali *et al.* 2001). Independently, the suppression of the mitochondrial permeability transition by HSP25 was observed (He and Lemasters 2003). Therefore, it is reasonable to hypothesize that the observed mitochondrial accumulation of HSP25 could constitute an important cellular response to limit the progression of mitochondrial injury after TFEC treatment. However, a minimal change in viability as observed after *HSP25* gene silencing in TFEC treated TAMH cells may also suggest that multiple stress proteins are involved in the process simultaneously.

Overall, this study provides compelling evidence for preferential cytosolic heat shock protein upregulation in response to specific intramitochondrial damage mediated by TFEC. While the signaling events linking the mitochondrial lesions to cytosolic responses are not well understood, the induction may play a role in limiting the progression of this chemical-induced cellular injury.

Table 3.1 **Microarray analyses of TFEC treated TAMH cells.** TAMH cells were treated with 200 mM TFEC for 2, 4, and 6 h. Gene expressions were normalized by their respective vehicle treated controls and displayed as a function of fold changes. Total number of genes significantly upregulated (at least 2 fold greater than control) or down-regulated (at least 2-fold lesser than control) at respective time points are tabulated as shown.

Treatment (h)	2-fold increase	2-fold decrease	Total
2	47	20	67
4	105	74	179
6	153	150	303

Table 3.2 **A representative list of genes with significant changes in their expression levels.** Genes that are significantly upregulated or down-regulated (i.e. greater than 2-fold change) were categorized by their biological function. Genes that were down-regulated are displayed in shaded boxes.

	Fold Induction		
Apoptosis	**2 h**	**4 h**	**6 h**
BCL2-associated anthogene 3 (BAG3)	1.3	2.0	2.9
CCAAT/enhancer binding protein (C/EBP)	2.0	1.9	2.3
Programmed cell death 2 (PDCD2)	1.6	2.5	2.2
Baculoviral IAP repeat containing 5 (BIRC5)	0.9	0.7	0.5
Fas-associating protein with death domain (FADD)	0.8	0.6	0.5
BCL2-related ovarian killer protein (BOK)	0.7	0.4	0.4
Baculoviral IAP repeat containing 3 (BIRC3)	0.4	0.3	0.3
Cell cycling			
V-Maf oncogene family, protein K (MAF-K)	2.2	3.6	4.7
Cyclin-dependent kinase inhibitor 1A (CDKN1A)	2.2	1.5	2.6
Protein tyrosine phosphatase (PTPN16)	1.3	1.9	2.2
Cell division cycle 25 homolog B (CDC25B)	0.8	0.7	0.5
ECT2 oncogene (ECT2)	0.9	0.6	0.5
Cyclin B2 (CCNB2)	0.9	0.7	0.5
Cyclin A2 (CCNA2)	0.8	0.7	0.5
Cyclin E2 (CCNE2)	0.8	0.7	0.4
Cyclin E1 (CCNE1)	0.7	0.5	0.4
Cyclin D1 (CCND1)	0.6	0.4	0.4
Cyclin F (CCNF)	0.6	0.5	0.3
DNA maintenance/repair			
Transformed mouse 3T3 cell double minute (MDM2)	1.8	2.5	2.7
Thymidine kinase 1 (TK1)	0.9	0.5	0.4
FLAP structure specific endonuclease 1 (FEN1)	0.8	0.7	0.5
Chromatin assembly factor 1	0.8	0.6	0.5
MUTS homolog 6 (MSH6)	0.9	0.6	0.5
Topoisomerase II-alpha (TOP2A)	1.0	0.7	0.5
Growth			
Growth differentiation factor 15 (GDF15)	5.9	16.2	19.7
Vascular endothelial growth factor (VEGF)	3.3	5.5	7.1
Nuclear protein 95 (NP95)	1.0	0.7	0.5
Platelet derived growth factor, B polypeptide (PDGFB)	1.0	0.6	0.4
Hepatocyte growth factor (NK1)	0.7	0.6	0.5

Table 3.2 (continued)

	Fold Induction		
Immune response	**2 h**	**4 h**	**6 h**
Lymphotoxin B (LTB)	0.8	0.5	0.5
Eukaryotic translation initiation factor 2α kinase 2 (EIF2AK2)	0.7	0.5	0.5
Interferon regulatory factor 2 (IRF1)	0.4	0.5	0.5
CD14 antigen (CD14)	0.8	0.6	0.4
Metabolism			
Glutathione S-transferase-α2 (GSTA2)	9.2	26.4	40.8
Aldehyde oxidase 1 (AOX1)	1.9	3.1	4.0
Cytochrome P450 3A13 (CYP3A13)	1.3	2.1	2.8
Glutathione S-transferase-α4 (GSTA4)	2.0	2.6	2.8
Glutathione S-transferase-α3 (GSTA3)	1.5	2.0	2.4
Stress response			
Heat shock protein 68 (HSP68 or HSP70)	1.7	19.6	35.7
Heme oxygenase-1 (HO-1)	17.2	29.4	31.0
DNA-damage inducible transcript 3 (DDIT3 or GADD153)	3.6	10.4	13.5
Myeloid differentiation response gene (MYD116 or GADD34)	1.8	7.0	10.8
Arsenite inducible RNA association protein (AIRAP)	2.5	5.9	9.7
Growth arrest and DNA-damage inducible 45α (GADD45A)	3.8	7.0	9.2
Growth arrest and DNA-damage inducible 45γ (GADD45G)	2.0	4.3	9.2
Heat shock protein 105 (HSP105)	1.3	3.5	4.8
Heat shock protein 25 (HSP25)	1.4	3.4	4.7
Glutamate cysteine ligase, regulatory subunit (GCLM)	2.7	4.0	4.5
DNAJ homolog B1 (HSP40B1)	1.2	3.2	4.1
DNAJ homolog B9 (HSP40B9)	1.9	3.2	4.0
N-Myc downstream regulated-like (NDRL)	1.8	3.0	3.2
Glutamate cysteine ligase, catalytic subunit (GCLC)	3.0	3.9	3.2
Thioredoxin reductase 1 (TXNRD1)	2.9	3.2	3.2
Oxidative stress induced gene (STAP or A170)	2.0	2.5	2.5
Heat shock protein 86-1 (HSP86-1)	1.3	2.0	2.5
N-Myc downstream regulated 1 (NDR1)	1.7	2.0	2.3
Glutathione reductase 1 (GSR)	1.4	1.7	2.3
Crystallin, alpha c (CRYAC)	1.2	1.9	2.1

Table 3.2 (continued)

	Fold Induction		
Transcriptional control	**2 h**	**4 h**	**6 h**
Activating transcription factor 3 (ATF3)	2.9	8.3	11.5
Four and a half LIM domains 2 (FHL2)	1.7	3.0	3.1
TG interacting factor (TGIF)	2.3	2.3	2.7
Inhibitor of kappa light polypeptide gene enhancer (IKBKG)	1.2	2.0	2.6
Peroxisome proliferator activated receptor gamma (PPARγ)	1.3	2.2	2.4
Cellular repressor of E1A-stimulated genes (CREG)	1.5	1.9	2.4
Kruppel-like factor 5 (KLF5)	2.0	2.5	2.3
Krox-20 family containing zinc finger (KROX20)	3.4	2.7	2.2
Signal transducer and activator of transcription 5A (STAT5α)	0.8	0.7	0.5
Transcription factor DP1 (TFDP1)	0.9	0.7	0.5
Kruppel-like factor 13 (KLF13)	0.9	0.5	0.5
Transporters			
Cationic amino acid transporter (SLC7A11)	5.4	11.5	15.1
Glutamate/neutral amino acid transporter (SLC1A4)	3.4	8.8	10.4
Activators of dibasic and neutral amino acid transport (SLC3A2)	1.8	2.9	3.9
ATP-binding cassette, subfamily c (ABCC2)	2.0	3.4	3.6
Organic cation transporter (SLC22A5)	1.9	2.5	3.3
Solute carrier family 20, member 1 (SLC 20A1)	1.5	2.5	2.5
Cationic amino acid transporter (SLC 7A5)	1.5	1.9	2.1
Monocarboxylic acid transporters (SLC16A2)	0.8	0.7	0.5

Table 3.3 **Microarray analyses of *de novo* TFEC-inducible *hsp* genes.** Analyses were performed on TAMH cultures treated with 200 μM TFEC for 2, 4 or 6 h. Results have been expressed as a normalized ratio of the gene expression in the TFEC-treated samples against aqueous vehicle treated controls. Selected highly expressed *HSP* genes are listed according to fold induction at 6 h.

Gene name	Fold Induction		
	2 h	4 h	6 h
HSP68 (or HSP70i)	1.7	19.6	35.7
Heme oxygenase-1	17.2	29.4	31.0
HSP 105	1.3	3.5	4.8
HSP25	1.4	3.4	4.7
HSP68A	1.3	1.9	4.6
HSP40B1	1.2	3.2	4.1
HSP40B9	1.9	3.2	4.0
HSP86	1.3	2.0	2.5

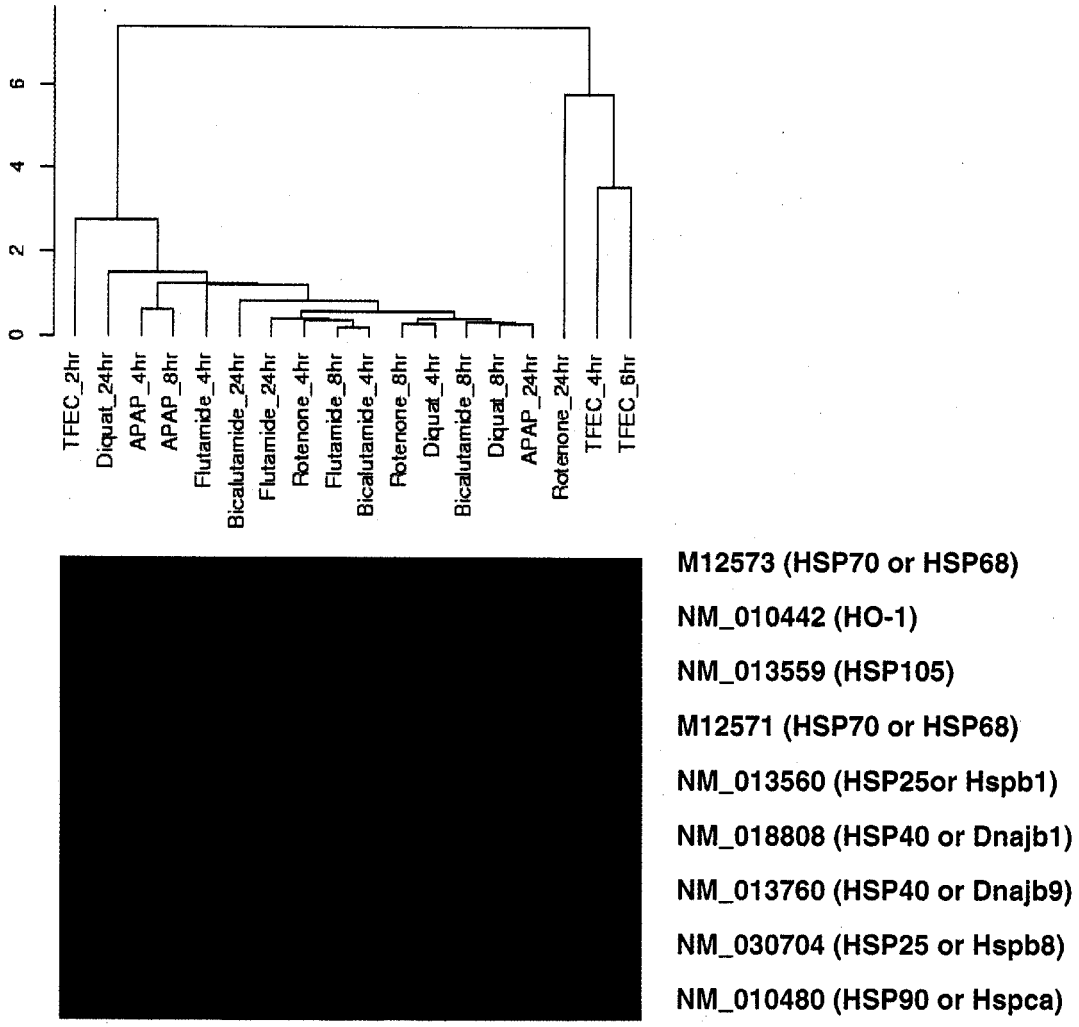

Figure 3.1 **Heat map display of the 8 TFEC-inducible *HSP*s.** Genes with > 2 fold upregulation are shaded in red. Intensity of the shading is proportional to the magnitude of mRNA induction. Responses were compared with other known hepatotoxicant treatments including rotenone (1 μM), acetaminophen (5 mM), diquat (20 μM) and flutamide (75 μM) dosed for 4, 8 and 24 h. The expression profiles were compared and clustered by similarity using the GeneSifter software. Red shading denotes upregulation, green shading denotes down regulation and black shading denotes genes with no significant change in expression level.

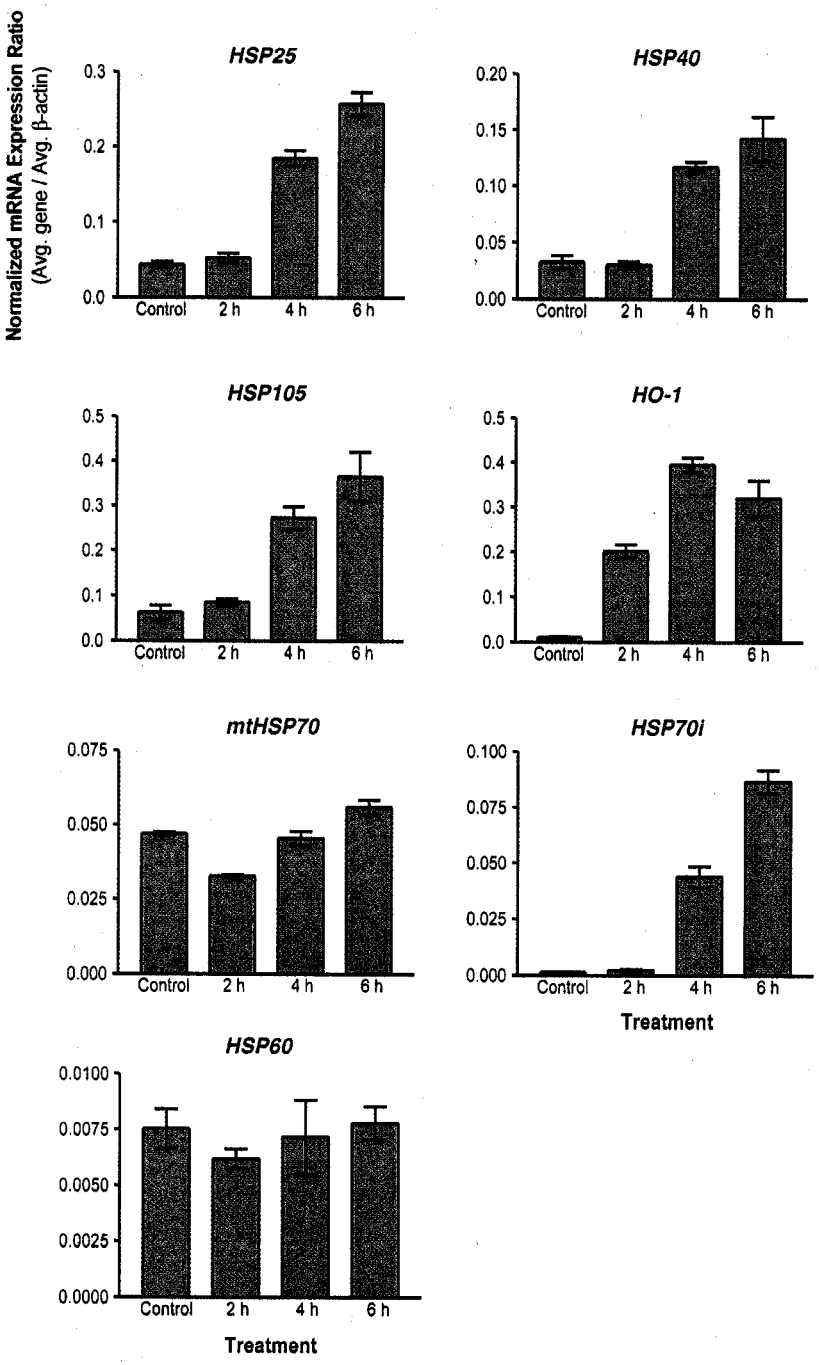

Figure 3.2 **Real time quantitative RT-PCR for selected genes.** Genes were validated with real-time quantitative RT-PCR using SYBR Green fluorogenic probes. Results are expressed as a normalized ratio using the housekeeping gene GAPDH as reference. Each profile is displayed as a separate graph including *HSP25*, *HSP40*, *HSP70i*, *mtHSP70*, *HSP60*, *HSP 105* and *HO-1*. Each data point is the taken as the average of 3 replicates with SEM displayed as the y-error bars.

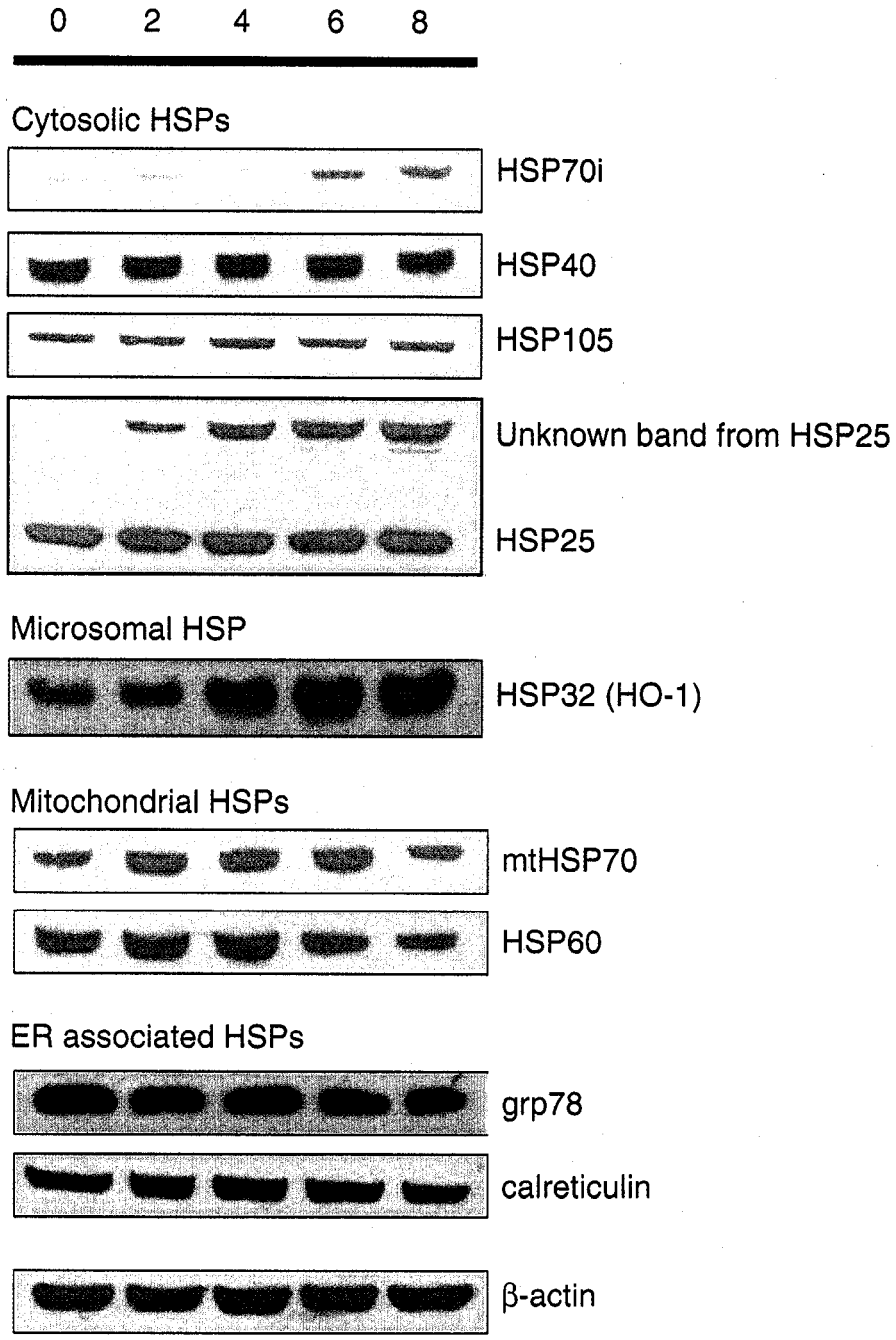

Figure 3.3A **Immunoblot assay for various HSPs following TFEC treatment of TAMH cells.** TAMH cells were treated with 250 μM TFEC for 0, 2, 4, 6 and 8 h. Total cell lysates were blotted with polyclonal anti-HSP25, anti-HSP40, anti-HSP60, anti–HSP70i, anti-HO-1, anti-mtHSP70, anti-HSP105, anti-grp78 and anti-calreticulin. Loading control was anti-β-actin.

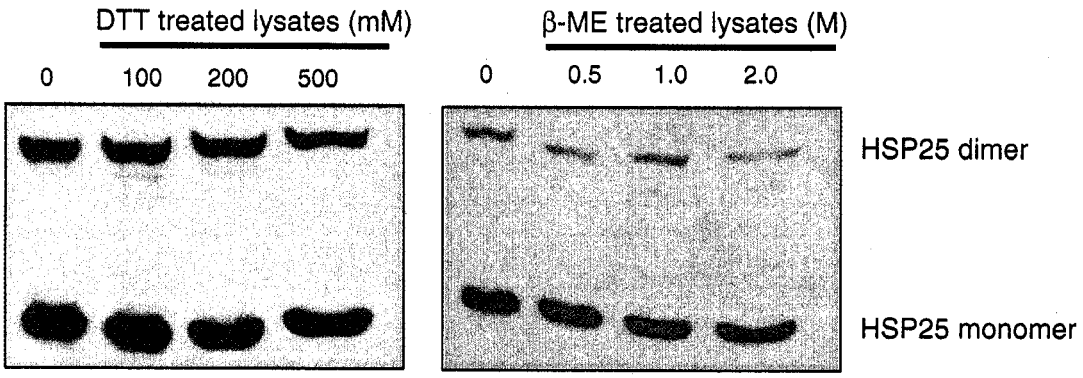

Figure 3.3B **Immunoblot assay for various HSPs following TFEC treatment of TAMH cells.** TAMH cells treated with TFEC (250 μM) for 6 h were incubated with different concentrations of DTT (100, 250, 500 mM) and β-mercaptoethanol (0.5, 1, 2 M) before SDS-PAGE and Western blot analysis with polyclonal anti-HSP25.

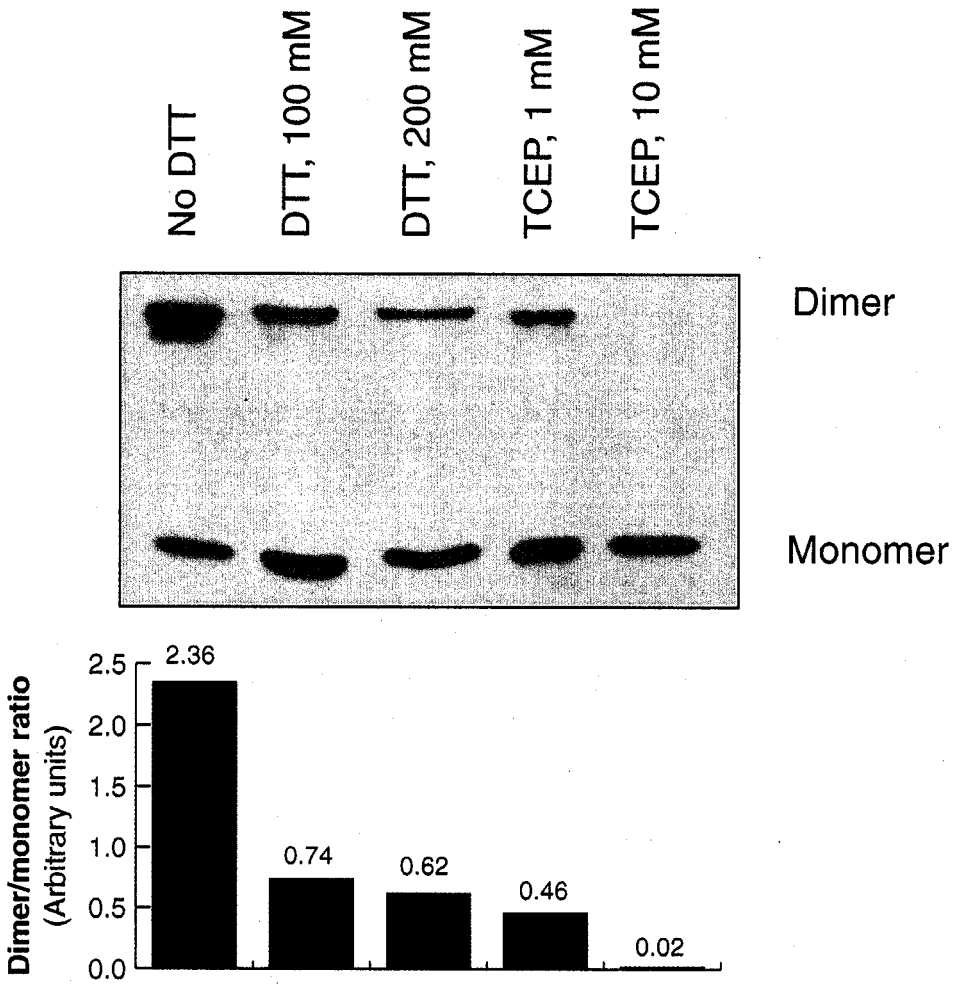

Figure 3.3C **Immunoblot assay for various HSPs following TFEC treatment of TAMH cells.** Samples of TAMH cells treated with TFEC (6 h, 250 μM) were purified on a DEAE-sepharose column. The fraction positive for HSP25 was applied for DTT (100 and 200 mM) and TCEP (1 and 10 mM) incubations (20 min at 95 °C) before SDS-PAGE and Western Blot analysis with polyclonal anti-HSP25.

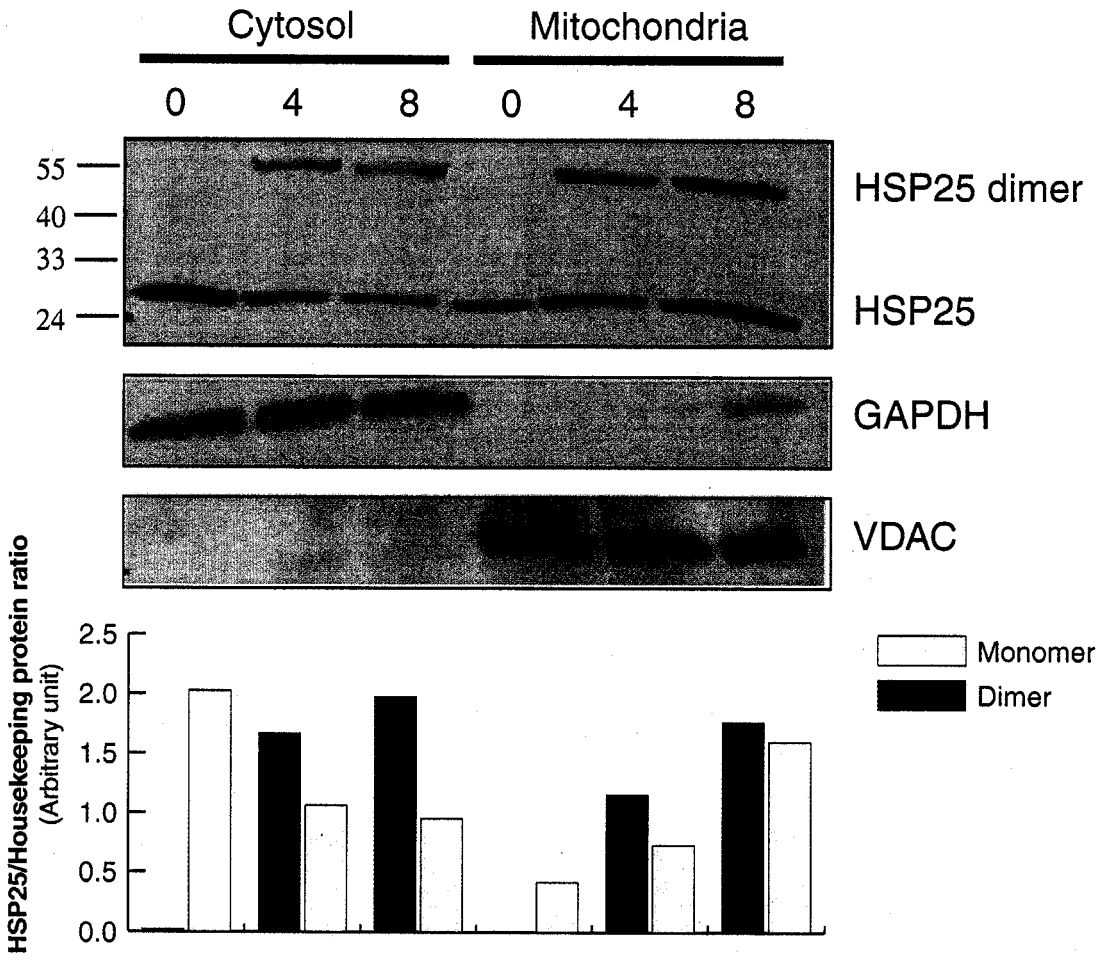

Figure 3.3D **Immunoblot assay for various HSPs following TFEC treatment of TAMH cells.** TAMH cells were subsequently treated with TFEC for 0, 4 and 8 h. Mitochondrial and cytosolic fractions were blotted with polyclonal anti-HSP25. Polyclonal anti-GAPDH and anti-VDAC were used as loading controls for cytosol and mitochondria respectively. Intensity of each HSP25 band is quantified by densitometry and displayed as a graph below the blot.

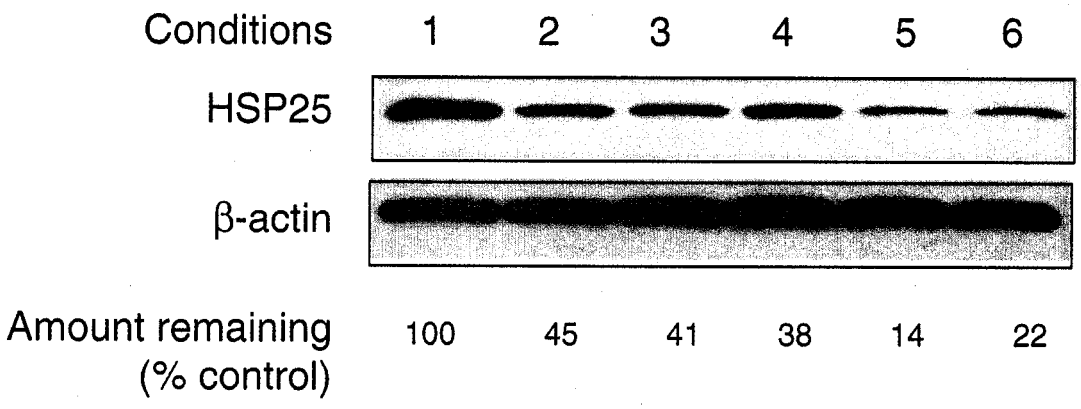

Figure 3.4A **Silencing of *HSP25* by siRNA.** TAMH cells were transfected with different ratios of siRNA-to-transfection reagent for 48 h. These conditions were: **1**. Untransfected control; **2**. 4 μL siRNA, 4 μL transfection reagent; **3**. 6 μL siRNA, 4 μL transfection reagent; **4**. 8 μL siRNA, 4 μL transfection reagent; **5**. 4 μL siRNA, 6 μL transfection reagent; **6**. 4 μL siRNA, 8 μL transfection reagent. HSP25 protein expression was monitored by immunoblot assay using specific polyclonal anti-HSP25 antibodies. HSP25 protein levels are expressed as a normalized ratio of the respective β-actin levels.

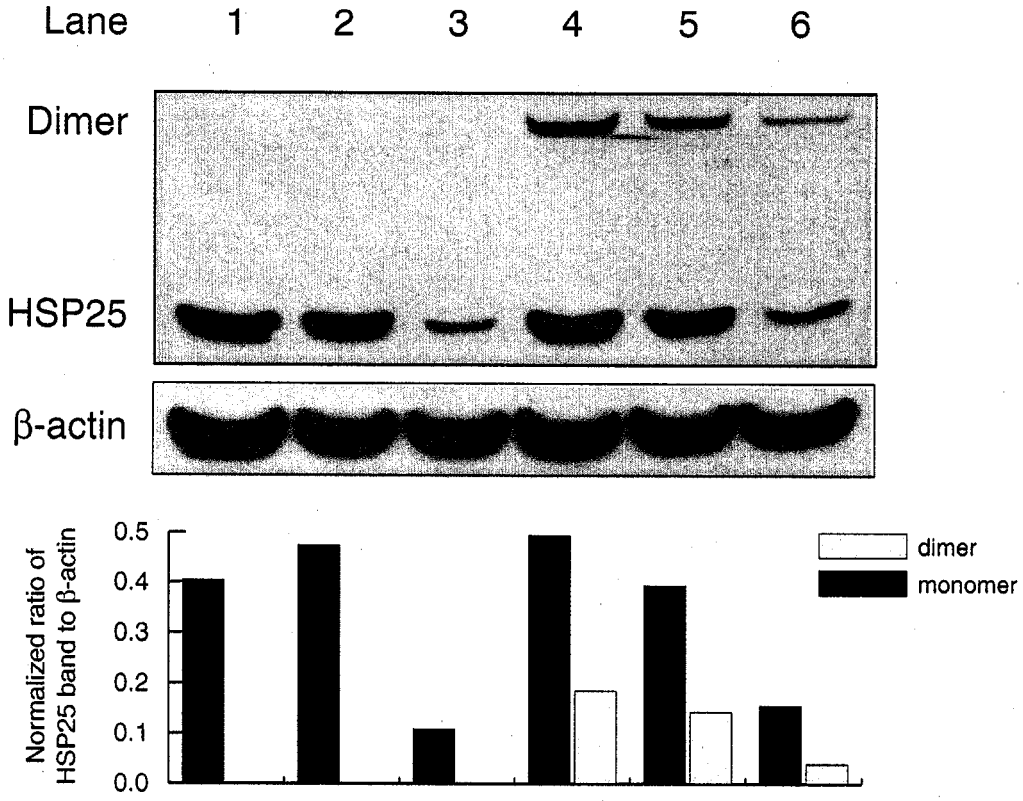

Figure 3.4B **Silencing of *HSP25* by siRNA.** TAMH cells were transfected with condition **5** as described earlier. At 30 h post-transfection, TFEC (250 μM) was administered and immunoblot assay was performed on cell lysates that were subjected to 8 h treatment with TFEC. Lane 1 and 4 are untransfected cells, 2 and 5 are cells transfected with the negative control siRNA, and 3 and 6 are transfected with HSP25 siRNA. Lane 1-3 are untreated cells and 4-6 are cells treated with TFEC. The relative protein levels and HSP25 monomer and the apparent dimer are expressed as a normalized ratio of the β-actin loading control.

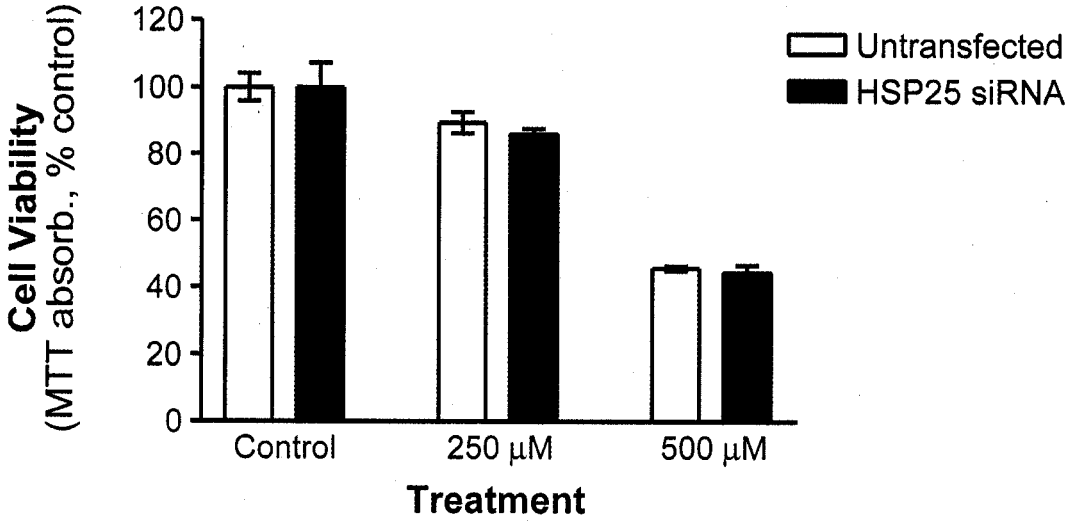

Figure 3.4C **Silencing of *HSP25* by siRNA.** MTT viability was performed on cells treated with vehicle or TFEC (250 and 500 μM) for 8 h, administered at 30 h post-transfection with either vehicle or condition **5**. Results are expressed as a percentage of viable cells in the untreated controls with +/- SD (n=6).

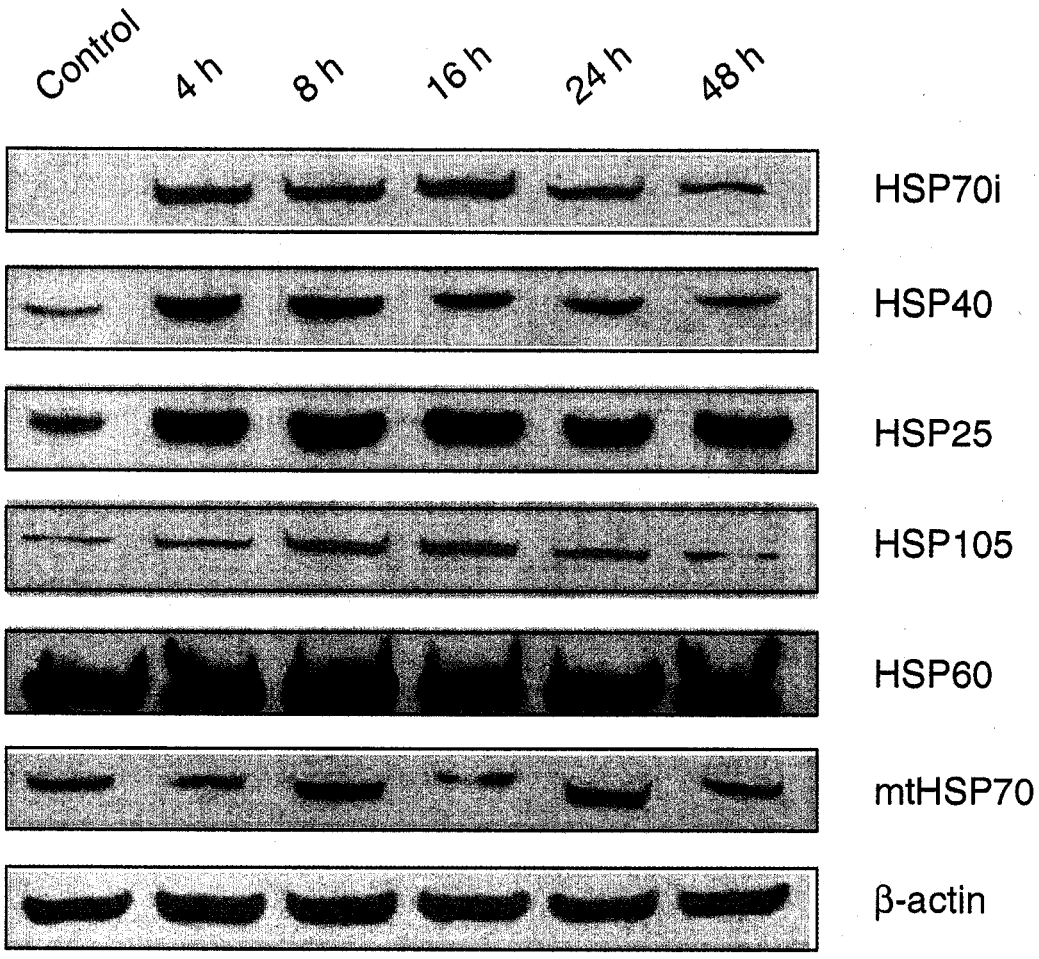

Figure 3.5 **Immunoblot assay for various HSPs after heat shock pretreatment of TAMH cells.** TAMH cells were shocked at 43°C for 30 min and replaced into the 37°C CO_2 incubator before they were harvested at 4, 8, 16, 24 and 48 h. They were blotted with a representative list of HSPs including HSP25, HSP40, HSP60, HSP70i, mtHSP70 and HSP105. The loading control was β-actin.

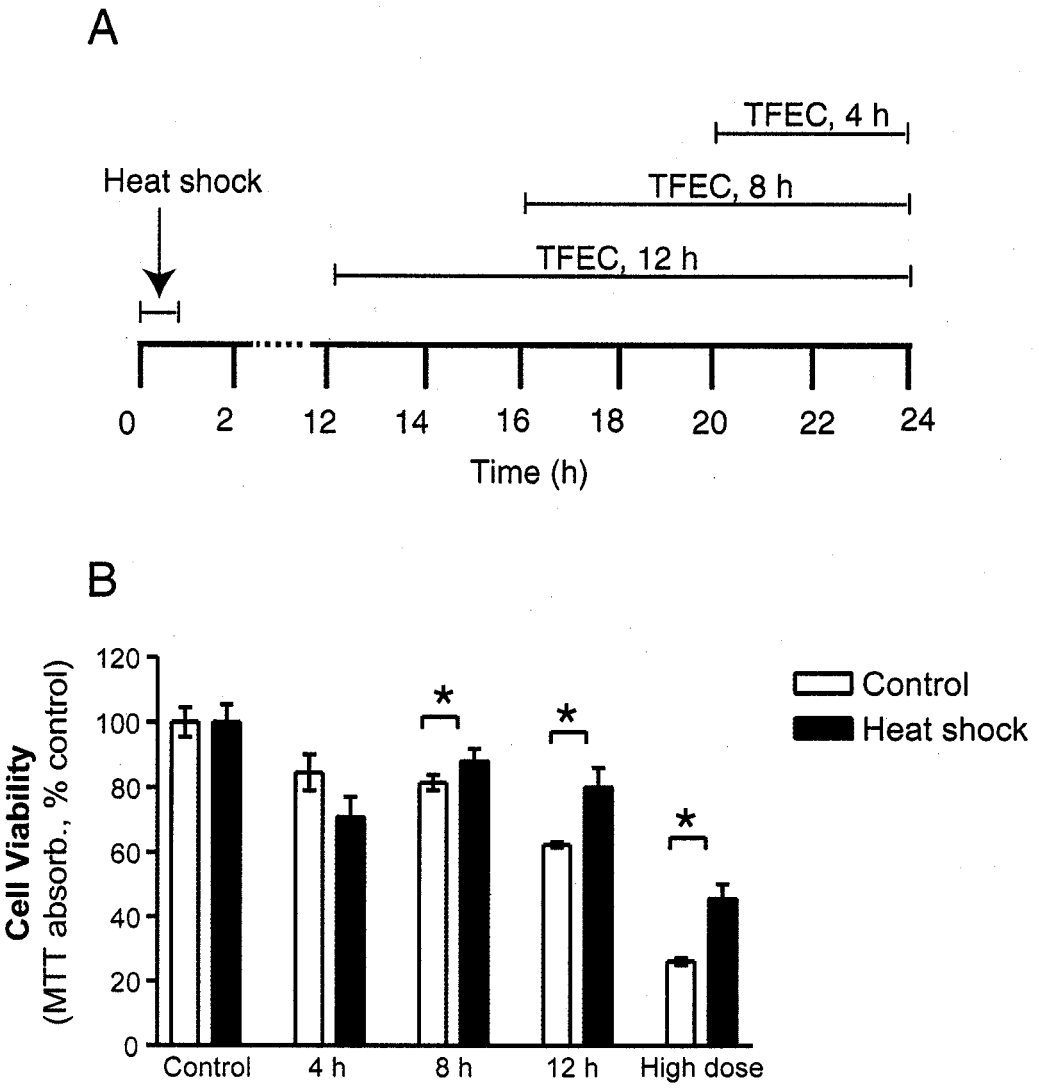

Figure 3.6 **MTT viability assay of heat shocked TAMH cells after various durations of TFEC (250 μM) treatment.** (A) Cells were heat shocked at 43 °C for 1 h, pre-incubated for another 11, 15, 19 h and treated for 12, 8 and 4 h respectively. (B) Viability was measured by MTT assay. Results are expressed as a percentage of viable cells in the untreated controls with +/- SD (n=6). (* denotes a statistically significant difference between control and heat shock cells with $p<0.05$).

A

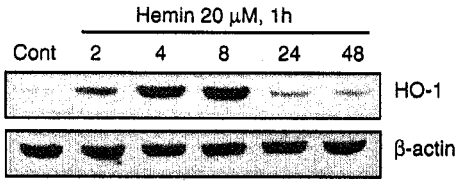

B

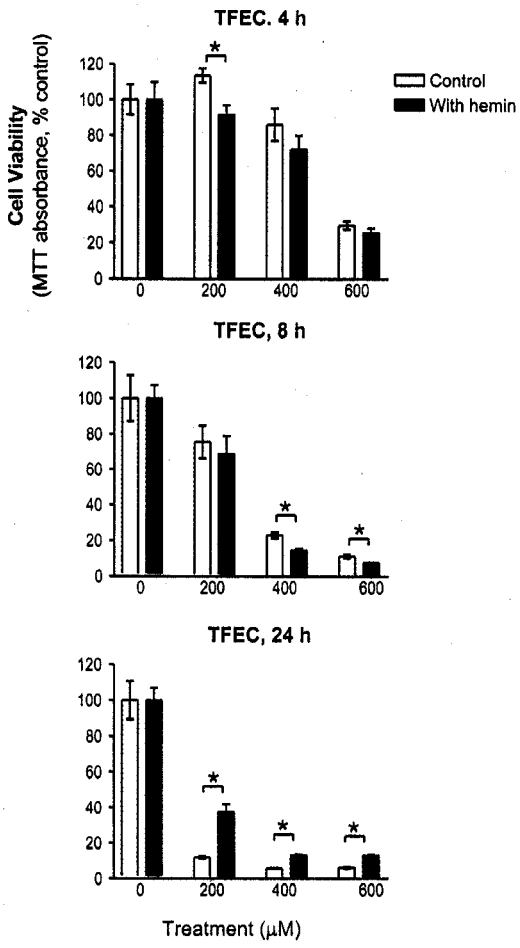

Figure 3.7 **Effect of hemin pretreatment on TFEC-induced cytotoxicity.** TAMH cells were treated with hemin (20 μM) for 1 h and fresh medium was replaced thereafter. (A) Cells were harvested at 2, 4, 8, 24 and 48 h and expression of HO-1 was monitored by Western blot using polyclonal anti-HO-1 antibody. Loading control was β-actin. (B) Cells were subsequently treated with TFEC (200-600 μM) for 4, 8 and 24 h respectively. Cell viability was monitored by MTT. Results are expressed as a percentage of viable cells in the untreated controls with +/- SD (n=6). (* denotes a statistically significant difference between control and heat shock cells with $p<0.05$).

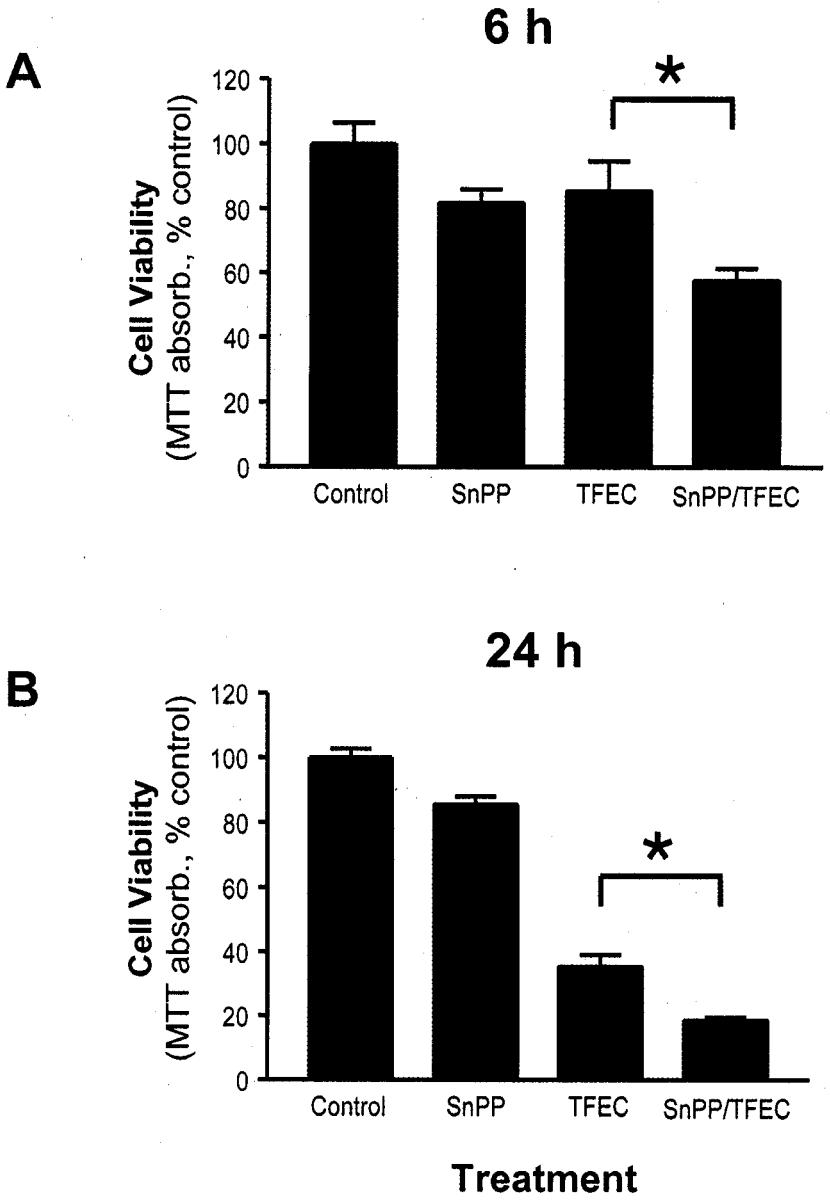

Figure 3.8 **Effect of SnPP on TFEC-induced cytotoxicity.** Cells were treated with TFEC (200 μM) for 6 and 24 h, with or without SnPP (20 μM) coadministration. Cell viability was monitored by MTT. Results are expressed as a percentage of viable cells in the untreated controls with +/- SD (n=6). (* denotes a statistically significant difference between control and heat shock cells with $p<0.05$).

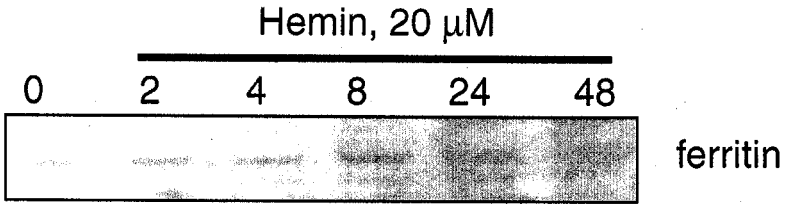

Figure 3.9 **Induction of ferritin by hemin pretreatment.** TAMH cells were treated with hemin (20 μM) for 1 h and the expression of ferritin was monitored by immunoblot assay using a goat polyclonal ferritin antibody.

Chapter 4

The Oxidative Stress Response In TFEC-induced Cytotoxicity

4.1 Introduction

Oxidative stress occurs commonly in chemical-induced cellular injury. It is often the result of : (1) an increase in ROS/RNS production; and/or (2) a decrease in cellular antioxidants. These changes can occur through direct and indirect mechanisms. Some compounds can be metabolized to free radicals directly, like the reductive dehalogenation of carbon tetrachloride by P450 enzymes to generate a radical that causes lipid peroxidation. Other compounds can form ROS through redox recycling. For example, the pesticides paraquat and diquat are known to be enzymatically reduced into radical anions by P450 reductases. The radical anions can then be reoxidized by reaction with molecular oxygen to form superoxide anion (Halliwell and Gutteridge 1999). ROS/RNS generation can also occur via the inhibition of some biochemical pathways like the ETC. For example, rotenone binds to Complex I and inhibits electron flow down the electrochemical gradient such that there is a local buildup of electrons to react directly with oxygen (as discussed in Chapter 1).

On the other hand, drugs and other chemicals can cause decreases in antioxidants in cells and tissues. Many compounds can be metabolized to electrophilic intermediates that can react with sulfydryl-containing antioxidants such as GSH and thioredoxin. If a large or sustained dose of such chemical is administered, it can overwhelm the ability of the cells to supply these protective factors, resulting in a depletion of these thiol-containing antioxidants. A classical example is the depletion of GSH by a reactive metabolite of the drug, acetaminophen. Acetaminophen is metabolized to its electrophilic reactive intermediate, N-acetyl-*p*-quinoneimine (NAPQI) that reacts with GSH, to both form GSH conjugates and oxidize GSH to GSSG (Chen *et al.* 1999;

Dahlin *et al.* 1984). Both reactions can cause oxidative stress that contributes to the hepatotoxicity caused by large doses of acetaminophen.

The current consensus on the mechanism of TFEC toxicity involves bioactivation of TFEC by cysteine S-conjugate β-lyase to an unstable DFTAL intermediate (Cooper *et al.* 2002a; James *et al.* 2002). This reactive electrophilic species covalently modifies a very small, but well-defined group of intramitochondrial proteins including aconitase, αKGDH subunits, AST, HSP60 and HSP70 (Bruschi *et al.* 1998; Bruschi *et al.* 1993; James *et al.* 2002). As discussed in Chapter 2, it is generally accepted that these binding events are the initiating lesions in the mitochondrial dysfunction, necrotic cell death and tissue damage produced by TFEC. However, it is not obvious if oxidative stress is participating as a parallel or intervening pathway to exacerbate the toxicity. Rick Schnellmann's group has shown that inhibition of lipid peroxidation in proximal renal tubular cells incubated with TFEC, did not increase cell survival, suggesting that oxidative stress as measured by lipid peroxidation is not an important contributory factor to toxicity (Groves *et al.* 1991). However, at the time these studies were initiated, conclusive evidence was not available.

Currently, there is a renewed interest in the role of oxidative stress in TFEC toxicity. A recently characterized transcription factor, Nrf2, has been found to be a key transcriptional activator for genes possessing the antioxidant response element (ARE) in their promoter region. This include *GSTs*, *ferritin*, *glutamylcysteine ligase* subunits (*GCLc*, *GCLm*) *glutathione reductase*, *heme oxygenase-1* (*HO-1*) and *NADPH-dependent quinone oxidoreductase* (*NQO1*), and many others are still being discovered (Alam *et al.* 1999; Jaiswal 2004; Numazawa and Yoshida 2004; Sakurai *et al.* 2005; Wild *et al.* 1999). These effector genes have ubiquitous roles in coding for enzymes that protect cells from reactive metabolite of xenobiotics that can cause oxidative stress in cells. Hence, there is intense interest in understanding the role of Nrf2 in chemoprevention and detoxification processes (Lee and Johnson 2004; Zhang and Gordon 2004). Some groups are also re-visiting other well-studied cytotoxicants

to determine how Nrf2 may participate in their mechanism of toxicity. For example, enhanced hepatotoxicity of acetaminophen was recently shown in *Nrf2* knockout mice, and the hepatic activation of Nrf2 by acetaminophen was also demonstrated (Chan *et al.* 2001; Goldring *et al.* 2004).

Previously, it has been shown that the reactive metabolite of TFEC, DFTAF, forms adducts with aconitase and αKGDH that leads to inhibition of these two TCA cycle enzymes (Chapter 1). TCA cycle inhibition, specifically the depletion of NADH, can attenuate the transhydrogenation of NADPH (Garrett and Grisham 1995; Rydstrom 1977). NADP/NADPH coupling to GSH/GSSG makes this an important determinant for the overall redox status of the host cell. Through this association, it is likely that a decreased antioxidant potential may arise from TCA inhibition. Moreover, studies with the TCA cycle inhibitor, sodium arsenite ($NaAsO_2$), have recently demonstrated an oxidative stress response (Lee *et al.* 2005b; Pourahmad *et al.* 2005).

Thus, the studies reported in this chapter represent a logical continuation of those in Chapter 3 that use global gene expression profiles to identify cellular and biochemical responses to help assess the involvement of oxidative stress in cytotoxicity caused by TFEC in TAMH cells. Parts of this chapter were previously published in *Toxicological Sciences* (Ho *et al.* 2005b).

4.2 Materials and Methods

4.2.1 Cell culture

Serum-free cell culture of the TAMH line between passages 21-35 was undertaken as previously described in Chapter 2. For glucose-free experiments, cells were grown and subsequently treated in Dulbecco's modified Eagle's medium, with or without glucose. Hepa-1 cells overexpressing GCL were developed and maintained as previously described (Botta *et al.* 2004). Mouse embryonic fibroblast wild-type (MEF-WT), *Nrf1* knock-out (MEF-*Nrf1*-/-) and *Nrf2* knock-out (MEF-*Nrf2*-/-) cell lines were developed by Dr. Jeff Chan (University of California, San Francisco) and

made available through Dr. Terry Kavanagh (University of Washington). The cell lines were maintained according to protocols described previously (Leung *et al.* 2003).

4.2.2 Microarray analysis procedures

TAMH cells were grown on 150 cm^2 tissue culture dishes before they were subjected to various treatments for RNA isolation and microarray analyses as described previously (Chapter 3).

4.2.3 Quantitative RT-PCR

The method for real time RT-PCR was described in Chapter 3. The gene-specific sequences of the primer pairs and probes used in the assays are as follows: *GCLc* (U85498): forward primer, ATGTGGACACCCGATGCAGTATT; reverse primer, TGTCTTGCTTGTAGTCAGGATGGTTT; probe, CCTAAAGCTAATTAAGAAGAGAGC. *GCLm* (NM_008129): forward primer, GCCACCAGATTTGACTGCCTTT; reverse primer, CAGGGATGCTTTCTTGAAGAGCTT; probe, TCTGAGGCAAGTTTCCA. *GSTA3* (NM_010356): forward primer, AGGAACAAACCAGGAACCGTTACTT; reverse primer, CAGCGCTCCTCAGCCTGTT; probe, TCTTCAACACCTTTTCAAAGG. *GSTA2* (NM_008182): forward primer, GTATTATGTCCCCCAGACCAAAGAG; reverse primer, CTGTTGCCCACAAGGTAGTCTTGT. *GAPDH* (NM_008084): forward primer, TCCTGCACCACCAACTGCTT; reverse primer, GAGGGGCCATCCACAGTCTT; probe, CACTCATGACCACAGTCCATGCCATCAC. *GSTA2* was analyzed by SYBR green instead of TaqMan and no probe was needed.

4.2.4 Isolation of cytosolic/nuclear fractions

Nuclear and cytosolic fractions were isolated with slight modifications to the protocol described previously (Buckley *et al.* 2003). Briefly, the harvested cells were pelleted and resuspended in 475 μL of cytosolic extraction buffer (10 mM Tris-base, 60 mM KCl, 1 mM EDTA, 1 mM DTT, protease inhibitor cocktail) and kept on ice for 10

min. Subsequently, 25 μL of 10 % v/v Igepal CA-630 was added to the cell suspension and mixed with gentle pipetting for 10-15 s. This mixture was spun at 12,000 g for 5 min at 4°C. The resultant supernatant was removed as the cytosolic fraction. The pellet which contained the nuclear-enriched fraction was then resuspended again in nuclear extraction buffer (20 mM Tris-base, 400 mM NaCl, 1.5 mM $MgCl_2$, 1.5 mM EDTA, 1 mM DTT, 25% v/v glycerol, protease inhibitor cocktail). Independent verification of the relative purity of subcellular fractions was by immunoblot (as described below).

4.2.5 Immunoblot procedures

All the fractions collected were assayed for protein concentration using the BCA protein assay kit (Pierce Chemical Co., Rockford, IL). Proteins (30-50 μg) were resolved by denaturing electrophoresis, SDS-PAGE (Mini-PROTEAN II; Bio-Rad Laboratories, Hercules, CA) and transferred to nitrocellulose membranes for 1 h at 15 V using Trans-Blot SD Semi-Dry Transfer Cell (Bio-Rad). Immunodetection was by chemiluminescence (SuperSignal ULTRA; Pierce, Rockford, IL) using specific antibodies diluted in PBS with 0.05% v/v Tween 20 and 5% w/v powdered milk. Anti-Nrf2 (1:1,000), anti-Nrf1, anti-Gadd153, anti-Gadd34 and anti-Histone-H1 were from Santa Cruz Biotechnology (San Diego CA), anti-HO-1 from Stressgen (Victoria, BC, Canada), and anti-GAPDH was developed in-house (Dietze *et al.* 1997). Secondary anti-mouse and anti-rabbit horseradish peroxidase conjugated secondary antibodies (Pierce) were used at 1:20,000 dilution. All primary antibodies were used at 1:2,000 dilution unless otherwise stated. Densitometric analyses were performed on selected immunoblots using Bio-Rad ChemiDoc and the Quantity One Version 4.3.0 program (Bio-Rad).

4.2.6 Immunocytochemistry

Immunocytochemical staining of TAMH cells was performed exactly as described in Chapter 2. Immunostaining was with anti-Nrf2 and anti-rabbit fluorescein isothiocyanate (FITC) conjugated IgG (Molecular Probes) in the presence of saponin

(0.2% w/v) to enhance antibody accessibility. Nuclear staining was performed by incubating 4',6-diamidine-2'-phenylindoledihydrochloride (DAPI) at 0.5 μg/mL in PBS for 5 min. Cells were washed extensively with PBS before being mounted with Fluoromount G (Southern Biotechnologies, Birmingham, AL), and were examined using a Nikon Eclipse fluorescence microscope (Nikon, Melville, NY) with 40X lenses. Images were then processed with Q-Imaging software (Burnaby, BC, Canada).

4.2.7 Spectrofluorometric analyses of hydrogen peroxide formation and free cytosolic calcium

Cells were grown on 6-well dishes and treated with TFEC as indicated. Cells were then incubated with either 10 μM dihydro-dichlorofluorescein-diacetate (H_2DCFDA) for measuring intracellular hydrogen peroxide, or 2 μM Indo-1 AM for measuring intracellular calcium. Cells were rinsed, harvested and re-suspended in 1 mL Hanks' BSS. Fluorescence was monitored using a SLM-Aminco 8100 spectrofluorometer (Spectronic Instruments, Rochester, NY), at 468 nm (excitation λ) and 528 nm (emission λ) for H_2DCFDA. Indo-1 detection and calcium quantification required a ratiometric analysis using the following equation:

Ratio = [absorbance (320 nm excitation λ, 405 nm emission λ) / absorbance (355 nm excitation λ, 475 nm emission λ)].

4.2.8 Viability assay by MTT

Cell viability was determined using 3-(4,5-dimethylthiazol-2-yl)-2,5-diphenyl-tetrazolium bromide (MTT) to assess cell viability according to protocols previously described (Chapter 2). Experiments investigating the impact of antioxidants on TFEC toxicity were with Trolox (1 mM) and t-butylhydroperoxide (TBHP) was used as a positive control to induce oxidative stress.

4.2.9 ATP depletion assay

Intracellular ATP levels were measured by its activity using the CellTiter-Glo Luminescent Cell Viability Assay (Promega, Madison, WI) according to the

manufacturer's protocol. Briefly, cells were treated with 250 μM TFEC for 0-8 h on 96-well plates. After incubation, an equivolume of the luminescent substrate and lysis buffer mix from the assay kit was added. The mixture was transferred to an opaque 96-well plate and luminescence was read and analyzed with PlateLumino (Phenix, Hayward, CA).

4.2.10 Flow cytometry

Flow cytometry methods were adopted from a previously described procedure (Botta *et al.* 2004). Briefly, cells were grown on 12-well dishes and treated for the time periods indicated. All cells were harvested, re-suspended and incubated in nonylacridine orange (NAO, Molecular Probes; 2 μM; 488 nm excitation λ, 530 nm emission λ), as a measure of mitochondrial cardiolipin content; with monochlorobimane (4 μM; 351-362 nm excitation λ, 450 nm λ) for reduced glutathione (GSH) content, or with hydroethidine for superoxide (Molecular Probes; 5 μM; 488 nm excitation λ, 590 nm emission λ). Diethylmaleate (DEM) was used as a positive control for GSH depletion (125 μM; 4 h). After staining for 30 min at 37 °C in the dark, the cells were examined by flow cytometry (Epics Elite, Beckman-Coulter Corp, Miami, FL) for the intensity of fluorescence. The PMTs were gated for live cells using propidium iodide (2 μM) added just before acquisition. NAD(P)H redox status was also monitored concurrently with a UV-excited blue autofluorescence (351-362 nm excitation λ, 450 nm emission λ). Data from at least 5,000 cells were collected in list mode, and processed with MPlus Software (Phoenix Flow Systems, San Diego, CA).

4.3 Results

4.3.1 Induction of oxidative stress-related genes

Microarray analyses were performed on TAMH cells treated with 200 μM TFEC for 2, 4 and 6 h using a 10K mouse oligonucleotide array (Codelink). Here, we highlight a group of oxidative stress related genes that were highly upregulated in a time-dependent fashion, with the expression level increasing from 2 to 6 h treatment with

TFEC. These genes included *heme oxygenase-1* (HO-1), *GST-alpha* isoforms, *GCL* subunits, *glutathione reductase* and *thioredoxin reductase* (Table 4.1). *Heme oxygenase-1* was the most upregulated gene in the entire array as measured at 4 h of TFEC treatment (29.4 fold higher than control cells). The mRNA expression of *GCL* subunits, *GSTA2* and *GSTA3* were validated by quantitative RT-PCR (Table 4.2). These confirmatory data demonstrate a good correlation with the microarray analyses. For example, *GSTA2*, the most highly upregulated of the 4 genes validated (26.4 fold induction at 4 h with microarray), was also the most highly expressed by RT-PCR (111.5 fold induction at 6 h).

4.3.2 Nrf2 induction and translocation is an early event in TFEC toxicity

Many of the oxidative stress related genes identified in these studies share an antioxidant response element (ARE) in their promoter sequences. Consequently, Nrf2 expression was assessed using Western blot analyses following treatment with 200 μM of TFEC for 0-6 h. An almost negligible level of Nrf2 protein was observed in control cells, but the level increased markedly after only 2 h of TFEC treatment (Figure 4.1A). Higher doses of TFEC (250 μM) produced similar induction at 6 h but with a lower absolute amount of Nrf2 induced (Figure 4.1A). Furthermore, Western blot analyses demonstrated a dramatic protein induction at 6 h treatment, which is completely reversed by the specific protein synthesis inhibitor, cycloheximide (Figure 4.1B). Similar cycloheximide-dependent inhibition of expression was also observed with HO-1 (Figure 4.1C).

Determination of Nrf2 translocation from the cytosol to the nucleus was used as a functional correlate for Nrf2 induction. As shown in Figure 4.2, cytosolic Nrf2 levels increased in a time-dependent manner from 0-2 h and thereafter, decreased. Meanwhile, nuclear Nrf2 reached a maximum at about 1 h and remained at that level. This translocation was also specific for Nrf2 since the highly homologous Nrf1 did not display any change in expression level or subcellular distribution following TFEC treatment (Figure 4.2). Likewise, complementary immunocytochemical staining of

Nrf2 and fluorescence microscopy demonstrated the translocation with a distinct nuclear staining pattern after similar treatment (Figure 4.3). Thus, these data clearly indicate that Nrf2 is rapidly mobilized from the cytosol to the nucleus in response to TFEC treatment, consistent with the induction of ARE-controlled genes.

4.3.3 Lack of an early phase oxidative stress in TFEC toxicity

Nrf2 activation and the upregulation of effector ARE genes suggest that TFEC might act by an oxidative stress mechanism. GSH depletion, oxidation of membrane cardiolipin, levels of reduced pyridine nucleotides (NAD(P)H), and intracellular hydrogen peroxide/superoxide formation were examined as indicators of cellular redox perturbations. Using flow cytometric measurements with a thiol-reactive dye, monochlorobimane, no significant change was observed in cellular concentrations of GSH from 0-6 h treatment with 250 μM TFEC (Figure 4.4A). A supratoxicological dose of TFEC (400 μM) caused a decrease (approx. 20%) in reduced GSH that was not as pronounced as the decrease (approx. 80%) caused by diethylmaleate (Figure 4.4A). Likewise, there was little change in membrane cardiolipin oxidation as measured by NAO staining and flow cytometry, nor any significant increase in intracellular hydrogen peroxide or superoxide formation within the first 2 h (Figure 4.4B, 4.4C, 4.4D). NAD(P)H levels, as detected by UV-excited autofluorescence, were significantly reduced at 4 and 6 h (Figure 4.4E). The reduction is time-dependent such that cells after 6 h of treatment had approximately 50% lower levels of reduced pyridine dinucleotides in comparison to controls. Arguably, it is still possible that oxidative stress was transient and/or below our detection limits. Hence, the significance of any low-level oxidative stress was investigated by looking at the cytoprotective action of an antioxidant, as well as the transgenic overexpression of GCL subunits. An effective dose of Trolox (1 mM) failed to reverse the toxicity of TFEC (250 μM) as demonstrated with the MTT viability assay (Figure 4.4F). Likewise, Hepa-1 cells overexpressing GCL subunits (i.e. CR17) did not alter the dose-dependent profile of TFEC toxicity (Figure 4.4G).

4.3.4 Cellular calcium dysregulation

ER stress is known to result in non-physiological mobilizations of calcium from this compartment. Therefore, intracellular calcium was measured spectrofluorometrically using the ratiometric UV-excitable dye, Indo-1 AM which fluoresces strongly at 405 nm with high cytosolic calcium concentrations, and at 475 nm with low concentrations. Ratiometric analysis also corrects for differential dye-loading between samples. The results show an increasing intracellular calcium concentration with time following TFEC treatment (Figure 4.5A). Significant increases were observed after 4 and 6 h with ratios of 0.57 and 0.72, respectively. These values were comparable to those found with calcium ionophore, A23187 (100 nM) treated cells (0.85) as a positive control indicative of calcium dysregulation from more generalized ER stress following TFEC exposure.

4.3.5 Depletion of intracellular ATP

Changes to cellular ATP levels are expected as a consequence of TFEC-mediated inhibition of the TCA cycle and were investigated using a commercially available luminescent procedure (CellTiter-Glo Luminescent Cell Viability Assay, Promega). There was a rapid depletion of intracellular ATP within the first 2 h of TFEC treatment (to approx. 50% of starting levels). By 8 h, the levels were reduced even further to less than 20% of control levels (Figure 4.5A).

To further determine the importance of intracellular ATP to subsequent cell signaling, TAMH cells were preincubated in glucose-free or high-glucose (4,500 mg/L) medium before subjecting them to cytotoxic concentrations of TFEC (250 μM) for an additional 24 h. Our results show that cells survived significantly longer in the presence of high glucose medium (Figure 4.5B) and this was associated with the maintenance of cellular ATP content (approx. 4-fold higher) by glucose supplementation (Figure 4.5C).

4.3.6 Induction of ER stress response genes

Activation of Nrf2 in the absence of oxidative stress suggests involvement of another signaling pathway known to occur at the level of the ER (Cullinan *et al.* 2003; Liu *et al.* 2005). Our microarray analyses have indicated a strong link to ER stress with an early and pronounced upregulation of a number of ER-stress response genes (Table 4.3). This list includes genes encoding for four ER resident proteins (Gadd153, Gadd45, Gadd34, Atf3) as well as cytosolic proteins that have been well-established to be induced in response to ER stress (i.e. Ndr1). At least one of these genes was shown here to be upregulated at the protein level (Gadd153) while Gadd34 did not show any increase in protein level despite significant transcriptional changes (Figure 4.6 and Table 4.3). Western blot analyses for both Hsp70i and Atf3 showed that Atf3 is strongly upregulated temporally from 4 to 8 h after the initiation of TFEC treatment, whereas Hsp70i levels remained high even at 20 h (Figure 4.7).

4.3.7 Effect of *Nrf2*-/- in TFEC toxicity

The role of Nrf2 transcriptional activation of ARE genes to TFEC-induced cytotoxicity was examined with the use of mouse embryonic fibroblasts (MEF), and transgenic cells either with *Nrf1* or *Nrf2* knock-out (*Nrf1*-/- or *Nrf2*-/-). The basal level of Nrf2 protein expression in all 3 lines was determined by Western blot as shown in Figure 4.8. By treating these cell lines with TFEC at various concentrations for 24 h, it was observed that *Nrf2*-/- fibroblasts were significantly less viable than either the WT or the *Nrf1*-/- fibroblasts. *Nrf1*-/- did not display any change in toxicity profile versus the WT fibroblasts (Figure 4.9).

4.4 Discussion

The work presented here has shown that despite a highly focused mitochondrial origin of subcellular damage, signal transduction of the initial chemical insult caused by TFEC rapidly expands to affect other organelles such as the ER. We previously demonstrated that the initial damage to mitochondrial proteins results in the

translocation of cytosolic BAX to the outer mitochondrial membrane (Chapter 2). This translocation is pivotal to the activation of subsequent mitochondrial effects including a mitochondrial permeability transition (MPT) (James *et al.* 2002), and the release of cytochrome *c* into the cytosol where it mediates downstream proteolysis (Chapter 2). Gene expression profiling has now revealed a previously undetected early induction of ARE responsive genes including *heme oxygenase-1*, *GCL*, *thioredoxin reductase* and *GSTs* during TFEC cytotoxicity. Subsequent RT-PCR has confirmed this high level of *HO-1* induction (Chapter 3) as well as the induction of *GCL* subunits and *GST-alpha* isoforms. Further independent microarray studies using the same samples but run on a different platform (NIA 15K mouse cDNA array) have also shown that many of the same genes were upregulated as well as other oxidative stress related genes, including various *ferritin* subunits and *GST-pi* (Hu *et al.*, manuscript in preparation). This was a surprising observation since previous reports had indicated that the level of oxidative stress in TFEC-mediated cell death was absent or minimal, and inconsequential to toxicity (Groves *et al.* 1991). To establish a link from the initial mitochondrial protein binding events to the upregulation of these genes, we considered the possible role of a predominant and well-characterized transcription factor, Nrf2.

Nrf2 is an important stress-responsive transcription factor of the "cap-and-collar" β-leucine zipper family, that is activated during oxidative stress (Nguyen *et al.* 2003). It regulates the expression of a number of Phase II enzymes (e.g. NQO1, GSTs) and antioxidant proteins (e.g. GCL, HO-1, thioredoxin). This process is driven by the association of Nrf2 to the ARE consensus sequence (5'-TGACnnnGCA-3') on the promoter region of these genes (Itoh *et al.* 2004; Jaiswal 2004; Lee and Johnson 2004; Numazawa and Yoshida 2004). Recent reports continue to identify new downstream effector genes for Nrf2, including *thioredoxin reductase* and *MafG* (Katsuoka *et al.* 2005; Sakurai *et al.* 2005).

At present, the mechanisms of Nrf2 upstream activation are not completely understood. A few independent, yet not mutually exclusive, theories have emerged in

this respect. Nrf2 has been shown to be constitutively expressed and localized in the cytosol, and maintained in a repressed state by complexing with the actin-associating protein, Keap1. This heterodimerization confines most of Nrf2 to the cytoskeleton and away from the nucleus. Keap1 has a cysteine-rich surface which is subject to oxidation in cases of oxidative and nitrosative stress, and to thiol adduction in cases of reaction with electrophiles. This apparently results in global conformational changes to Keap1 thereby, leading to the liberation of Nrf2. The monomeric Nrf2 is then available to translocate to the nucleus. In this manner, Keap1 acts as a redox-sensor that upregulates ARE antioxidant responses through Nrf2 (Itoh *et al.* 2004; Itoh *et al.* 2003; Kang *et al.* 2004; Levonen *et al.* 2004; Zhang and Hannink 2003). More recently, it has also been suggested that oxidation of selective cysteines on Keap1 might not change its affinity to Nrf2, but rather result in self-ubiquitination, and hence, releasing Nrf2 to transmigrate (Eggler *et al.* 2005).

Nrf2 activation also has been shown to be mediated through phosphorylation by mitogen-activated protein kinases (MAPKs), protein kinase C (atypical isoform) and phosphoinositol-3-kinase (PI3K) (Nakaso *et al.* 2003; Nguyen *et al.* 2003; Numazawa *et al.* 2003; Yu *et al.* 2000). Further upstream kinases may also play a role in these events. In addition, it has been proposed that Nrf2 can be activated through a redox-independent pathway. This involves a prior ER stress that induces an ER-specific protein kinase, termed PERK, which can directly phosphorylate Nrf2 (Cullinan and Diehl 2004; Cullinan *et al.* 2003).

From the studies reported here, TFEC can be seen to induce some Phase II enzymes and antioxidant responsive genes in TAMH cells, and this is likely a consequence of early Nrf2 induction. This phenomenon has not been previously reported for TFEC or other halogenated aliphatics. To establish mechanistic links to the activation of Nrf2, we examined numerous indicators of cellular oxidative stress, but the overall lack of any significant changes in these parameters suggests that classical oxidative stress does not contribute significantly to TFEC-mediated cytotoxicity in TAMH cells.

These findings are consistent with previously reported *in vivo* findings (Groves *et al.* 1991). While this does not rule out a role for Keap1 in the regulation of Nrf2 translocation, it does imply that redox changes related to GSH status or ROS production are not pivotal in the activation pathway. In future studies it will be of interest to examine the possibility of Keap1 modification following transient, low-level oxidative stress or reactions with electrophilic reactive metabolites using highly sensitive mass spectrometry techniques.

One of the earliest effects of TFEC observed was a rapid depletion of intracellular ATP. TFEC-mediated modification and inhibition of mitochondrial aconitase and αKGDH activities (both important enzymes in the TCA cycle) might result in a localized intramitochondrial oxidative stress leading to the rapid inhibition of ATP production- an important determinant of the commitment to necrosis or apoptosis (Leist *et al.* 1997; Leist *et al.* 1999). Intracellular ATP concentrations are critical for cell viability, and marked ATP depletion (15-25% of control) has been hypothesized to switch the cell death mechanism from apoptosis to necrosis (Lieberthal *et al.* 1998). In fact, our previous studies with TFEC have shown that despite mitochondrial changes supporting apoptosis (e.g. cytochrome *c* release), activation of pro-apoptotic caspases does not occur. Rather, energy-independent cysteine proteases, like calpains, replace caspases as the major enzymes catalyzing proteolysis (Chapter 2). The present work provides direct evidence for an immediate loss of ATP that is consistent with the decay of early apoptotic signals into a secondary necrosis. More importantly, we have also demonstrated that replenishment of ATP by glucose supplementation significantly restored cell viability. Even though depletion of ATP in glucose supplemented cells was still significant, it appears that a higher basal level was sufficient to "cushion" some of the damage produced by TFEC. These data confirm the importance of low intracellular ATP levels on critical downstream energy-dependent processes.

The lack of clear evidence for a generalized cellular oxidative stress, coupled to significant ATP depletion, implicates an alternative pathway for the activation of Nrf2

in this cell death model. One possibility is an ER-stress mediated Nrf2 induction. An ER resident protein kinase, PERK, is known to directly phosphorylate Nrf2 and trigger dissociation from Keap1 without the involvement of ROS (Cullinan *et al.* 2003). PERK itself is strongly activated as part of the unfolded protein response (UPR) and has been shown to be critical for cell survival during ER stress (Cullinan and Diehl 2004). A recent study has also reported that ER stress stimulated HO-1 induction occurs through Nrf2 binding to ARE, consistent with our findings (Liu *et al.* 2005). Furthermore, regulation of calcium homeostasis appears to be important during Nrf2 activation (Lee *et al.* 2003), and recently, a selective calmodulin/CaMK inhibitor, KN93, was shown to block Nrf2 activation of ARE gene induction in HepG2 cells treated with diallyl trisulfide (Chen *et al.* 2004).

The role of ER stress in TFEC-induced cytotoxicity is not well-studied, but there are scattered reports which suggest that this might be a significant and under-appreciated phenomenon. For example, a role for calpains in renal cell death following TFEC treatment has been demonstrated (Schnellmann and Williams 1998), in agreement with our previous work using TAMH cells (Chapter 2). Of particular significance, calpain activation was blocked by overexpression of anti-apoptotic BCL-xL (Chapter 2). These studies provided additional evidence for ER stress coupled with induction of specific ER stress proteins in TFEC-induced cytotoxicity. For example, Atf3 is recognized as an important stress responsive ER-bound transcription factor that has been shown to induce Gadd153 (Wolfgang *et al.* 1997). Accordingly, Gadd153 is another ER stress responsive gene shown to be strongly induced by TFEC. Since covalent binding precedes all other events, these findings suggest that ER stress occurs as a result of some prior mitochondrial dysfunction. Because a strong link has already been made between ATP depletion and calcium release from the ER (Harriman *et al.* 2002), we hypothesize that interruption of mitochondrial function causes a rapid depletion of intracellular ATP by TFEC, which leads to ER calcium release and an unfolded protein response (UPR) which is an energy-dependent process (Figure 4.10). It is also possible that ATP depletion directly inhibits Ca-ATPase such that calcium is

released from ER stores. Our ongoing efforts will include attempts to detect activation of PERK, as well as other calcium-dependent signaling pathways, in Nrf2 phosphorylation and activation.

Overall, to the best of our knowledge, this is the first evidence of Nrf2 activation in halogenated aliphatics-induced cytotoxicity. The apparent lack of oxidative stress, despite clear transcriptional upregulation of classical antioxidant response genes, suggests that a pathway independent of classical oxidative stress might be involved in this mitochondrially-initiated pathway of toxicity. A strong ER response following ATP deprivation provides important clues to support further investigations of ER stress mediated Nrf2 activation.

Table 4.1. **Microarray analyses of *de novo* TFEC-inducible and ARE responsive genes.** Analyses were performed on TAMH cultures treated with 200 μM TFEC for 2, 4 or 6 h. Results have been expressed as a normalized ratio of gene expression in the TFEC-treated samples vs. aqueous vehicle treated controls. Selected ARE-possessing and highly expressed genes are listed and ranked among all genes according to fold induction at 4 h.

Rank	Gene name	Fold induction		
		2 h	4 h	6 h
1	Heme oxygenase (Decycling) 1	17.2	29.4	31.0
2	Glutathione S-transferase, (GSTA2)	9.2	26.4	40.8
26	Glutamate cysteine ligase, regulatory subunit	2.6	4.0	4.5
29	Glutamate cysteine ligase, catalytic subunit	3.0	3.9	3.2
40	Thioredoxin reductase 1 (TXNRD1)	2.9	3.2	3.2
73	Glutathione S-transferase, (GSTA4)	2.0	2.6	2.8
77	Oxidative stress induced gene (STAP or A170)	2.0	2.5	2.5
126	Glutathione S-transferase, (GSTA3)	1.5	2.0	2.4
211	Glutathione reductase 1 (GSR)	1.4	1.7	2.3

Table 4.2. **RT-PCR analyses of ARE responsive genes.** Selected genes shown to be upregulated by microarray analyses were validated with real-time quantitative RT-PCR using TaqMan (for *GSTA3*, *GCLC* and *GCLM*) and SYBR Green (for *GSTA2*) fluorogenic probes. Results are expressed as a normalized ratio using the housekeeping gene GAPDH as reference. Standard deviation for each data point is shown in parentheses. All expression levels show a statistically significant difference as compared to their respective untreated controls ($0.001<p<0.05$).

Gene name	Ratio of (gene/GAPDH) mRNA expression			
	0 h	2 h	4 h	6 h
Glutathione S-transferase, (GSTA2)	0.002 (0.000)	0.026 (0.000)	0.122 (0.003)	0.223 (0.016)
Glutamate cysteine ligase, regulatory subunit	0.130 (0.005)	0.383 (0.079)	0.572 (0.022)	0.702 (0.000)
Glutamate cysteine ligase, catalytic subunit	0.199 (0.002)	0.527 (0.045)	0.740 (0.108)	0.800 (0.083)
Glutathione S-transferase, (GSTA3)	0.110 (0.001)	0.294 (0.026)	0.418 (0.063)	0.455 (0.048)

Table 4.3. **Microarray analyses of TFEC-mediated induction of ER stress response genes.** Microarray experiments were performed on TAMH cultures treated with 200 μM TFEC for 2, 4 or 6 h. Results have been expressed as a normalized ratio of gene expression in the TFEC-treated samples vs. aqueous vehicle treated controls. Selected genes previously known to play prominent roles in the mammalian ER stress response are listed and ranked among all genes based on fold induction at 4 h.

Rank	Gene name	Fold induction		
		2 h	4 h	6 h
6	DNA-damage inducible transcript 3 (DDIT3 or GADD153)	3.6	10.4	13.5
10	Activating transcription factor 3 (ATF3)	2.9	8.3	11.5
12	Growth arrest and DNA-damage inducible 45α (GADD45a)	3.8	7.0	9.2
13	Myeloid differentiation primary response gene 116 (MYD116 or GADD34)	1.8	7.0	10.8
23	Growth arrest and DNA-damage inducible 45γ (GADD45g)	2.0	4.3	9.2
124	N-Myc downstream regulated 1 (NDR1)	1.7	2.0	2.3

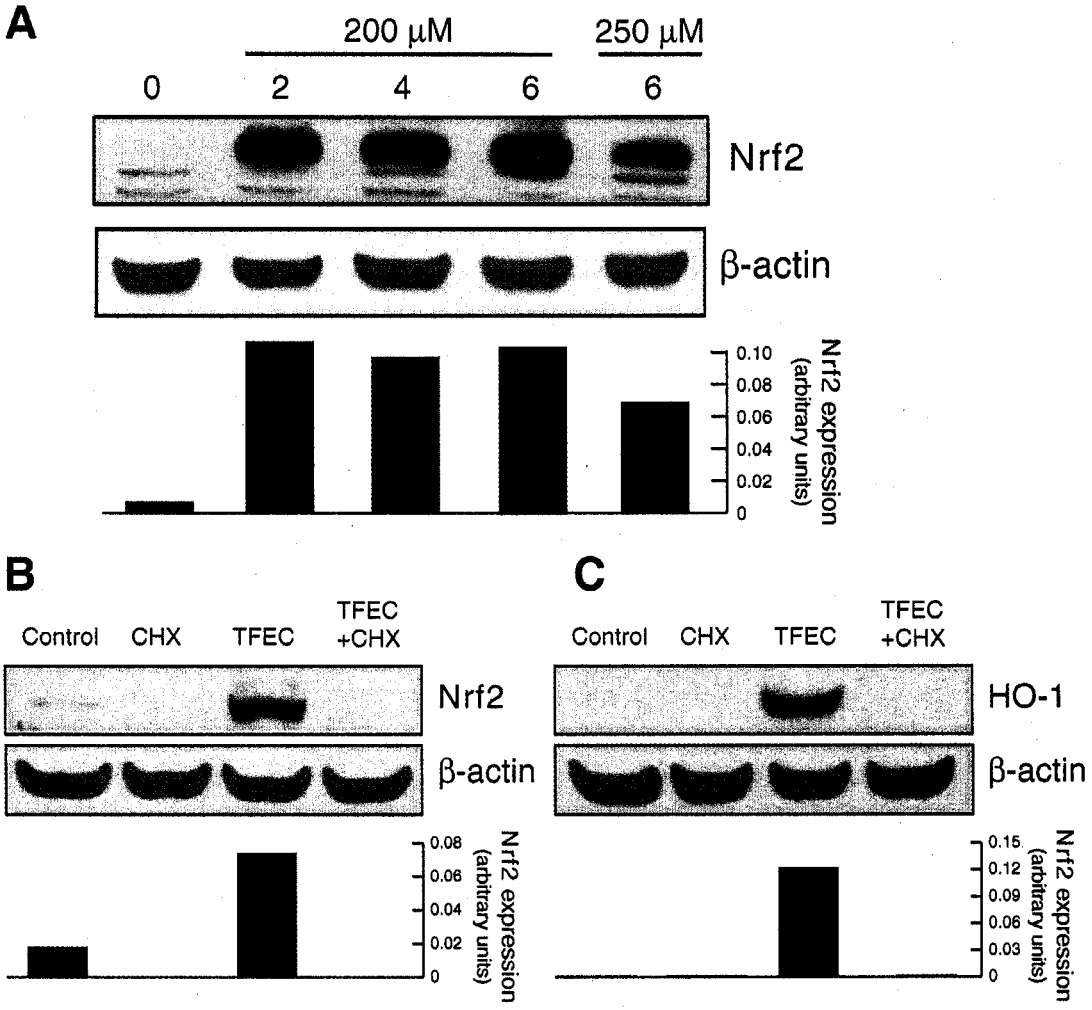

Figure 4.1. **Confirmation of Nrf2 induction following TFEC treatment by immunoblot assay.** (A) TAMH cells were treated with 200 or 250 μM TFEC for 0 to 6 h. Whole cell lysates were resolved by SDS-PAGE and immunoblotted with polyclonal antibodies to Nrf2. Monoclonal antibodies to β–actin were employed as loading control. (B,C) TAMH cell lysates were treated with 250 μM TFEC, in the presence or absence of cycloheximide (10 μg/mL) and immunoblotted for Nrf2 or HO-1 using polyclonal antisera. Nrf2 expression was quantified by densitometric analyses as displayed below each sub-figure.

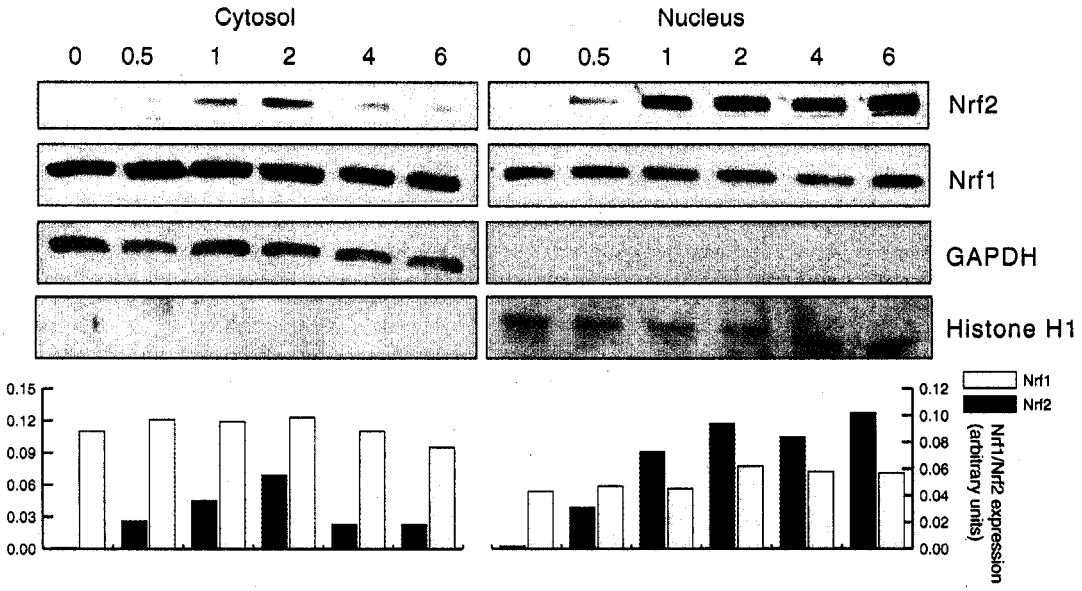

Figure 4.2. **Subcellular distribution of Nrf2 in response to TFEC treatment.** TAMH cultures were treated with 200 μM TFEC for 0, 0.5, 1, 2, 4 and 6 h. Subcellular fractions of cytosol and nuclei were separated by standard centrifugation procedures, resolved by SDS-PAGE, and subsequently immunoblotted with polyclonal anti-sera to Nrf2 and to Nrf1. Expression of Nrf1 and Nrf2 were quantified by densitometric analyses as shown below the immunoblots.

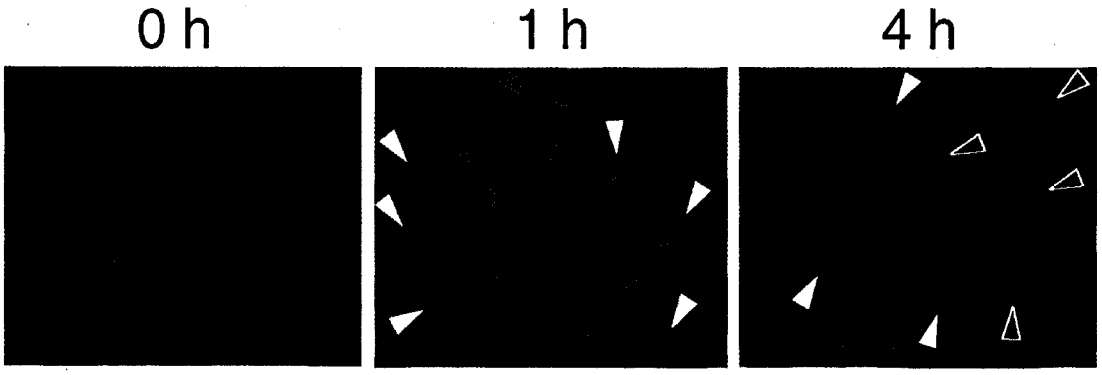

Figure 4.3. **Immunocytochemical detection of Nrf2 subcellular localization.** TAMH cells were treated with 200 μM for 0 to 4 h. Nuclei were stained with DAPI and Nrf2 with FITC-conjugated anti-rabbit antibody. The cells were fixed to slides with paraformaldehyde and viewed using fluorescence microscopy. Movement of Nrf2 from the cytosol to the nucleus was observed as decreased cytosolic staining of FITC-conjugated secondary antibody at both 1 h and 4 h, and increasing co-localization of FITC green dye with blue DAPI-stained nuclei (indicated by solid white arrowheads). Nuclear condensation of treated cells at 4 h is also shown (black arrowheads).

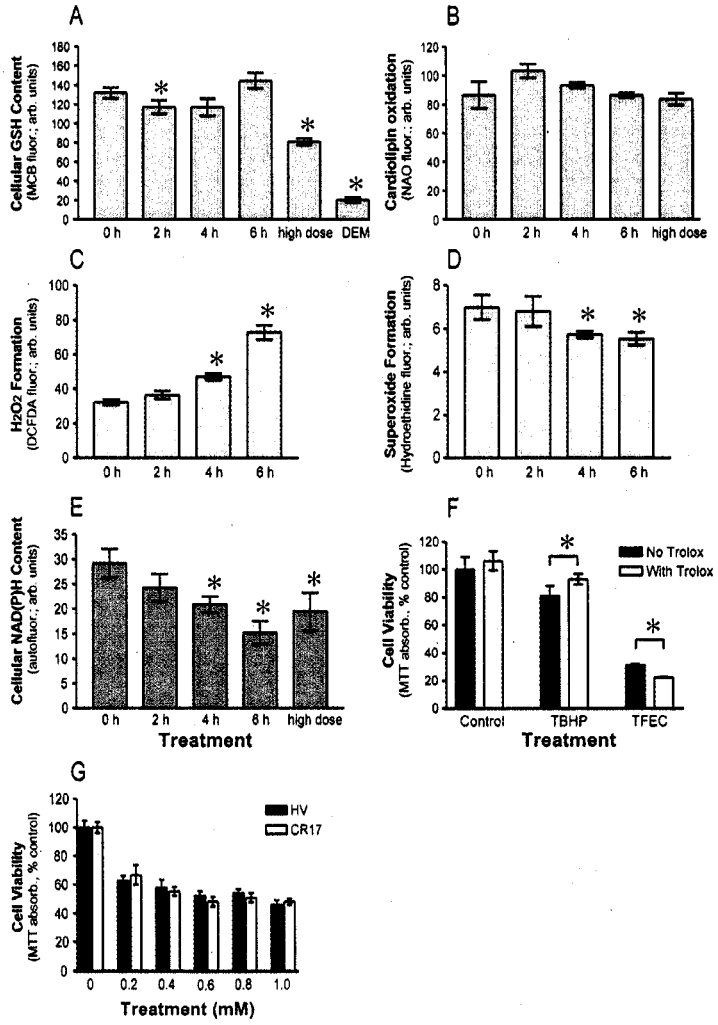

Figure 4.4. **Detection of oxidative stress in TFEC toxicity.** TAMH cells were treated with 250 μM TFEC for 0 to 6 h and subjected to the following analyses: (A) Cellular reduced GSH levels as determined by flow cytometry using MCB staining. DEM (125 μM, 4 h) was administered as a positive control for GSH depletion. (B) Mitochondrial membrane cardiolipin oxidation as measured by flow cytometry using NAO staining. A higher dose of TFEC beyond the toxicological range (400 μM) at 4 h was used to confirm a lack of response. (C) Hydrogen peroxide release was determined spectrofluorometrically using DCFDA staining. (D) Superoxide was determined by oxidation of hydroethidine (5 μM) using flow cytometry. (E) NAD(P)H was measured by flow cytometry using UV excitable autofluorescence. (F) The effect of the antioxidant, Trolox (1 mM) was investigated by MTT viability using TFEC (250 μM) for 24 h. Positive control was with t-butylhydroperoxide (TBHP, 500 μM, 3 h). (G) Wild-type Hepa-1 cells (HV) and GCL subunits-overexpressing cells (CR17) were dosed with up to 1 mM TFEC for 24 h. Cell viability was assayed by MTT. (* indicates a statistically significant difference from control cells as determined by unpaired *t-test*, $p < 0.05$).

A

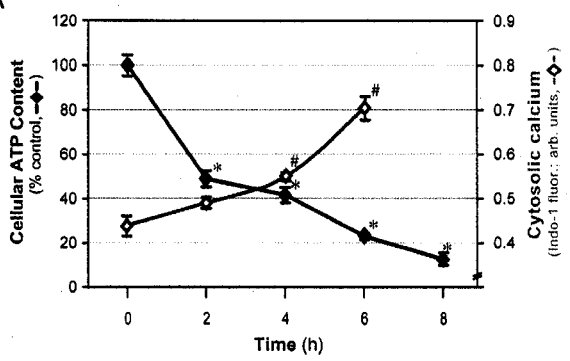

B

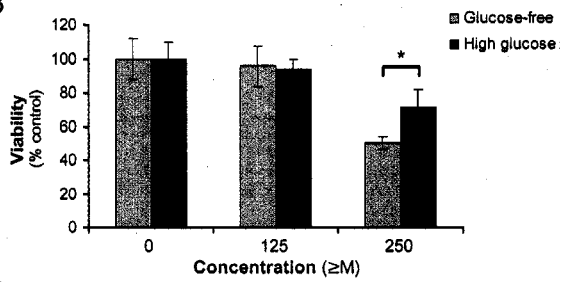

C

Treatment	Average RLU reading (n=4)	% control	SD
Glucose-free, no treatment	113.87	100.0	9.44
Glucose-free, 125 uM TFEC	176.93	155.4	14.14
Glucose-free, 250 uM TFEC	51.98	45.6	4.95
High glucose, no treatment	450.64	395.8	28.15
High glucose, 125 uM TFEC	332.07	291.6	30.78
High glucose, 250 uM TFEC	263.09	231.1	14.07

Figure 4.5. **Changes in intracellular calcium and ATP levels.** (A) TAMH cells were treated with 250 μM TFEC for 0 to 8 h for ATP measurement. Results are expressed on the left as a percentage of the luminescence detected in comparison to control cells (solid symbols). Intracellular calcium was measured spectrofluorometrically using Indo-1 AM staining of TAMH cells treated with 250 μM TFEC for 0 to 6 h. Results are expressed as a ratio of the fluorescence detected at 405 nm and 475 nm as indicated (open symbols). (* and # indicate a statistically significant difference from respective control cultures for intracellular ATP and calcium respectively, as determined by unpaired *t-test*, $P < 0.05$). (B) TAMH cells were treated with 250 μM TFEC for 24 h in glucose-free or high glucose DMEM medium. Viability was measured by MTT assay. Results are expressed as a percentage of viable cells in the untreated controls with +/- SD (n=6). (* indicates a statistically significant difference between glucose-free and high glucose treatment, $p<0.05$). (C) Intracellular ATP content in glucose-free or glucose-supplemented medium. TAMH cells were treated with 250 μM TFEC for 24 h in glucose-free or high glucose DMEM medium. Raw ATP levels are quantified in relative luminescence units (RLU). These values are subsequently expressed as a percentage of the luminescence detected in comparison to glucose-free incubated control cells.

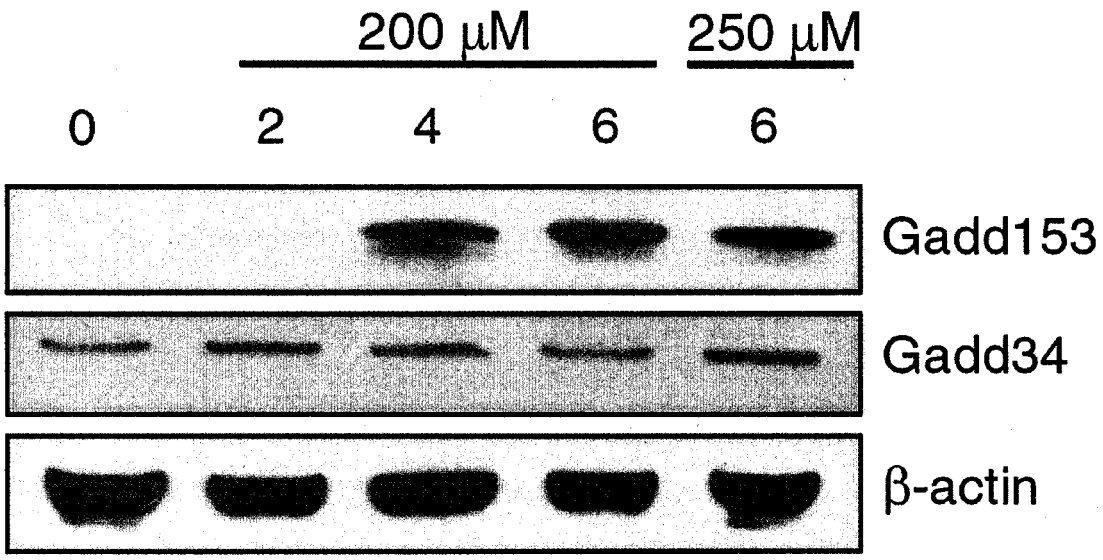

Figure 4.6. **Immunoblot assay for Gadd153 and Gadd34 protein following TFEC treatment.** TAMH cells were treated with 200 or 250 μM TFEC for 0 to 6 h. Whole cell lysates were resolved by SDS-PAGE and immunoblotted with polyclonal anti-Gadd153 and anti-Gadd34. Equal loading between lanes was confirmed by reprobing blots with monoclonal β–actin antibody.

Figure 4.7. **Immunoblot analysis for Atf3 and HSP70i protein expression following TFEC treatment.** TAMH cultures were treated with 200 or 250 μM TFEC for 0 to 4 h. Cells treated at 200 μM were replaced with fresh medium at 4 h and kept for a total of 8 and 20 h. Whole cell lysates were resolved by SDS-PAGE and immunoblotted with polyclonal antibodies to Atf3 and monoclonal antibodies to HSP70i.

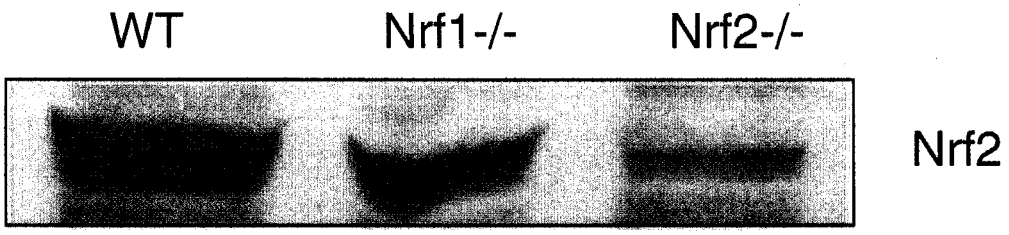

Figure 4.8 **Immunoblot analysis for Nrf2 in MEFs.** The constitutive expression of Nrf2 was compared in MEF-WT, *-Nrf1-/-* and *Nrf2-/-* using polyclonal anti-Nrf2 antibody.

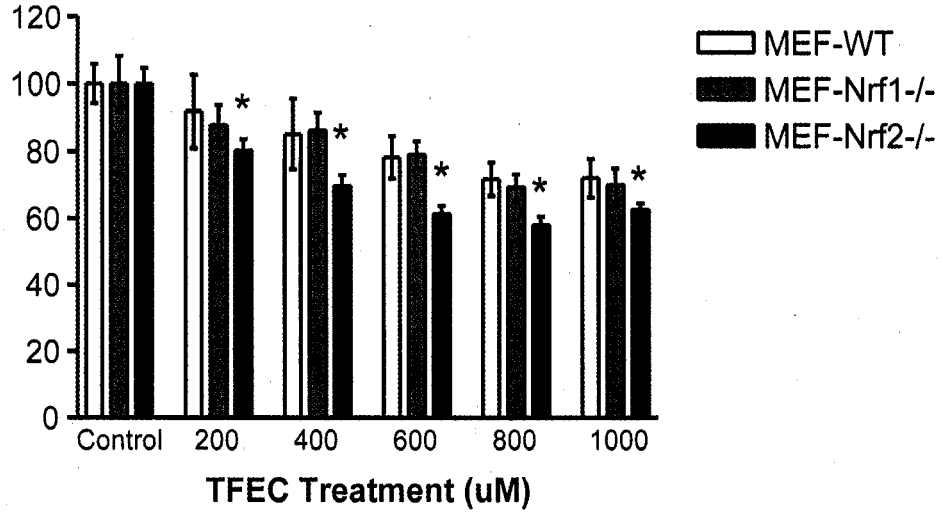

Figure 4.9 **Cell viability assay for TFEC toxicity in MEFs.** Wildtype, *Nrf1*-/- and *Nrf2*-/- MEF were treated with TFEC (0-1000 μM) for 24 h. Cell viability was measured by MTT. Results are expressed as a percentage of viable cells in the untreated controls with +/- SD (n=6). (* indicates a statistically significant difference between glucose-free and high glucose treatment, $p<0.05$).

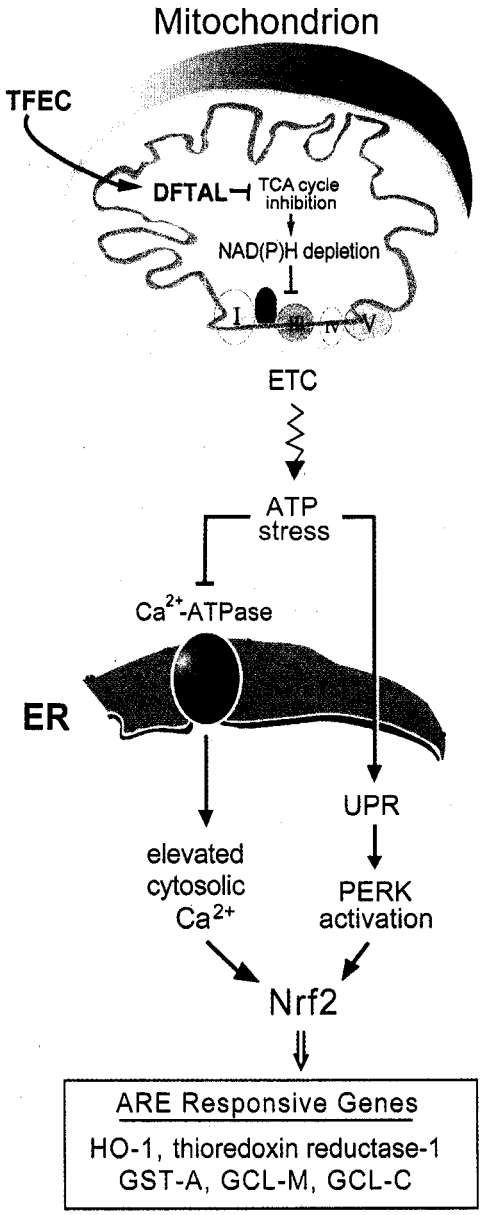

Figure 4.10. **Proposed events leading to Nrf2 activation in TFEC toxicity.** TFEC is taken into the mitochondria and metabolized by β-lyase activities to generate a reactive intermediate (DFTAL) that readily binds lysine residues of neighboring proteins. Specific binding to the TCA enzymes αKGDH and aconitase result in a depletion of TCA function and NAD(P)H production. Reduced NAD(P)H may suppress the electron transport chain (ETC) and bioenergetics as exemplified by intracellular ATP depletion (refer to Figure 5). This "ATP stress" can lead to ER changes through two possible pathways: (1) inhibition of ER-resident calcium-ATPase pumps and release of ER calcium into the cytosol where it can activate subsequent signaling pathways; and/or, (2) direct stimulation of the UPR and other ER protein kinases. Both pathways have previously been shown to activate Nrf2 transcription activities.

Chapter 5

Is There A Critical Target? Searching For Answers And Future Studies

5.1 Introduction

Thus far, we have examined the biochemical pathways and consequences of TFEC-induced toxicity, primarily in a well-characterized mouse hepatocyte cell line, TAMH. The data gathered from Chapter 2 confirmed the role of an early mitochondrial dysfunction in effecting downstream mitochondrial changes, leading ultimately to a secondary necrosis. We also learned that early mitochondrial perturbations rapidly dissipated to other organelles, resulting in a generalized cellular stress response, involving both cytosolic (HSPs) and ER (e.g. ATF3 and Gadd153) stress proteins. We have considered a dual mechanism of toxicity, implicating both protein modification and oxidative stress. However, the lack of a convincing early oxidative stress as described in Chapter 4, likely suggests that oxidative stress, if any, is a consequence of earlier biochemical changes, rather than an initiation event for cytotoxicity. Therefore, despite a highly coordinated induction of ARE genes (including *HO-1*, *GCL*, *GST-alpha* etc.) through the Nrf2 pathway (Chapter 4), a direct and early link to oxidative damage was absent.

In light of these recent findings, it is plausible that mitochondrial dysfunction in TFEC-treated TAMH cells is primarily, if not exclusively, dependent on an early modification of mitochondrial proteins, including AST, aconitase, αKGDH, HSP60 and mtHSP70 (Bruschi *et al.* 1998; Bruschi *et al.* 1993; James *et al.* 2002). A widely accepted paradigm for protein modification in toxicology is the existence of some critical target(s). The hypothesis is that damage to these critical targets initiates pathways that lead to toxicity (Chapter 1). Therefore, this possibility was considered as a mechanism in TFEC-induced cytotoxicity. In Chapter 1, the targets were reviewed and a model for mitochondrial damage was proposed. Briefly, aspartate aminotransferase (AST) was proposed as a likely candidate for β-lyase scission of

TFEC to generate the electrophilic, DFTAF (Cooper *et al.* 2002b). This intermediate readily adducts the lysine groups of mitochondrial proteins in its vicinity, including aconitase and αKGDH, whose resulting functional deficits have already been characterized (Bruschi *et al.* 1998; James *et al.* 2002). Mitochondrial stress proteins, HSP60 and mtHSP70 were also adducted, possibly as part of a battery of mitochondrial stress responses to alleviate protein damage. Furthermore, mtHSP70 co-immunoprecipitated with a high molecular weight mitochondrial β-lyase which may partially explain its adduction by DFTAF (Cooper *et al.* 2001). A pertinent question to address is whether adduction of some of these targets has more extensive toxicological consequences. Mitochondrial aconitase and αKGDH being key enzymes in the TCA cycle, were considered important targets to focus upon. The conversion of α-ketoglutarate to succinyl-CoA by αKGDH is the rate-limiting step in the TCA cycle (Huang *et al.* 2003a). Thus, it is conceivable that adduction by TFEC could have a direct and detrimental impact on cell bioenergetics and downstream processes. Furthermore, a novel role of aconitase has been shown in the maintenance of mtDNA stability in yeast (Chen *et al.* 2005). Hence, adduction of aconitase may contribute to mtDNA instability, in addition to its role in ATP synthesis. This mechanism may exacerbate, or even be the major determinant for TFEC-induced toxicity.

Therefore, it was of interest to investigate if aconitase and/or αKGDH were critical targets in TFEC-induced cytotoxicity. An attempt was made to compare the toxicological profile of TFEC with known TCA cycle inhibitors of aconitase and αKGDH: sodium fluorocitrate and sodium arsenite respectively, using microarray clustering analysis and toxicity assays. In addition, some unresolved questions from earlier studies (Chapters 2 to 4) are addressed, to provide a better understanding of mechanisms of TFEC-mediated cytotoxicity.

5.2 Materials and Methods

5.2.1 Cell culture

Serum-free cell culture of the TAMH line between passages 21-35 was undertaken as previously described in Chapter 2. The human hepatocarcinoma cell line, HepG2/C3A (ATCC, Manassas, VA) was maintained in F12 nutrient mixture (Invitrogen) supplemented with 5% FBS, 50 U/mL penicillin and 50 μg/mL streptomycin (Invitrogen). Medium was replaced every third day.

5.2.2 Stable transfection

Keap1/FLAG mammalian expression vector was obtained as a gift from Dr. Dan Liebler (Vanderbilt University, Nashville, TN). Transfection in TAMH cells was carried out according to methods described previously (Sekhar *et al.* 2003). Briefly, cells grown in 6-well dishes were transfected with 4 μg of plasmid with lipofectamine (Invitrogen) in Opti-MEM medium (Invitrogen). Twenty-four hours after the initial transfection, cells were trypsinized and passed into 35 mm dishes with standard TAMH cell growth medium (see Chapter 2 for description) enriched with G418 (1000 μg/mL). Individual clones were isolated and expanded. These clones were subsequently maintained in 500 μg/mL G418 and screened for successful transfection using an anti-FLAG antibody (Sigma) for detection of Keap1/FLAG protein by Western blot.

5.2.3 Microarray analysis procedures

HepG2/C3A cells were grown on 150 cm^2 tissue culture dishes before they were subjected to various treatments for RNA isolation and microarray analyses according to the method described in Chapter 3. Affymetrix Human Genome U133A version 2.0 arrays (Affymetrix, Santa Clara, CA) were used for microarray analysis.

5.2.4 Immunoblot procedures

All the fractions collected were assayed for protein concentration using the BCA protein assay kit (Pierce Chemical Co., Rockford, IL). Each 30-50 μg of sample

proteins were resolved by denaturing electrophoresis, SDS-PAGE (Mini-PROTEAN II; Bio-Rad Laboratories, Hercules, CA) and transferred to nitrocellulose membrane for 1 h at 15 V using Trans-Blot SD Semi-Dry Transfer Cell (Bio-Rad). Immunodetection was by chemiluminescence (SuperSignal ULTRA; Pierce, Rockford, IL) using specific antibodies diluted in PBS with 0.05% v/v Tween 20 and 5% w/v powdered milk. Anti-FLAG and anti-β-actin (1:20,000) were from Sigma, anti-GCLc and anti-GCLm were gifts from Dr. Terry Kavanagh, University of Washington, anti-MnSOD was from Stressgen and another similar antibody was made available through Dr. Naoyuki Taniguchi, Osaka University, Japan. Anti-mouse and anti-rabbit horseradish peroxidase conjugated secondary antibodies (Pierce) were used at 1:20,000 dilutions. All primary antibodies were used at 1:2,000 dilutions unless otherwise stated.

5.2.5 Viability assay by MTT

Cell viability was determined by 3-(4,5-dimethylthiazol-2-yl)-2,5-diphenyl-tetrazolium bromide (MTT) viability assay according to protocols as described previously (Chapter 2).

5.2.6 SOD activity assays

Total and MnSOD activities were determined using a colorimetric SOD determination kit (Sigma). The method is based upon the reduction of 2-(4-iodophenyl)-3-(4-nitrophenyl)-5-(2,4-disulfophenyl)-2H-tetrazolium salt (WST-1) into a formazan dye by reaction with superoxide, performed according to manufacturer's instruction. MnSOD specific activities were measured with the addition of 1 mM KCN to the cell lysates to inhibit cytosolic SOD activities.

5.2.7 Assessment of mtDNA damage in *Saccharomyces cerevisiae*

Mitochondrial dysfunction and mutation was assessed using a color colony method as described previously (Kim *et al.* 2002). This assay was performed by our collaborator, Dr. Ron Butow, University of Texas Southwestern Medical Center, Dallas, TX.

Briefly, *ade* mutant colonies were treated with various concentrations of TFEC for 72 h. Pictures of the resultant colonies were taken to evaluate the extent of discoloration as an indicator of mitochondrial dysfunction and mutation. Furthermore, petite colonies after each treatment were scored, tested and expressed as a percentage of total colonies formed (i.e. petite frequency), according to methods described previously (Chen and Clark-Walker 1993).

5.3 Results

5.3.1 Microarray analysis of TFEC treated HepG2/C3A cells

HepG2/C3A cells were employed as a human equivalent of the murine TAMH cell line used previously as described in Chapters 2-4. Microarray analyses were conducted on these cells treated with aqueous vehicle, TFEC (150 μM) or the specific aconitase inhibitor, sodium fluorocitrate (1 mM) at their respective LD_{50} (24 h). RNAs were isolated at 6 and 24 post-treatment respectively. This microarray experiment was part of a larger scale toxicogenomics study which involved establishing the gene expression profile of HepG2/C3A cells treated with a number of well-characterized mitochondrial toxicants including flutamide, antimycin A and rotenone. When clustering analysis was performed on these samples, it was observed that the gene expression profile of TFEC treated cells resembled most closely that of sodium fluorocitrate (data not shown).

When examining exclusively the top 600 most differentially regulated genes in each treatment (i.e. 300 most up-regulated and 300 most down-regulated genes), a significant number of genes that were strongly induced in TFEC-treated TAMH cells (Chapter 3 and 4) were correspondingly up-regulated in the human HepG2/C3A cells. Major genes involved in heat shock, oxidative stress and ER stress response were highly induced (Table 5.1). Examples include various isoforms of *HSP70*, *HSP40* and *HSP105* of the heat shock protein family; *heme oxygenase-1*, *GCL* subunits and thioredoxin reductase of the oxidative stress responsive genes; as well as *ATF3*, *ATF4* and *Gadd45B* of the ER-stress responsive genes. It was also observed that 191 of the

600 differentially expressed genes after TFEC treatment were identical to those differentially expressed after fluorocitrate treatment. These similarities were particularly significant among genes regulating stress response, transcriptional control, metabolism, growth and differentiation. A representative subset of these genes is displayed in Table 5.2.

5.3.2 Comparison of cellular responses: TFEC vs. αKGDH inhibitors

To investigate if the binding and inhibition of αKGDH by DFTAF is an important initiating event in TFEC-mediated cytotoxicity, cellular responses to TFEC treatment were compared against classical αKGDH inhibitors (sodium arsenite and α-ketomethylvaleric acid, a.k.a. KMV). A number of studies (Table 5.3) have shown that both arsenite and KMV cause necrosis through a mitochondrial pathway, just as in TFEC-induced cytotoxicity, including initiation of the mitochondrial membrane permeability transition (MPT) and the release of cytochrome *c* to the cytosol. Conflicting results were obtained for the activation of caspases by KMV, as well as the major role of oxidative stress in arsenite-induced toxicity. A significant Nrf2 induction and activation was also observed after arsenite treatment as after TFEC treatment (Chapter 4).

Separately, toxicity of TFEC in TAMH was compared against fluorocitrate and KMV using an MTT viability assay. At 24 h treatment, LD_{50} of fluorocitrate was approximately 1000 μM (Figure 5.1A). KMV did not display any significant toxicity even up to 2 mM treatment (Figure 5.1B). On the other hand, TFEC at 250 μM reduced viability to approximately 30% while previous data demonstrated an LD_{50} of 125 μM (Figure 2.2).

5.3.3 Effects of TFEC on mitochondrial DNA in yeast

In view of a recent literature report of a novel role for aconitase in the maintenance of mitochondrial DNA (mtDNA) stability (Chen *et al.* 2005), the possible indirect effect of TFEC to destabilize mtDNA through inhibition of aconitase was examined.

Saccharomyces cerevisiae ade2 mutant cultures were exposed to varying concentrations of TFEC. These cells produce red colonies, which decolorizes (i.e. turns to white) during mitochondrial dysfunction and mutagenesis. A progressive loss of mitochondrial DNA and function was observed with increasing TFEC concentrations (up to 1 mM), as shown with the dose-dependent discoloration of the yeast cultures (Figure 5.2). Colonies turned completely white between 500 and 1000 μM. Effects of the treatment on mtDNA were also assessed by the formation of structurally abnormal petite cells. These cells have either a partial or complete loss of mtDNA and were incapable of oxidative phosphorylation. A quantitation of petite frequency is shown in Figure 5.3. Notably, a mediocre but significant increase in petite cells was observed between 250 to 500 μM TFEC (i.e. from 4 to 7 %).

5.3.4 Post-translational modification of GCL by TFEC

The expression of GCL subunits after TFEC (250 μM, 0-8 h) treatment was monitored by immunoblot assays. As shown in Figure 5.4A, minimal increase in expression was observed for native GCLC and GCLM at 73 and 30 kDa, respectively. Conversely, an unknown band of approximately 130-140 kDa increased in intensity in a time-dependent manner with TFEC treatment. This band was immunoreactive to both polyclonal GCLC and GCLM antibodies, suggesting that it could be a heterodimer, comprised of both GCL subunits. Additional information about this band was obtained by the co-administration of the specific protein synthesis inhibitor, cycloheximide (10 μg/mL). After treatment for 6 h with TFEC in the presence of cycloheximide, the immunoreactive band at 130-140 kDa was still formed (Figure 5.4B).

5.3.5 Effects of TFEC on MnSOD expression and activity

The expression of another oxidative stress responsive enzyme, mitochondrial manganese superoxide dismutase (MnSOD), was monitored after TFEC treatment for 0-8 h. By immunoblot analysis, it was demonstrated that a high molecular weight band (at 40-45 kDa), suggestive of a dimer of MnSOD (native protein at 22 kDa), progressively increased with increasing duration of TFEC treatment. The use of a

different MnSOD-specific antibody (obtained as kind gift from Dr. Naoyuki Taniguchi, Osaka University, Japan) gave the same result (Figure 5.5).

The activity of MnSOD was subsequently measured to determine the functional significance of the apparent dimer. Total SOD and MnSOD specific activities were quantified using a colorimetric method (Sigma product no. 19160). It was shown that the increase in the MnSOD "dimer" did not alter MnSOD or total SOD activities (Figure 5.6).

5.3.6 Stable transfection of Keap1 and impact on TFEC-induced cytotoxicity

Other than the ER-stress mediated Nrf2 induction hypothesized in Chapter 4, Nrf2 activation may also be triggered by direct alkylation of the cytosolic Nrf2 represssor, Keap1 protein, leading to a possible conformational change in this protein (Dietz *et al.* 2005; Dinkova-Kostova *et al.* 2001; Hong *et al.* 2005). To investigate this possibility, Keap1/FLAG plasmid was transfected into TAMH cells. Clonal selection for positive stable transfectants was by immunoblot assay using anti-FLAG antibody. Of the 5 clones screened, only Clone 2.2 was positive for Keap1/FLAG expression (Figure 5.8). This clone was subsequently expanded and exposed to 0, 50, 250 or 500 μM TFEC for 24 h. Using the MTT viability assay, it was revealed that Keap1/FLAG overexpression potentiated the toxicity of TFEC. At a TFEC concentration of 50 μM, viability of these cells decreased from approximately 100% to 60 % (Figure 5.9). Statistically significant decreases in viability were also observed at higher concentrations, albeit less pronounced.

To detect direct binding of TFEC to Keap1, TFEC treated Keap1/FLAG overexpressing TAMH cells were immunoprecipitated with anti-FLAG antibody and subsequently immunoblotted with the DFTAL cross-reactive antibody, anti-TFA (Satoh *et al.* 1985). However, no DFTAL adducts were observed (data not shown).

5.4 Discussion

The direct functional impact of TFEC binding to the TCA cycle enzymes, aconitase and αKGDH, has already been established. Previous studies in murine TAMH cells (James *et al.* 2002) and PC12 cells (Park *et al.* 1999) have demonstrated inhibition of enzymatic function for both enzymes. Results of studies reported in this dissertation also described reduction of mitochondrial NADH production, as well as a generalized depletion of intracellular ATP (Chapter 4). Here, we provide further evidence supporting the hypothesis that major cellular responses to TFEC treatment exhibit remarkable congruence with chemically-induced inhibition of both aconitase and αKDGH by alternative procedures.

Cytotoxicity caused by TFEC was also reproduced in a human HepG2/C3A cell line, (LD_{50} of 150 μM at 24 h, data not shown). A large number of genes that were strongly induced in the TAMH cells after TFEC treatment were correspondingly induced in C3A cells, e.g. *HSP70*, *HSP40*, *HO-1*, *ATF3* and *GCL* subunits. More importantly, it was shown that the generalized gene expression profile overlapped significantly with that for the specific aconitase inhibitor, sodium fluorocitrate. Approximately one-third of the most differentially expressed genes were common between the two treatments. This high homology in genomic response strongly suggests that inhibition of aconitase is an important mechanism of TFEC-induced cytotoxicity.

While the primary role of mitochondrial aconitase in the TCA cycle is undisputable, some recent findings expanded our current understanding of its physiological role(s). In a February 2005 issue of *Science*, a novel function for yeast aconitase in the maintenance and packaging of mtDNA was reported (Chen *et al.* 2005). It was shown that aconitase, along with about twenty other mitochondrial proteins (including mitochondrial HSP60), associated directly with the mtDNA. This action was observed to be surprisingly independent of the catalytic role of aconitase within the TCA cycle Hence, it became logical to question if the binding of aconitase by DFTAF may

indirectly disrupt mtDNA packaging, leading to mitochondrial dysfunction. Accordingly, studies described herein supported an increase in mtDNA loss and mitochondrial dysfunction in yeast after treatment with toxicological doses of TFEC. However, this finding is still inconclusive because the bioactivation of TFEC in yeast might differ from the mammalian system. Thus, future studies using mammalian models will be necessary to evaluate the relevance of this observation. Nonetheless, it is suggestive that mtDNA instability may be another mechanism contributing to TFEC-mediated mitochondrial toxicity. By inference, the multiple physiological impact aconitase has on the cell can render it a critical target for toxicity.

Apart from aconitase, another important adducted protein to consider is αKGDH. Even though earlier studies have demonstrated that the extent of inhibition of aconitase was greater than for αKGDH, the status of αKGDH as the rate-limiting step in the TCA cycle qualify this enzyme as a likely critical lesion resulting in toxicity. A number of neurodegenerative diseases have been associated with an early loss of αKGDH function (Huang *et al.* 2003b). For example, the earliest metabolic consequences of Wernicke-Korsakoff syndrome, which occur during thiamine deficiency, have been traced to the loss of αKGDH function (Desjardins and Butterworth 2005). In Alzheimers' disease, a reduction of αKGDH enzymatic activity correlated well with the extent of disease severity (Mastrogiacomo *et al.* 1993). Thus, the toxicological impact of αKGDH inhibition needs to be considered.

Arsenite binds and inhibits αKGDH by covalently modifying the lipoic acid moiety of the enzyme complex (Chacin *et al.* 1979). A survey of current literature has revealed a number of important similarities with TFEC. Firstly, both compounds result in a rapid depletion of ATP as a direct consequence of TCA cycle inhibition (Pourahmad *et al.* 2005). There is also clear involvement of a mitochondrial cell death pathway involving the membrane permeability transition and release of cytochrome *c* (Bustamante *et al.* 2005; Scholz *et al.* 2005). Even more convincingly, despite an early mitochondrial apoptotic signaling, necrosis ensued in both chemical-induced toxicities

(Scholz *et al.* 2005). Additionally, a competitive inhibitor of αKGDH, α-ketomethylvaleric acid (KMV), exhibited similar patterns of mitochondrial changes and necrotic cell death (Huang *et al.* 2003a; Huang *et al.* 2003b).

To put these comparative studies between TFEC and the various TCA cycle inhibitors (fluorocitrate, arsenite and KMV) into perspective, it is clear that the cellular responses in TFEC-induced toxicity is intricately linked to the effects of TCA cycle inhibition. A close resemblance between TFEC-induced toxicity and toxicity caused by both aconitase and αKGDH inhibitors implicates these enzymes in the mechanism of initiation of TFEC-induced toxicity. Moreover, preliminary studies demonstrated that fluorocitrate (LD_{50} approx. 1000 μM at 24 h) and KMV (LD_{50} > 2 mM at 24 h) are both significantly less toxic than TFEC (LD_{50} approx. 125 μM at 24 h) in TAMH cells, suggesting that inhibition of either enzyme alone is insufficient to reproduce the full complement of effects observed in TFEC-induced toxicity. Another interesting observation is that TCA cycle inhibition, caused by aconitase inhibition can be overcome by supplementation of α-ketoglutarate through transamination of glutamate via the ancilliary TCA cycle enzyme, AST. This alternative source of TCA cycle substrates helps sustain the production of NADH, bypassing the need for aconitase (Tretter and Adam-Vizi 2000). Therefore, this leads to the possibility that the binding and inhibition of AST by DFTAF may reinforce the blockade of the TCA cycle, thereby exacerbating mitochondrial dysfunction. Thus, the overall toxicity of TFEC might be due to inhibition of multiple and functionally interdependent critical targets, including aconitase, αKGDH and AST. The combined inhibition of all three enzymes effectively shuts down most NADH biosynthesis, triggering a rapid onset of ATP depletion and subsequent necrosis. A detailed analysis of their relative contribution would require specific silencing of individual enzymes and this is achievable with currently available technologies.

One other outstanding issue that remains to be addressed is post-translational modification of proteins after TFEC treatment. In Chapter 3, we discussed the

formation of a HSP25 dimer that was apparently resilient to standard reducing conditions (100 mM DTT). Interestingly, this phenomenon was observed in a few other instances. For example, it was observed that GCL subunits appear to heterodimerize to a 130-140 kDa complex (Figure 5.4). The molecular weight of this immunoreactive band matched a 138 kDa band (Davis *et al.* 1973), as well as a 2:1 heterotrimer (GCLM:GCLC), a biologically active GCL assembly that has previously been reported (Fraser *et al.* 2002). Furthermore, another oxidative stress response protein, MnSOD, formed an immunoreactive band that migrated at the expected homodimer mass (Figure 5.5). Just like the HSP25 dimer, the apparent MnSOD dimer and GCL trimer were resistant to standard reducing conditions (Figure 5.4A and 5.5). There was also a lack of clear functional correlations attributed to these complexes, since there was no significant change in intracellular GSH levels (Chapter 4) or MnSOD activity (Figure 5.6). Thus, it is not certain if this phenomenon has any biological significance. However, the uniqueness of this behavior makes TFEC a candidate toxicant to investigate the mechanism of formation of some novel protein complexes. Interestingly, another stress protein, calreticulin, is known to exist as a functional dimer (Jorgensen *et al.* 2003). Upon treatment of TAMH cells with TFEC, it was observed that calreticulin formed an apparent dimer that was resistant to standard DTT reducing conditions (Figure 5.7). The formation of this band over time also was consistent with the effects observed for the formation of both GCL and HSP25 multimers which were resistant to reducing conditions. Further characterization of these complexes will be necessary to verify their composition. The exact molecular mechanism for this occurrence is currently unknown, and also would require further investigation through a combination of protein purification and mass spectrometric analyses.

The final aspect of this discussion will address other possible molecular pathways regulating the activation of a Nrf2 response in TFEC-induced cytotoxicity. Results reported in Chapter 4 support an ER stress-mediated phosphorylation and activation of Nrf2. This mechanism obviates the need for an early oxidative stress as the stimulus.

An alternative explanation for an oxidative-stress independent route could be a direct alkylation of the cytosolic Nrf2 repressor, Keap1 (Dietz *et al.* 2005; Dinkova-Kostova *et al.* 2001; Hong *et al.* 2005). Just as with the oxidation of reactive thiols on the surface of Keap1, covalent modification with an electrophilic species could result in global conformational changes in Keap1, thereby liberating Nrf2 to undergo nuclear translocation. Through this mechanism, metabolic activation of TFEC would be sufficient for mediating downstream Nrf2 responses. This could account for a more rapidly acting Nrf2 activation pathway than if the activation cascade has to go through a prior redox perturbation. However, the lack of Keap1 modification (data not shown) by DFTAL rendered this an unlikely mechanistic route. Nonetheless, it is possible that Keap1 might play a modulatory role in Nrf2 activation and its subsequent cytoprotective effects, since TAMH cells stably transfected with Keap1/FLAG potentiated the toxicity of TFEC (Figure 5.9). The increase in Keap1 expression in the cytosol most likely limited the availability of Nrf2 to translocate to the nucleus. Ultimately, cytoprotective effects of antioxidant responses would be significantly attenuated. A confirmation of this postulation would require assessment of the various Nrf2-responsive genes under these conditions.

5.5 Future directions/conclusions

The heterogeneity of cellular pathways and responses in mitochondrial dysfunction has confounded our understanding of the subject. Even with the use of a highly selective mitochondrial toxicant, TFEC, the subsequent biochemical changes and modulation of regulatory pathways are multi-faceted and complex. However, our research has provided new information which adds to our knowledge of this particular chemical-induced mitochondrial damage.

Metabolic activation of TFEC through a β-lyase mediated pathway is the initiating event in cytotoxicity. Studies described in Chapter 2 conclusively demonstrated that DFTAL covalent modification of the TCA cycle enzymes by the reactive metabolite formed, DFTAF, likely activated a signaling pathway that initiated in mitochondria

and propagated more generally through the cell. These signals primed the cell for a classical apoptosis, which eventually decayed into a secondary necrosis. More intuitively, these findings have re-affirmed the concept that intracellular ATP is an important biological "rheostat" that determines the route for toxicity and cell death (a higher ATP level favoring apoptosis and low level favoring necrosis). Furthermore, it was revealed that despite a mitochondrial origin for toxicity, subcellular changes rapidly implicated other cellular components including the ER and cytosol.

The use of microarray as a preliminary tool helped identify the major extra-mitochondrial responses, including heat shock response (Chapter 3) and the oxidative stress response (Chapter 4). The induction of cytosolic HSPs supported the notion of an early, exported signal that radiated out from the mitochondria. Such induction may be cytoprotective by inhibition of downstream signaling processes. For example, a generalized heat shock protein induction was shown to be cytoprotective. However, protein-specific contributions have yet to be characterized. In addition, some of the specific protein responses should be investigated using siRNA against specific genes, e.g. *HO-1*, *HSP70i* and *GCL*, the most strongly up-regulated of the genes.

Global gene expression profiling has also led to the discovery of a major role for the stress-mediated transcription factor, Nrf2, in TFEC-mediated toxicity. Interestingly, evidence argued against an early oxidative stress, a well-established stimulus for the activation of the Nrf2 pathway. Instead, indirect evidence has suggested another route for Nrf2 activation through an ER stress response. While this hypothesis has to be tested more rigorously in the future, it is clear that mitochondrial damage is intricately linked to an ER response with upregulation of ER stress genes and ER calcium mobilizations (Chapter 4). Furthermore, crosstalk between these organelles may be more than just physiological. Recent studies using electron microscopic tomography have provided images of an intimate physical contact between the ER and the mitochondria. It has been suggested that this close interaction facilitates their

communication, e.g., the exportation of calcium signals (Mannella 2000; Mannella *et al.* 1998).

In conclusion, the investigation of TFEC-induced cytotoxicity has provided us with a useful tool to study biochemical changes in response to mitochondrial dysfunction. The research work described here is a good illustration of the use of genomic tools (i.e. microarray technology) to guide subsequent functional characterization of selected protein changes and responses. It is our hope that some aspects of this research will trigger new ideas, which may help identify novel targets and strategies against related mitochondrial pathologies.

Table 5.1 **Microarray analyses of *de novo* TFEC-inducible genes in HepG2/C3A cells.** Analyses were performed on HepG2/C3A human hepatocarcinoma cells treated with 150 μM TFEC for 6 and 24 h. Results have been expressed as a normalized ratio of the gene expression in the TFEC-treated samples against aqueous vehicle treated controls. At the time of this writing, information for data analyses was only available for the 300 most highly inducible genes for each treatment. Thus, genes whose expression did not fall within this category are currently denoted as "unavailable". Three major functional categories of gene changes are displayed here: (A) heat shock protein genes, (B) oxidative stress responsive genes and (C) ER stress responsive genes. Within each category, the genes are listed according to the fold induction at 24 h treatment.

A

Heat Shock Protein Genes	Fold Induction	
	6 h	24 h
Heat shock protein 22 kDa (HPB8)	4.4	87.3
Heat shock protein 70 kDa (HSPA6)	Unavailable	78.5
Heat shock protein 70 kDa (HSPA1B)	6.2	52.6
Heat shock protein 70 kDa (HSPA1A)	7.6	49.9
Heme oxygenase-1	17.1	38.1
DnaJB4 (HSP40)	10.8	24.2
DnaJB1 (HSP40)	2.9	12.9
DnaJB9 (HSP40)	4.6	8.2
DnaJB2 (HSP40)	2.7	Unavailable
DnaJC3 (HSP40)	Unavailable	6.6
Heat shock protein 105kDa/110kDa (HSPH1)	Unavailable	11.7

B

Oxidative Stress Responsive Genes	Fold Induction	
	6 h	24 h
Metallothionein 1X (MT1X)	2.8	41.4
Heme oxygenase-1	17.1	38.1
Metallothionein 1E (MT1E)	3.3	24.1
Metallothionein 1G (MT1G)	3.4	22.1
Glutamate cysteine ligase (GCLM)	5.9	18.4
Metallothionein 1H (MT1H)	Unavailable	18.4
Metallothionein 1F (MT1F)	Unavailable	13.0
Glutamate cysteine ligase (GCLC)	4.6	Unavailable
Thioredoxin reductase (TXNRD1)	3.5	7.4

Table 5.1 (continued)

C

ER Stress Responsive Genes	Fold Induction	
	6 h	24 h
Growth arrest and DNA-damage inducible B (Gadd45B)	Unavailable	42.6
Activating transcription factor 3 (ATF3)	9.8	9.6
Stanniocalcin 2 (STC2)	3.3	Unavailable
Activating transcription factor 4 (ATF4)	2.7	Unavailable

Table 5.2 **A comparison of gene expression profile of TFEC and fluorocitrate.** Analyses were performed on HepG2/C3A human hepatocarcinoma cells treated with either 150 μM TFEC or 1 mM sodium fluorocitrate for 6 and 24 h. Results have been expressed as a normalized ratio of the gene expression in the TFEC-treated samples against aqueous vehicle treated controls. A representative list of the commonly up- or down-regulated genes between the two treatments is shown in the table. Gene expression whose data was not available at the time of this writing is denoted as unavailable, "U".

	Fold Induction			
	TFEC		Fluorocitrate	
Common up- or down-regulated genes	**6 h**	**24 h**	**6 h**	**24 h**
Apoptosis				
Survivin (BIRC5)	0.31	0.07	U	0.31
Caspase recruitment domain, 10 (CARD10)	3.98	U	3.43	U
Cell cycling				
Cyclin B1	0.27	U	0.40	0.30
Cyclin E2	0.23	U	0.33	U
Growth and differentiation				
Early growth response 1 (EGR1)	2.95	14.17	5.93	18.70
Kruppel-like factor 5 (KLF5)	U	7.61	U	4.70
Kruppel-like factor 6 (KLF6)	4.69	11.15	5.04	9.68
Immediate early response (IER5)	U	13.52	U	8.66
Growth differentiation factor 15 (GDF15)	6.23	U	3.01	3.08
Immune response				
Chemokine ligand 2 (XCL1)	2.71	U	4.62	U
Interleukin 11 (IL11)	4.02	61.36	U	7.30
Interleukin 8 (IL8)	U	8.21	3.64	6.48
Metabolism and transporters				
Aldehyde dehydrogenase 8, A1(ALDH8A1)	0.05	U	0.34	U
ATP-binding cassette, G5 (ABCG5)	U	0.09	U	0.15
Cytochrome P450, 1A1 (CYP1A1)	0.08	U	0.33	37.81
Cytochrome P450, 39A1 (CYP39A1)	U	0.14	U	0.16
Solute carrier, 1A4 (SLC1A4)	3.50	U	4.52	U
Solute carrier. 2A2 (SLC2A2)	U	0.02	U	0.29
Solute carrier, 2A3 (SLC2A3)	0.27	U	0.29	U
Sulfotransferase, 1E1 (SULT1E1)	0.25	0.05	U	0.15

Table 5.2 (Continued)

Common up- or down-regulated genes	Fold Induction			
	TFEC		Fluorocitrate	
	6 h	24 h	6 h	24 h
Stress response				
DnaJB1 (HSP40B1)	3.03	9.76	U	5.04
Growth arrest and DNA damage 45 (Gadd45B)	U	42.65	10.09	24.58
HSP70 (A1A)	7.59	12.93	0.17	20.26
HSP70 A1B	6.15	52.64	0.11	30.58
Metallothionein 1E (MT1E)	3.27	24.13	0.41	3.34
Metallothionein 1F (MT1F)	U	12.97	0.38	3.22
Metallothionein 1X (MT1X)	2.80	41.43	0.30	5.17
Stanniocalcin 2 (STC2)	3.32	U	8.79	U
Thioredoxin reductase 1 (TXNRD1)	3.46	7.38	U	3.15
Transcriptional control				
Activating transcription factor 3 (ATF3)	9.77	9.59	47.83	25.30
Activating transcription factor 4 (ATF4)	2.72	U	2.90	U
v-Fos	U	125.88	3.02	41.24
MDM1	0.22	U	0.44	U
MAPK-activated protein kinase 2 (MAPKAPK)	3.62	U	2.96	U
v-jun (JUN)	U	18.42	2.75	37.14
v-maf homolog f (MAFF)	6.30	13.60	3.96	4.98
v-maf homolog g (MAFG)	3.67	U	3.38	U
BACH transcription factor 1 (BACH1)	U	11.17	U	3.27

Table 5.3 **A comparison of major cellular responses: TFEC vs. αKGDH inhibitors.** The major cellular responses during TFEC mediated cytotoxicity in TAMH cells was compared against well-characterized αKGDH inhibitors: sodium arsenite and α-ketomethylvaleric acid (KMV). Information for comparison was taken from our investigation (Chapters 2 to 4) as well as current literature (PubMed search).

Event	TFEC	αKGDH inhibitors
Differences:		
Early oxidative stress	Minimal ROS increase within the first 2 h of TFEC treatment (Chapter 4).	Arsenite generates ROS in Wistar rats. Ascorbic acid and a-tocopherol co-administration reduce lipid peroxidation and inhibit arsenite mediated toxicity (Ramanathan *et al.* 2003).
Caspase(s) activation	Minimal caspase activation is observed (Chapter 2).	Caspase-3 activation is observed in KMV-treated PC12 cells (Huang *et al.* 2003a).

Table 5.3 (continued)

Event	TFEC	αKGDH inhibitors
Similarities:		
Necrotic cell death	Early apoptotic signaling decayed rapidly into a secondary necrosis (Chapter 2).	Arsenite and KMV both induced necrotic cell death through a mitochondrial pathway (Huang *et al.* 2003a; Scholz *et al.* 2005).
Membrane permeability transition (MPT)	Inhibitor of MPT, bongkrekic acid, effectively inhibited TFEC induced-cell death (James *et al.* 2002).	Arsenite induced MPT (Bustamante *et al.* 2005; Scholz *et al.* 2005). Cyclosporin A blocked KMV-induced cell death (Huang *et al.* 2003a).
Cytochrome *c* release	Cytochrome *c* released into the cytosol at 8 h post-treatment with TFEC (Chapter 2).	Arsenite and KMV both stimulated cytochrome *c* release from mitochondria (Bustamante *et al.* 2005; Huang *et al.* 2003a).
Caspase(s) activation	Minimal caspase activation was observed (Chapter 2).	Arsenite triggered caspase-independent necrosis (Scholz *et al.* 2005).
ATP depletion	TFEC induced rapid ATP depletion (Chapter 4).	Arsenite-induced cytotoxicity was reversed with ATP generators fructose, xylitol and glutamine (Pourahmad *et al.* 2005).
Activation of Nrf2	TFEC induced an early Nrf2 expression and nuclear translocation (Chapter 4).	Arsenite induced Nrf2 activation in cultured keratinocytes (Pi *et al.* 2003).
HO-1 induction	TFEC strongly induced HO-1 expression (Chapter 3).	Arsenite induced HO-1 expression in vascular smooth muscle cells (Lee *et al.* 2005b).
Early oxidative stress	Minimal ROS increase within the first 2 h of TFEC treatment (Chapter 4).	Toxicity of arsenite in rat hepatocytes was not reversed with ROS scavengers (Pourahmad *et al.* 2005). KMV-mediated changes were not linked to ROS formation in PC12 cells (Huang *et al.* 2003a).
Effects of BCL-xL	BCL-xL overexpression prevented BAX translocation and cell death (Chapter 2).	BCL-xL overexpression prevented cell death in arsenite treated BJAB cells (Scholz *et al.* 2005).

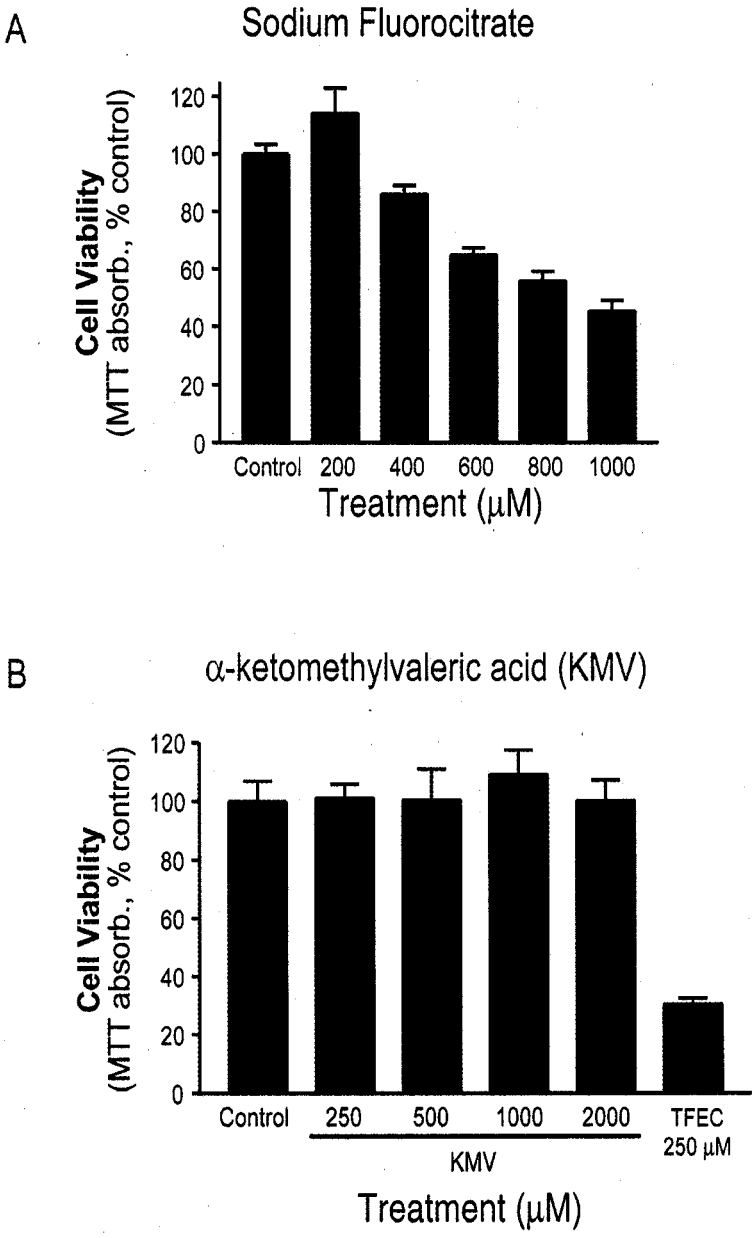

Figure 5.1 **MTT viability assay of fluorocitrate- and KMV-treated TAMH cells.** The viability of TAMH cells after (A) fluorocitrate (0-1000 μM) and (B) KMV (0-2000 μM) treatments for 24 h were assayed by MTT. Results are expressed as a percentage of viable cells in the untreated controls with +/- SD (n=6).

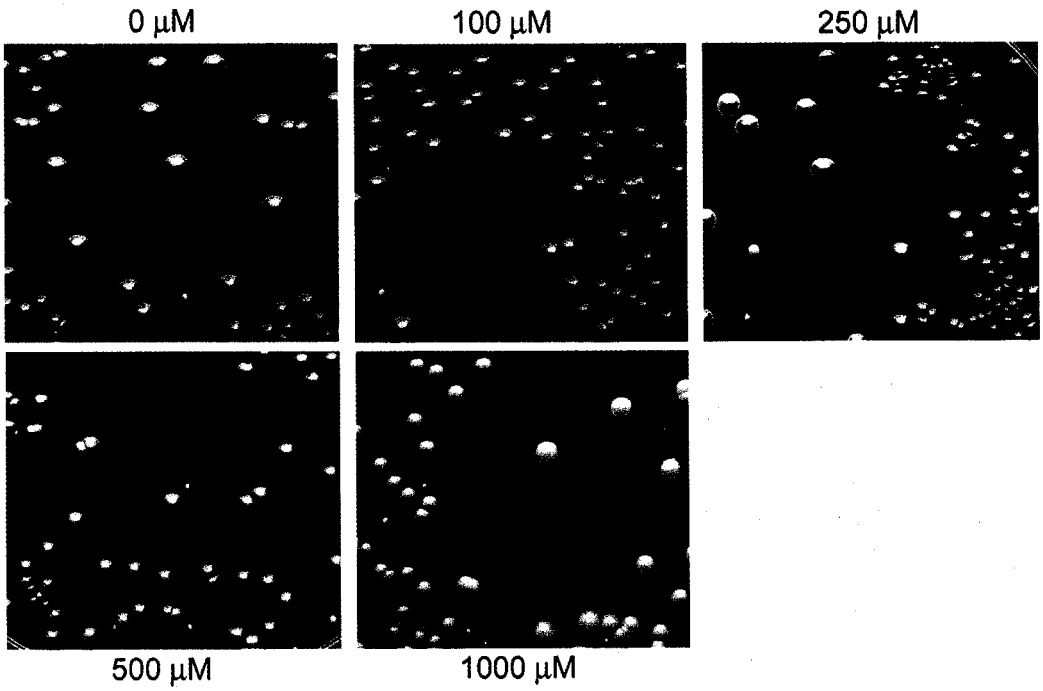

Figure 5.2 **Effects of TFEC on yeast mitochondria.** TFEC (0-1000 μM) was added to the growth medium containing the *Saccharomyces cerevisiae ade2* mutant. The mixture was plated and incubated at 37 °C for 5 days. Pictures were taken at the end of incubation and the colonies were evaluated. Red colonies indicate fully functional mitochondria and white colonies had significant mitochondrial damage and mtDNA mutation.

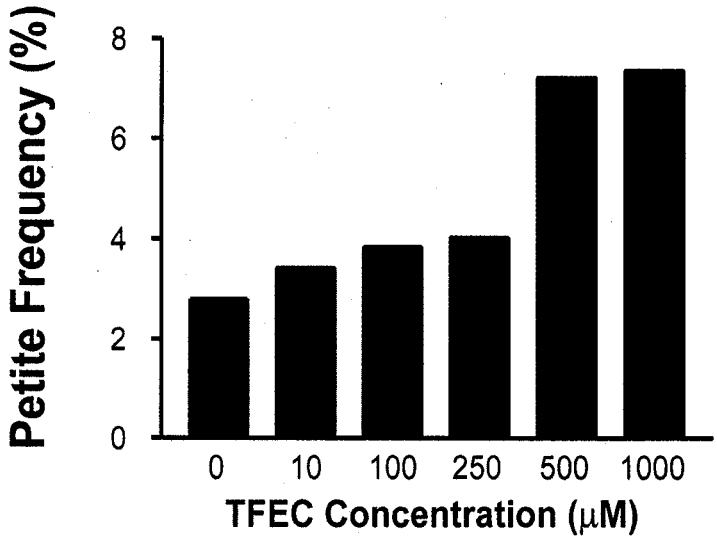

Figure 5.3 **Effects of TFEC on the increase in petite frequency in yeast.** The same yeast strain used for color colony assay (Figure 5.2) was treated with TFEC (0-1000 μM) for 5 days. Petite colonies were tested and confirmed by growth in glucose-containing medium, and expressed as a percentage of total colonies.

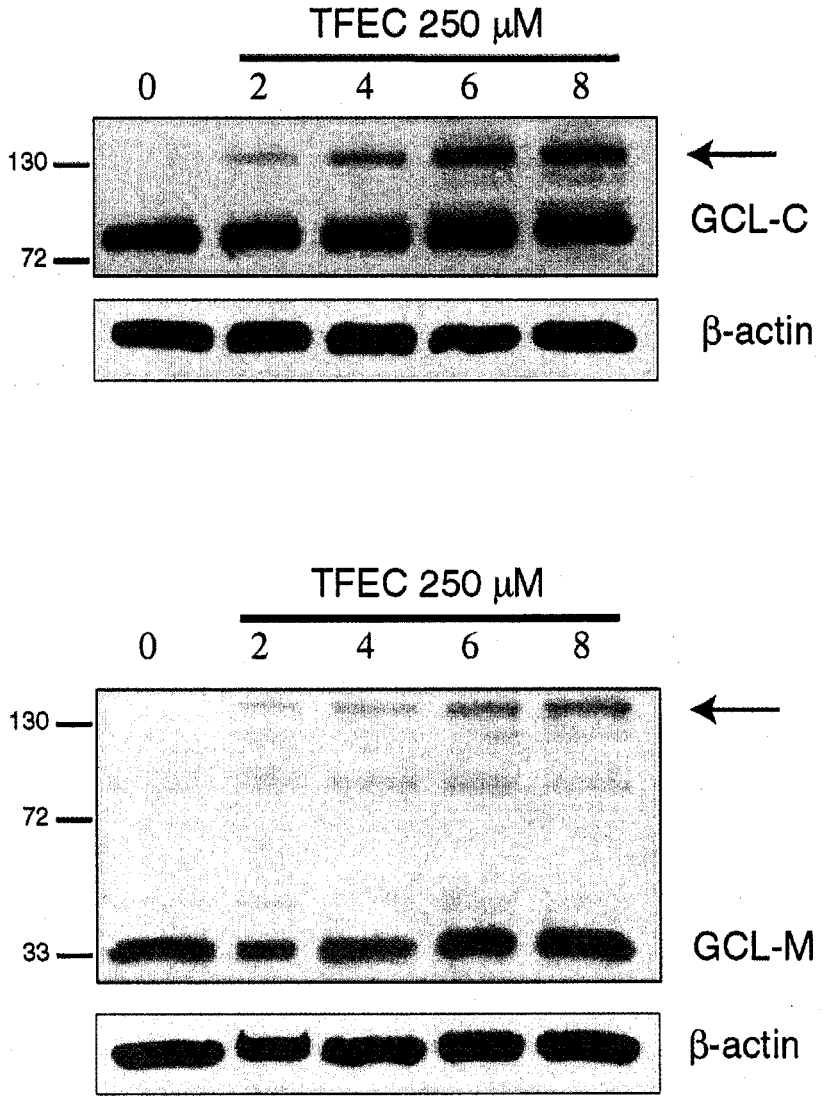

Figure 5.4A **Effects of TFEC treatment on GCL expression.** TAMH cells were treated with 250 μM TFEC for 0-8 h. Total cell lysates were subjected to immunoblot assay using polyclonal anti-GCL-C and anti-GCL-M antibodies. The black arrow indicates an increase in expression of an uncharacterized band with increasing duration of TFEC treatment.

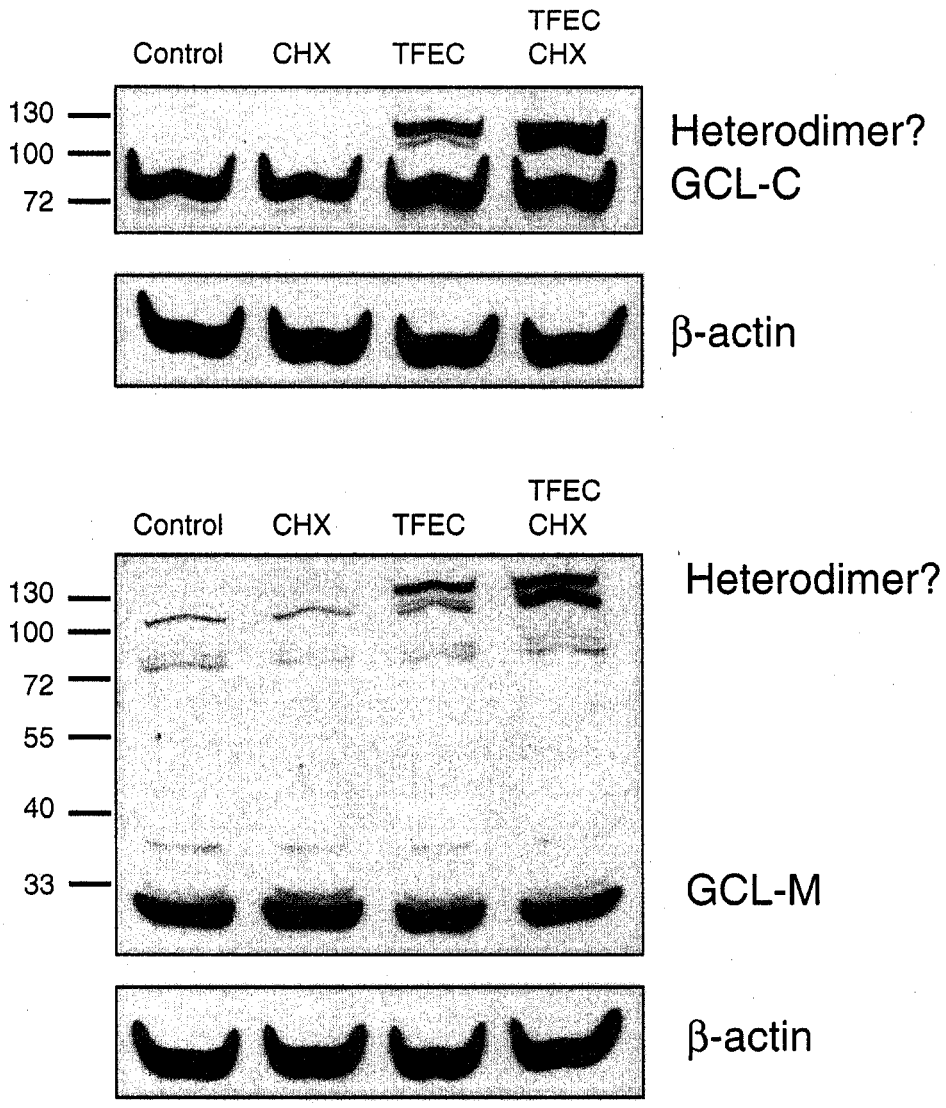

Figure 5.4B **Effects of TFEC treatment on GCL expression.** TAMH cells with or without TFEC treatment (250 μM, 6 h) were co-administered with or without cycloheximide (CHX, 10 μg/mL). The resulting cell lysates were subjected to similar immunoblot assay as in (A). A common band was formed with antibodies against both subunits of GCL and is denoted as an apparent heterodimer. Monoclonal anti-β-actin was used as the loading control.

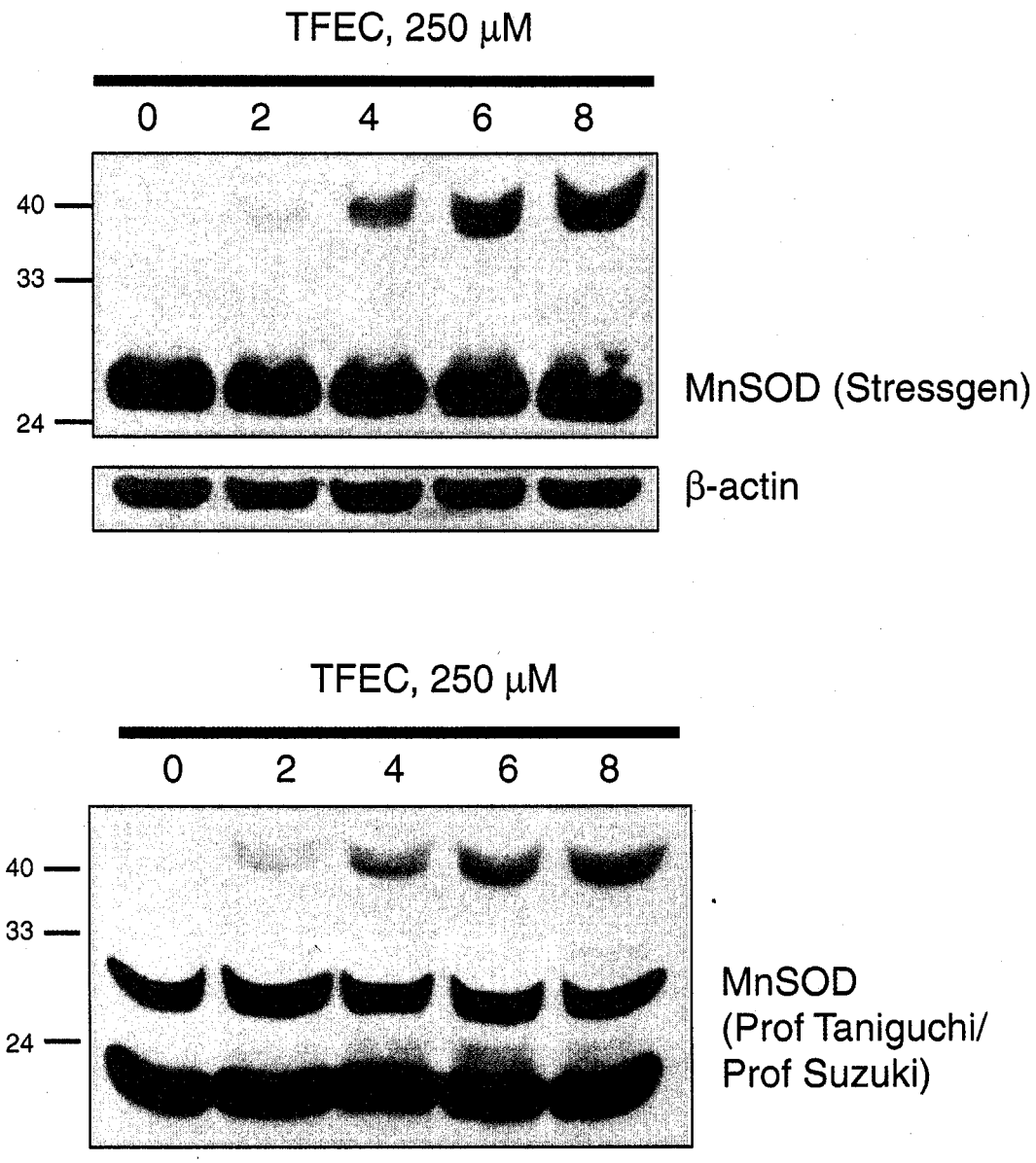

Figure 5.5 **Effects of TFEC treatment on MnSOD expression.** TAMH cells were treated with 250 μM TFEC for 0-8 h. Total cell lysates were subjected to immunoblot assay using polyclonal anti-MnSOD antibodies. Immunoblots were obtained using two different antibodies: Top panel with polyclonal MnSOD from Stressgen and bottom panel with polyclonal MnSOD developed by Prof Taniguchi/Prof Suzuki from Osaka University. Monoclonal anti-β-actin was used as the loading control.

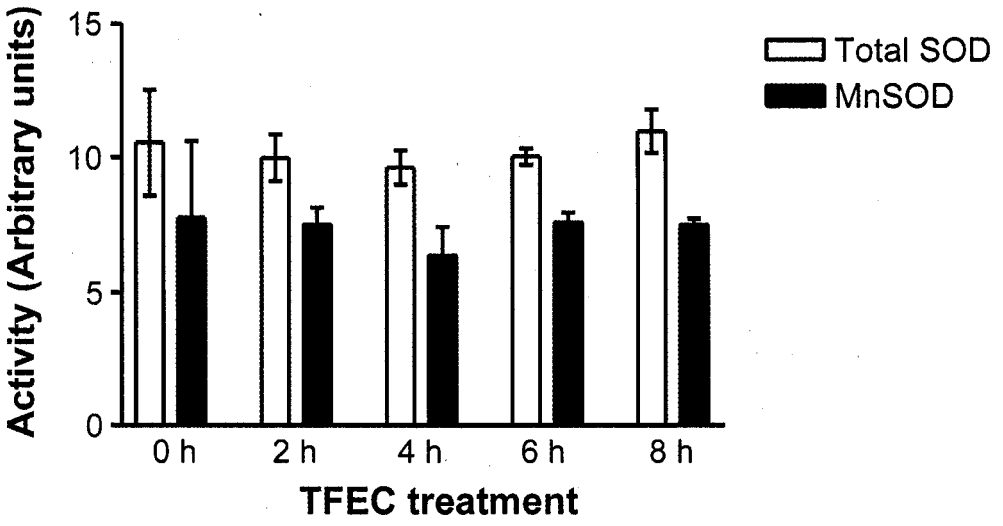

Figure 5.6 **Total and MnSOD activity assays.** TAMH cells were treated with 250 mM TFEC for 0-8 h. Total cell lysates were subjected to total SOD and MnSOD activity assays using SOD determination kit from Sigma. Results are expressed as an arbitrary unit derived from the absorbance measurements with +/- SD (n=3).

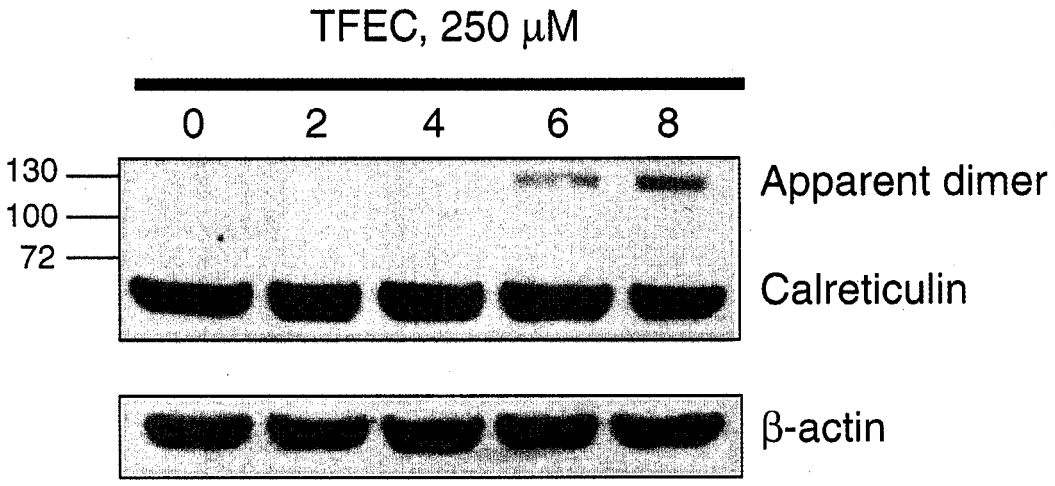

Figure 5.7 **Effects of TFEC treatment on calreticulin expression.** TAMH cells were treated with 250 μM TFEC for 0-8 h. Total cell lysates were subjected to immunoblot assay using polyclonal anti-calreticulin antibodies. Monoclonal anti-β-actin was used as the loading control. Blot was obtained as a longer exposure of the same membrane used in Figure 3.3.

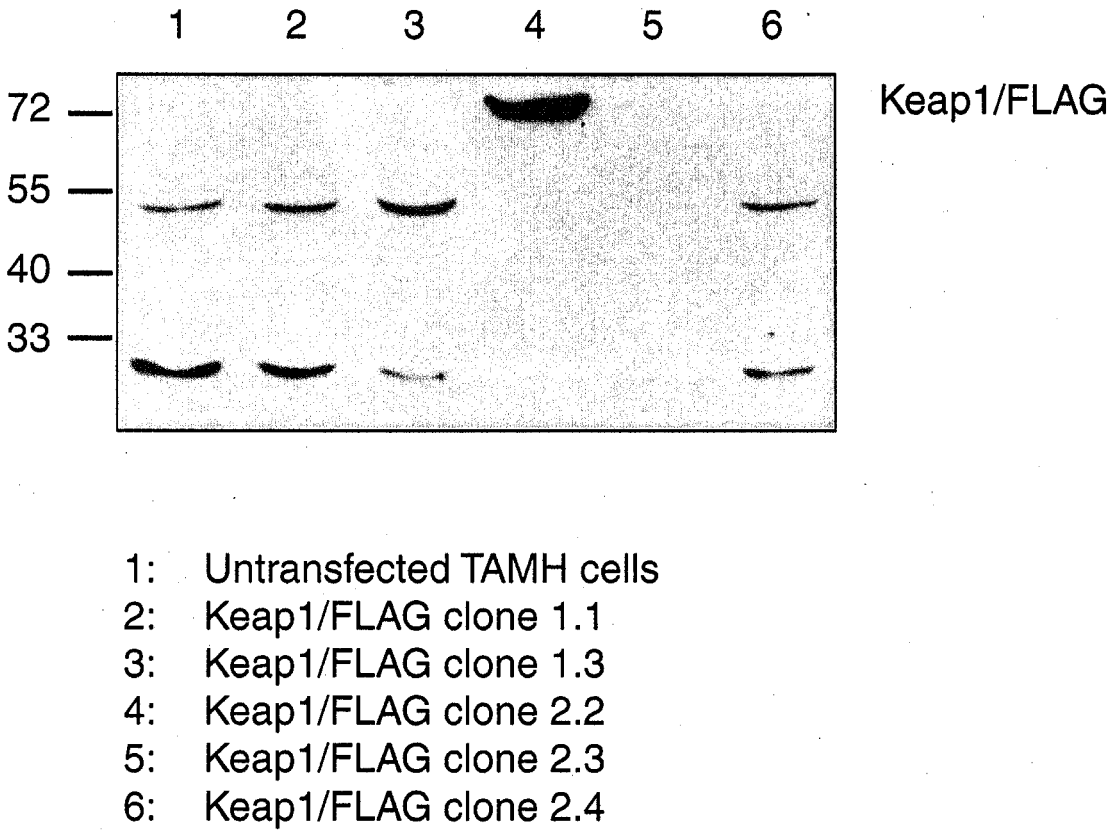

Figure 5.8 **Stable transfection of Keap1/FLAG in TAMH cells.** TAMH cells were transfected with Keap1/FLAG plasmid. Clones were isolated and expanded in the presence of 1000 μg/mL G418 as the selection antibiotics. Five clones were harvested for immunoblot assay using polyclonal anti-FLAG antibody. Native Keap1/FLAG has an apparent molecular weight of approximately 70 kDa. Clone 2.2 appeared to be successfully transfected.

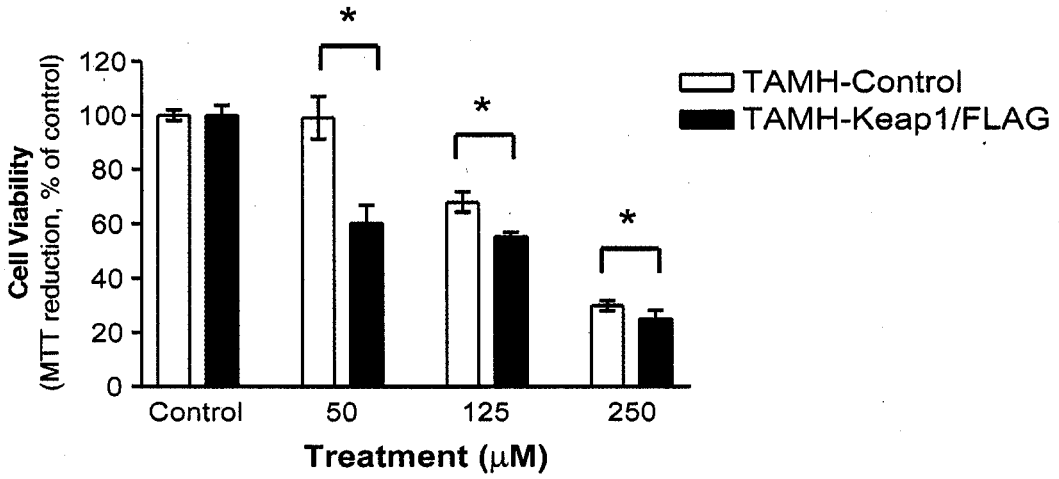

Figure 5.9 **MTT viability assay of TFEC treated TAMH cells with Keap1 stable transfection.** TAMH control cell line or TAMH stably transfected with Keap1/FLAG (Clone 2.2) were subjected to various concentrations of TFEC for 24 h. The viability of the cells after respective treatments were assayed by MTT. Results are expressed as a percentage of viable cells in the untreated controls with +/- SD (n=6). (* denotes a statistically significant difference between control and Keap1/FLAG stably transfected cells with $p<0.05$).

Bibliography

Abramov, A. Y., Canevari, L., and Duchen, M. R. (2004). Beta-amyloid peptides induce mitochondrial dysfunction and oxidative stress in astrocytes and death of neurons through activation of NADPH oxidase. *J Neurosci* **24**, 565-75.

Adams, M. L. (2003). The involvement of mitochondria in the cell death process: communication from mitochondria to the nucleus. In Medicinal Chemistry, p. 143. University of Washington, Seattle.

Alam, J., Stewart, D., Touchard, C., Boinapally, S., Choi, A. M., and Cook, J. L. (1999). Nrf2, a Cap'n'Collar transcription factor, regulates induction of the heme oxygenase-1 gene. *J Biol Chem* **274**, 26071-8.

Aliev, G., Seyidova, D., Lamb, B. T., Obrenovich, M. E., Siedlak, S. L., Vinters, H. V., Friedland, R. P., LaManna, J. C., Smith, M. A., and Perry, G. (2003). Mitochondria and vascular lesions as a central target for the development of Alzheimer's disease and Alzheimer disease-like pathology in transgenic mice. *Neurol Res* **25**, 665-74.

Aliev, G., Seyidova, D., Neal, M. L., Shi, J., Lamb, B. T., Siedlak, S. L., Vinters, H. V., Head, E., Perry, G., Lamanna, J. C., Friedland, R. P., and Cotman, C. W. (2002). Atherosclerotic lesions and mitochondria DNA deletions in brain microvessels as a central target for the development of human AD and AD-like pathology in aged transgenic mice. *Ann N Y Acad Sci* **977**, 45-64.

Allen-Jennings, A. E., Hartman, M. G., Kociba, G. J., and Hai, T. (2002). The roles of ATF3 in liver dysfunction and the regulation of phosphoenolpyruvate carboxykinase gene expression. *J Biol Chem* **277**, 20020-5.

Anders, M. W. (2004). Glutathione-dependent bioactivation of haloalkanes and haloalkenes. *Drug Metab Rev* **36**, 583-94.

Anders, M. W., and Dekant, W. (1998). Glutathione-dependent bioactivation of haloalkenes. *Annu Rev Pharmacol Toxicol* **38**, 501-37.

Andersen, M. H., Becker, J. C., and Straten, P. (2005). Regulators of apoptosis: suitable targets for immune therapy of cancer. *Nat Rev Drug Discov* **4**, 399-409.

Antonawich, F. J., Krajewski, S., Reed, J. C., and Davis, J. N. (1998). Bcl-x(l) Bax interaction after transient global ischemia. *J Cereb Blood Flow Metab* **18**, 882-6.

Antonsson, B., Montessuit, S., Lauper, S., Eskes, R., and Martinou, J. C. (2000). Bax oligomerization is required for channel-forming activity in liposomes and to trigger cytochrome c release from mitochondria. *Biochem J* **345**, 271-8.

Antonsson, B., Montessuit, S., Sanchez, B., and Martinou, J. C. (2001). Bax is present as a high molecular weight oligomer/complex in the mitochondrial membrane of apoptotic cells. *J Biol Chem* **276**, 11615-23.

Arrigo, A. P. (2001). Hsp27: novel regulator of intracellular redox state. *IUBMB Life* **52**, 303-7.

Beere, H. M., and Green, D. R. (2001). Stress management - heat shock protein-70 and the regulation of apoptosis. *Trends Cell Biol* **11**, 6-10.

Beere, H. M., Wolf, B. B., Cain, K., Mosser, D. D., Mahboubi, A., Kuwana, T., Tailor, P., Morimoto, R. I., Cohen, G. M., and Green, D. R. (2000). Heat-shock protein 70 inhibits apoptosis by preventing recruitment of procaspase-9 to the Apaf-1 apoptosome. *Nat Cell Biol* **2**, 469-75.

Biswas, G., Guha, M., and Avadhani, N. G. (2005). Mitochondria-to-nucleus stress signaling in mammalian cells: Nature of nuclear gene targets, transcription regulation, and induced resistance to apoptosis. *Gene* **354**, 132-9.

Boelsterli, U. A. (2003). *Mechanistic Toxicology*. Taylor & Francis, New York.

Bolstad, B. M., Irizarry, R. A., Astrand, M., and Speed, T. P. (2003). A comparison of normalization methods for high density oligonucleotide array data based on variance and bias. *Bioinformatics* **19**, 185-93.

Botta, D., Franklin, C. C., White, C. C., Krejsa, C. M., Dabrowski, M. J., Pierce, R. H., Fausto, N., and Kavanagh, T. J. (2004). Glutamate-cysteine ligase attenuates TNF-induced mitochondrial injury and apoptosis. *Free Radic Biol Med* **37**, 632-42.

Brady, H. J., and Gil-Gomez, G. (1998). Bax. The pro-apoptotic Bcl-2 family member, Bax. *Int J Biochem Cell Biol* **30**, 647-50.

Browne, G. S., Nelson, C., Nguyen, T., Ellis, B. A., Day, R. O., and Williams, K. M. (1999). Stereoselective and substrate-dependent inhibition of hepatic mitochondria beta-oxidation and oxidative phosphorylation by the non-steroidal anti-inflammatory drugs ibuprofen, flurbiprofen, and ketorolac. *Biochem Pharmacol* **57**, 837-44.

Bruschi, S. A., Crabb, J. W., and Stevens, J. L. (1994). The E3 subunit of 2-oxoglutarate, branched-chain alpha-keto acid, and malate dehydrogenase are adducted during nephrotoxic cysteine-conjugate injury., Vol. 14, p. 428.

Bruschi, S. A., Lindsay, J. G., and Crabb, J. W. (1998). Mitochondrial stress protein recognition of inactivated dehydrogenases during mammalian cell death. *Proc Natl Acad Sci U S A* **95**, 13413-8.

Bruschi, S. A., West, K. A., Crabb, J. W., Gupta, R. S., and Stevens, J. L. (1993). Mitochondrial HSP60 (P1 protein) and a HSP70-like protein (mortalin) are major targets for modification during S-(1,1,2,2-tetrafluoroethyl)- L-cysteine-induced nephrotoxicity. *J Biol Chem* **268**, 23157-61.

Buckley, B. J., Marshall, Z. M., and Whorton, A. R. (2003). Nitric oxide stimulates Nrf2 nuclear translocation in vascular endothelium. *Biochem Biophys Res Commun* **307**, 973-9.

Bustamante, J., Nutt, L., Orrenius, S., and Gogvadze, V. (2005). Arsenic stimulates release of cytochrome c from isolated mitochondria via induction of mitochondrial permeability transition. *Toxicol Appl Pharmacol* **207**, 110-6.

Butow, R. A. (2002). Cellular responses to mitochondrial dysfunction: it's not always downhill. *Cell Death Differ* **9**, 1043-5.

Butow, R. A., and Avadhani, N. G. (2004). Mitochondrial signaling: the retrograde response. *Mol Cell* **14**, 1-15.

Castellani, R., Hirai, K., Aliev, G., Drew, K. L., Nunomura, A., Takeda, A., Cash, A. D., Obrenovich, M. E., Perry, G., and Smith, M. A. (2002). Role of mitochondrial dysfunction in Alzheimer's disease. *J Neurosci Res* **70**, 357-60.

Castillo, J. L., Milgrom, P., Kharasch, E., Izutsu, K., and Fey, M. (2001). Evaluation of fluoride release from commercially available fluoride varnishes. *J Am Dent Assoc* **132**, 1389-92; quiz 1459-60.

Chacin, J., Rincon, R., Inciarte, D., Canizales, A., Martinez, G., and Alonso, D. (1979). Effect of Krebs cycle intermediates and inhibitors on toad gastric mucosa. *Am J Physiol* **236**, E692-700.

Chan, K., Han, X. D., and Kan, Y. W. (2001). An important function of Nrf2 in combating oxidative stress: detoxification of acetaminophen. *Proc Natl Acad Sci U S A* **98**, 4611-6.

Chao, D. T., and Korsmeyer, S. J. (1998). BCL-2 family: regulators of cell death. *Annu Rev Immunol* **16**, 395-419.

Chen, C., Pung, D., Leong, V., Hebbar, V., Shen, G., Nair, S., Li, W., and Tony Kong, A. N. (2004). Induction of detoxifying enzymes by garlic organosulfur compounds through transcription factor Nrf2: effect of chemical structure and stress signals. *Free Radic Biol Med* **37**, 1578-90.

Chen, K., Gunter, K., and Maines, M. D. (2000). Neurons overexpressing heme oxygenase-1 resist oxidative stress- mediated cell death. *J Neurochem* **75**, 304-13.

Chen, W., Shockcor, J. P., Tonge, R., Hunter, A., Gartner, C., and Nelson, S. D. (1999). Protein and nonprotein cysteinyl thiol modification by N-acetyl-p-benzoquinone imine via a novel ipso adduct. *Biochemistry* **38**, 8159-66.

Chen, X. J., and Clark-Walker, G. D. (1993). Mutations in MGI genes convert Kluyveromyces lactis into a petite-positive yeast. *Genetics* **133**, 517-25.

Chen, X. J., Wang, X., Kaufman, B. A., and Butow, R. A. (2005). Aconitase couples metabolic regulation to mitochondrial DNA maintenance. *Science* **307**, 714-7.

Chiba, K., Peterson, L. A., Castagnoli, K. P., Trevor, A. J., and Castagnoli, N., Jr. (1985). Studies on the molecular mechanism of bioactivation of the selective nigrostriatal toxin 1-methyl-4-phenyl-1,2,3,6-tetrahydropyridine. *Drug Metab Dispos* **13**, 342-7.

Chipuk, J. E., Kuwana, T., Bouchier-Hayes, L., Droin, N. M., Newmeyer, D. D., Schuler, M., and Green, D. R. (2004). Direct activation of Bax by p53 mediates mitochondrial membrane permeabilization and apoptosis. *Science* **303**, 1010-4.

Commandeur, J. N., De Kanter, F. J., and Vermeulen, N. P. (1989). Bioactivation of the cysteine-S-conjugate and mercapturic acid of tetrafluoroethylene to acylating reactive intermediates in the rat: dependence of activation and deactivation activities on acetyl coenzyme A availability. *Mol Pharmacol* **36**, 654-63.

Cooper, A. J., Bruschi, S. A., and Anders, M. W. (2002a). Toxic, halogenated cysteine S-conjugates and targeting of mitochondrial enzymes of energy metabolism. *Biochem Pharmacol* **64**, 553-64.

Cooper, A. J., Bruschi, S. A., Iriarte, A., and Martinez-Carrion, M. (2002b). Mitochondrial aspartate aminotransferase catalyses cysteine S-conjugate beta-lyase reactions. *Biochem J* **368**, 253-61.

Cooper, A. J., Wang, J., Gartner, C. A., and Bruschi, S. A. (2001). Co-purification of mitochondrial HSP70 and mature protein disulfide isomerase with a functional rat kidney high-M(r) cysteine S-conjugate beta-lyase. *Biochem Pharmacol* **62**, 1345-53.

Cotran, R. S., Kumar, V., and Collins, T. (1999). *Robbins Pathologic Basis of Disease*. W.B. Saunders Company.

Cottrell, D. A., Borthwick, G. M., Johnson, M. A., Ince, P. G., and Turnbull, D. M. (2002). The role of cytochrome c oxidase deficient hippocampal neurones in Alzheimer's disease. *Neuropathol Appl Neurobiol* **28**, 390-6.

Cullinan, S. B., and Diehl, J. A. (2004). PERK-dependent activation of Nrf2 contributes to redox homeostasis and cell survival following endoplasmic reticulum stress. *J Biol Chem* **279**, 20108-17.

Cullinan, S. B., Zhang, D., Hannink, M., Arvisais, E., Kaufman, R. J., and Diehl, J. A. (2003). Nrf2 is a direct PERK substrate and effector of PERK-dependent cell survival. *Mol Cell Biol* **23**, 7198-209.

Dahlin, D. C., Miwa, G. T., Lu, A. Y., and Nelson, S. D. (1984). N-acetyl-p-benzoquinone imine: a cytochrome P-450-mediated oxidation product of acetaminophen. *Proc Natl Acad Sci U S A* **81**, 1327-31.

Darrouzet, E., Issartel, J. P., Lunardi, J., and Dupuis, A. (1998). The 49-kDa subunit of NADH-ubiquinone oxidoreductase (Complex I) is involved in the binding of piericidin and rotenone, two quinone-related inhibitors. *FEBS Lett* **431**, 34-8.

Davis, J. S., Balinsky, J. B., Harington, J. S., and Shepherd, J. B. (1973). Assay, purification, properties and mechanism of action of gamma-glutamylcysteine synthetase from the liver of the rat and Xenopus laevis. *Biochem J* **133**, 667-78.

De Maio, A. (1999). Heat shock proteins: facts, thoughts, and dreams. *Shock* **11**, 1-12.

Decker, T., and Lohmann-Matthes, M. L. (1988). A quick and simple method for the quantitation of lactate dehydrogenase release in measurements of cellular cytotoxicity and tumor necrosis factor (TNF) activity. *J Immunol Methods* **115**, 61-9.

Degli Esposti, M., and Dive, C. (2003). Mitochondrial membrane permeabilisation by Bax/Bak. *Biochem Biophys Res Commun* **304**, 455-61.

Dekant, W. (2001). Chemical-induced nephrotoxicity mediated by glutathione S-conjugate formation. *Toxicol Lett* **124**, 21-36.

Desagher, S., and Martinou, J. C. (2000). Mitochondria as the central control point of apoptosis. *Trends Cell Biol* **10**, 369-77.

Desjardins, P., and Butterworth, R. F. (2005). Role of mitochondrial dysfunction and oxidative stress in the pathogenesis of selective neuronal loss in Wernicke's encephalopathy. *Mol Neurobiol* **31**, 17-25.

Diaz-Latoud, C., Buache, E., Javouhey, E., and Arrigo, A. P. (2005). Substitution of the unique cysteine residue of murine Hsp25 interferes with the protective activity of this stress protein through inhibition of dimer formation. *Antioxid Redox Signal* **7**, 436-45.

Dietz, B. M., Kang, Y. H., Liu, G., Eggler, A. L., Yao, P., Chadwick, L. R., Pauli, G. F., Farnsworth, N. R., Mesecar, A. D., van Breemen, R. B., and Bolton, J. L. (2005). Xanthohumol isolated from Humulus lupulus Inhibits menadione-induced DNA damage through induction of quinone reductase. *Chem Res Toxicol* **18**, 1296-305.

Dietze, E. C., Schafer, A., Omichinski, J. G., and Nelson, S. D. (1997). Inactivation of glyceraldehyde-3-phosphate dehydrogenase by a reactive metabolite of acetaminophen and mass spectral characterization of an arylated active site peptide. *Chem Res Toxicol* **10**, 1097-103.

Dinkova-Kostova, A. T., Massiah, M. A., Bozak, R. E., Hicks, R. J., and Talalay, P. (2001). Potency of Michael reaction acceptors as inducers of enzymes that protect against carcinogenesis depends on their reactivity with sulfhydryl groups. *Proc Natl Acad Sci U S A* **98**, 3404-9.

Downs, C. A., Jones, L. R., and Heckathorn, S. A. (1999). Evidence for a novel set of small heat-shock proteins that associates with the mitochondria of murine PC12 cells and protects NADH:ubiquinone oxidoreductase from heat and oxidative stress. *Arch Biochem Biophys* **365**, 344-50.

Duchen, M. R. (2000). Mitochondria and calcium: from cell signalling to cell death. *J Physiol* **529**, 57-68.

Duchen, M. R. (2004). Roles of mitochondria in health and disease. *Diabetes* **53**, S96-102.

Eggler, A. L., Liu, G., Pezzuto, J. M., van Breemen, R. B., and Mesecar, A. D. (2005). Modifying specific cysteines of the electrophile-sensing human Keap1 protein is insufficient to disrupt binding to the Nrf2 domain Neh2. *Proc Natl Acad Sci U S A* **102**, 10070-5.

Ehrnsperger, M. (1997). *Molecular Chaperones in the Life Cycle of Proteins*. Marcel Dekker, New York.

El-Hassan, H., Anwar, K., Macanas-Pirard, P., Crabtree, M., Chow, S. C., Johnson, V. L., Lee, P. C., Hinton, R. H., Price, S. C., and Kass, G. E. (2003). Involvement of mitochondria in acetaminophen-induced apoptosis and hepatic injury. Roles of cytochrome c, Bax, Bid, and caspases. *Toxicol Appl Pharmacol* **191**, 118-29.

Eskes, R., Desagher, S., Antonsson, B., and Martinou, J. C. (2000). Bid induces the oligomerization and insertion of Bax into the outer mitochondrial membrane. *Mol Cell Biol* **20**, 929-35.

Finucane, D. M., Bossy-Wetzel, E., Waterhouse, N. J., Cotter, T. G., and Green, D. R. (1999). Bax-induced caspase activation and apoptosis via cytochrome c release from mitochondria is inhibitable by Bcl-xL. *J Biol Chem* **274**, 2225-33.

Fischer, U., Janicke, R. U., and Schulze-Osthoff, K. (2003). Many cuts to ruin: a comprehensive update of caspase substrates. *Cell Death Differ* **10**, 76-100.

Fraser, J. A., Saunders, R. D., and McLellan, L. I. (2002). Drosophila melanogaster glutamate-cysteine ligase activity is regulated by a modifier subunit with a mechanism of action similar to that of the mammalian form. *J Biol Chem* **277**, 1158-65.

Fromenty, B., and Pessayre, D. (1995). Inhibition of mitochondrial beta-oxidation as a mechanism of hepatotoxicity. *Pharmacol Ther* **67**, 101-54.

Ganju, N., and Eastman, A. (2002). Bcl-X(L) and calyculin A prevent translocation of Bax to mitochondria during apoptosis. *Biochem Biophys Res Commun* **291**, 1258-64.

Garrett, R. H., and Grisham, C. M. (1995). *Biochemistry*. Saunders College Publishing, Orlando.

Garrido, C., Gurbuxani, S., Ravagnan, L., and Kroemer, G. (2001). Heat shock proteins: endogenous modulators of apoptotic cell death. *Biochem Biophys Res Commun* **286**, 433-42.

Gerlach, M., Riederer, P., Przuntek, H., and Youdim, M. B. (1991). MPTP mechanisms of neurotoxicity and their implications for Parkinson's disease. *Eur J Pharmacol* **208**, 273-86.

Gewies, A. (2003). Introduction to Apoptosis.

Ghatan, S., Larner, S., Kinoshita, Y., Hetman, M., Patel, L., Xia, Z., Youle, R. J., and Morrison, R. S. (2000). p38 MAP kinase mediates bax translocation in nitric oxide-induced apoptosis in neurons. *J Cell Biol* **150**, 335-47.

Goldring, C. E., Kitteringham, N. R., Elsby, R., Randle, L. E., Clement, Y. N., Williams, D. P., McMahon, M., Hayes, J. D., Itoh, K., Yamamoto, M., and Park, B. K. (2004). Activation of hepatic Nrf2 in vivo by acetaminophen in CD-1 mice. *Hepatology* **39**, 1267-76.

Gonzales, S., Erario, M. A., and Tomaro, M. L. (2002). Heme oxygenase-1 induction and dependent increase in ferritin. A protective antioxidant stratagem in hemin-treated rat brain. *Dev Neurosci* **24**, 161-8.

Goormaghtigh, E., Pollakis, G., and Ruysschaert, J. M. (1983). Mitochondrial membrane modifications induced by adriamycin-mediated electron transport. *Biochem Pharmacol* **32**, 889-93.

Gotoh, T., Terada, K., Oyadomari, S., and Mori, M. (2004). hsp70-DnaJ chaperone pair prevents nitric oxide- and CHOP-induced apoptosis by inhibiting translocation of Bax to mitochondria. *Cell Death Differ* **11**, 390-402.

Green, D. R., and Reed, J. C. (1998). Mitochondria and apoptosis. *Science* **281**, 1309-12.

Gross, A., McDonnell, J. M., and Korsmeyer, S. J. (1999). BCL-2 family members and the mitochondria in apoptosis. *Genes Dev* **13**, 1899-911.

Groves, C. E., Hayden, P. J., Lock, E. A., and Schnellmann, R. G. (1993). Differential cellular effects in the toxicity of haloalkene and haloalkane cysteine conjugates to rabbit renal proximal tubules. *J Biochem Toxicol* **8**, 49-56.

Groves, C. E., Lock, E. A., and Schnellmann, R. G. (1990). The effects of haloalkene cysteine conjugates on cytosolic free calcium levels in suspensions of rat renal proximal tubules. *J Biochem Toxicol* **5**, 187-92.

Groves, C. E., Lock, E. A., and Schnellmann, R. G. (1991). Role of lipid peroxidation in renal proximal tubule cell death induced by haloalkene cysteine conjugates. *Toxicol Appl Pharmacol* **107**, 54-62.

Hai, T., Wolfgang, C. D., Marsee, D. K., Allen, A. E., and Sivaprasad, U. (1999). ATF3 and stress responses. *Gene Expr* **7**, 321-35.

Halestrap, A. P., Doran, E., Gillespie, J. P., and O'Toole, A. (2000). Mitochondria and cell death. *Biochem Soc Trans* **28**, 170-7.

Halliwell, B., and Gutteridge, J. M. C. (1999). *Free Radicals in Biology and Medicine*. Oxford University Press, New York.

Harriman, J. F., Liu, X. L., Aleo, M. D., Machaca, K., and Schnellmann, R. G. (2002). Endoplasmic reticulum Ca(2+) signaling and calpains mediate renal cell death. *Cell Death Differ* **9**, 734-41.

Hayden, P. J., Ichimura, T., McCann, D. J., Pohl, L. R., and Stevens, J. L. (1991a). Detection of cysteine conjugate metabolite adduct formation with specific mitochondrial proteins using antibodies raised against halothane metabolite adducts. *J Biol Chem* **266**, 18415-8.

Hayden, P. J., and Stevens, J. L. (1990). Cysteine conjugate toxicity, metabolism, and binding to macromolecules in isolated rat kidney mitochondria. *Mol Pharmacol* **37**, 468-76.

Hayden, P. J., Yang, Y., Ward, A. J., Dulik, D. M., McCann, D. J., and Stevens, J. L. (1991b). Formation of difluorothionoacetyl-protein adducts by S-(1,1,2,2-tetrafluoroethyl)-L-cysteine metabolites: nucleophilic catalysis of stable lysyl adduct formation by histidine and tyrosine. *Biochemistry* **30**, 5935-43.

He, L., and Lemasters, J. J. (2003). Heat shock suppresses the permeability transition in rat liver mitochondria. *J Biol Chem* **278**, 16755-60.

Hengartner, M. O. (2000). The biochemistry of apoptosis. *Nature* **407**, 770-6.

Hightower, L. E. (1991). Heat shock, stress proteins, chaperones, and proteotoxicity. *Cell* **66**, 191-7.

Ho, H. K., Hu, Z. H., Tzung, S. P., Hockenbery, D. M., Fausto, N., Nelson, S. D., and Bruschi, S. A. (2005a). BCL-xL overexpression effectively protects against tetrafluoroethylcysteine-induced intramitochondrial damage and cell death. *Biochem Pharmacol* **69**, 147-57.

Ho, H. K., White, C. C., Fernandez, C., Fausto, N., Kavanagh, T. J., Nelson, S. D., and Bruschi, S. A. (2005b). Nrf2 activation involves an oxidative-stress independent pathway in tetrafluoroethylcysteine-induced cytotoxicity. *Toxicol Sci* **86**, 354-64.

Hong, F., Sekhar, K. R., Freeman, M. L., and Liebler, D. C. (2005). Specific patterns of electrophile adduction trigger Keap1 ubiquitination and Nrf2 activation. *J Biol Chem* **280**, 31768-31775.

Hsu, Y. T., Wolter, K. G., and Youle, R. J. (1997). Cytosol-to-membrane redistribution of Bax and Bcl-X(L) during apoptosis. *Proc Natl Acad Sci U S A* **94**, 3668-72.

Huang, H. M., Ou, H. C., Xu, H., Chen, H. L., Fowler, C., and Gibson, G. E. (2003a). Inhibition of alpha-ketoglutarate dehydrogenase complex promotes cytochrome c release from mitochondria, caspase-3 activation, and necrotic cell death. *J Neurosci Res* **74**, 309-17.

Huang, H. M., Zhang, H., Xu, H., and Gibson, G. E. (2003b). Inhibition of the alpha-ketoglutarate dehydrogenase complex alters mitochondrial function and cellular calcium regulation. *Biochim Biophys Acta* **1637**, 119-26.

Isenberg, J. S., and Klaunig, J. E. (2000). Role of the mitochondrial membrane permeability transition (MPT) in rotenone-induced apoptosis in liver cells. *Toxicol Sci* **53**, 340-51.

Itoh, K., Tong, K. I., and Yamamoto, M. (2004). Molecular mechanism activating Nrf2-Keap1 pathway in regulation of adaptive response to electrophiles. *Free Radic Biol Med* **36**, 1208-13.

Itoh, K., Wakabayashi, N., Katoh, Y., Ishii, T., O'Connor, T., and Yamamoto, M. (2003). Keap1 regulates both cytoplasmic-nuclear shuttling and degradation of Nrf2 in response to electrophiles. *Genes Cells* **8**, 379-91.

Jaiswal, A. K. (2004). Nrf2 signaling in coordinated activation of antioxidant gene expression. *Free Radic Biol Med* **36**, 1199-207.

James, E. A., Gygi, S. P., Adams, M. L., Pierce, R. H., Fausto, N., Aebersold, R. H., Nelson, S. D., and Bruschi, S. A. (2002). Mitochondrial aconitase modification, functional inhibition, and evidence for a supramolecular complex of the TCA cycle by the renal toxicant S-(1,1,2,2-tetrafluoroethyl)-L-cysteine. *Biochemistry* **41**, 6789-97.

Jenner, P. (2001). Parkinson's disease, pesticides and mitochondrial dysfunction. *Trends Neurosci* **24**, 245-7.

Jiang, H. Y., Wek, S. A., McGrath, B. C., Lu, D., Hai, T., Harding, H. P., Wang, X., Ron, D., Cavener, D. R., and Wek, R. C. (2004). Activating transcription factor 3 is integral to the eukaryotic initiation factor 2 kinase stress response. *Mol Cell Biol* **24**, 1365-77.

Jiang, X., and Wang, X. (2004). Cytochrome C-mediated apoptosis. *Annu Rev Biochem* **73**, 87-106.

Jorgensen, C. S., Ryder, L. R., Steino, A., Hojrup, P., Hansen, J., Beyer, N. H., Heegaard, N. H., and Houen, G. (2003). Dimerization and oligomerization of the chaperone calreticulin. *Eur J Biochem* **270**, 4140-8.

Kabakov, A. E., Budagova, K. R., Latchman, D. S., and Kampinga, H. H. (2002). Stressful preconditioning and HSP70 overexpression attenuate proteotoxicity of cellular ATP depletion. *Am J Physiol Cell Physiol* **283**, C521-34.

Kagan, V. E., Borisenko, G. G., Tyurina, Y. Y., Tyurin, V. A., Jiang, J., Potapovich, A. I., Kini, V., Amoscato, A. A., and Fujii, Y. (2004). Oxidative lipidomics of apoptosis: redox catalytic interactions of cytochrome c with cardiolipin and phosphatidylserine. *Free Radic Biol Med* **37**, 1963-85.

Kang, M. I., Kobayashi, A., Wakabayashi, N., Kim, S. G., and Yamamoto, M. (2004). Scaffolding of Keap1 to the actin cytoskeleton controls the function of Nrf2 as key regulator of cytoprotective phase 2 genes. *Proc Natl Acad Sci U S A* **101**, 2046-51.

Katsuoka, F., Motohashi, H., Engel, J. D., and Yamamoto, M. (2005). Nrf2 transcriptionally activates the mafG gene through an antioxidant response element. *J Biol Chem* **280**, 4483-90.

Kaufmann, S. H., and Hengartner, M. O. (2001). Programmed cell death: alive and well in the new millennium. *Trends Cell Biol* **11**, 526-34.

Keller, D. A., Kennedy, G. L., Jr., Ross, P. E., Kelly, D. P., and Elliott, G. S. (2000). Toxicity of tetrafluoroethylene and S-(1,1,2, 2-tetrafluoroethyl)-L-cysteine in rats and mice. *Toxicol Sci* **56**, 414-23.

Kerr, J. F., Wyllie, A. H., and Currie, A. R. (1972). Apoptosis: a basic biological phenomenon with wide-ranging implications in tissue kinetics. *Br J Cancer* **26**, 239-57.

Kim, G., Sikder, H., and Singh, K. K. (2002). A colony color method identifies the vulnerability of mitochondria to oxidative damage. *Mutagenesis* **17**, 375-81.

Kim, J. S., He, L., and Lemasters, J. J. (2003). Mitochondrial permeability transition: a common pathway to necrosis and apoptosis. *Biochem Biophys Res Commun* **304**, 463-70.

Krahenbuhl, S. (2001). Mitochondria: important target for drug toxicity? *J Hepatol* **34**, 334-6.

Kregel, K. C. (2002). Heat shock proteins: modifying factors in physiological stress responses and acquired thermotolerance. *J Appl Physiol* **92**, 2177-86.

Krueger, M. J., Singer, T. P., Casida, J. E., and Ramsay, R. R. (1990). Evidence that the blockade of mitochondrial respiration by the neurotoxin 1-methyl-4-phenylpyridinium (MPP+) involves binding at the same site as the respiratory inhibitor, rotenone. *Biochem Biophys Res Commun* **169**, 123-8.

Lee, H. J., Wang, C. J., Kuo, H. C., Chou, F. P., Jean, L. F., and Tseng, T. H. (2005a). Induction apoptosis of luteolin in human hepatoma HepG2 cells involving mitochondria translocation of Bax/Bak and activation of JNK. *Toxicol Appl Pharmacol* **203**, 124-31.

Lee, J. M., and Johnson, J. A. (2004). An important role of Nrf2-ARE pathway in the cellular defense mechanism. *J Biochem Mol Biol* **37**, 139-43.

Lee, J. M., Shih, A. Y., Murphy, T. H., and Johnson, J. A. (2003). NF-E2-related factor-2 mediates neuroprotection against mitochondrial complex I inhibitors and increased concentrations of intracellular calcium in primary cortical neurons. *J Biol Chem* **278**, 37948-56.

Lee, P. C., Ho, I. C., and Lee, T. C. (2005b). Oxidative stress mediates sodium arsenite-induced expression of heme oxygenase-1, monocyte chemoattractant protein-1, and interleukin-6 in vascular smooth muscle cells. *Toxicol Sci* **85**, 541-50.

Lei, K., Nimnual, A., Zong, W. X., Kennedy, N. J., Flavell, R. A., Thompson, C. B., Bar-Sagi, D., and Davis, R. J. (2002). The Bax subfamily of Bcl2-related proteins is essential for apoptotic signal transduction by c-Jun NH(2)-terminal kinase. *Mol Cell Biol* **22**, 4929-42.

Leist, M., Single, B., Castoldi, A. F., Kuhnle, S., and Nicotera, P. (1997). Intracellular adenosine triphosphate (ATP) concentration: a switch in the decision between apoptosis and necrosis. *J Exp Med* **185**, 1481-6.

Leist, M., Single, B., Naumann, H., Fava, E., Simon, B., Kuhnle, S., and Nicotera, P. (1999). Inhibition of mitochondrial ATP generation by nitric oxide switches apoptosis to necrosis. *Exp Cell Res* **249**, 396-403.

Leung, L., Kwong, M., Hou, S., Lee, C., and Chan, J. Y. (2003). Deficiency of the Nrf1 and Nrf2 transcription factors results in early embryonic lethality and severe oxidative stress. *J Biol Chem* **278**, 48021-9.

Levonen, A. L., Landar, A., Ramachandran, A., Ceaser, E. K., Dickinson, D. A., Zanoni, G., Morrow, J. D., and Darley-Usmar, V. M. (2004). Cellular mechanisms of redox cell signalling: role of cysteine modification in controlling antioxidant defences in response to electrophilic lipid oxidation products. *Biochem J* **378**, 373-82.

Li, N., Ragheb, K., Lawler, G., Sturgis, J., Rajwa, B., Melendez, J. A., and Robinson, J. P. (2003). Mitochondrial complex I inhibitor rotenone induces apoptosis through enhancing mitochondrial reactive oxygen species production. *J Biol Chem* **278**, 8516-25.

Lieberthal, W., Menza, S. A., and Levine, J. S. (1998). Graded ATP depletion can cause necrosis or apoptosis of cultured mouse proximal tubular cells. *Am J Physiol* **274**, F315-27.

Liu, X. M., Peyton, K. J., Ensenat, D., Wang, H., Schafer, A. I., Alam, J., and Durante, W. (2005). Endoplasmic reticulum stress stimulates heme oxygenase-1 gene expression in vascular smooth muscle. Role in cell survival. *J Biol Chem* **280**, 872-7.

Lock, E. A., and Ishmael, J. (1998). The nephrotoxicity and hepatotoxicity of 1,1,2,2-tetrafluoroethyl-L- cysteine in the rat. *Arch Toxicol* **72**, 347-54.

Luo, X., Budihardjo, I., Zou, H., Slaughter, C., and Wang, X. (1998). Bid, a Bcl2 interacting protein, mediates cytochrome c release from mitochondria in response to activation of cell surface death receptors. *Cell* **94**, 481-90.

Maniratanachote, R., Minami, K., Katoh, M., Nakajima, M., and Yokoi, T. (2005). Chaperone proteins involved in troglitazone-induced toxicity in human hepatoma cell lines. *Toxicol Sci* **83**, 293-302.

Mannella, C. A. (2000). Introduction: our changing views of mitochondria. *J Bioenerg Biomembr* **32**, 1-4.

Mannella, C. A., Buttle, K., Rath, B. K., and Marko, M. (1998). Electron microscopic tomography of rat-liver mitochondria and their interaction with the endoplasmic reticulum. *Biofactors* **8**, 225-8.

Marzo, I., Brenner, C., Zamzami, N., Jurgensmeier, J. M., Susin, S. A., Vieira, H. L., Prevost, M. C., Xie, Z., Matsuyama, S., Reed, J. C., and Kroemer, G. (1998). Bax and adenine nucleotide translocator cooperate in the mitochondrial control of apoptosis. *Science* **281**, 2027-31.

Mastrogiacomo, F., Bergeron, C., and Kish, S. J. (1993). Brain alpha-ketoglutarate dehydrogenase complex activity in Alzheimer's disease. *J Neurochem* **61**, 2007-14.

McGoldrick, T. A., Lock, E. A., Rodilla, V., and Hawksworth, G. M. (2003). Renal cysteine conjugate C-S lyase mediated toxicity of halogenated alkenes in primary cultures of human and rat proximal tubular cells. *Arch Toxicol* **77**, 365-70.

Mikhailov, V., Mikhailova, M., Degenhardt, K., Venkatachalam, M. A., White, E., and Saikumar, P. (2003). Association of Bax and Bak homo-oligomers in mitochondria. Bax requirement for Bak reorganization and cytochrome c release. *J Biol Chem* **278**, 5367-76.

Mikhailov, V., Mikhailova, M., Pulkrabek, D. J., Dong, Z., Venkatachalam, M. A., and Saikumar, P. (2001). Bcl-2 prevents Bax oligomerization in the mitochondrial outer membrane. *J Biol Chem* **276**, 18361-74.

Miller, E. C., and Miller, J. A. (1981). Mechanisms of chemical carcinogenesis. *Cancer* **47**, 1055-64.

Mosser, D. D., Caron, A. W., Bourget, L., Denis-Larose, C., and Massie, B. (1997). Role of the human heat shock protein hsp70 in protection against stress- induced apoptosis. *Mol Cell Biol* **17**, 5317-27.

Murphy, K. M., Ranganathan, V., Farnsworth, M. L., Kavallaris, M., and Lock, R. B. (2000). Bcl-2 inhibits Bax translocation from cytosol to mitochondria during drug-induced apoptosis of human tumor cells. *Cell Death Differ* **7**, 102-11.

Nakaso, K., Yano, H., Fukuhara, Y., Takeshima, T., Wada-Isoe, K., and Nakashima, K. (2003). PI3K is a key molecule in the Nrf2-mediated regulation of antioxidative proteins by hemin in human neuroblastoma cells. *FEBS Lett* **546**, 181-4.

Nguyen, T., Sherratt, P. J., and Pickett, C. B. (2003). Regulatory mechanisms controlling gene expression mediated by the antioxidant response element. *Annu Rev Pharmacol Toxicol* **43**, 233-60.

Nicklas, W. J., Vyas, I., and Heikkila, R. E. (1985). Inhibition of NADH-linked oxidation in brain mitochondria by 1-methyl-4-phenyl-pyridine, a metabolite of the neurotoxin, 1-methyl-4-phenyl-1,2,5,6-tetrahydropyridine. *Life Sci* **36**, 2503-8.

NTP (1997). NTP Toxicology and Carcinogenesis Studies of Tetrafluoroethylene (CAS No. 116-14-3) in F344 Rats and B6C3F1 Mice (Inhalation Studies). *Natl Toxicol Program Tech Rep Ser* **450**, 1-321.

Numazawa, S., Ishikawa, M., Yoshida, A., Tanaka, S., and Yoshida, T. (2003). Atypical protein kinase C mediates activation of NF-E2-related factor 2 in response to oxidative stress. *Am J Physiol Cell Physiol* **285**, C334-42.

Numazawa, S., and Yoshida, T. (2004). Nrf2-dependent gene expressions: a molecular toxicological aspect. *J Toxicol Sci* **29**, 81-9.

Odum, J., and Green, T. (1984). The metabolism and nephrotoxicity of tetrafluoroethylene in the rat. *Toxicol Appl Pharmacol* **76**, 306-18.

Oltvai, Z. N., Milliman, C. L., and Korsmeyer, S. J. (1993). Bcl-2 heterodimerizes in vivo with a conserved homolog, Bax, that accelerates programmed cell death. *Cell* **74**, 609-19.

Orrenius, S. (2004). Mitochondrial regulation of apoptotic cell death. *Toxicol Lett* **149**, 19-23.

Otterbein, L. E., Bach, F. H., Alam, J., Soares, M., Tao Lu, H., Wysk, M., Davis, R. J., Flavell, R. A., and Choi, A. M. (2000). Carbon monoxide has anti-inflammatory effects involving the mitogen-activated protein kinase pathway. *Nat Med* **6**, 422-8.

Otterbein, L. E., and Choi, A. M. (2000). Heme oxygenase: colors of defense against cellular stress. *Am J Physiol Lung Cell Mol Physiol* **279**, L1029-37.

Pan, G., O'Rourke, K., and Dixit, V. M. (1998). Caspase-9, Bcl-XL, and Apaf-1 form a ternary complex. *J Biol Chem* **273**, 5841-5.

Park, L. C., Gibson, G. E., Bunik, V., and Cooper, A. J. (1999). Inhibition of select mitochondrial enzymes in PC12 cells exposed to S-(1,1,2,2-tetrafluoroethyl)-L-cysteine. *Biochem Pharmacol* **58**, 1557-65.

Pastorino, J. G., Tafani, M., Rothman, R. J., Marcinkeviciute, A., Hoek, J. B., Farber, J. L., and Marcineviciute, A. (1999). Functional consequences of the sustained or transient activation by Bax of the mitochondrial permeability transition pore. *J Biol Chem* **274**, 31734-9.

Pei, W., Liou, A. K., and Chen, J. (2003). Two caspase-mediated apoptotic pathways induced by rotenone toxicity in cortical neuronal cells. *Faseb J* **17**, 520-2.

Pi, J., Qu, W., Reece, J. M., Kumagai, Y., and Waalkes, M. P. (2003). Transcription factor Nrf2 activation by inorganic arsenic in cultured keratinocytes: involvement of hydrogen peroxide. *Exp Cell Res* **290**, 234-45.

Pierce, R. H., Campbell, J. S., Stephenson, A. B., Franklin, C. C., Chaisson, M., Poot, M., Kavanagh, T. J., Rabinovitch, P. S., and Fausto, N. (2000). Disruption of redox homeostasis in tumor necrosis factor-induced apoptosis in a murine hepatocyte cell line. *Am J Pathol* **157**, 221-36.

Pierce, R. H., Franklin, C. C., Campbell, J. S., Tonge, R. P., Chen, W., Fausto, N., Nelson, S. D., and Bruschi, S. A. (2002). Cell culture model for acetaminophen-induced hepatocyte death in vivo. *Biochem Pharmacol* **64**, 413-24.

Plumb, J. A., Milroy, R., and Kaye, S. B. (1989). Effects of the pH dependence of 3-(4,5-dimethylthiazol-2-yl)-2,5- diphenyl-tetrazolium bromide-formazan absorption on chemosensitivity determined by a novel tetrazolium-based assay. *Cancer Res* **49**, 4435-40.

Pourahmad, J., Rabiei, M., Jokar, F., and O'Brien P, J. (2005). A comparison of hepatocyte cytotoxic mechanisms for chromate and arsenite. *Toxicology* **206**, 449-60.

Putcha, G. V., Deshmukh, M., and Johnson, E. M., Jr. (1999). BAX translocation is a critical event in neuronal apoptosis: regulation by neuroprotectants, BCL-2, and caspases. *J Neurosci* **19**, 7476-85.

Qiu, Y., Benet, L. Z., and Burlingame, A. L. (1998). Identification of the hepatic protein targets of reactive metabolites of acetaminophen in vivo in mice using two-dimensional gel electrophoresis and mass spectrometry. *J Biol Chem* **273**, 17940-53.

Qiu, Y., Benet, L. Z., and Burlingame, A. L. (2001). Identification of hepatic protein targets of the reactive metabolites of the non-hepatotoxic regioisomer of

acetaminophen, 3'-hydroxyacetanilide, in the mouse in vivo using two-dimensional gel electrophoresis and mass spectrometry. *Adv Exp Med Biol* **500**, 663-73.

Raffray, M., and Cohen, G. M. (1997). Apoptosis and necrosis in toxicology: a continuum or distinct modes of cell death? *Pharmacol Ther* **75**, 153-77.

Ramanathan, K., Shila, S., Kumaran, S., and Panneerselvam, C. (2003). Ascorbic acid and alpha-tocopherol as potent modulators on arsenic induced toxicity in mitochondria. *J Nutr Biochem* **14**, 416-20.

Ravagnan, L., Roumier, T., and Kroemer, G. (2002). Mitochondria, the killer organelles and their weapons. *J Cell Physiol* **192**, 131-7.

Ritossa, F. (1996). Discovery of the heat shock response. *Cell Stress Chaperones* **1**, 97-8.

Robertson, J. D., Datta, K., and Kehrer, J. P. (1997). Bcl-xL overexpression restricts heat-induced apoptosis and influences hsp70, bcl-2, and Bax protein levels in FL5.12 cells. *Biochem Biophys Res Commun* **241**, 164-8.

Robertson, J. D., and Orrenius, S. (2000). Molecular mechanisms of apoptosis induced by cytotoxic chemicals. *Crit Rev Toxicol* **30**, 609-27.

Robertson, J. D., and Orrenius, S. (2002). Role of mitochondria in toxic cell death. *Toxicology* **181-182**, 491-6.

Roth, W., and Reed, J. C. (2002). Apoptosis and cancer: when BAX is TRAILing away. *Nat Med* **8**, 216-8.

Rydstrom, J. (1977). Energy-linked nicotinamide nucleotide transhydrogenases. *Biochim Biophys Acta* **463**, 155-84.

Sakurai, A., Nishimoto, M., Himeno, S., Imura, N., Tsujimoto, M., Kunimoto, M., and Hara, S. (2005). Transcriptional regulation of thioredoxin reductase 1 expression by cadmium in vascular endothelial cells: Role of NF-E2-related factor-2. *J Cell Physiol* **203**, 529-37.

Salminen, W. F., Jr., Voellmy, R., and Roberts, S. M. (1997). Protection against hepatotoxicity by a single dose of amphetamine: the potential role of heat shock protein induction. *Toxicol Appl Pharmacol* **147**, 247-58.

Samali, A., Nordgren, H., Zhivotovsky, B., Peterson, E., and Orrenius, S. (1999). A comparative study of apoptosis and necrosis in HepG2 cells: oxidant- induced caspase inactivation leads to necrosis. *Biochem Biophys Res Commun* **255**, 6-11.

Samali, A., Robertson, J. D., Peterson, E., Manero, F., van Zeijl, L., Paul, C., Cotgreave, I. A., Arrigo, A. P., and Orrenius, S. (2001). Hsp27 protects mitochondria of thermotolerant cells against apoptotic stimuli. *Cell Stress Chaperones* **6**, 49-58.

Sammut, I. A., and Harrison, J. C. (2003). Cardiac mitochondrial complex activity is enhanced by heat shock proteins. *Clin Exp Pharmacol Physiol* **30**, 110-5.

Satoh, H., Fukuda, Y., Anderson, D. K., Ferrans, V. J., Gillette, J. R., and Pohl, L. R. (1985). Immunological studies on the mechanism of halothane-induced hepatotoxicity: immunohistochemical evidence of trifluoroacetylated hepatocytes. *J Pharmacol Exp Ther* **233**, 857-62.

Schafler, A. E., Kirmanoglou, K., Pecher, P., Hannekum, A., and Schumacher, B. (2002). Overexpression of heat shock protein 60/10 in myocardium of patients with chronic atrial fibrillation. *Ann Thorac Surg* **74**, 767-70.

Scheffler, I. E. (1999). *Mitochondria*. John Wiley & Sons, New York.

Schnellmann, R. G., and Williams, S. W. (1998). Proteases in renal cell death: calpains mediate cell death produced by diverse toxicants. *Ren Fail* **20**, 679-86.

Scholz, C., Wieder, T., Starck, L., Essmann, F., Schulze-Osthoff, K., Dorken, B., and Daniel, P. T. (2005). Arsenic trioxide triggers a regulated form of caspase-independent necrotic cell death via the mitochondrial death pathway. *Oncogene* **24**, 1904-13.

Scorrano, L., and Korsmeyer, S. J. (2003). Mechanisms of cytochrome c release by proapoptotic BCL-2 family members. *Biochem Biophys Res Commun* **304**, 437-44.

Sekhar, K. R., Crooks, P. A., Sonar, V. N., Friedman, D. B., Chan, J. Y., Meredith, M. J., Starnes, J. H., Kelton, K. R., Summar, S. R., Sasi, S., and Freeman, M. L. (2003). NADPH oxidase activity is essential for Keap1/Nrf2-mediated induction of GCLC in response to 2-indol-3-yl-methylenequinuclidin-3-ols. *Cancer Res* **63**, 5636-45.

Shangary, S., and Johnson, D. E. (2002). Peptides derived from BH3 domains of Bcl-2 family members: a comparative analysis of inhibition of Bcl-2, Bcl-x(L) and Bax oligomerization, induction of cytochrome c release, and activation of cell death. *Biochemistry* **41**, 9485-95.

Sherer, T. B., Betarbet, R., and Greenamyre, J. T. (2002). Environment, mitochondria, and Parkinson's disease. *Neuroscientist* **8**, 192-7.

Shimizu, H., Takahashi, T., Suzuki, T., Yamasaki, A., Fujiwara, T., Odaka, Y., Hirakawa, M., Fujita, H., and Akagi, R. (2000). Protective effect of heme oxygenase induction in ischemic acute renal failure. *Crit Care Med* **28**, 809-17.

Shou, Y., Li, L., Prabhakaran, K., Borowitz, J. L., and Isom, G. E. (2003). p38 Mitogen-activated protein kinase regulates Bax translocation in cyanide-induced apoptosis. *Toxicol Sci* **75**, 99-107.

Single, B., Leist, M., and Nicotera, P. (1998). Simultaneous release of adenylate kinase and cytochrome c in cell death. *Cell Death Differ* **5**, 1001-3.

Stocker, R., Yamamoto, Y., McDonagh, A. F., Glazer, A. N., and Ames, B. N. (1987). Bilirubin is an antioxidant of possible physiological importance. *Science* **235**, 1043-6.

Tada-Oikawa, S., Hiraku, Y., Kawanishi, M., and Kawanishi, S. (2003). Mechanism for generation of hydrogen peroxide and change of mitochondrial membrane potential during rotenone-induced apoptosis. *Life Sci* **73**, 3277-88.

Takehara, T., Liu, X., Fujimoto, J., Friedman, S. L., and Takahashi, H. (2001). Expression and role of Bcl-xL in human hepatocellular carcinomas. *Hepatology* **34**, 55-61.

Tirmenstein, M. A., and Nelson, S. D. (1989). Subcellular binding and effects on calcium homeostasis produced by acetaminophen and a nonhepatotoxic regioisomer, 3'-hydroxyacetanilide, in mouse liver. *J Biol Chem* **264**, 9814-9.

Tirmenstein, M. A., and Nelson, S. D. (1990). Acetaminophen-induced oxidation of protein thiols. Contribution of impaired thiol-metabolizing enzymes and the breakdown of adenine nucleotides. *J Biol Chem* **265**, 3059-65.

Tretter, L., and Adam-Vizi, V. (2000). Inhibition of Krebs cycle enzymes by hydrogen peroxide: A key role of [alpha]-ketoglutarate dehydrogenase in limiting NADH production under oxidative stress. *J Neurosci* **20**, 8972-9.

Trost, L. C., and Lemasters, J. J. (1997). Role of the mitochondrial permeability transition in salicylate toxicity to cultured rat hepatocytes: implications for the pathogenesis of Reye's syndrome. *Toxicol Appl Pharmacol* **147**, 431-41.

Tzung, S. P., Fausto, N., and Hockenbery, D. M. (1997). Expression of Bcl-2 family during liver regeneration and identification of Bcl-x as a delayed early response gene. *Am J Pathol* **150**, 1985-95.

Tzung, S. P., Kim, K. M., Basanez, G., Giedt, C. D., Simon, J., Zimmerberg, J., Zhang, K. Y., and Hockenbery, D. M. (2001). Antimycin A mimics a cell-death-inducing Bcl-2 homology domain 3. *Nat Cell Biol* **3**, 183-91.

van Gurp, M., Festjens, N., van Loo, G., Saelens, X., and Vandenabeele, P. (2003). Mitochondrial intermembrane proteins in cell death. *Biochem Biophys Res Commun* **304**, 487-97.

Van Loo, G., Saelens, X., Van Gurp, M., MacFarlane, M., Martin, S. J., and Vandenabeele, P. (2002). The role of mitochondrial factors in apoptosis: a Russian roulette with more than one bullet. *Cell Death Differ* **9**, 1031-42.

Vila, M., Jackson-Lewis, V., Vukosavic, S., Djaldetti, R., Liberatore, G., Offen, D., Korsmeyer, S. J., and Przedborski, S. (2001). Bax ablation prevents dopaminergic neurodegeneration in the 1-methyl- 4- phenyl-1,2,3,6-tetrahydropyridine mouse model of Parkinson's disease. *Proc Natl Acad Sci U S A* **98**, 2837-42.

Wang, K. K. (2000). Calpain and caspase: can you tell the difference? *Trends Neurosci* **23**, 20-6.

Waters, S. L., Sarang, S. S., Wang, K. K., and Schnellmann, R. G. (1997). Calpains mediate calcium and chloride influx during the late phase of cell injury. *J Pharmacol Exp Ther* **283**, 1177-84.

Wild, A. C., Moinova, H. R., and Mulcahy, R. T. (1999). Regulation of gamma-glutamylcysteine synthetase subunit gene expression by the transcription factor Nrf2. *J Biol Chem* **274**, 33627-36.

Wolfgang, C. D., Chen, B. P., Martindale, J. L., Holbrook, N. J., and Hai, T. (1997). gadd153/Chop10, a potential target gene of the transcriptional repressor ATF3. *Mol Cell Biol* **17**, 6700-7.

Wolter, K. G., Hsu, Y. T., Smith, C. L., Nechushtan, A., Xi, X. G., and Youle, R. J. (1997). Movement of Bax from the cytosol to mitochondria during apoptosis. *J Cell Biol* **139**, 1281-92.

Wu, J. C., Merlino, G., Cveklova, K., Mosinger, B., Jr., and Fausto, N. (1994). Autonomous growth in serum-free medium and production of hepatocellular carcinomas by differentiated hepatocyte lines that overexpress transforming growth factor alpha 1. *Cancer Res* **54**, 5964-73.

Yu, R., Chen, C., Mo, Y. Y., Hebbar, V., Owuor, E. D., Tan, T. H., and Kong, A. N. (2000). Activation of mitogen-activated protein kinase pathways induces antioxidant response element-mediated gene expression via a Nrf2-dependent mechanism. *J Biol Chem* **275**, 39907-13.

Zavialov, A. V., Gaestel, M., Korpela, T., and Zav'yalov, V. P. (1998). Thiol/disulfide exchange between small heat shock protein 25 and glutathione. *Biochim Biophys Acta* **1388**, 123-32.

Zhang, C., Gao, C., Kawauchi, J., Hashimoto, Y., Tsuchida, N., and Kitajima, S. (2002). Transcriptional activation of the human stress-inducible transcriptional repressor ATF3 gene promoter by p53. *Biochem Biophys Res Commun* **297**, 1302-10.

Zhang, C., Kawauchi, J., Adachi, M. T., Hashimoto, Y., Oshiro, S., Aso, T., and Kitajima, S. (2001). Activation of JNK and transcriptional repressor ATF3/LRF1 through the IRE1/TRAF2 pathway is implicated in human vascular endothelial cell death by homocysteine. *Biochem Biophys Res Commun* **289**, 718-24.

Zhang, D. D., and Hannink, M. (2003). Distinct cysteine residues in Keap1 are required for Keap1-dependent ubiquitination of Nrf2 and for stabilization of Nrf2 by chemopreventive agents and oxidative stress. *Mol Cell Biol* **23**, 8137-51.

Zhang, H., Heim, J., and Meyhack, B. (1998). Redistribution of Bax from cytosol to membranes is induced by apoptotic stimuli and is an early step in the apoptotic pathway. *Biochem Biophys Res Commun* **251**, 454-9.

Zhang, Y., and Gordon, G. B. (2004). A strategy for cancer prevention: stimulation of the Nrf2-ARE signaling pathway. *Mol Cancer Ther* **3**, 885-93.

Zhou, H., Kato, A., Yasuda, H., Odamaki, M., Itoh, H., and Hishida, A. (2003). The induction of heat shock protein-72 attenuates cisplatin-induced acute renal failure in rats. *Pflugers Arch* **446**, 116-24.

Zimmermann, K. C., Bonzon, C., and Green, D. R. (2001). The machinery of programmed cell death. *Pharmacol Ther* **92**, 57-70.

Zou, H., Li, Y., Liu, X., and Wang, X. (1999). An APAF-1.cytochrome c multimeric complex is a functional apoptosome that activates procaspase-9. *J Biol Chem* **274**, 11549-56.

Vita

Han Kiat Ho was born in 1975 and raised as the younger of two children in Singapore. At the National University of Singapore, he earned a Bachelor of Science (Pharmacy) with First Class Honors in 2000. In 2005, he earned a Doctor of Philosophy in Medicinal Chemistry at the University of Washington.